



**HAL**  
open science

# Homogenization-based, higher-gradient dynamical response of micro-structured media

Mohammad Ayad

► **To cite this version:**

Mohammad Ayad. Homogenization-based, higher-gradient dynamical response of micro-structured media. Mechanics of materials [physics.class-ph]. Université de Lorraine; Université libanaise, 2020. English. NNT : 2020LORR0062 . tel-02956259

**HAL Id: tel-02956259**

**<https://hal.univ-lorraine.fr/tel-02956259>**

Submitted on 2 Oct 2020

**HAL** is a multi-disciplinary open access archive for the deposit and dissemination of scientific research documents, whether they are published or not. The documents may come from teaching and research institutions in France or abroad, or from public or private research centers.

L'archive ouverte pluridisciplinaire **HAL**, est destinée au dépôt et à la diffusion de documents scientifiques de niveau recherche, publiés ou non, émanant des établissements d'enseignement et de recherche français ou étrangers, des laboratoires publics ou privés.



## AVERTISSEMENT

Ce document est le fruit d'un long travail approuvé par le jury de soutenance et mis à disposition de l'ensemble de la communauté universitaire élargie.

Il est soumis à la propriété intellectuelle de l'auteur. Ceci implique une obligation de citation et de référencement lors de l'utilisation de ce document.

D'autre part, toute contrefaçon, plagiat, reproduction illicite encourt une poursuite pénale.

Contact : [ddoc-theses-contact@univ-lorraine.fr](mailto:ddoc-theses-contact@univ-lorraine.fr)

## LIENS

Code de la Propriété Intellectuelle. articles L 122. 4

Code de la Propriété Intellectuelle. articles L 335.2- L 335.10

[http://www.cfcopies.com/V2/leg/leg\\_droi.php](http://www.cfcopies.com/V2/leg/leg_droi.php)

<http://www.culture.gouv.fr/culture/infos-pratiques/droits/protection.htm>



Université Libanaise  
Ecole Doctorale des  
Sciences et de  
Technologie



Université Libanaise  
Faculté de Génie

**LEM3**  
LABORATOIRE D'ÉTUDE DES MICROSTRUCTURES  
ET DE MÉCANIQUE  
DES MATÉRIAUX



**UNIVERSITÉ  
DE LORRAINE**

**THESE de doctorat en Cotutelle**  
Pour obtenir le grade de Docteur délivré par  
**L'Université Libanaise Et l'Université de Lorraine**

Spécialité : Mécanique et Énergétique

Présentée et soutenue publiquement par

**Mohammad Ayad**

Le 02 Juillet 2020

**Homogenization-based, higher-gradient  
dynamical response of micro-structured media**

**Membres du Jury:**

<b>M. Luigi Gambarotta</b> , Pr, University of Genoa	<i>Rapporteur</i>
<b>M. Andrei Metrikine</b> , Pr, Delft University of Technology	<i>Rapporteur</i>
<b>M. Fodil Meraghni</b> , Pr, Ecole Nationale Supérieure d'Arts et Métiers	<i>Président</i>
<b>M. khaled Khalil</b> , Pr, Université Libanaise	<i>Examineur</i>
<b>M. Jean-François Ganghoffer</b> , Pr, Université de Lorraine	<i>Directeur de thèse</i>
<b>M. Hassan Lakiss</b> , Pr, Université Libanaise	<i>Directeur de thèse</i>
<b>M. Mohamad Hammoud</b> , Dr, Lebanese International University	<i>Examineur</i>
<b>Mme. Florence Dinzart</b> , Dr, Université de Lorraine	<i>Examinatrice</i>
<b>M. Hilal Reda</b> , Dr, Université Libanaise	<i>Invité</i>
<b>M. Nikos Karathansopoulos</b> , Dr, ETH Zurich	<i>Invité</i>
<b>M. Gerard Maurice</b> , Pr, Université de Lorraine	<i>Invité</i>
<b>M. Rachid Rahouadj</b> , Pr, Université de Lorraine	<i>Invité</i>

## Acknowledgments

First, I would like to send special and warm thanks to my parents and my family (My wife, my brothers, my sisters...). I wouldn't have been able to pursue this project without your support.

I would like to thank all the teaching staff at the Lebanese University (Faculty of Engineering) and to renew my gratitude for Dr. Marwan Fahs and Dr. Daoud Baalbaki who encouraged me to continue in this field. A special thanks to my teachers Ibrahim Cheaitou and Hassan Chour, who advised me to carry on my dream by doing this Ph.D. I am also very grateful for the "Association de Specialisation et d'Orientation Scientifique" for giving me the Ph.D. grant.

My deepest appreciation and thanks to my supervisors, Pr. Jean-Francois Ganghoffer, Pr. Hassan Lakiss and Dr. Hilal Reda . I thank them for their recommendations, suggestions and support.

Then, I would like to express my sincere appreciation to Dr. Nikolaos Karathanasopoulos, for his continuous guidance, encouragement and support throughout my Ph.D. period. He provided counsel and assistance that greatly enhanced my skills.

I would like to thank Pr. Rachid Rahouadj for his guidance, encouragement, wisdom throughout my Ph.D. period. I am also grateful to all the workers in LEM3 who provided me with the tools and the needed ambiance for working.

These lines cannot express all my feelings. I would like to dedicate this work to my friends, my family and mostly the one person who I'm waiting for his/her arrival "My future son or daughter".

## Résumé – Abstract

**Titre de la thèse en français :** Réponse dynamique de milieux à microstructure par des formulations à gradient d'ordre supérieur obtenues par des méthodes d'homogénéisation.

### Résumé

Une approche dynamique discrète (DDM) est proposée dans le contexte de la mécanique des poutres pour calculer les caractéristiques de dispersion des structures périodiques. Cette démarche permet de calculer les caractéristiques de dispersion de milieux périodiques unidimensionnels et bidimensionnels. Il est montré qu'un développement d'ordre supérieur suffisamment élevé des forces et des moments d'éléments structuraux est nécessaire pour décrire avec précision les modes de propagation d'ordre supérieur. Ces résultats montrent dans l'ensemble que les calculs des caractéristiques de dispersion de systèmes structurels périodiques peuvent être abordés avec une bonne précision par la dynamique des éléments discrets.

Les comportements non classiques peuvent être capturés non seulement par une expansion d'ordre supérieur mais aussi par des formulations à gradient supérieur. Nous calculons ainsi les paramètres constitutifs macroscopiques jusqu'au deuxième gradient du déplacement en utilisant deux formulations différentes, soit selon une méthode d'homogénéisation dynamique à gradient supérieur (DHGE) prenant en compte les effets de micro-inertie, ou alternativement selon le principe de Hamilton. Nous analysons ensuite la sensibilité des termes constitutifs du second gradient aux paramètres microstructuraux pour des matériaux composites à microstructure périodique de type laminés. En plus, on montre que les modèles du deuxième gradient formulés à partir de l'énergie interne totale en tenant compte des termes de gradient d'ordre supérieur donnent la meilleure description de la propagation d'onde à travers ces milieux.

On analyse les contributions d'ordre supérieur et de microinertie sur le comportement mécanique de structures composites en utilisant une méthode d'homogénéisation dynamique d'ordre supérieur qui intègre les effets de microinertie. Nous calculons la réponse effective statique longitudinale à gradient d'ordre supérieur, en quantifiant la différence relative par rapport à la formulation classique de type Cauchy qui repose sur le premier gradient du déplacement. Nous analysons ensuite les propriétés de propagation d'ondes longitudinales en termes de fréquence propre de composites, en tenant compte de la contribution de la microinertie. La longueur interne joue un rôle crucial dans les contributions de microinertie

avec un effet substantiel pour les faibles valeurs de longueur interne, et qui correspond à une large gamme de matériaux utilisés en ingénierie des structures.

La méthode d'homogénéisation développée montre un effet de taille important pour les modules élastiques homogénéisés d'ordre supérieur. Par conséquent, nous développons une formulation indépendante de la taille qui est basée sur des termes de correction liée aux moment quadratique. Dans ce contexte, on analyse l'influence des termes de correction sur le comportement statique et dynamique de composites à inclusion.

**Mots clés :** Homogénéisation, Cauchy, micro-inertie, second gradient, dynamique, acoustique, vibration, stratifiés périodiques, composites.

**Titre de la thèse en anglais :** Homogenization-based higher-gradient dynamical response of micro-structured media.

## **Abstract**

A discrete dynamic approach (DDM) is developed in the context of beam mechanics to calculate the dispersion characteristics of periodic structures. Subsequently, based on this dynamical beam formulation, we calculate the dispersion characteristics of one-dimensional and two-dimensional periodic media. A sufficiently high order development of the forces and moments of the structural elements is necessary to accurately describe the propagation modes of higher order. These results show that the calculations of the dispersion characteristics of structural systems can be approached with good accuracy by the dynamics of the discrete elements.

Besides, non-classical behaviors can be captured not only by higher order expansion but also by higher gradient formulations. To that scope, we develop a higher gradient dynamic homogenization method with micro-inertia effects. Using this formulation, we compute the macroscopic constitutive parameters up to the second gradient, using two distinct approaches, namely Hamilton's principle and a total internal energy formulation. We analyze the sensitivity of the second gradient constitutive terms on the inner material and geometric parameters for the case of composite materials made of a periodic, layered microstructure. Moreover, we show that the formulations based on the total internal energy taking into account higher order gradient terms give the best description of wave propagation through the composite.

We analyze the higher order and micro-inertia contributions on the mechanical behavior of composite structures by calculating the effective static and dynamic properties of composite beams using a higher order dynamic homogenization method. We compute the effective longitudinal static response with higher order gradient, by quantifying the relative difference compared to the classical formulation of Cauchy type, which is based on the first gradient of displacement. We then analyze the propagation properties of longitudinal waves in terms of the natural frequency of composite structural elements, taking into account the contribution of micro-inertia. The internal length plays a crucial role in the contributions of micro-inertia, which is particularly significant for low internal length values, therefore for a wide range of materials used in structural engineering. The developed method shows an important size effect for the higher gradients, and to remove these effects correction terms have been incorporated which are related to the quadratic moment of inertia. We analyze in this context the influence

## Résumé – Abstract

of the correction terms on the static and dynamic behavior of composites with a central inclusion.

**Keywords:** Homogenization, Cauchy, micro-inertia, second gradient, dynamic, acoustic, vibration, Periodic laminates, composites.

## Table of Contents

### Contents

Acknowledgments .....	2
Résumé – Abstract.....	3
Résumé.....	3
Abstract.....	5
Table of Contents .....	7
List of Figures .....	10
List of Tables .....	14
Résumé de la Thèse en Français .....	15
<b>Chapter 1: General Introduction .....</b>	<b>27</b>
1.1 Overview .....	27
1.1.1 Higher order static homogenization.....	30
1.1.2 Impact of higher order homogenization on static and dynamic behavior.....	32
1.2 Motivation of the thesis.....	36
1.2.1 Dispersion characteristics of periodic structural systems using higher order beam dynamics .....	36
1.2.2 Strain gradient homogenization based on dynamic higher gradient strain energy and effects on wave propagation .....	36
1.2.3 Strain gradient homogenization with micro inertia effects for vibration analyses...37	
1.2.4. Wave propagation analysis of composites structures using independent size higher gradient formulation .....	37
1.3 Organization of the thesis.....	38
References.....	39
<b>Chapter 2: Dispersion characteristics of periodic structural systems using higher order beam element dynamics.....</b>	<b>47</b>
2.1 Introduction .....	48
2.2 Structural dynamics of discrete and continuous systems .....	51
2.2.1 Dispersion characteristics of discrete systems based on the asymptotic description of their inner forces and moments .....	51
2.3 Dispersion Diagrams for 1D periodic media.....	54
2.3.1 One-Cell periodic system $\Omega_1$ .....	54
2.3.2 Two-cell systems $\Omega_2$ .....	58
2.3.3 Three-cells system $\Omega_3$ .....	61
2.4 Dynamical response of a 2D network material .....	65
2.5 Discussion .....	68
2.6 Conclusion.....	69

References .....	70
<b>Chapter 3: On the role of second gradient constitutive parameters in the static and dynamic analysis of heterogeneous media with micro-inertia effects</b> .....	75
3.1 Introduction .....	76
3.2 Homogenization methods.....	79
3.2.1 Second gradient mechanics and Hill-Mandel principle .....	79
3.2.2 Hamilton principle based second gradient mechanics .....	82
3.2.3 Dynamic higher gradient energy formulation of the constitutive law .....	85
3.3 Results.....	86
3.3.1 Composite laminated media .....	86
3.3.2 Homogenized higher gradient static effective properties .....	92
3.3.3 Wave propagation in layered, periodic media.....	96
3.4. Discussion .....	105
3.5 Conclusion.....	107
References.....	108
<b>Chapter 4: Higher-gradient and micro-inertia contributions on the mechanical response of composite beam structures</b> .....	114
4.1 Introduction .....	115
4.2 Materials and methods .....	117
4.2.1 Composite beams.....	117
4.2.2 Higher gradient and micro-inertia constitutive material modeling .....	119
4.2.3 Static and dynamic equilibrium of the homogenized structure.....	121
4.3 Results.....	122
4.3.1 Static response .....	122
4.3.2 Micro-inertia effects on the higher-gradient, eigenfrequency properties .....	125
4.3.3 Sensitivity of the dynamic properties on the micro-inertia contributions for different second-gradient material designs .....	132
4.4 Discussion .....	135
4.5 Conclusion.....	136
References.....	137
<b>Chapter 5: Wave Propagation in 2D composites Structure using Higher Gradient Size Independent Homogenization</b> .....	141
5.1 Introduction .....	142
5.2 Materials and methods .....	146
5.2.1 Theoretical formulation .....	146
5.2.2 Homogenization modeling.....	150
5.2.3 Wave dispersion for 2D structures .....	152
5.3 Application to inclusion based composite materials.....	153

## Table of Contents

5.3.1 Overview of inclusion based composite models .....	153
5.3.2 Static properties of 2D composite microstructures.....	155
5.3.3 Wave propagation analysis within 2D second gradient media .....	161
5.4 Discussion .....	167
5.5 Conclusion.....	169
References .....	170
<b>Conclusions and Perspectives.....</b>	<b>174</b>
<b>Appendices.....</b>	<b>177</b>
Appendix 1.A: Expression of the dynamic forces and moments .....	177
1.A.1 Dynamical expression of the Normal Force.....	177
1.A.2 Dynamical expression of the transverse force and bending moments .....	178
Appendix 2.A: Hamilton principle .....	179
2.A.1 Second gradient from surface to volume integration.....	179
2.A.2 Hamiltonian principle up to second gradient .....	180
2.A.3 Simplification of $F_i$ .....	183
Appendix 2.B: Higher gradient dynamic homogenization method.....	185
Appendix 2.C: Elasticity Solution.....	186
Appendix 3.A: Identification of micromechanical constants upon normal deformations ..	186
Appendix 4. A: Homogenized elasticity tensors .....	189
Appendix 4.B: Corrected higher gradient formulation.....	189
Appendix 4. C: Microscopic elastic matrix .....	191

## List of Figures

Figure R.1: Treillis carré avec ses éléments répétitifs de base (gris foncé) (a). Le nœud principal 1, ainsi que les quatre éléments nécessaires à la description de son équilibre discret (b). L'équilibre de la force normale, du cisaillement et des moments pour le nœud principal 1 est représenté en (c). .....	17
Figure R.2 : Courbes de dispersion pour une structure en treillis carré de la Fig. R1b en utilisant l'expression dynamique des forces et des moments intérieurs jusqu'au quatrième ordre pour le cisaillement et la solution issue du théorème de Bloch (lignes pointillées) (a). Courbes de dispersion du même réseau pour une expansion d'ordre supérieur (8ème ordre) du cisaillement interne et des moments (lignes continues) et solution du théorème de Bloch (lignes pointillées) (b). .....	18
Figure R.3 : Géométrie périodique de matériaux composites stratifiés (à gauche) et les paramètres de la cellule unitaire (à droite).....	19
Figure R.4 : Courbes de vitesse de phase obtenues par le principe de Hamilton jusqu'au second ordre (Cyan), pour le premier gradient (vert), premier gradient avec effets de micro-inertie d'ordre supérieur (jaune) dans (Bacigalupo et Gambarotta, 2014b) et la solution exacte (rouge) fournie par (Sun et al.,1968). .....	19
Figure R.5: Fréquence des ondes longitudinales (a) et transversales (b) et vitesse de groupe pour les ondes longitudinales (c) et transverses (d) pour les deux méthodes d'homogénéisation dynamique en fonction de la valeur du nombre d'onde. ....	20
Figure R.6 : Déformation et déplacement le long d'une poutre en utilisant la formulation du second gradient pour une déformation fixée à l'extrémité de la poutre $\varepsilon_{SG} = 0$ (Vert) et la solution linéaire pour $\varepsilon_{SG} = \varepsilon_0$ (Rouge) pour un chargement $P_0 / A = 0.02C_1^1$ à l'extrémité chargée de la poutre.....	21
Figure R.7 : Différence relative des valeurs de fréquence propre calculées pour le deuxième gradient (SG) et le deuxième gradient avec micro-inertie (SG + $\mu I$ ) ((a) et (b) respectivement) pour les trois premiers modes propres pour différentes valeurs de la longueur interne $l_e$ .....	22
Figure R.8: Variation des longueurs internes $l_{e_{ij}}$ (mm) en fonction du rayon de l'inclusion $R$ (mm) pour $(E_1 / E_2) = 20, 100$ en (a) et (b) respectivement, et en fonction du rapport des modules élastiques $(E_1 / E_2)$ pour $R = 0.25mm, 0.4mm$ en (c) et (d) respectivement.....	23
Figure R.9: Courbes de dispersion en utilisant une approximation classique (Bleu), une approximation du second gradient sans termes de correction (Rouge) et avec des termes de correction (Vert) pour le mode de cisaillement (bande inférieure) et le mode longitudinal (bande supérieure) dans la première partie de la zone de Brillouin de la matrice.....	24
Figure R.10 : Différence relative maximale des courbes de dispersion entre la formulation du second gradient pour $k = 0.6m^{-1}$ sans termes de correction (SG en rouge) et avec des termes de correction (SG * en vert) pour différents rayons d'inclusion R avec un contraste de modules $(E_1 / E_2 = 100MPa)$ pour les modes transverses (a) et longitudinal (b), et pour différents rapports d'élasticité $(E_1 / E_2)$ avec $R = 0.4mm$ , pour les modes transverse (c) et longitudinal (d). .....	24
Figure 1.1: Architected materials with anisotropic designs (left),(Karathanasopoulos et al., 2017) and chiral structures (tetrachiral lattice, right), (Karathanasopoulos et al., 2020). .....	27
Figure 1.2: Dispersion analysis on a hexachiral material with superposed domains of validity of the continuum models (Rosi & Auffray, 2016). .....	34

## List of Figures

Figure 2.1 : Propagating wave lengths $L_c$ within repetitive network materials with repetitive unit cells of size $l_0$ . Scale separation applies when $L_c \gg l_0$ . .....	50
Figure 2.2 : Forces and moments acting at the end nodes of each beam element (a). A single unit-cell structure in a one dimensional domain without transverse forces and moments (a) and its two neighboring cell representation (c). .....	51
Figure 2.3 : Longitudinal dispersion curve obtained for the Cauchy effective continuum (in blue) and by the dynamic discrete method (in Red). .....	55
Figure 2.4 : Displacement of a series of 5 nodes in the 1D space, when the wave frequency is accounted for in the periodic solution. ....	57
Figure 2.5 : A basic system of two-cells with an internal node $v$ considered as the basic material unit (a). Two adjacent material units comprising a total of 4 unit-cells (b). ....	58
Figure 2.6: Dispersion curves for a two-cell system that includes an optical branch (blue line) and an acoustic branch (red line). .....	60
Figure 2.7 : Three-cells system $\Omega_3$ with two internal nodes $v_1$ and $v_2$ considered as the basic material unit (a). Two adjacent material units comprised of a total of 6 unit-cells (b). ....	61
Figure 2.8 : Dispersion curve of the three-cells system including an acoustic (blue) and two optimal branches (green and red). .....	63
Figure 2.9 : Square lattice along with its basic elements (dark grey) in each material direction (a). The principal node 1, along with the four elements required for the description of its discrete equilibrium (b). The equilibrium of the normal, shear and moments for the principal node 1 is pictured in (c). .....	65
Figure 2.10 : Dispersion curves for a square lattice structure of Fig. 2.9b using the dynamic expression of the inner forces and moments up to the fourth order for the inner shear and moments along with the Bloch theorem solution (dashed lines) (a). Dispersion curves of same lattice for a higher order expansion (8 <sup>th</sup> order) of the inner shear and moments (continuous lines) along with the Bloch theorem solution (dashed lines) (b). .....	67
Figure 3.1: Homogenization concept from micro to macro model .....	80
Figure 3.2: Periodic layered composite material geometry (left) and its unit cell material parameters (right). .....	87
Figure 3.3: Homogenized second gradient and coupling tensors in function of layers thickness ratio $d_1/d_2$ for longitudinal (a) and for transverse (b). .....	95
Figure 3.4 : Second gradient characteristic length as a function of the elastic modulus ratio $\phi$ for the case of longitudinal and b) for transverse deformations (b) for different thickness ratio values. ....	96
Figure 3.5: Phase velocity curves obtained by Hamilton principle up to second order (Cyan), for first gradient (green), first gradient with higher order micro-inertia effects (yellow) in (Bacigalupo & Gambarotta, 2014b) and the exact solution (red) provided by (Sun et al.,1968) (Appendix 2.C). .....	100
Figure 3.6 : Variation of dynamic second gradient characteristic length as a function of the normalized wavenumber for different values of the phase velocity for the case of longitudinal (a) and transverse (b) deformation mode. ....	102
Figure 3.7: Normalized phase velocity curves for longitudinal wave (a) and for transverse wave (b) obtained by the DHGE method with first and second gradient constitutive parameters (blue and red respectively). The exact solution is presented in black (Sun et al., 1968), while the yellow color curves correspond to the first gradient constitutive formulation with higher gradient inner micro-inertia terms provided in (Bacigalupo & Gambarotta, 2014). .....	104
Figure 3.8: Frequency of the longitudinal (a) and transverse waves (b) and group velocity for the longitudinal (c) and transverse waves (d) for both dynamic homogenization methods as a function of the propagating wave number value. ....	105

## List of Figures

Figure 4.1: A two-phase composite beam structure (a) with effective Cauchy (C), Second-Gradient (SG) and micro-inertia ( $\mu I$ ) properties (b) which depend on its micro-scale material parameters. Upon loading, the obtained static (c) and dynamic (d) characteristics directly depend on the modeling formulation employed for the assessment of its structural response at the effective continuum scale.....	118
Figure 4.2 : Strain and displacement along the beam using the second gradient formulation for $\varepsilon_{SG} = 0$ (Red), and the linear solution for $\varepsilon_{SG} = \varepsilon_0$ (Black) for a loading $P_0 / A = 0.02C_1^l$ at the loaded extremity of the beam. ....	124
Figure 4.3 : Macroscopic strain (a) and displacement (b) profiles for a total of four internal length values, starting from the Cauchy-mechanics case ( $l_e = 0$ ) up to a substantially high internal length value of $l_e = 0.92mm$ . The loading is kept constant to $P_0 / A = 0.02C_1^l$ as in the results of Fig. 4.2.....	125
Figure 4.4: Mesh (a) and longitudinal displacement profiles for the first three eigenfrequency values (b, c and d accordingly) along with the corresponding eigenfrequency value for the Borosilicate Glass and Silicon Carbide unit-cell design of Table 4.2.....	127
Figure 4.5 : Relative difference of the eigenfrequency values computed for the second-gradient (SG) and the second-gradient with micro-inertia (SG+ $\mu I$ ) formulation (subplots (a) and (b) accordingly) for the first three eigenmodes for different values of the internal length $l_e$ . ....	133
Figure 4.6 : Relative difference of the $SG + \mu I$ response with respect to the Cauchy-mechanics (C) predictions as a function of the variation of the density ratio of the individual material phases contained in the unit-cell for different internal lengths values $l_e = 0.153mm$ (a), $l_e = 0.205mm$ (b), $l_e = 0.25mm$ (c) and $l_e = 0.29mm$ (d).....	134
Figure 5.1: Centrosymmetric matrix and central hole (a) and reinforcement material (b).....	155
Figure 5.2: Square pattern (a) with three different square unit-cell choices (b, c, d and e) of dimension $l, 2l, 3l$ and $4l$ accordingly.....	158
Figure 5.3 : Second gradient constitutive moduli variation for different RVE sizes without correction terms $A_{ijklmn}^{hom}$ in (a) and with correction terms $A_{ijklmn}^{hom*}$ in (b). ....	159
Figure 5.4 : Variation of internal length parameters $le_{ij}$ (mm) as function of the inclusion radius $R$ (mm) for $(E_1 / E_2) = 20, 100$ in (a) and (b) accordingly as function of the microscopic elasticity ratio $(E_1 / E_2)$ for $R = 0.25mm, 0.4mm$ in (c) and (d) accordingly. ....	160
Figure 5.5 : Variation of internal length parameters $le_{ij^*}$ (mm) as function of inclusion radius $R$ (mm) for $(E_1 / E_2) = 20, 100$ in (a) and (b) accordingly, and as function of the elasticity ratio $(E_1 / E_2)$ for $R = 0.2mm, 0.4mm$ in (c) and (d) accordingly. ....	161
Figure 5.6 : Mesh of the composite structure (a), and displacement shape for the transverse (b) and longitudinal (c) propagating modes. ....	162
Figure 5.7 : Longitudinal (Green) and transverse (Blue) wave dispersion (b) through the 2D composite structure from Fig. 5.1b in Brillouin zone (a). ....	163
Figure 5.8: Dispersion relation of the composite structure (Fig. 5.1b) using Cauchy approximation (Blue), and COMSOL with the diamond points for the shear (lower band) and longitudinal modes (upper band).....	164
Figure 5.9: Wave dispersion diagram using the first gradient theory (Blue), the higher gradient approximation without correction terms (Red) and with correction terms (Green) for the shear mode (lower band) and the longitudinal mode (upper band).....	165
Figure 5.10 : Maximum relative difference in the dispersion curves at $k = 0.6m^{-1}$ between the higher gradient formulation without correction terms (SG in Red) and with correction terms	

## List of Figures

(SG\* in Green) for different inclusion radii  $R$  with a contrast of moduli ( $E_1 / E_2 = 100MPa$ ) for the transverse and longitudinal modes in (a) and (b) accordingly, and for different elasticity ratio ( $E_1 / E_2$ ) with  $R = 0.4mm$ , for the transverse and longitudinal modes in (c) and (d) accordingly.....166

Figure 5.11: Pantographic structure with perpendicular diagonal. ....168

## List of Tables

Table 2.1 : Geometric and mechanical characteristics of the beam. ....	52
Table 2.2 : Frequency values that satisfy the separation of scales as a function of the number of unit-cells considered within the basic period of the structural system. ....	69
Table 3.1: Geometric and mechanical layers properties the laminate layers.....	97
Table 3.2: Constant values obtained by the Hamilton principle based on second gradient mechanics.....	99
Table 3.3: Constants value obtained by the DHGE method. ....	103
Table 4.1 : Mechanical properties of the materials used in the design of the microstructure of the composite beam of Fig. 4.1a. ....	118
Table 4.2 : Homogenized stiffness coefficients and internal length values for different Carbon and Glass-based unit-cell material designs using the material properties of Table 4.1 and the definitions of Eq. (4.3).....	122
Table 4.3 : Homogenized static and dynamic properties of the composite unit-cell material designs of Tables 1 and 2 for equal micro-scale layer thickness $d_i$ in Fig. 4.1a.....	129
Table 4.4 : Eigenfrequency values of the composite Silicon Carbide-Borosilicate Glass (Tables 4.2, 4.3) beam structure upon a Cauchy (C), Second-Gradient (SG) and Second-Gradient with micro-inertia (SG+ $\mu$ I) modeling formulation. ....	130
Table 4.5 :Eigenfrequency values of the composite E-Glass and Epoxy (Tables 4.2, 4.3) beam structure upon a Cauchy (C), Second-Gradient (SG) and Second-Gradient with micro-inertia contributions (SG+ $\mu$ I) modeling formulation. ....	131
Table 4.6 : Eigenfrequency values of the composite Carbon and Epoxy (Tables 4.2, 4.3) beam structure upon a Cauchy (C), Second-Gradient (SG) and Second-Gradient with micro-inertia effects (SG+ $\mu$ I).....	131
Table 5.1 : Relative difference between the homogenized second gradient constitutive parameters of the 2D composite structure in Fig. 1a using HGE without the correction terms and the analytical results of (Li, 2011). ....	157
Table 5.2 : Relative difference between of the homogenized second gradient constitutive parameters of the 2D composite structure in Fig. 5.1a using HGE with corrections terms and the analytical results of (Li, 2011).....	157

## Résumé de la Thèse en Français

**Titre de la thèse en français :** Réponse dynamique de milieux à microstructure par des formulations à gradient d'ordre supérieur obtenues par des méthodes d'homogénéisation.

Les modèles micromécaniques prédictifs visant à comprendre l'impact de la géométrie et des propriétés du renfort et de la matrice sur la réponse de composites à l'échelle macroscopique font l'objet de développements significatifs, la détermination expérimentale des propriétés mécaniques des composites étant délicate. Par conséquent, des approches prédictives d'inspiration micromécanique s'avèrent très utiles afin de lier le comportement aux différentes échelles et de construire une loi de comportement à l'échelle d'un milieu continu effectif, grâce auxquelles les propriétés équivalentes du milieu continu de substitution peuvent être liées aux paramètres microstructuraux géométriques et mécaniques des constituants individuels du composite. En outre, la conception optimale de matériaux architecturés et de composites nécessite de comprendre de façon quantitative la relation entre l'architecture interne et les propriétés physiques, et de formuler les approches théoriques et numériques adéquates pour évaluer ces propriétés en prenant en compte les effets de microstructure dans des conditions tant statique que dynamique.

La mécanique des milieux continus généralisés peut être définie comme une théorie des milieux continus où la mécanique des milieux continus classiques développée par Cauchy est insuffisante pour la description des phénomènes physiques (Kröner, 1968). Afin de conserver une description de type milieu continu, il faut adopter une modélisation de type milieux continus enrichis pour modéliser le milieu homogène équivalent résultant du processus d'homogénéisation. Les techniques d'homogénéisation classiques rencontrent des limites lorsque la longueur d'onde du chargement ou de la déformation deviennent comparable à la taille de la microstructure ou de celle d'un volume élémentaire représentatif de cette dernière (Trinh et al., 2012). L'objectif de l'homogénéisation vers des milieux continus généralisés est de remédier à ces limitations et d'étendre la plage de validité de l'approche de type milieu continu au-delà de l'hypothèse stricte de la séparation d'échelle (Mindlin, 1964; Eringen et Suhubi, 1964). L'incorporation de l'échelle microstructurale dans les formulations de type milieux continus enrichis implique la relaxation de l'hypothèse de localité des interactions et l'introduction d'une interaction spatiale à grande distance et d'échelles de longueur internes pour tenir compte de l'influence des points voisins dans la définition des variables cinématique, statiques et la formulation des équations constitutives. Il existe essentiellement deux façons de généraliser la définition classique d'un continuum, classées en milieux continus d'ordre

supérieur et milieux à gradient supérieur. Les milieux d'ordre supérieur impliquent des degrés de liberté supplémentaires comme le milieu de Cosserat développé par les frères Cosserat (Cosserat et Cosserat, 1909) et le milieu micromorphe (Eringen et Suhubi, 1964; Mindlin, 1964; Germain, 1973). Dans l'élasticité de Cosserat encore appelée micropolaire (Cosserat et Cosserat, 1909), des rotations locales sont ajoutées comme degrés de liberté. Dans les milieux à gradient d'ordre supérieur, on garde les mêmes degrés de liberté mais des gradients d'ordre supérieur du champ de déplacement ou de la déformation complètent le jeu de degrés de liberté.

L'objectif général de la thèse est de formuler des méthodes d'homogénéisation dynamiques de milieux hétérogènes en prenant en compte l'impact de la microstructure sous-jacente par des formulations enrichies de type milieux continus du second gradient pour la description des interactions spatiales à longue portée ainsi que les effets de micro-inertie.

Dans cette thèse, nous déterminons dans une première étape le développement asymptotique d'ordre supérieur des forces et des moments dans les éléments structuraux de type poutres pour des sollicitations dynamiques (Ayad et al., 2020a). Par la suite, nous utilisons les résultats obtenus pour calculer les caractéristiques de dispersion de milieux périodiques unidimensionnels et bidimensionnels. L'équilibre de la cellule irréductible d'un milieu périodique permet d'obtenir la structure fondamentale du diagramme de dispersion aux basses fréquences, décrivant le comportement acoustique de la structure au-delà de la limite de la théorie non dispersive de Cauchy. Nous montrons que la dynamique discrète permet d'accéder aux modes de fréquence plus élevés pour un domaine incluant plusieurs cellules, ces plages de fréquence dispersive n'étant pas accessibles par des formulations classiques. Ces analyses sont ensuite étendues pour des structures bidimensionnelles (Fig. R1) afin d'en décrire les caractéristiques de dispersion.

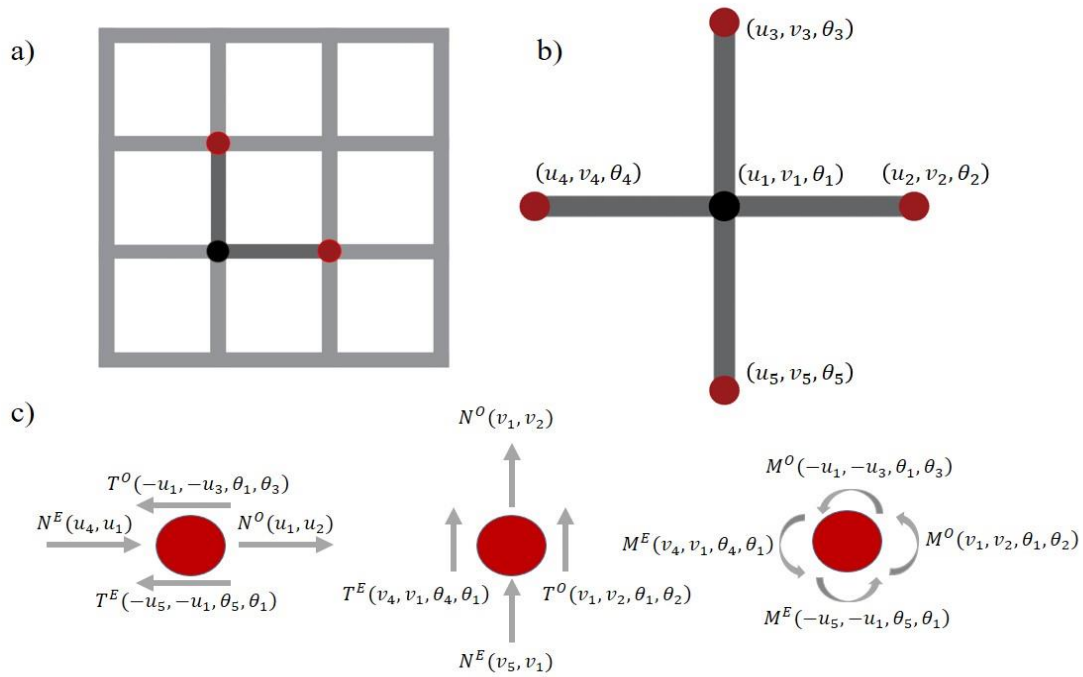


Figure R.1: Treillis carré avec ses éléments répétitifs de base (gris foncé) (a). Le nœud principal 1, ainsi que les quatre éléments nécessaires à la description de son équilibre discret (b). L'équilibre de la force normale, du cisaillement et des moments pour le nœud principal 1 est représenté en (c).

Les résultats de dispersion dynamique discrète sont validés par comparaison avec les prédictions du théorème de Bloch (Fig. R2) (Phani et al., 2006). Un développement d'ordre supérieur suffisamment élevé des forces et des moments des éléments structuraux est nécessaire pour décrire avec précision les modes de propagation d'ordre supérieur. A l'inverse, nous montrons que les modes de propagation longitudinaux et transverses peuvent être capturés en utilisant une expansion du quatrième ordre des forces et moments dynamiques. Ces résultats montrent que le calcul des caractéristiques de dispersion de systèmes structuraux périodiques peut être abordés avec une bonne précision par la dynamique d'éléments discrets de type poutres.

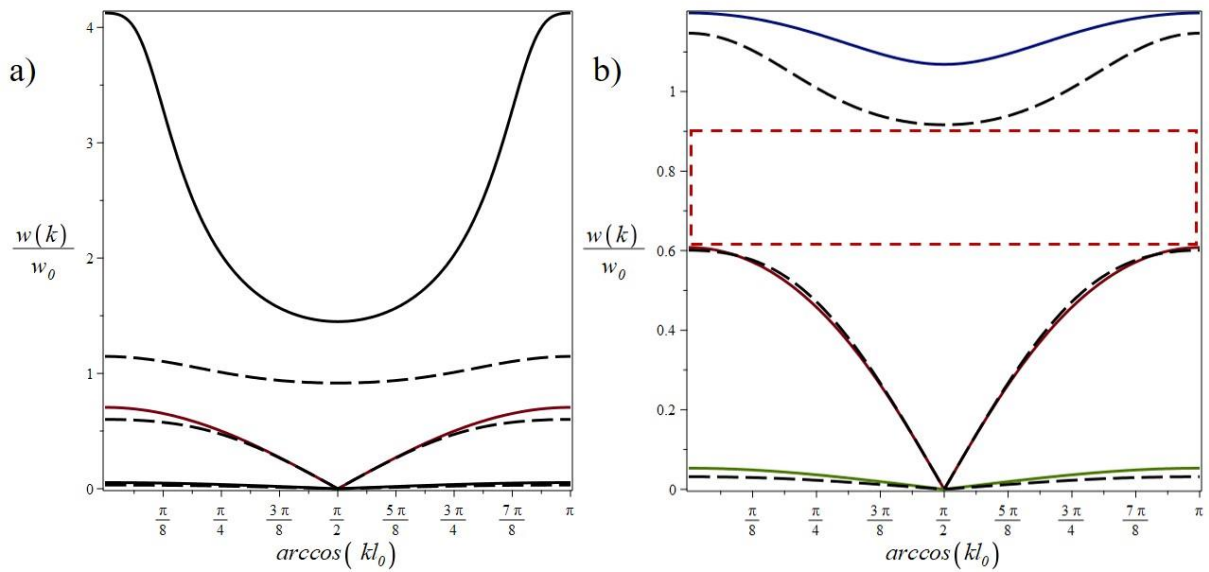


Figure R.2 : Courbes de dispersion pour une structure en treillis carré de la Fig. R1b en utilisant l'expression dynamique des forces et des moments intérieurs jusqu'au quatrième ordre pour le cisaillement et la solution issue du théorème de Bloch (lignes pointillées) (a). Courbes de dispersion du même réseau pour une expansion d'ordre supérieur (8ème ordre) du cisaillement interne et des moments (lignes continues) et solution du théorème de Bloch (lignes pointillées) (b).

Au-delà de la méthode discrète développée, qui permet d'accéder à des propriétés acoustiques dispersives, nous développons dans cette thèse des méthodes d'homogénéisation dynamiques à gradient supérieur avec des effets de micro-inertie qui décrit le comportement au-delà des prédictions du milieu effectif de Cauchy (Ayad et al., 2020b). Dans cette optique, nous calculons les paramètres constitutifs macroscopiques jusqu'au second gradient en utilisant deux formulations, celle de l'énergie interne totale et le principe de Hamilton. Nous analysons ensuite la sensibilité des termes constitutifs du second gradient aux paramètres microstructuraux pour des matériaux composites à microstructure périodique de type laminés (Fig. R3).

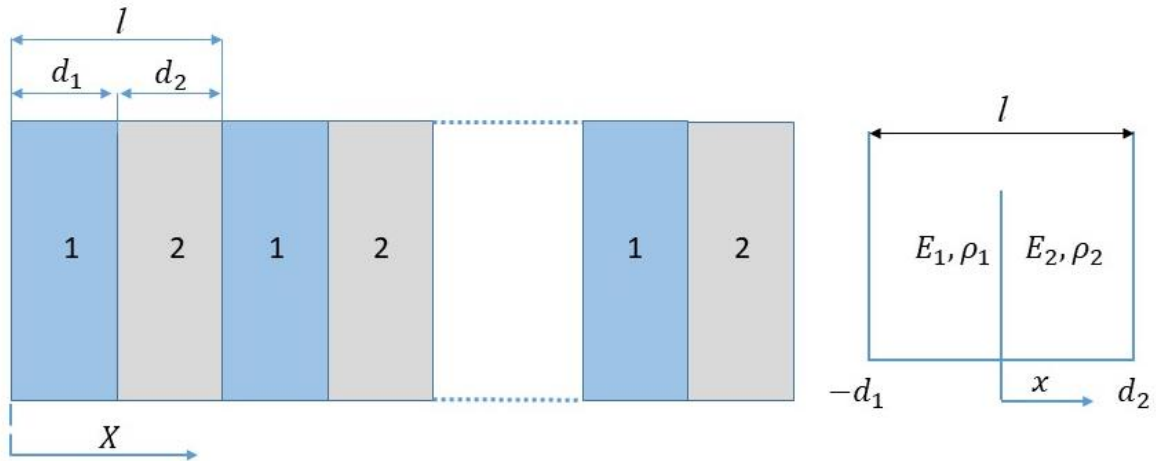


Figure R.3 : Géométrie périodique de matériaux composites stratifiés (à gauche) et les paramètres de la cellule unitaire (à droite).

Les résultats suggèrent que l'importance des termes du second gradient dépend fortement du contraste de propriétés géométriques et mécaniques des constituants, ainsi que du mode de déformation, longitudinal ou transverse. De plus, l'étude de propagation d'ondes indique que les deux formulations utilisées conduisent à des diagrammes de dispersion qui diffèrent selon la plage de variation du nombre d'onde. En particulier, les modèles du second gradient formulés à partir du principe de Hamilton décrivent mal la plage de faibles nombre d'ondes par rapport au premier gradient ou aux solutions analytiques (Fig. R4).

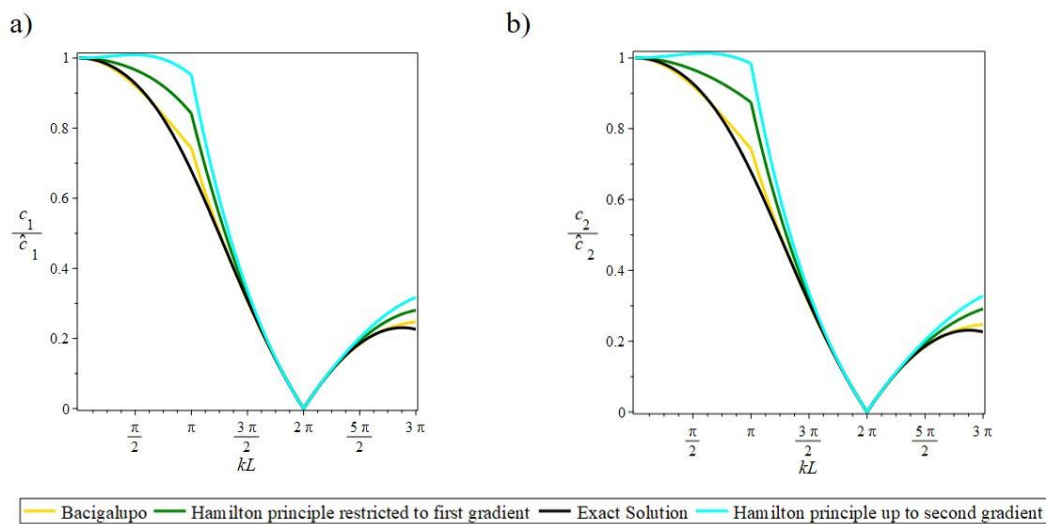


Figure R.4 : Courbes de vitesse de phase obtenues par le principe de Hamilton jusqu'au second ordre (Cyan), pour le premier gradient (vert), premier gradient avec effets de micro-inertie d'ordre supérieur (jaune) dans (Bacigalupo et Gambarotta, 2014b) et la solution exacte (rouge) fournie par (Sun et al., 1968).

Au contraire, les formulations qui s'appuient sur l'énergie interne totale avec prise en compte des termes de gradient d'ordre supérieur et de la micro-inertie donnent une meilleure description des diagrammes de fréquence et des vitesses de phase et de groupe (Fig. R5).

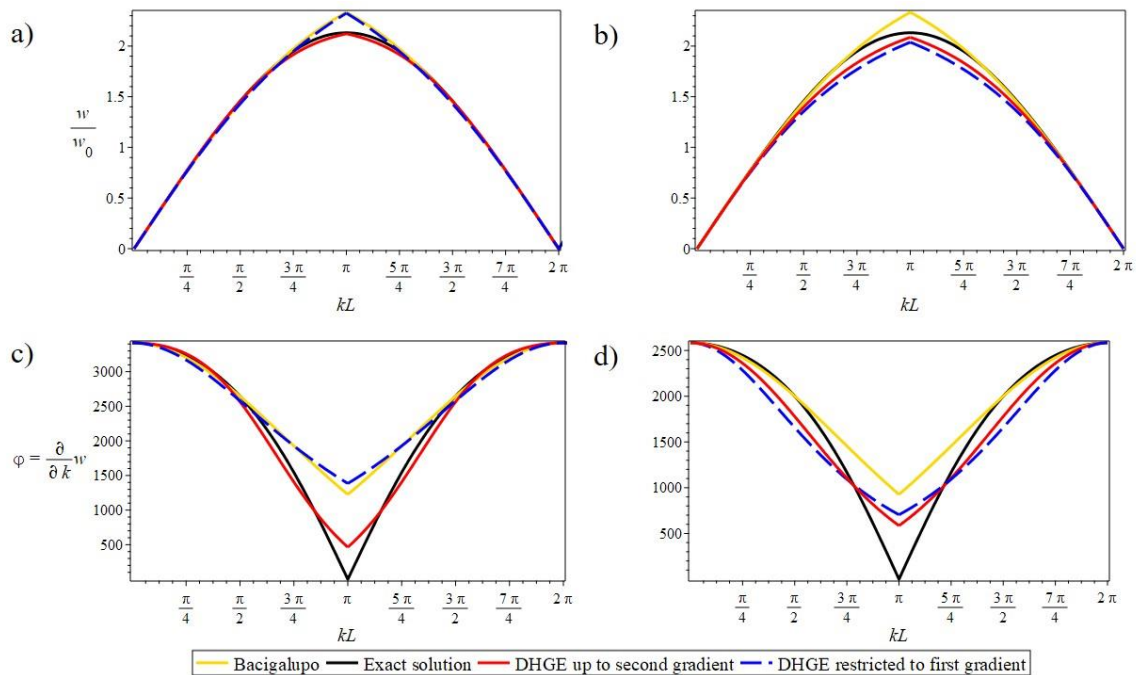


Figure R.5: Fréquence des ondes longitudinales (a) et transversales (b) et vitesse de groupe pour les ondes longitudinales (c) et transverses (d) pour les deux méthodes d'homogénéisation dynamique en fonction de la valeur du nombre d'onde.

Le rôle des contributions d'ordre supérieur et de la micro-inertie sur le comportement mécanique de structures composites est analysé en calculant les propriétés statiques et dynamiques effectives de poutres composites en utilisant une méthode d'homogénéisation dynamique d'ordre supérieur qui intègre les effets de micro-inertie. Nous calculons la réponse effective statique longitudinale à gradient d'ordre supérieur, en quantifiant la différence relative par rapport à la formulation classique de type Cauchy qui repose sur la prise en compte du seul premier gradient du déplacement (Fig. R6).

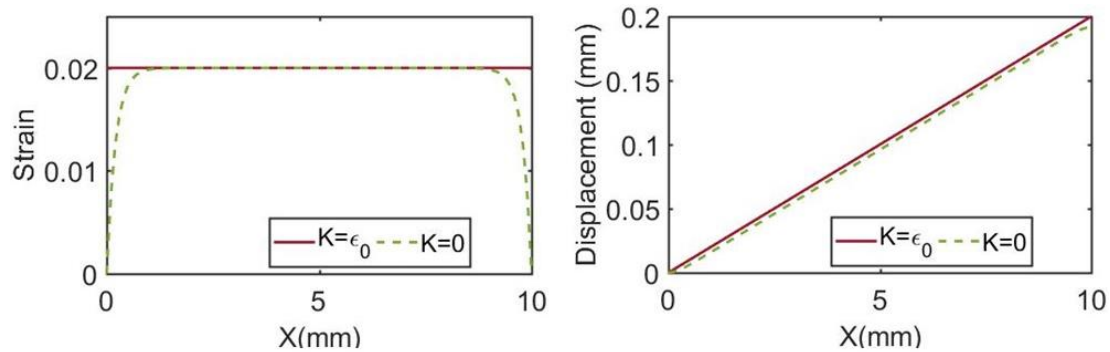


Figure R.6 : Déformation et déplacement le long d'une poutre en utilisant la formulation du second gradient pour une déformation fixée à l'extrémité de la poutre  $\varepsilon_{SG} = 0$  (Vert) et la solution linéaire pour  $\varepsilon_{SG} = \varepsilon_0$  (Rouge) pour un chargement  $P_0 / A = 0.02C_1^1$  à l'extrémité chargée de la poutre.

Nous observons que dans la plage d'analyse statique, les effets d'ordre supérieur nécessitent des valeurs de longueur interne élevées et des distributions de profil de déformation fortement non linéaires pour que des effets d'ordre supérieur non négligeables apparaissent. Nous analysons ensuite les propriétés de propagation d'ondes longitudinales en termes de fréquence propre des structures composites, en tenant compte de la contribution de la micro-inertie. Des expressions analytiques sont obtenues qui relient les paramètres constitutifs effectifs du matériau composite à ses caractéristiques de vibration à l'échelle macroscopique. Un aspect novateur réside dans l'établissement de la preuve que les contributions de micro-inertie peuvent contrebalancer l'effet des termes du second gradient sur les fréquences propres de la structure, leur importance relative dépendant du mode de propagation considéré. La longueur interne joue un rôle crucial dans les contributions de micro-inertie, avec un effet substantiel pour des valeurs de longueur interne faibles, qui seront ainsi observés pour une large gamme de matériaux utilisés en ingénierie des structures (Fig. R7).

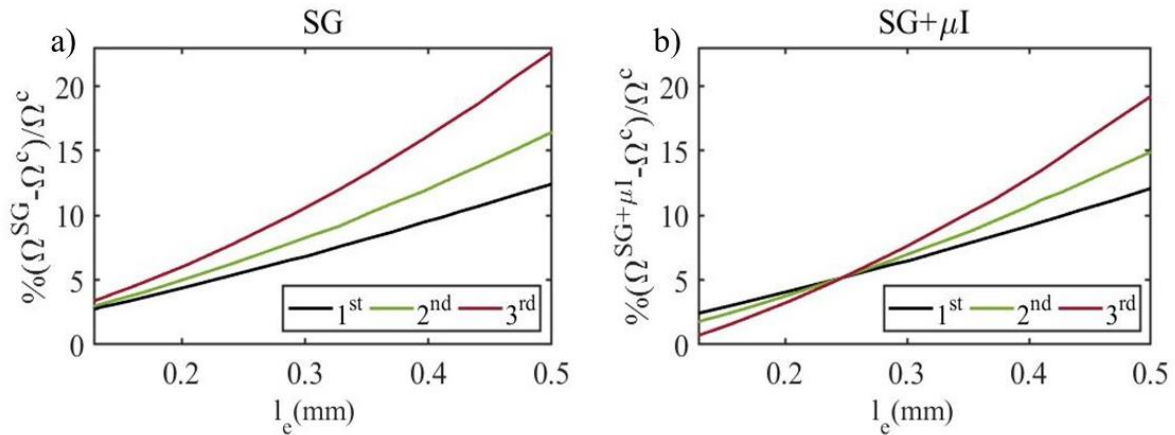


Figure R.7 : Différence relative des valeurs de fréquence propre calculées pour le deuxième gradient (SG) et le deuxième gradient avec micro-inertie (SG +  $\mu I$ ) ((a) et (b) respectivement) pour les trois premiers modes propres pour différentes valeurs de la longueur interne  $l_e$ .

Nous appliquons ensuite la méthodes d'homogénéisation à des composites en 2D en prenant en compte l'effet de taille par le biais des modules mécanique du comportement à gradients supérieurs. Dans cette optique, des termes de correction des modules du second gradient sont intégrés dans la formulation, ces derniers s'annulant pour des structures homogènes et étant indépendant de la taille du volume élémentaire représentatif (Li, 2011), corrigeant ainsi les déficiences des modèles du second gradient de la littérature. On considère une matrice comportant une inclusion circulaire centrale; afin de quantifier l'importance des effets du second gradient, on calcule les longueurs caractéristiques en fonction des contrastes de paramètres géométrique et mécanique de la structure (Fig. R8).

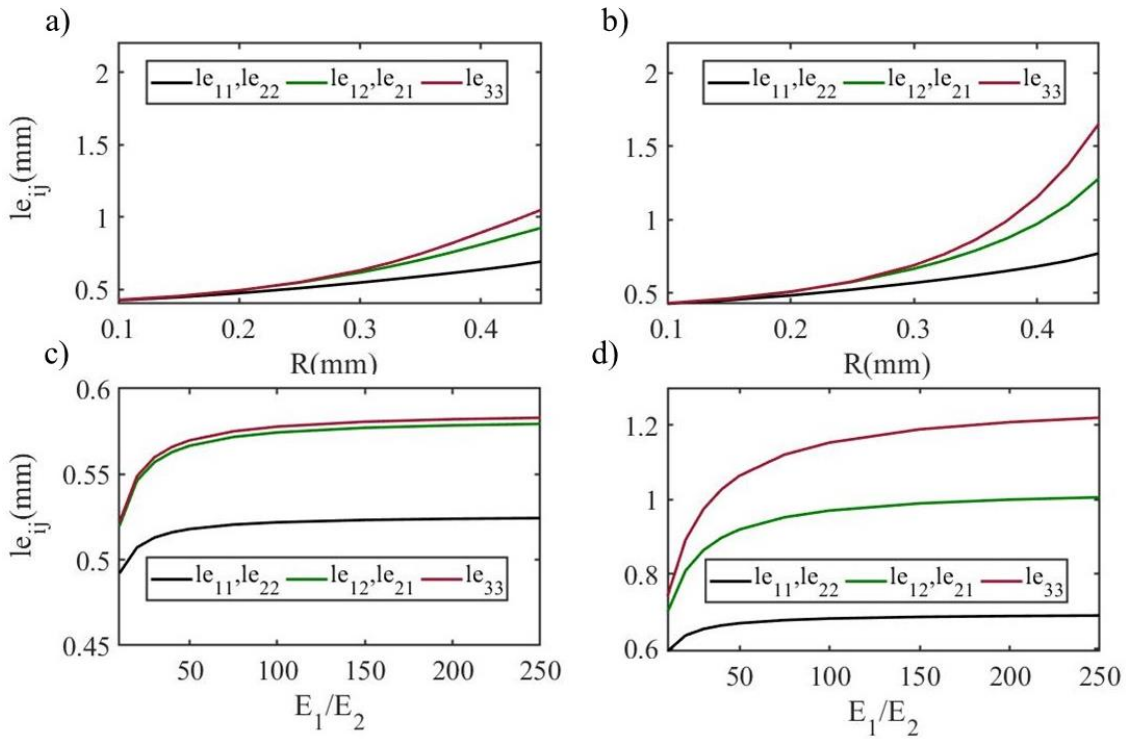


Figure R.8: Variation des longueurs internes  $le_{ij}$  (mm) en fonction du rayon de l'inclusion  $R$  (mm) pour  $(E_1 / E_2) = 20, 100$  en (a) et (b) respectivement, et en fonction du rapport des modules élastiques  $(E_1 / E_2)$  pour  $R = 0.25$  mm, 0.4 mm en (c) et (d) respectivement.

Les paramètres de longueur interne dépendent fortement des caractéristiques géométrique (la fraction volumique d'inclusion), tandis que les propriétés mécaniques de la microstructure (rapport des modules élastiques de la matrice à celui de l'inclusion) ont un impact moindre sur les longueurs internes qui convergent à fort contraste des modules. On note que les termes de correction diminuent les valeurs de longueur internes ainsi que leur intervalle de variation en fonction des propriétés microscopique de la composites mais avec les mêmes profils de variation que ceux obtenus Fig. R8. On étudie ensuite le comportement acoustique de la structure composite en utilisant la formulation du second gradient développée sans et avec les termes de corrections, qui est comparée avec le comportement classique de Cauchy pour des petites valeurs du vecteur d'onde (Fig. R.9).

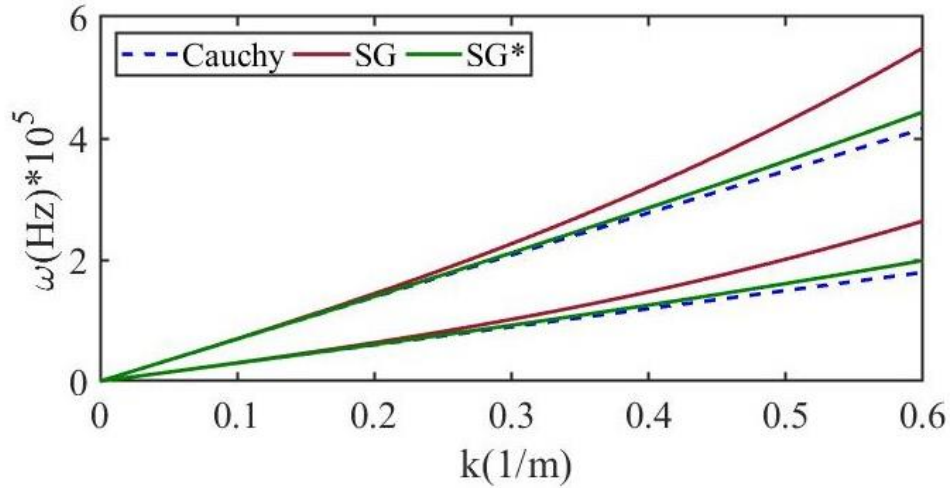


Figure R.9: Courbes de dispersion en utilisant une approximation classique (Bleu), une approximation du second gradient sans termes de correction (Rouge) et avec des termes de correction (Vert) pour le mode de cisaillement (bande inférieure) et le mode longitudinal (bande supérieure) dans la première partie de la zone de Brillouin de la matrice.

On remarque que les gradients supérieurs apportent de la dispersion au comportements acoustique de la structure ; la différence entre les formulations à gradients supérieurs et la théorie classique est analysée pour différentes fractions de l'inclusion et différents rapport d'élasticité entre la matrice et l'inclusion en Fig. R10.

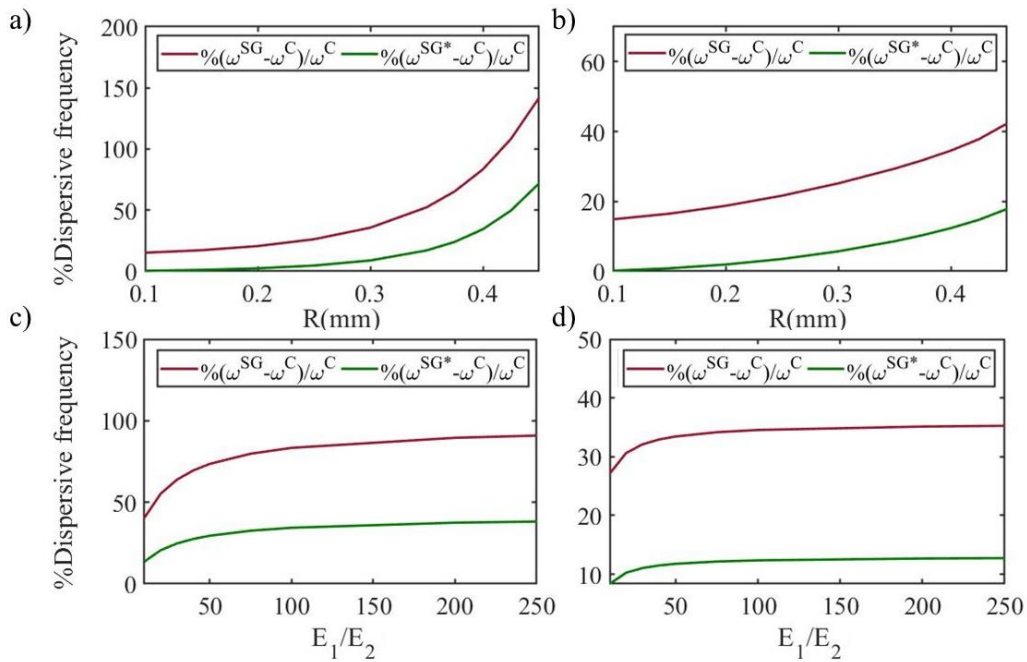


Figure R.10 : Différence relative maximale des courbes de dispersion entre la formulation du second gradient pour  $k = 0.6m^{-1}$  sans termes de correction (SG en rouge) et avec des termes de correction (SG \* en vert) pour différents rayons d'inclusion  $R$  avec un contraste de modules ( $E_1 / E_2 = 100MPa$ ) pour les modes transverses (a) et longitudinal (b), et pour différents rapports d'élasticité ( $E_1 / E_2$ ) avec  $R = 0.4mm$ , pour les modes transverse (c) et longitudinal (d).

La fréquence de dispersion obtenue en utilisant la formulation à gradient supérieur dépend des propriétés de la microstructure; cette dépendance est plus importante pour le mode transversal que pour le mode longitudinal pour les propriétés des composites considérées. Les méthodes développées et les résultats obtenus serviront de référence pour le calcul des propriétés statiques et dynamiques des structures composites et de matériaux architecturés au sens large, fournissant une base théorique et numérique pour la quantification de la sensibilité des propriétés mécaniques effectives enrichies aux paramètres microstructuraux.

## Références

- [1] Ayad, M., Karathanasopoulos, N., Reda, H., Ganghoffer, J.F., Lakiss, H., (2020a). Dispersion characteristics of periodic structural systems using higher order beam element dynamics. *Mathematics and Mechanics of Solids*, 25 (2) 457-474. <https://doi.org/10.1177/1081286519880227>.
- [2] Ayad, M., Karathanasopoulos, N., Reda, H., Ganghoffer, J.F., Lakiss, H., (2020b). On the role of second gradient constitutive parameters in the static and dynamic analysis of heterogeneous media with micro-inertia effects. <https://doi.org/10.1016/j.ijsolstr.2019.10.017>.
- [3] Bacigalupo, A., Gambarotta, L., (2014). Second-gradient homogenized model for wave propagation in heterogeneous periodic media. *International Journal of Solids and Structures*, 51(5) 1052-1065. <https://doi.org/10.1016/j.ijsolstr.2013.12.001>.
- [4] Cosserat E., Cosserat F., 1909. *Théorie des corps déformables*. Herman et Fils, Paris. <https://doi.org/10.1038/081067a0>. A. S. Phani, J. Woodhouse, N. A. Fleck, Wave propagation in two-dimensional periodic lattices, *J. Acoust. Soc. Am.* 119 (2006) 1995-2005. <https://doi.org/10.1121/1.2179748>.
- [5] Eringen, A.C., Suhubi, E.S., (1964). Nonlinear theory of simple micro-elastic solids—I. *International Journal of Engineering Science*, 2 (2) 189–203, 389-40. [https://doi.org/10.1016/0020-7225\(64\)90004-7](https://doi.org/10.1016/0020-7225(64)90004-7).
- [6] Kröner, E., (1968). Elasticity theory of materials with long range cohesive forces *International Journal of Solids and Structures*, 3(5), 731-742. [https://doi.org/10.1016/0020-7683\(67\)90049-2](https://doi.org/10.1016/0020-7683(67)90049-2).
- [7] Li, J. (2011). A micromechanics-based strain gradient damage model for fracture prediction of brittle materials – Part I: Homogenization methodology and constitutive relations. *International Journal of Solids and Structures*, 48 (24) 3336-3345. <https://doi.org/10.1016/j.ijsolstr.2011.08.007>.
- [8] Mindlin, R.D., Eshel, N.N. (1968). On first strain-gradient theories in linear elasticity. *Int J Solids Struct*, 4(1) 109-124. [https://doi.org/10.1016/0020-7683\(68\)90036-X](https://doi.org/10.1016/0020-7683(68)90036-X).
- [9] Sun, C.T., Achenbach, J.D., Herrmann, G., (1968). Time-harmonic waves in a stratified medium propagating in the direction of the layering. *Journal of Applied Mechanics*, 35(2), 408-411. doi:10.1115/1.3601212.
- [10] Trinh, D. K., Janicke, R., Auffray, N., Diebels, S., Forest, S., (2012). Evaluation of generalized continuum substitution models for heterogeneous materials. *International Journal for Multiscale Computational Engineering*, 10 (6), 527-549, DOI: 10.1615/IntJMCompEng.2012003105.

# **Chapter 1**

## **Introduction**

## Chapter 1: General Introduction

### 1.1 Overview

The development of additive manufacturing has allowed the engineering of a new class of materials that obtain their effective mechanical attributes by their inner topological design rather than their chemical composition, and generate exceptional material performances far beyond those of the base material. Artificial materials of this kind deserve the epithet “architected materials or metamaterials” (with a base material being metal, polymer or ceramic), considering their potential to yield effective static and dynamic attributes that can well extend the design space of the base material used (Cui et al., 2010; Vaezi et al., 2013). Architected materials define a new class of artificial materials with exceptional static and dynamic characteristics typically not encountered in natural materials (Reda et al., 2018). The mechanical response of periodic architected materials can be analyzed at the macroscopic level, on the scale of a unit cell that is multiplied to build a regular (periodic) lattice. They are used in a wide range of engineering applications, such as vibration control, energy absorption (Mei et al., 2012; Clayes et al., 2016) and noise reduction (Reda et al., 2017; Bacigalupo, & Gambarotta, 2014). Different strategies can be followed to reach properties beyond those of conventional materials, including adjusting the degree of anisotropy, the average density by tuning the inner microstructural design, or designing microstructures with non-centrosymmetric or chiral features to activate interactions between different deformation modes and thereby access new effective properties. Examples of architected materials designs prone to strong anisotropy or exhibiting chiral effects are given in Fig. 1.1.

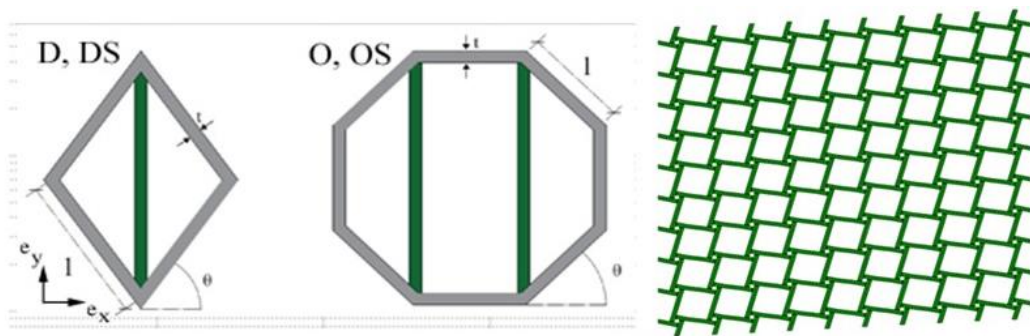


Figure 1.1: Architected materials with anisotropic designs (left), (Karathanasopoulos et al., 2017) and chiral structures (tetrachiral lattice, right), (Karathanasopoulos et al., 2020).

A lot of attention has been given in the last years to the static behavior of architected materials. In particular, an emphasis has been posed on the design of 2D unit cells with tailored stiffness attributes. Designing materials of controlled mechanical properties has opened new possibilities in a series of engineering applications, such as in morphing and mechanical engineering, wave propagation and vibration (Xu et al., 2016, Cheng et al., 2018). Architected materials designed with a quasi-periodic inner topology have witnessed a rapid expansion in the recent period; the complex internal topology of architected materials prohibits the use of direct numerical simulations or full-field computations of macrostructures made of architected materials, which become numerically too expensive. Whereas, the mechanical response of periodic architected materials can be analyzed at the unit cell scale.

For the computation of the effective mechanical properties of architected media, homogenization methods have been commonly employed. The determination of a homogenized material behavior in the static regime constitutes the first step towards the characterization of its wave propagation characteristics (Reda et al., 2017; Bacigalupo and Gambarotta, 2014). The latter can be obtained by computing the material's dynamic attributes at the scale of their representative building blocks (Lachenal et al., 2013).

Artificial materials demonstrate not only uncommon static properties, but also dynamic mechanical attributes. A primal design objective has been to obtain inner material architectures that favor the development of bandgap frequency regions. Different lattice configurations have been shown to provide wave propagation isolation characteristics. More specifically, triangular and hexagonal honeycomb lattices have been identified to exhibit isolation properties (Karathanasopoulos et al., 2017), while tetrachiral honeycombs have been shown to permit a veering of certain modes. The latter have found direct applications in both passive and active vibration control (Bacigalupo and Gambarotta, 2017). Recently, architected materials that make use of inner folding mechanisms have attracted researchers' attention for their ability to control elastic waves (Bacigalupo and Gambarotta, 2017).

The use of resonant elements has been associated to material designs of enhanced dynamic properties. More specifically, resonant internal units have been related to acoustic band gaps (Collet et al., 2011; Pennec et al., 2008; Liu, and Hu, 2010) along with a tuning capability at low frequencies (Bigoni et al., 2013). Their wave propagation characteristics are highly sensitive to their inner material topology, with different inner architectures that exhibit utterly different dynamical properties (Bacigalupo and De Bellis, 2015).

In the realm of composite engineering, the development of predictive micromechanical models is both appealing and necessary in order to bridge the scales and to provide a constitutive law at a continuum scale, whereby the effective continuum properties can be evaluated from the geometrical and microstructural parameters of the individual constituents of the composite. The presence of a strong contrast of properties between the reinforcement and the surrounding matrix entails the development of strong strain gradients within the composite, leading very often to the need of modeling the composite as an enriched continuum in the framework of the mechanics of generalized continua (like a strain gradient or a micromorphic substitution medium). Homogenization theory has become over the last four decades a fundamental tool to analyze the overall behavior of highly heterogeneous media such as composites. It most often relies on the determination of a representative elementary volume (RVE), which implicitly assumes that the structure of the RVE is found almost everywhere in the structure, which amounts in fact to a disguised pseudo-periodicity.

For this reason, periodic homogenization plays a privileged role as a theory to account for the overall homogenized behavior of multiphase materials like composites. Initiated by the works of (Bensoussan et al., 1978; Sanchez-Palencia, 1980), several authors analyzed more recently the influence of higher-order terms in the asymptotic expansions of the fields on the macroscopic behavior of linear elastic composites (Gambin and Kröner, 1989; Boutin, 1996; Triantafyllidis and Bardenhagen, 1996; Smyshlyaev and Cherednichenko, 2000; Tran et al., 2012). Furthermore, designing architected and composite materials in an optimal way requires understanding the relation between the internal architecture and physical properties, and suitable ways to evaluate these properties. In classical continuum mechanics (Truesdell and Noll, 1965), all higher order displacement gradients are neglected and only the first order displacement gradient is involved in measuring the deformations of a body. Such kinematic framework turns out not to be rich enough to describe a variety of important mechanical and physical phenomena (Auffray, 2010). Especially, the classical continuum mechanics proves to be intrinsically size independent, as reported by (Truesdell and Noll, 1992). Particularly, size effects and a non-local behavior may arise due to the discrete nature of matter at a sufficiently small-scale level.

### 1.1.1 Higher order static homogenization

Classical homogenization techniques limits to large wavelength of the loading or deformation field when it is comparable with the typical microstructure size. In situations where strict scale separation assumption fails, the classical Cauchy theory proves unable to predict the overall behavior; particularly, size effects and even non-local behaviors may arise due to the discrete nature of matter at sufficiently small scales level. The lack of a material length scale parameter in the classical continuum elasticity theory leads however to an inaccurate description of the macroscopic structural behaviors (Goda and Ganghoffer, 2015).

Two distinct strategies emerged to remedy the lack of scale separation in the modeling of homogenized media: the first strategy is phenomenological in nature and uses generalized continuum mechanics. The incorporation of the microstructural scale within enhanced continuum formulations involves the relaxation of the local action hypothesis and the introduction of a spatial interaction and typical length scales to account for the influence of neighboring points in the formulation of constitutive equations.

The mechanics of generalized continua can be defined as the mechanics of matter for circumstances in which the conventional continuum mechanics cannot offer a promising approach (Kröner, 1968). In order to keep a continuum description, one has to consider a generalized continuum to model the substitution material resulting from the homogenization process. The objective of homogenization towards generalized continua is to remedy the classical homogenization techniques limitations and to extend the range of validity of the continuum approach beyond the strict assumption of the scale separation (Mindlin, 1964; Eringen and Suhubi, 1964). There are essentially two ways to generalize the classical definition of a continuum, classified into higher-order and higher-gradient continua. Higher-order continua involves additional degrees of freedom like the Cosserat medium promoted by the Cosserat brothers (Cosserat and Cosserat, 1909) and the micromorphic medium (Eringen and Suhubi, 1964; Mindlin, 1964; Germain, 1973). In Cosserat elasticity (Cosserat and Cosserat, 1909), local rotations are added as degrees of freedom. In higher-gradient continua, one keeps the same degrees of freedom but higher gradients of the displacement field are added as arguments of the strain energy density.

Amongst the possible a priori choices of the effective substitution medium mentioned previously (Cosserat, micromorphic, strain-gradient ...), the strain gradient elastic continuum introduced in (Mindlin, 1964) and (Mindlin & Eshel, 1968) offers several advantages as

underlined in (Yvonnet et al., 2020) since it is rich enough to represent emergent properties without having recourse to the micromorphic medium that has many more inherent parameters (Auffray et al., 2015) and such a model can be constructed using asymptotic homogenization (Boutin, 1996; Bacigalupo and Gambarotta, 2010, 2014; Tran et al., 2012).

A large body of works has been devoted to strain gradient homogenization in the literature since more than 40 years (Ben-Amoz, 1976; Forest and Sab, 1998; Forest, 1998; Forest et al., 2001; Trinh et al., 2012; Tran et al., 2012; Rahali et al., 2015; Bacigalupo and Gambarotta, 2010) for composites with periodic or random microstructures (Goda & Ganghoffer, 2016), auxetic architected materials (Bacigalupo & Gambarotta, 2014) and random fibrous media (Berkache et al., 2017). Different approaches have been employed in the literature for the derivation of the effective mechanical properties of strain gradient models of heterogeneous microstructures.

Periodic homogenization methods relying on the asymptotic expansion of the searched solution versus a small parameter representative of the relative scale of the unit cell (with respect to the macroscale of the overall structure) have been developed in (Bensoussan et al., 1978; Sanchez-Palencia, 1980) considering the main proponents. Expansion of the series up to the second order leads to the formulation of an effective strain gradient continuum whereby the local solution depends on the macroscopic strain gradient (Gambin and Kröner, 1989; Boutin, 1996; Triantafyllidis and Bardenhagen, 1996; Smyshlyaev and Cherednichenko, 2000; Tran, 2012). The strain gradient elastic moduli are computed by solving in a sequential manner two unit cell boundary value problems, a classical one leading to the Cauchy moduli and a higher order BVP associated with the macroscopic strain gradient as a kinematic source term.

Pure asymptotic expansion methods (Boutin, 1996; Smyshlyaev and Cherednichenko, 2000) are sometimes combined with a Fast Fourier Transform FFT method to compute the effective properties (Tran et al., 2012; Li and Zhang, 2013). A quite common strategy to compute the strain gradient moduli is to use suitable quadratic boundary conditions over the RVE as the minimum kinematic loading capturing a gradient of the strain at the macroscopic level, an approach followed by many authors (Gologanu et al., 1997; Forest, 1998; Forest et al., 2001; Kanit et al., 2003; Geers et al., 2001; Kouznetsova et al., 2004; Auffray et al., 2010; Barboura and Li, 2018). This method extends the classical kinematic uniform boundary conditions employed in Cauchy type homogenization (Huet, 1990). The method however suffers from two major flaws, since the effective strain gradient moduli remain non-zero for homogeneous materials or under conditions of scale separation (Forest and Trinh, 2011). Corrections to these spurious effects were recently proposed (Yvonnet et al., 2020), where they

added a body force field to the quadratic boundary conditions together with a correction of the localization tensor to get a convergence effective strain gradient modulus for big number of cells. Very recently, (Monchiet et al., 2020) made a correction to the employed quadratic boundary conditions, thereby getting rid of the strain gradient effects (the effective medium remains of Cauchy type). Furthermore, the computed strain gradient effects converge asymptotically with the number of periods. Note that this asymptotic homogenization method avoids the spurious effect since the source term in the second order unit cell problem vanishes for a homogeneous medium. Moreover, another type of correction was provided in (Li, 2011) where second gradient moduli not only vanish for homogenous media but are independent of periods number; the correction terms used the first gradient moduli and the quadratic inertia of the structure. Furthermore, the author provides an analytical solution of the higher gradient constitutive parameters for 1D and 2D composites structures.

### 1.1.2 Impact of higher order homogenization on static and dynamic behavior

The descriptions of microstructural effects analyzed in wave propagation are most of the time phenomenological in nature, following either the line of micromorphic models (Berezovski et al., 2013) or second gradient continuum models (Fafalis et al., 2012). The phenomenological nature of these models entails that the material parameters involved in the wave propagation formulations need to be calibrated to experiments, and consequently such models are not predictive. The large number of intrinsic parameters to be identified requires a somewhat difficult measurement protocol; this issue is addressed especially in (Polyzos et al., 2015; Iliopoulos et al., 2016; Réthoré et al., 2015). In order to circumvent this drawback, multiscale methods have been developed to link the dispersive aspects of wave propagation to the microstructure of the material. Amongst these, homogenization techniques derive the dynamical macroscopic behavior by upscaling the microscopic one, so obtaining a more coarse description of the dispersive wave propagation features, but still reflecting in a predictive manner the impact of the underlying material microstructure.

It is experimentally proven that materials with a heterogeneous microstructure exhibit a dispersive wave propagation behavior, that is, each wavenumber travels with a different phase velocity (Erofeyev, 2003). However, homogenization models based on the classical, Cauchy-type elasticity theory are not able to reproduce different aspects of the physical behavior of heterogeneous media, such as wave dispersion.

The impact of the heterogeneous microstructure on the wave propagation characteristics of materials was first recognized and analyzed by Mindlin (1964), who proposed several non-local continuum models to capture the dispersion of planar waves. Since the early works in the 1960s by Toupin (1962) and Koiter (1969), there have been several literature contributions to the topic, recently summarized in (Askes and Aifantis, 2009). Generalized continuum theories offer an attractive alternative for capturing dynamic behaviors overlooked by classical elasticity, especially dispersion relations (Lombardo and Askes, 2012). In order to study low frequency wave propagation in effective continuum media, enriched second gradient elasticity descriptions have been developed which account for microstructural effects descriptive of the dispersive wave behavior (Aifantis, 1998). Different theories based on an enrichment of the classical elasticity framework by higher order gradients have been proposed in the past to overcome deficiencies of classical elasticity (see Aifantis, 1992,1998; Askes and Aifantis 2009; Reda et al. 2018) and plasticity (see Askes and Metrikine, 2002; Askes et al., 2008; Askes and Aifantis, 2011; Askes et al., 2012). Their formulation has aimed at describing both static and dynamic phenomena (Gourgiotis and Georgiadis, 2009; Gonella and Ruzzene, 2010; Gonella et al., 2011; Ostoja-Starzewki, 2002; Papargyri-Beskou, 2004; Askes and Aifantis, 2011).

Gradient elasticity models are useful to predict the wave dispersion characteristics in heterogeneous materials or discrete systems (see Mindlin, 1964; Muhlhaus and Oka, 1996; Gonella et al., 2011, Gonella and Ruzzene, 2010). A thorough analysis of the effects brought about by gradient elasticity models can be found in (Papargyri-Beskou et al., 2009; Fafalis et al., 2012), especially the impact of the higher-order inertial terms (see Metrikine and Askes, 2002; Askes and Aifantis, 2009; Askes and Metrikine, 2002). A detailed comparison between the dispersive characteristics of various simplified models of gradient elasticity can be found in (Askes et al., 2008). Accordingly, differences between classical elasticity considerations and formulations that account for the role of higher order inner material kinematics or finite strains can be found in (Reda et al. 2018, Karathanasopoulos et al., 2019). These homogenization methods encounters limitations in describing the wave dispersion on all the structure Brillouin zone as shown in the figure below.

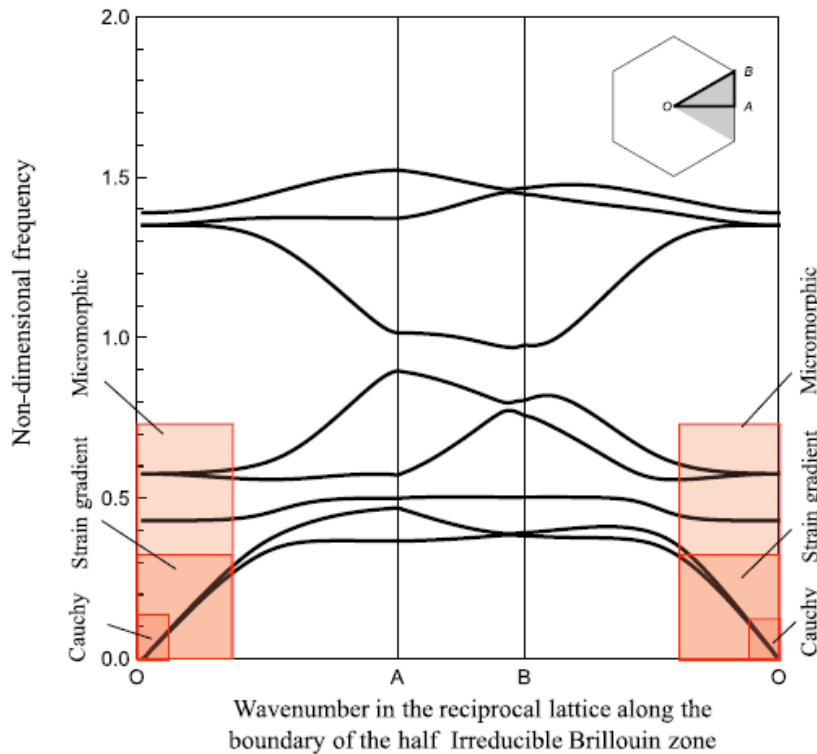


Figure 1.2: Dispersion analysis on a hexachiral material with superposed domains of validity of the continuum models (Rosi & Auffray, 2016).

Amongst the employed micromechanical methods, asymptotic homogenization is quite appealing and has developed importantly in the field of wave propagation over the last decade (Fish and Chen, 2001; Guenneau et al., 2013; Bacigalupo and Gambarotta, 2010, 2014). Boutin and Auriault (1993). Extending the approach developed by Bensoussan et al., 1978; Sanchez-Palencia, 1980, and Bakhvalov and Panasenko, 1984) have proposed the long wave propagation in periodic media based on homogenization. The asymptotic expansion of the displacement field includes terms up to the third order to describe wave scattering. The high frequency behavior of composite structures has been first analyzed in (Boutin et al., 2012, 2014). The authors employ an asymptotic multiscale method to address large scale modulations of high frequency mechanical waves. The developed theoretical formulation allows the identification of the physical behavior of composite structures in frequency ranges that are not accessible by the methods typically used for low frequency analysis.

Homogenization in the time domain has also been proposed by several authors, see e.g. (Chen and Fish, 2000), considering both fast and slow time scales. In many studies, gradient elasticity theories have been derived from the continualization of the response of a discrete lattice consisting of discrete masses and springs, see for example the early work of Mindlin (1972). One important challenge of gradient elasticity theories is a physical interpretation of

the involved length-scale parameters as a function of the given microstructure (Askes and Aifantis, 2011).

Resorting to computational approaches, finite element computations over the unit cell with periodic Bloch type boundary conditions have been performed to model acoustic waves scattering and to evaluate the band structure (Hussein, 2009; Huang, 2011). As an alternative strategy for the solution of the Floquet-Bloch problem, plane wave expansions of the displacement vector, elastic moduli and mass are done in Fourier series with respect to the periodicity vectors (Nemat-Nasser et al., 2011).

Since the aforementioned approaches apply restrictively to the low frequency range, they cannot describe the high frequency features encountered in microstructured periodic materials, like the presence of band gaps or negative refraction. High frequency behaviors were investigated in both discrete materials and composites with a high contrast of their elastic properties using asymptotic expansion methods (Andrianov et al., 2008, 2011; Craster et al., 2010; Zhikov, 2000; Smyshlyaev, 2009; Auriault and Boutin, 2012). First strain gradient formulations such as the ones elaborated in Mindlin (Mindlin 1964) have further interest due to the possibility of associating them to higher order inertia terms, where the kinetic energy depends on the velocity gradient. These effects allow to better describe strain singularities at sharp crack tips and to capture size effects within the dynamic material behavior (dispersion relations) manifested by real materials such as porous materials, polymer foams (see Mindlin, 1964; Askes and Aifantis, 2011). In the same spirit, a continuum model of Cauchy type including micro-inertia terms in the kinetic and potential energy was proposed (Wang and Sun, 2002; Sun and Huang, 2007) with applications to the computation of the dispersion diagram for laminates which is compared with the exact solution for laminated media (Sun et al., 1968) obtained by the elasticity theory. The exact solution has been proven experimentally in (Robinson and al., 1974), where the existence of propagating bands and gaps in layered media was experimentally demonstrated.

Apart from the sufficient description of the wave propagation characteristics of engineering materials, eigenfrequency analysis has been of interest for a lot of research in the last decades especially for lattice structures. Moreover, different studies have been done on the impact of geometrical and mechanical microstructure properties on the macroscopic response. For certain geometries, first mode eigenfrequency will be increased which helps to isolate lower frequencies (Syam et al., 2018; Andresen et al., 2020). Impact of higher gradient formulation has been analyzed on eigenfrequency studies (Altan et al., 1996; Salehian & Inman, 2008;

Bisegna & Caruso, 2011). Higher gradient shows a huge influence on the eigenfrequency values as described in (Altan et al.,1996) with respect to classic continuum.

### **1.2 Motivation of the thesis**

The general objective of the thesis is to develop higher gradient homogenization methods to predict the response of periodic structures and composites covering successively the static, vibratory and acoustic responses at a macroscopic level of description, intermediate between the microscopic and structural scales.

Higher gradient formulation has been applied to different composite structures and different architecture materials. In this thesis, we analyze the impact of higher gradient formulation on the macroscopic response; moreover, we relate this impact to the microstructure properties.

The need to employ such enriched formulations going beyond Cauchy elasticity adopting in a first step discrete models of structural systems is highlighted in the first part of the thesis.

#### **1.2.1 Dispersion characteristics of periodic structural systems using higher order beam dynamics**

Lattice configurations have been shown to provide special wave propagation characteristics. Moreover, wave motion in triangular and hexagonal honeycomb lattices exhibits characteristic pass and stop band as shown in (Karathanasopoulos et al., 2017). Floquet-Bloch principle has been used to explore the dispersion characteristics of periodic structures (Phani et al; 2006) which is based on the mass and stiffness matrix of the structure, by considering the structure as a discrete system.

In this thesis, we derive higher order discrete mechanics methods (DDM) using the internal forces and moments and we show that this method is not limited to Cauchy linear dispersion behavior.

Furthermore, we show the size dependence of this method, where studying two or three unit-cell structure will increase the degree of freedom and obtain the optical dispersion curves.

#### **1.2.2 Strain gradient homogenization based on dynamic higher gradient strain energy and effects on wave propagation**

In this thesis, we develop a higher gradient dynamic homogenization method with micro-inertia effects. To that scope, we compute the macroscopic constitutive parameters up to the second gradient, using two distinct approaches, namely the Hamilton's principle and the total strain energy formulation.

Using the derived formulation, we calculate the dispersion characteristics of the composite materials with a periodic, layered microstructure, where we show that second gradient macroscopic constitutive formulations derived using the dynamic higher gradient strain energy (DHGE) outperform first gradient approaches, better approximating the wave propagation characteristics of the effective medium.

### **1.2.3 Strain gradient homogenization with micro inertia effects for vibration analyses**

We compute the complete set of the effective static and dynamic properties of composite beam structures using a dynamic higher gradient energy homogenization method (DHGE), which incorporates micro-inertia effects.

We observe that within the static analysis case, higher-order effects require high internal length values and highly non-linear strain profile distributions for non-negligible higher-order effects to appear. We subsequently analyze the longitudinal, higher-gradient eigenfrequency properties of composite structural members, accounting for the role of micro-inertia contributions. Thereupon, we derive analytical expressions that relate the composite material's effective constitutive parameters with its macroscale vibration characteristics. We provide for the first time evidence that micro-inertia contributions can counteract the effect of second-gradient properties on the eigenfrequencies of the structure, with their relative significance depending on the mode of interest. Moreover, we show that the internal length plays a crucial role in the significance of micro-inertia contributions, with their effect to be substantial for low, rather than for high internal length values, thus for a wide range of materials used in engineering practice.

### **1.2.4. Wave propagation analysis of composites structures using independent size higher gradient formulation**

We use a higher gradient energy formulation (HGE) to compute the complete set of effective properties, including the correction terms of the higher gradient moduli involving the quadratic inertia tensor, which has the benefit to generate size independent higher gradient constitutive parameters. The static homogenized properties of inclusion-based composites are

computed together with their internal lengths as an application of the proposed homogenization method, highlighting the importance of the correction terms. We subsequently analyze the variation of these parameters for different microstructural mechanical and geometrical parameters, showing that the mechanical effect is limited to low contrast, whereas the volume fraction of reinforcement has a stronger effect on internal lengths. We provide as a novel aspect a study of the influence of correction terms on the wave propagation features of composite structures, showing a decrease of the dispersive frequency due to the correction. In addition, we show that frequencies computed depend on the propagation mode of interest, with the shear frequency mode being more affected than the longitudinal mode irrespective of the formulation employed.

### 1.3 Organization of the thesis

The thesis aims to handle the lack of space and time scale separation within periodic microstructured media (architected materials, composites) by resorting to generalized continua. This motivation serves as a starting point in chapter 2, where we develop a discrete dynamic method (DDM) to evaluate the dispersion diagrams of 1D and 2D architected materials described with beams as structural elements. The performed analyses show the limitations of Cauchy elasticity in describing the dynamics of simple structural systems, calling for the consideration of higher spatial gradients in their modeling.

Chapter 3 advances novel homogenization methods towards effective strain gradient medium for composite materials, based on a higher gradient strain energy formulation. A systematic sensitivity of microstructural parameters is performed to highlight the factors responsible for strain gradient effects at the macroscopic level. We analyze the influence of higher gradient formulation on the dispersion characteristics through a layered microstructure. Apart from the wave propagation, we study the impact of higher gradient and micro-inertia terms calculated using the dynamical higher gradient energy formulation (DHGE) on the resonance response in chapter 4. Moreover, we calculate the correction terms that eliminate the higher gradient terms for homogenous structures and provide independent size moduli in chapter 5. We analyze the impact of these terms on the wave propagation behavior through these composites for different microstructure properties. Each chapter includes a thorough discussion of the employed method and obtained results. Finally, we conclude with an overview of the main thrust of the thesis, a critical analysis of the proposed methods and results, a synthetic overview of ongoing works, and proposals for future developments.

## References

- [1] Aifantis, E., (1992). International Journal of Engineering Science 30(10):1279-1299. [https://doi.org/10.1016/0020-7225\(92\)90141-3](https://doi.org/10.1016/0020-7225(92)90141-3).
- [2] Aifantis, E., (1998). Strain gradient interpretation of size effects. International Journal of Fracture, 95(1), 299-314. <https://doi.org/10.1023/A:1018625006804>.
- [3] Altan, B. S., Evensen, H. A., Aifantis, E.C.(1996). Longitudinal vibrations of a beam: a gradient elasticity approach, Mech. Res. Comm., 23(1), 35-40. [https://doi.org/10.1016/0093-6413\(95\)00074-7](https://doi.org/10.1016/0093-6413(95)00074-7).
- [4] Andresen, S., Bäger, A., Hamm, C. (2020). Eigenfrequency maximisation by using irregular lattice structures, J. Sound Vib., 465 (115027). <https://doi.org/10.1016/j.jsv.2019.115027>.
- [5] Andrianov, I. V., Bolshakov, V. I., Danishevs'kyi, V. V., and Weichert, D. (2008). Higher order asymptotic homogenization and wave propagation in periodic composite materials. Proc. R. Soc. A., 464(2093), 1181–1201. <https://doi.org/10.1098/rspa.2007.0267>.
- [6] Andrianov, I.V., Awrejcewicz, J., Danishevs'kyi, V.V., Weichert, D., (2011). Wave propagation in periodic composites: higher-order asymptotic analysis versus plane-wave expansion method. Journal of Computational and Nonlinear Dynamics 6(1), 011015-1 - 011015-8.DOI: 10.1115/1.4002389.
- [7] Askes, H., Metrikine, A., (2002). One-dimensional dynamically consistent gradient elasticity models derived from a discrete microstructure: Part 2: Static and dynamic response. European Journal of Mechanics - A/Solids, 21(4), 573-588. [https://doi.org/10.1016/S0997-7538\(02\)01217-2](https://doi.org/10.1016/S0997-7538(02)01217-2).
- [8] Askes, H., Metrikine, A., Pichugin, A., Bennett, T., (2008). Four simplified gradient elasticity models for the simulation of dispersive wave propagation. Journal Philosophical Magazine , 88(28-29) 3415-3443. [doi.org/10.1080/14786430802524108](https://doi.org/10.1080/14786430802524108).
- [9] Askes, H., Aifantis, E., (2009). Gradient elasticity and flexural wave dispersion in carbon nanotubes. Phys. Rev. B 80, 195412. <https://doi.org/10.1103/PhysRevB.80.195412>.
- [10] Askes, H., Aifantis, E., (2011). Gradient elasticity in statics and dynamics: An overview of formulations, length scale identification procedures, finite element implementations and new results. International Journal of Solids and Structures, 48(13), 1962-1990. <https://doi.org/10.1016/j.ijsolstr.2011.03.006>.
- [11] Askes, H., Calik-Carakose, U., Susmel, L., (2012). Gradient elasticity length scale validation using static fracture experiments of PMMA and PVC. International Journal of Fracture, 176(2), 223–227. <https://doi.org/10.1007/s10704-012-9735-x>.
- [12] Auffray, N., Bouchet, R., Brechet, Y., (2010). Strain gradient elastic homogenization of bidimensional cellular media. Int. J. Solids Struct. 47 (13), 1698–1710. <https://doi.org/10.1016/j.ijsolstr.2010.03.011>.
- [13] Auffray, N., Dirrenberger, J., Rosi, G., (2015). A complete description of bi-dimensional anisotropic strain-gradient elasticity. Int. J. Solids Struct., 69-70, 195–206 . <https://doi.org/10.1016/j.ijsolstr.2015.04.036>.
- [14] Auriault, J.L., Boutin, C., (2012). Long wavelength inner-resonance cut-off frequencies in elastic composite materials. Int. J. Solid. Struct. 49, 3269-3281. <https://doi.org/10.1016/j.ijsolstr.2012.07.002>.
- [15] Bacigalupo, A., Gambarotta, L., (2010). Second-order computational homogenization of heterogeneous materials with periodic microstructure. ZAMM-J. Appl. Math. Mech., 90 (10–11), 796–811. <https://doi.org/10.1002/zamm.201000031>.

- [16] Bacigalupo, A., Gambarotta, L., (2014). Homogenization of periodic hexa-and tetrachiral cellular solids. *Compos. Struct.* 116, 461–476. <https://doi.org/10.1016/j.compstruct.2014.05.033>.
- [17] Bacigalupo, A., & De Bellis, M.L. (2015). Auxetic anti-tetrachiral materials: Equivalent elastic properties and frequency band-gaps. *Comp. Struct.*, 131, 530-544. <https://doi.org/10.1016/j.compstruct.2015.05.039>.
- [18] Bacigalupo, A., & Gambarotta, L. (2017). Wave propagation in non-centrosymmetric beam-lattices with lumped masses: Discrete and micropolar modeling. *International Journal of Solids and Structures*, 118–119, 128–145. <https://doi.org/10.1016/J.IJSOLSTR.2017.04.010>.
- [19] Bakhvalov, N.S., Panasenko, G.P., (1984). *Homogenization, Averaging process in periodic Media*. Kluwer Academic Publishers. Moscow.
- [20] Barboura, S., Li, J., (2018). Establishment of strain gradient constitutive relations by using asymptotic analysis and the finite element method for complex periodic microstructures. *Int. J. Solids Struct.* 136, 60–76. <https://doi.org/10.1016/j.ijsolstr.2017.12.003>.
- [21] Ben-Amoz, M., (1976). A dynamic theory for composite materials. *Z. Angew. Math. Phys.* 27 (1), 83–99. <https://doi.org/10.1007/BF01595244>.
- [22] Bensoussan, A., Lions, J. L., and Papanicolaou, G., (1978). *Asymptotic Analysis for Periodic Structures*. North Holland. Amsterdam.
- [23] Berezovski, A., Engelbrecht, J., Salupere, A., Tamm, K., Peets, T., and Berezovski, M. (2013). Dispersive waves in microstructured solids. *Int. J. Solids Struct.*, 50(11-12) 1981–1990. <https://doi.org/10.1016/j.ijsolstr.2013.02.018>.
- [24] Berkache, K., Deogekar, S., Goda, I., Picu, R., Ganghoffer, J.-F., (2017). Construction of second gradient continuum models for random fibrous networks and analysis of size effects. *Compos. Struct.* 181, 347–357. <https://doi.org/10.1016/j.compstruct.2017.08.078>.
- [25] Bigoni, D., Guenneau, S., Movchan, A. B., & Brun, M. , (2013). Elastic metamaterials with inertial locally resonant structures: Application to lensing and localization, *Phys. Rev. B* 87, 174303. <https://doi.org/10.1103/PhysRevB.87.174303>.
- [26] Bisegna, P., Caruso, G. (2011). Dynamical behavior of disordered rotationally periodic structures: A homogenization approach, *J. Sound Vib.*, 330 (11), 2608-2627. <https://doi.org/10.1016/j.jsv.2010.12.009>.
- [27] Boutin, C., Auriault, J. L., (1993). Rayleigh scattering in elastic composite materials. *Int. J. Eng. Sci.* 31 (12) 1669–1689. [https://doi.org/10.1016/0020-7225\(93\)90082-6](https://doi.org/10.1016/0020-7225(93)90082-6). [https://doi.org/10.1016/0020-7225\(93\)90082-6](https://doi.org/10.1016/0020-7225(93)90082-6).
- [28] Boutin, C., (1996). Microstructural effects in elastic composites. *International Journal of Solids and Structures*, 33 (7) 1023-105. [https://doi.org/10.1016/0020-7683\(95\)00089-5](https://doi.org/10.1016/0020-7683(95)00089-5).
- [29] Boutin, C., Rallu, A., & Hans, S. (2012). Large scale modulation of high frequency acoustic waves in periodic porous media. *The Journal of the Acoustical Society of America*, 132(6), 3622–3636. <https://doi.org/10.1121/1.4763553>.
- [30] Boutin, C., Rallu, A., Hans, S., (2014). Large scale modulation of high frequency waves in periodic elastic composites. *J. Mech. Phys. Solid*, 70, 362 – 381. <https://doi.org/10.1016/j.jmps.2014.05.015>.
- [31] Chen, W., Fish, J., (2000). A dispersive model for wave propagation in periodic heterogeneous media based on homogenization with multiple spatial and temporal scales. *Journal of Applied Mechanics*, 68(2), 153-161. <https://doi.org/10.1115/1.1357165>.
- [32] Cheng, L., Liang, X., Belski, E., Wang, X., Sietins, J.M., Ludwick, S., To, A. (2018). Natural Frequency Optimization of Variable-Density Additive Manufactured Lattice Structure: Theory and Experimental Validation, *J. Manuf. Sci. Eng.* 140(10): 105002 (16 pages). <https://doi.org/10.1115/1.4040622>.

- [33] Claves, C., Deckers, E., Pluymers, B., & Desmet, W. (2016). A lightweight vibro-acoustic metamaterial demonstrator: Numerical and experimental investigation. *Mech. Syst. and Signal Pr.*, 70-71, 853-880. <https://doi.org/10.1016/j.ymsp.2015.08.029>.
- [34] Collet, M., Ouisse, M., Ruzzene, M., & Ichchou, MN. (2011). Floquet-Bloch decomposition for the computation of dispersion of two-dimensional periodic, damped mechanical systems. *Int. J. Solids Struct.*, 48, 2837-2848. <https://doi.org/10.1016/j.ijsolstr.2011.06.002>.
- [35] Cosserat E., Cosserat F., 1909. *Théorie des corps déformables*. Herman et Fils, Paris. <https://doi.org/10.1038/081067a0>.
- [36] Craster, R.V., Kaplunov, J., Pichugin, A.V., (2010). High-frequency homogenization for periodic media. *Proceedings of the Royal Society A*, 466, 2341–2362. <https://doi.org/10.1098/rspa.2009.0612>.
- [37] Cui, T. J., Smith, D. R. , Liu, R. (2010). *Metamaterials: Theory, Design and Applications*. Springer US.
- [38] Eringen, A.C., Suhubi, E.S., (1964). Nonlinear theory of simple micro-elastic solids—I. *International Journal of Engineering Science*, 2 (2) 189–203, 389-40. [https://doi.org/10.1016/0020-7225\(64\)90004-7](https://doi.org/10.1016/0020-7225(64)90004-7).
- [39] Erofejev, V. I., (2003). *Wave Processes in Solids with Microstructure*. World Scientific. <https://doi.org/10.1142/5157>.
- [40] Fafalis, D.A., Filopoulos, S.P., Tsamasphyros, G.J., (2012). On the capability of generalized continuum theories to capture dispersion characteristics at the atomic scale. *European Journal of Mechanics - A/Solids* 36, 25-37. <https://doi.org/10.1016/j.euromechsol.2012.02.004>.
- [41] Fish, J., Chen, W. (2001). Higher-order homogenization of initial/boundary-value problem, *J. Eng. Mech.* 127, 1223-1230. [https://doi.org/10.1061/\(ASCE\)0733-9399\(2001\)127:12\(1223\)](https://doi.org/10.1061/(ASCE)0733-9399(2001)127:12(1223)).
- [42] Forest, S., Sab, K., (1998). Cosserat overall modelling of heterogeneous materials. *Mech. Res. Commun.* 25(4), 449–454. [https://doi.org/10.1016/S0093-6413\(98\)00059-7](https://doi.org/10.1016/S0093-6413(98)00059-7).
- [43] Forest, S., (1998). Mechanics of generalized continua: construction by homogenization. *Journal de Physique IV* (8), 39–48. <https://doi.org/10.1051/jp4:1998405>.
- [44] Forest, S., Pradel, F., Sab, K., (2001). Asymptotic analysis of heterogeneous Cosserat media. *Int. J. Solids Struct.* 38 (26-27), 4585–4608. [https://doi.org/10.1016/S0020-7683\(00\)00295-X](https://doi.org/10.1016/S0020-7683(00)00295-X).
- [45] Forest, S., Trinh, D., (2011). Generalized continua and non-homogeneous boundary conditions in homogenisation methods. *ZAMM-J. Appl. Math.Mech.* 91 (2), 90–109. <https://doi.org/10.1002/zamm.201000109>.
- [46] Gambin, B., Kroner, E., (1989). High order terms in the homogenized stress-strain relation of periodic elastic media. *Phys. Stat. Sol.(b)* 151, 513–519. <https://doi.org/10.1002/pssb.2221510211>.
- [47] Geers, M., Kouznetsova, V., Brekelmans, W., (2001). Gradient-enhanced computational homogenization for the micro-macro scale transition. *Le J. Phys. IV* 11 (PR5), Pr5–145. <https://doi.org/10.1051/jp4:2001518>.
- [48] Germain, P. (1973). The method of virtual power in continuum mechanics. Part 2 : Microstructure. *SIAM J. Appl. Math.*, 25(3) 556–575, 1973. <https://doi.org/10.1137/0125053>.
- [49] Goda, I., Ganghoffer, J.-F., (2015). Identification of couple-stress moduli of vertebral trabecular bone based on the 3D internal architectures, *Journal of the Mechanical Behavior of Biomedical Materials*, 51, 99-118. <https://doi.org/10.1016/j.jmbbm.2015.06.036>.
- [50] Goda, I., Ganghoffer, J.-F., (2016). Construction of first and second order grade anisotropic continuum media for 3D porous and textile composite structures. *Compos. Struct.* 141, 292–327. <https://doi.org/10.1016/j.compstruct.2016.01.061>.

- [51] Gologanu, M., Leblond, J-B., Perrin, G., Devaux, J. (1997). Recent Extensions of Gurson's Model for Porous Ductile Metals. In: Suquet P. (eds) Continuum Micromechanics. International Centre for Mechanical Sciences, 377. Springer, Vienna.
- [52] Gonella, S., Ruzzene, M., (2010). Multicell homogenization of one-dimensional periodic structures. *Journal of Vibration and Acoustics*, 132(1). <https://doi:10.1115/1.4000439>.
- [53] Gonella, S., Steven Greene, M., & Liu, W. K. (2011). Characterization of heterogeneous solids via wave methods in computational microelasticity. *Journal of the Mechanics and Physics of Solids*, 59(5), 959-974. <https://doi.org/10.1016/j.jmps.2011.03.003>.
- [54] Gourgiotis, P., Georgiadis, H., (2009). Plane-strain crack problems in microstructured solids governed by dipolar gradient elasticity. *Journal of the Mechanics and Physics of Solids* 57(11) 1898-1920. <https://doi.org/10.1016/j.jmps.2009.07.005>.
- [55] Guenneau, S., Craster, R., Antonakakis, T., Cherednichenko, K., Cooper, S., (2013). Homogenization Techniques for Periodic Structures. E. Popov. Gratings: Theory and Numeric Applications, AMU (PUP), pp.11.1-11.31. <https://hal.archives-ouvertes.fr/hal-00785718>.
- [56] Huang, Z.G., 2011. Analysis of Acoustic Wave in Homogeneous and Inhomogeneous Media Using Finite Element Method. *Acoustic Waves - From Microdevices to Helioseismology*, Marco G. Beghi, IntechOpen. [https://DOI: 10.5772/18792](https://DOI:10.5772/18792).
- [57] Huet, C., (1990). Application of variational concepts to size effects in elastic heterogeneous bodies. *J. Mech. Phys. Solids* 38 (6), 813–841. [https://doi.org/10.1016/0022-5096\(90\)90041-2](https://doi.org/10.1016/0022-5096(90)90041-2).
- [58] Hussein, M.I., (2009). Reduced Bloch mode expansion for periodic media band structure calculations. *Proceedings of the Royal Society A*, 465, 2825–2848. <https://doi.org/10.1098/rspa.2008.0471>.
- [59] Iliopoulos, S., Aggelis, D., Polyzos, D., (2016). Wave dispersion in fresh and hardened concrete through the prism of gradient elasticity, *International Journal of Solids and Structures*, 78–79, 149-159. <https://doi.org/10.1016/j.ijsolstr.2015.09.005>.
- [60] Kanit, T., Forest, S., Galliet, I., Mounoury, V., Jeulin, D., (2003). Determination of the size of the representative volume element for random composites: statistical and numerical approach. *Int. J. Solids Struct.* 40 (13-14), 3647–3679. [https://doi.org/10.1016/S0020-7683\(03\)00143-4](https://doi.org/10.1016/S0020-7683(03)00143-4).
- [61] Karathanasopoulos, N., Reda, H., Ganghoffer, J.-F., (2017). Designing two-dimensional metamaterials of controlled static and dynamic properties, *Comput. Materials Sci.* 138, 323-332. <https://doi.org/10.1016/j.commatsci.2017.06.035>.
- [62] Karathanasopoulos, N., Reda, H., & Ganghoffer, J. F. (2019). The role of non-slender inner structural designs on the linear and non-linear wave propagation attributes of periodic, two-dimensional architected materials. *Journal of Sound and Vibration*, 455, 312–323. <https://doi.org/10.1016/J.JSV.2019.05.011>
- [63] Karathanasopoulos, N., Dos Reis, F., Diamantopoulou, M., Ganghoffer, J.-F. (2020). Mechanics of beams made from chiral metamaterials: Tuning deflections through normal-shear strain couplings. *Materials & Design*, 189, 108520. <https://doi.org/10.1016/j.matdes.2020.108520>.
- [64] Koiter, W.T., (1969). Couple-stresses in the theory of elasticity: I and II. *Philosophical transactions of the royal society of London OF LONDON B*, 67, 17-44.
- [65] Kouznetsova, V., Geers, M., Brekelmans, W., (2004). Multi-scale second order computational homogenization of multi-phase materials: a nested finite element solution strategy. *Comput. Methods Appl. Mech. Eng.* 193 (48-51), 5525–5550. <https://doi.org/10.1016/j.cma.2003.12.073>.
- [66] Kröner, E., (1968). Elasticity theory of materials with long range cohesive forces *International Journal of Solids and Structures*, 3(5), 731-742. [https://doi.org/10.1016/0020-7683\(67\)90049-2](https://doi.org/10.1016/0020-7683(67)90049-2).

- [67] Lachenal, X., & Daynes, S., Weaver, P.M. (2013). Review of morphing concepts and materials for wind turbine blade applications. *Wind Energy*, 16, 283-307. <https://doi.org/10.1002/we.531>.
- [68] Li, J. (2011). A micromechanics-based strain gradient damage model for fracture prediction of brittle materials – Part I: Homogenization methodology and constitutive relations. *International Journal of Solids and Structure*, 48 (24) 3336-3345. <https://doi.org/10.1016/j.ijsolstr.2011.08.007>.
- [69] Li, J., Zhang, X.-B., (2013). A numerical approach for the establishment of strain gradient constitutive relations in periodic heterogeneous materials. *Eur. J. Mech.-A/Solids* 41, 70–85. <https://doi.org/10.1016/j.euromechsol.2013.03.001>.
- [70] Liu, Y., & Hu, H. (2010). A review on auxetic structures and polymeric materials. *Scientific Research and essays*, 5, 1052-1063.
- [71] Lombardo, M., Askes, H., (2012). Higher-order gradient continuum modelling of periodic lattice materials. *Computational Materials Science*, 52(1), 204-208. <https://doi.org/10.1016/j.commatsci.2011.05.025>.
- [72] Mei, J., Ma, G., Yang, M., Yang, Z., Wen, W., & Sheng, P. (2012). Dark acoustic metamaterials as super absorbers for low-frequency sound. *Nat. Communication*, 3, 756. <https://doi.org/10.1038/ncomms1758>.
- [73] Metrikine, A. V. and Askes, H. (2002). One-dimensional dynamically consistent gradient elasticity models derived from a discrete microstructure: Part 1: Generic formulation. *European Journal of Mechanics - A/Solids*, 21(4), 555-572. [https://doi.org/10.1016/S0997-7538\(02\)01218-4](https://doi.org/10.1016/S0997-7538(02)01218-4).
- [74] Mindlin, R., (1964). Microstructure in linear elasticity. *Arch. Ration. Mech. Anal.* 16 (1), 51–78. <https://doi.org/10.1007/BF00248490>.
- [75] Mindlin, R. Eshel, N., (1968). On first strain-gradient theories in linear elasticity. *Int. J. Solids Struct.* 4 (1), 109–124. [https://doi.org/10.1016/0020-7683\(68\)90036-X](https://doi.org/10.1016/0020-7683(68)90036-X).
- [76] Mindlin, R.D., (1972). Elasticity, piezoelectricity and crystal lattice dynamics. *Journal of Elasticity*, 2(4), 217–282. <https://doi.org/10.1007/BF00045712>.
- [77] Monchiet, V., Auffray, N., Yvonnet, J., (2020). Strain-gradient homogenization: a bridge between asymptotic expansion and quadratic boundary condition methods. *Mech. Mat.*, 143. <https://doi.org/10.1016/j.mechmat.2019.103309>.
- [78] Mühlhaus, H., Oka, F., (1996). Dispersion and wave propagation in discrete and continuous models for granular materials. *International Journal of Solids and Structures*, 33(19), 2841-2858. [https://doi.org/10.1016/0020-7683\(95\)00178-6](https://doi.org/10.1016/0020-7683(95)00178-6).
- [79] Nemat-Nasser, S., Willis, J.R., Srivastava, A., Amirkhizi, A.V., (2011). Homogenization of periodic elastic composites and locally resonant sonic materials. *Physical Review B* 83, 104103. <https://doi.org/10.1103/PhysRevB.83.104103>.
- [80] Ostoja-Starzewski, M., (2002). Lattice models in micromechanics. *Applied Mechanics Reviews*, 55(1), 35-60. <https://doi.org/10.1115/1.1432990>.
- [81] Papargyri-Beskou, S., Beskos, D.E., (2004). Response of gradient-viscoelastic bar to static and dynamic axial load. *Acta Mechanica*, 170(3–4), 199–212. <https://doi.org/10.1007/s00707-004-0106-1>.
- [82] Papargyri-Beskou, S., Polyzos, D., Beskos, D.E., (2009). Wave dispersion in gradient elastic solids and structures: A unified treatment. *International Journal of Solids and Structures*, 46 (21) 3751-3759. <https://doi.org/10.1016/j.ijsolstr.2009.05.002>.
- [83] Pennec, Y., Djafari-Rouhani, B., Larabi, H., Vasseur, J.O., & Hladky-Hennion, A.C. (2008). Low-frequency gaps in a phononic crystal constituted of cylindrical dots deposited on a thin homogeneous plate. *Phys. Rev. B*, 78, 104105-1-8. <https://doi.org/10.1103/PhysRevB.78.104105>.

- [84] Phani, S.A., Woodhouse, J., Fleck, N.A. (2006). Wave propagation in two-dimensional periodic lattices, *J. Acoust. Soc. Am.* 119, 1995-2005. <https://doi.org/10.1121/1.2179748>.
- [85] Polyzos, D., Huber, G., Mylonakis, G., Triantafyllidis, T., Papargyri-Beskou, S., Beskos, D.E., (2015). Torsional vibrations of a column of fine-grained material: A gradient elastic approach. *Journal of the Mechanics and Physics of Solids*, 76, 338-358. <https://doi.org/10.1016/j.jmps.2014.11.012>.
- [86] Rahali, Y., Giorgio, I., Ganghoffer, J.-F., dell'Isola, F., (2015). Homogenization à la Piola produces second gradient continuum models for linear pantographic lattices. *Int. J. Eng. Sci.* 97, 148–172. <https://doi.org/10.1016/j.ijengsci.2015.10.003>.
- [87] Reda, H., Karathanasopoulos, N., Rahali, Y., Ganghoffer, J. F., & Lakiss, H. (2018). Influence of first to second gradient coupling energy terms on the wave propagation of three-dimensional noncentrosymmetric architected materials. *Int. J. Engng Sci.*, 128, 151– 164. <https://doi.org/10.1016/J.IJENGSCI.2018.03.014>.
- [88] Reda, H., Ganghoffer, J.-F., & Lakiss, H. (2017). Micropolar dissipative models for the analysis of 2D dispersive waves in periodic lattices. *J Sound. Vib.*, 392, 325–345. <https://doi.org/10.1016/j.jsv.2016.12.007>.
- [89] Réthoré, J., Kaltenbrunner, C., Dang, T., Chaudet, P., Kuhn, M., (2015). Gradient-elasticity for honeycomb materials: Validation and identification from full-field measurements. *International Journal of Solids and Structures*, 72, 108-117. <https://doi.org/10.1016/j.ijsolstr.2015.07.015>.
- [90] Robinson, C. W., Leppelmeier, G. W., (1974). Experimental Verification of Dispersion Relations for Layered Composites. *Journal of Applied Mechanics*, 41(1). <https://doi.org/10.1115/1.3423280>.
- [91] Rosi, G., Auffray, N., (2016). Anisotropic and dispersive wave propagation within strain-gradient framework. *Wave Motion*, 63, 120-134. <https://doi.org/10.1016/j.wavemoti.2016.01.009>.
- [92] Salehian, A., Inman, D.J. (2008). Dynamic analysis of a lattice structure by homogenization: Experimental validation, *Journal of Sound and Vibration*, 316 (1–5) 180-197. <https://doi.org/10.1016/j.jsv.2008.02.031>.
- [93] Sanchez-Palencia, E. (1980). *Nonhomogeneous media and Vibration Theory*, Lecture Notes in Physics 127 Springer, Berlin. <https://doi.org/10.1007/3-540-10000-8>.
- [94] Smyshlyaev, V.P., Cherednichenko, K.D. (2000). On rigorous derivation of strain gradient effects in the overall behaviour of periodic heterogeneous media. *J. Mech. Phys. Solids* 48(6-7) 1325–1357. [https://doi.org/10.1016/S0022-5096\(99\)00090-3](https://doi.org/10.1016/S0022-5096(99)00090-3).
- [95] Smyshlyaev, V.P., (2009). Propagation and localization of elastic waves in highly anisotropic periodic composites via two-scale homogenization. *Mechanics of Materials*, 41(4), 434-447. <https://doi.org/10.1016/j.mechmat.2009.01.009>.
- [96] Sun, C.T., Achenbach, J.D., Herrmann, G., (1968). Time-harmonic waves in a stratified medium propagating in the direction of the layering. *Journal of Applied Mechanics*, 35(2), 408-411. <https://doi.org/10.1115/1.3601212>.
- [97] Sun, C.T., Huang, G.L., (2007). Modeling Heterogeneous Media with Microstructures of Different Scales. *Journal of Applied Mechanics*, 74(2), 203–209. <https://doi.org/10.1115/1.2188536>.
- [98] Syam, P.W., Jianwei, W., Zhao, B., Maskery, I., Elmadih, W., Leach, R. (2018). Design and analysis of strut-based lattice structures for vibration isolation, *Precision Engineering*, 52, 494-506. <https://doi.org/10.1016/j.precisioneng.2017.09.010>.
- [99] Tran, T.-H., Monchiet, V., Bonnet, G. (2012). A micromechanics-based approach for the derivation of constitutive elastic coefficients of strain-gradient media. *Int. J. Solids Struct.* 49(5) 783–792. <https://doi.org/10.1016/j.ijsolstr.2011.11.017>.

- [100] Triantafyllidis, N, Bardenhagen, S. (1996). The influence of scale size on the stability of periodic solids and the role of associated higher order gradient continuum models. *J. Mech. Phys. Solids* 44(11) 1891–1928. [https://doi.org/10.1016/0022-5096\(96\)00047-6](https://doi.org/10.1016/0022-5096(96)00047-6).
- [101] Trinh, D. K., Janicke, R., Auffray, N., Diebels, S., Forest, S., (2012). EVALUATION OF GENERALIZED CONTINUUM SUBSTITUTION MODELS FOR HETEROGENEOUS MATERIALS, *International Journal for Multiscale Computational Engineering*, 10 (6), 527-549, DOI: 10.1615/IntJMCompEng.2012003105.
- [102] Toupin, R.A., (1962). Elastic materials with couple-stresses. *Archive for Rational Mechanics and Analysis*, 11(1), 385–414. <https://doi.org/10.1007/BF00253945>.
- [103] Truesdell, C. and Noll, W. (1965) *The Non-Linear Field Theories of Mechanics*. In: Flügge, S., Ed., *Encyclopedia of Physics*, Vol. 3, Springer-Verlag, Berlin. [http://dx.doi.org/10.1007/978-3-642-46015-9\\_1](http://dx.doi.org/10.1007/978-3-642-46015-9_1).
- [104] Truesdell, C. and Noll, W. (1992). *The Non-Linear Field Theories of Mechanics*, Springer-Verlag Berlin. <https://doi.org/10.1007/978-3-662-13183-1>.
- [105] Vaezi, M., Seitz, H., Yang, S., (2013). A review on 3D micro-additive manufacturing technologies. *Int. J. Adv. Manuf. Technol.* 67 (5–8), 1721–1754. <http://dx.doi.org/10.1007/s00170-013-4962-5>.
- [106] Wang, Z.-P., Sun, C.T., (2002). Modelling micro-inertia in heterogeneous materials under dynamic loading. *Wave Motion*, 36(4), 473–485. [https://doi.org/10.1016/S0165-2125\(02\)00037-9](https://doi.org/10.1016/S0165-2125(02)00037-9).
- [107] Xu, S., Shen, J., Zhou, S., Huang, X., & Xie, YM. (2016). Design of lattice structures with controlled anisotropy. *Materials and Design*, 93, 443-447. <https://doi.org/10.1016/j.matdes.2016.01.007>.
- [108] Yvonnet, J., Auffray, N., Monchiet, V., (2020). Computational second-order homogenization of materials with effective anisotropic strain-gradient behavior. *International Journal of Solids and Structures*, 191–192 (15) 434-448. <https://doi.org/10.1016/j.ijsolstr.2020.01.006>.
- [109] Zhikov, V.V., (2000). On an extension of the method of two-scale convergence and its applications. *Sbornik: Mathematics*, 191(7), 973-1014. <https://doi.org/10.1070/SM2000v191n07ABEH000491>.

# **Chapter 2**

## Dispersion characteristics of periodic structural systems using higher order beam element dynamics

## **Chapter 2: Dispersion characteristics of periodic structural systems using higher order beam element dynamics**

### **Summary**

In the current chapter, we elaborate a beam mechanics based, discrete dynamics approach for the computation of the dispersion characteristics of periodic structures. To that scope, we compute the higher order, asymptotic expansion of the forces and moments developed within beam structural elements upon dynamic loads. Thereafter, we employ the obtained results to compute the dispersion characteristics of one and two-dimensional periodic media. In the one-dimensional space, we demonstrate that single unit-cell equilibrium can provide the fundamental, low frequency band diagram structure, which can be approximated by non-dispersive Cauchy media formulations. However, we show that the discrete dynamics method can access the higher frequency modes by considering multiple unit-cell systems for the dynamic equilibrium, frequency ranges that cannot be accessed by simplified formulations. We extend the analysis in the two-dimensional space computing, the dispersion attributes of square lattice structures. Thereupon, we demonstrate that the discrete dynamics dispersion results well compare to the once obtained using Bloch theorem computations. We show that a high order expansion of the structures' inner element forces and moments is required for the higher wave propagation modes to be accurately represented, contrary to the shear and the longitudinal mode which can be captured using a lower, fourth-order expansion of its inner dynamic forces and moments. The provided results can serve as a reference analysis for the computation of the dispersion characteristics of periodic structural systems with the use of discrete element dynamics.

## 2.1 Introduction

In order to compute the effective static and dynamic response of a microstructured medium, a homogenization process, relating microscale attributes with macroscale mechanical behaviors needs to be established, as introduced in different works (Sanchez-Palencia, 1980; Bensoussan et al., 1987; Auriault & Bonnet, 1985; Auriault & Boutin, 2012 ; Boutin & Auriault,1993; Craster et al., 2010). In the formulation of the different theories a common assumption has been made, that the wavelengths propagating within the medium (Fig. 2.1) are much longer than the underlying distributed microstructure (Bakhvalov & Panasenko, 1989; Panasenko, 2005).

Elastodynamic homogenization approaches have been developed for both periodic and random heterogeneous media (Willis, 1983, 1984 & 1997; Nassar et al., 2016). In contrast to asymptotic approaches, the elastodynamic homogenization formulation is exact and does not make any scale separation hypothesis. As such, the resulting effective continuum is nonlocal in space and time. However, its formulation is rather unfavorable for numerical implementation. Asymptotic elastodynamic homogenization strategies are in general non-exact, with their accuracy to depend on the order of expansion of the local fields versus the underlying small scale mechanical parameters. The macroscopic fields together with the effective homogenized continuum behavior are obtained as a volume averaging process over a representative unit cell. A key assumption typically made is the one of scale separation that is considering long wavelengths and low frequencies for the propagating waves within the effective dynamic continuum (Parnell & Abrahams, 2008).

However, it has been shown that frequency has an impact on wave propagation through photonic crystals and metamaterials. Furthermore, the homogenized model of the periodic structure is not unique. Contrariwise, it depends on both the microstructural behavior it aims to describe and on the frequency of the incident waves. This interdependence is expressed in the dispersion diagram, which relates the frequency of propagating waves to the wave number. The dispersion diagram provides information on the phase and group velocity magnitudes and on the possible existence of bandgaps for a particular microstructural design (Guenneau et al., 2012).

Wave propagation has been extensively analyzed within the context of artificial materials, as of their potential to create amongst others wave tuning and isolating properties, which are typically not encountered for conventional materials (Deymier, 2013; Hussein et al.,

2014; Ma & Sheng, 2016; Karathanasopoulos et al., 2017; Sridhar et al., 2018). The extraordinary mechanical attributes of artificial materials have been the primal motivation for their development and use in different engineering fields, such as in acoustic cloaking, seismic wave isolation and super-resolution imaging (Hu et al., 2011; Kaina et al., 2015; Mitchell et al.; 2014; Wen et al., 2011).

A need to accurately characterize the wave propagation characteristics of the effective continuum arose, which fostered the development of different analytical and numerical modeling techniques (Mace et al., 2005; Reda et al., 2018; Mencik & Ichchou, 2008; Mencik & Duhamel, 2015; Silva et al., 2015). The two phenomena that are primarily responsible for the effective material behavior are the so-called Bragg scattering and local resonance. While the appearance of resonance does not require a periodic microstructure and can be observed for both long and short wavelengths, Bragg scattering appears only in the short-wavelength regime, thus for high frequencies (Pasternak & Mühlhaus, 2005 & 2006).

Classical homogenization analysis methods however typically restrain to low frequencies, so that they typically prove insufficient for use in applications where high frequencies appear. As a result, high frequency techniques have been developed for the case where the propagating wavelengths and the characteristic microstructural length scales are of the same order of magnitude (Chesnais et al., 2015). In such cases, multiple scattering effects become important (Craster et al., 2010; Colquitt, 2018). In particular, amongst others, negative refraction phenomena may appear, created by appropriate modulation of the materials inner structural parameters, which can substantially modify the locality of the propagating wave fields, as showcased for two-dimensional mass-spring systems (Wang & Chen, 2019).

Considering multiple scales has led to the formulation of effective continua for artificial medium which are applicable to different frequency ranges. Thereupon, continualization approaches have been proposed based on asymptotic expansion schemes of the structures' inner elements (Suiker et al, 2001; Gonella & Ruzzene, 2008; Lombardo & Askes, 2012). What is more, a micropolar homogenization approach has been elaborated (Bacigalupo & Gambarotta, 2017), which can well capture the acoustic behavior of the effective medium. The development of such enhanced continualization techniques has been based on the higher order expansion of the underlying constitutive and micro-inertial parameters (Bacigalupo & Gambarotta, 2019). Methods of the kind have been as well used in the study of the wave propagation characteristics of both discrete lattices and plates (Antonakakis & Craster, 2012).

The dynamics of periodic discrete structures have been modeled in the literature using beam mechanics in the low frequency regime for which a homogenized continuous equivalent description can be obtained under the condition of scale separation (Caillerie et al., 1989; Hans & Boutin, 2008; Rallu et al., 2017). The validity of the method is accordingly limited below the diffraction frequency limit. However, when moving to the high frequency regime for which the wavelength becomes comparable to the unit cell size as shown in Fig. 2.1, a different formulation is required which goes beyond the assumption of scale separation, which is no more applicable. In higher frequencies the periodicity of the system needs to be satisfied for the scale separation to be also valid. The high frequency behavior of composite structures has been first analyzed in (Boutin et al., 2012 & 2014). The authors employ an asymptotic multiscale method to address the modeling of large scale modulations of high frequency mechanical waves. The developed theoretical formulation has allowed for the identification of the physical behavior of the composite structure in frequency ranges that are not accessible by the methods typically used for low frequency analysis.

However, up to now, no higher order discrete mechanics methods have been presented, which can inherently account for the effect of the propagating frequency on the considered media. What is more, the potential of dynamic discrete beam mechanics formulations to capture higher frequency ranges, which are not accessible for low frequency approaches has not been studied.

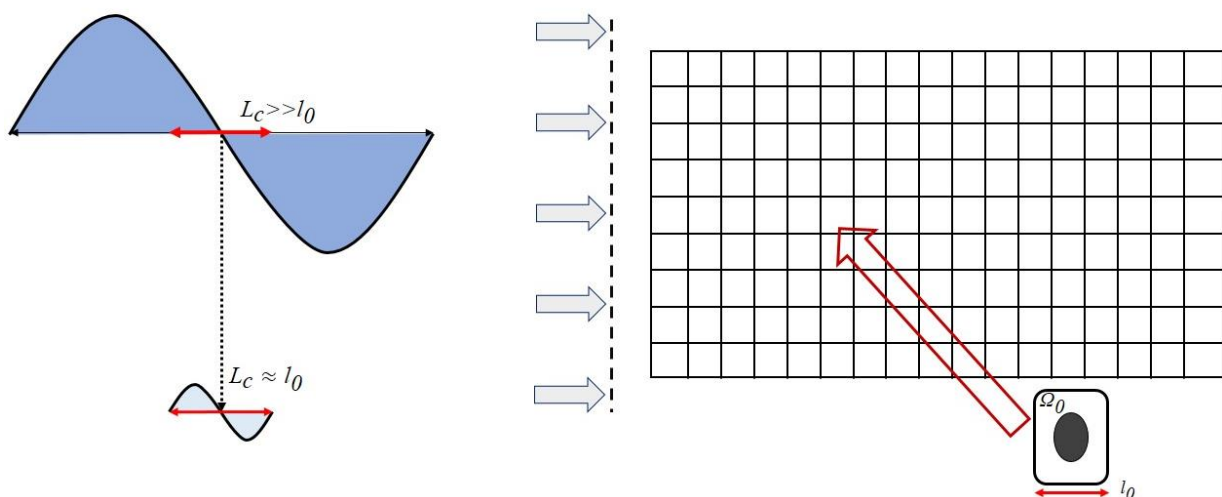


Figure 2.1 : Propagating wave lengths  $L_c$  within repetitive network materials with repetitive unit cells of size  $l_0$ . Scale separation applies when  $L_c \gg l_0$ .

In this chapter, we elaborate the higher order asymptotic expansion of the inner forces and moments developed within beam elements upon dynamic loads, which we employ to compute the dispersion characteristics of one and two-dimensional architected materials. The

elaborated discrete dynamics methods (DDM) incorporates the higher order frequency of the propagating waves for the first time, thus information on the wave characteristics of the media, in its very formulation. As such it can be used to characterize both low and high frequency propagation phenomena. In Section 2.2, we compute and provide the higher order, frequency-dependent asymptotic expansion forms for the normal, transverse forces and bending moments, making use of the dynamic equilibrium equations and of the beam constitutive law. We subsequently calculate the dispersion characteristics of one-dimensional periodic structures, providing insights into the frequency scale-separation domains and in the effects of the frequency magnitude on the dispersion diagram characteristics (Section 2.3). We extend the analysis to two-dimensional architected materials space, computing the band diagram structure of a square lattice, which we compare with the ones obtained by the Floquet-Bloch theorem predictions (Section 2.4). We comment on the main findings of the current work in Section 2.5 and conclude in Section 2.6.

## 2.2 Structural dynamics of discrete and continuous systems

### 2.2.1 Dispersion characteristics of discrete systems based on the asymptotic description of their inner forces and moments

In the current section, we express the forces and moments acting on beam element structure under dynamic loads. Each element is considered to consist of two mass-less end nodes, as schematically depicted in Fig. 2.2a. The kinematics of each beam are defined by the two nodal displacement components and by the node rotation (the rotation axis being perpendicular to the element plane, Fig. 2.2a).

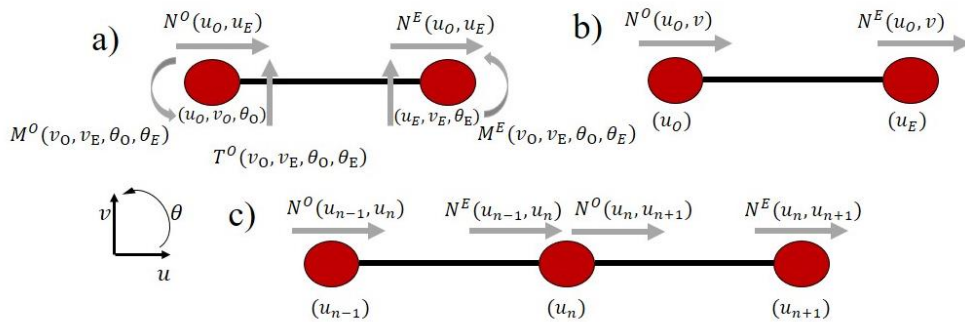


Figure 2.2 : Forces and moments acting at the end nodes of each beam element (a). A single unit-cell structure in a one dimensional domain without transverse forces and moments (a) and its two neighboring cell representation (c).

Chapter 2: Dispersion characteristics of periodic structural systems using higher order beam element dynamics

The elements have density  $\rho$ , length  $l_0$ , area  $A$  and elastic modulus  $E$ . Their geometric and mechanical parameters are summarized in Table 2.1.

Table 2.1 : Geometric and mechanical characteristics of the beam.

Element geometry		Mechanical Properties	
Area/Height	$A/h$	Density	$\rho$ (kg/m <sup>3</sup> )
Length	$l_0$	Young's modulus	$E$ (MPa)
Quadratic moment of inertia	$I = (Ah^2 / 12)$	Eigenfrequency	$w_0 = \sqrt{(E / \rho l_0^2)}$

In order to calculate the dynamic asymptotic expressions of the longitudinal force  $N$ , transverse force  $T$  and moment  $M$ , we use the following equilibrium equations and the element's constitutive law, linking the beam statics (force resultants and moments) to the kinematic variables:

$$\begin{aligned} \frac{dN}{dx} &= \rho A \ddot{u}, & \frac{dT}{dy} &= \rho A \ddot{v} \\ N &= -EA \frac{du}{dx}, & M &= -EI \frac{d^2v}{dy^2} \end{aligned} \quad (2.1)$$

Using the definitions of Eq. (2.1), we obtain through their asymptotic, frequency-based expansion as elaborated in **Appendix 1.A**, the following expressions for the forces  $N, T$  and moment  $M$  acting on each element ( $O$  represents the starting node and  $E$  represent the extremity node, and the beam is oriented from the left to the right):

$$N^O(u_1, u_2) = N(u_1, u_2) = \frac{EA}{l_0} \left( (u_1 - u_2) - \frac{(\chi l_0)^2}{6} (2u_1 + u_2) - \frac{(\chi l_0)^4}{a} (8u_1 + 7u_2) + o((\chi l_0)^5) \right) \quad (2.2)$$

$$N^E(u_1, u_2) = -N(u_2, u_1)$$

$$T^O(v_1, v_2, \theta_1, \theta_2) = T(v_1, v_2, \theta_1, \theta_2) = \frac{12EI}{l_0^3} \left( \begin{aligned} &(v_1 - v_2) + \frac{l_0}{2} (\theta_1 + \theta_2) - \frac{(\beta l_0)^4}{e} (26v_1 + 9v_2) - \frac{(\beta l)^4 l_0}{f} (22\theta_1 + 13\theta_2) - \\ &\frac{(\beta l)^8}{240} (gv_1 + hv_2) - \frac{(\beta l)^8 l_0}{m} (65.\theta_1 - 61.\theta_2) + o((\beta l_0)^{10}) \end{aligned} \right) \quad (2.3)$$

$$T^E(v_1, v_2, \theta_1, \theta_2) = T(-v_2, -v_1, \theta_2, \theta_1)$$

$$M^O(v_1, v_2, \theta_1, \theta_2) = M(v_1, v_2, \theta_1, \theta_2) = \frac{6EI}{l_0^2} \left( (v_1 - v_2) + \frac{l_0}{3}(2\theta_1 + \theta_2) - \frac{(\beta l_0)^4}{n}(22v_1 + 13v_2) - \frac{(\beta l_0)^4 l_0}{n}(4\theta_1 - 3\theta_2) \right) \\ M^E(v_1, v_2, \theta_1, \theta_2) = M(v_2, v_1, -\theta_2, -\theta_1) \quad (2.4)$$

In Eqs. (2.2-2.4), the coefficients a-s stand for numerical constants arising from the asymptotic expansion of the forces and moments, which are summarized in **Appendix 1.A**. The variables  $\chi$  and  $\beta$  stand accordingly for the compression and bending parameters defined as  $\chi = (\rho w^2 / E)^{1/2}$  and  $\beta = (\rho A w^2 / EI)^{1/4}$ ,  $w$  being the frequency of the propagating waves.

The asymptotic expansion of the transverse forces and moments in Eqs. (2.3) and (2.4) is carried out up to the 8<sup>th</sup> order, while the corresponding normal force expression up to the 4<sup>th</sup> order (which correspond to the same order of frequency. For the propagating waves to be characterized, the force and moment equilibrium needs to be formed and its non-trivial solution with respect to the frequency needs to be obtained. In Sections 2.3 and 2.4, we elaborate on the dispersion attributes of one-dimensional and two-dimensional systems.

### 2.2.1. Dispersion characteristics of 1D media based on Cauchy mechanics

The dispersion relation for an effective Cauchy continuum constitutes a first order approximation of the effective behavior of the medium. In the one-dimensional space the dynamic equilibrium equation along with the materials constitutive behavior are described as follows:

$$\frac{d\sigma(x,t)}{dx} = \rho \ddot{u}(x,t) \Rightarrow \frac{\partial^2 u(x,t)}{\partial x^2} = \frac{\rho}{E} \cdot \frac{\partial^2 u(x,t)}{\partial t^2} \quad (2.5)$$

Where in Eq. (2.5),  $E$  stands for the material's Young's modulus and  $\rho$  for its density. Inserting the harmonic plane wave solution ( $u_n = Ue^{i(\omega t - kx)}$ ) in Eq. (2.5), we obtain the dispersion relation ( $\omega-k$ ) in non-normalized and normalized form ( $\omega_0 = \sqrt{E / \rho l^2}$ ) accordingly, as follows:

$$\omega = \sqrt{E / \rho} k, \quad \frac{\omega}{\omega_0} = \sqrt{\frac{E}{\rho}} k / \sqrt{\frac{E}{\rho l^2}} = kl \quad (2.6)$$

## 2.3 Dispersion Diagrams for 1D periodic media

In the current section, we analyze the dispersion behavior of one-dimensional periodic media that are simulated as discrete systems (Section 2.2.1). Thereupon, we discuss the limits of validity of the homogenized Cauchy continuum consideration, while we address the issue of scale separation and frequency dependence of the solution. We study, one-cell, two-cell and three-cell systems.

### 2.3.1 One-Cell periodic system $\Omega_1$

In this section we analyze the case of 1D systems described by a sole unit-cell. The cell is described as a beam of length  $l = l_0$ , with a horizontal displacement  $u$ . Since, we solely analyze its one-dimensional behavior, the media acts in traction and compression, so that the sole force resultant acting is the longitudinal force  $N$  defined by Eq. (2.2). We next write the equilibrium of an internal node  $n$ , by considering a set of two neighboring cells as shown in Fig. 2.2c. Using Eq. (2.2) up to its fourth order expansion, we derive the equilibrium of the  $n$  node as the following expression for the normalized frequency  $X = w/w_0$  :

$$\begin{aligned} N^O(u_n, u_{n+1}) - N^E(u_n, u_{n-1}) = 0 \Rightarrow & \left( u_n + \frac{7}{6}u_{n-1} + \frac{7}{6}u_{n+1} \right) X^4 + \\ & \left( 15u_n + \frac{15}{4}u_{n-1} + \frac{15}{4}u_{n+1} \right) X^2 - 45u_n + \frac{45}{2}u_{n-1} + \frac{45}{2}u_{n+1} = 0 \end{aligned} \quad (2.7)$$

Where in Eq. (2.7)  $X(w)$  includes the frequency of the propagating waves, while  $n$  defines the index of the nodes along the structure (Fig. 2.2c). Inserting the harmonic plane wave solution  $u_{n-1} = Ue^{i(\omega t - k \cdot (n-1) \cdot l_0)}$ ,  $u_n = Ue^{i(\omega t - k \cdot n \cdot l_0)}$ ,  $u_{n+1} = Ue^{i(\omega t - k \cdot (n+1) \cdot l_0)}$ , Eq. (2.7) simplifies into the following dispersion relation of order  $O(w^4)$ :

$$X^4 \left( 1 + \frac{7}{8} \cos(kl_0) \right) + X^2 \left( 15 + \frac{15}{2} \cos(kl_0) \right) - 45 + 45 \cdot \cos(kl_0) = 0 \quad (2.8)$$

The solution of Eq. (2.8) leads to two identical real solutions (double root) upon which the dispersion relation of the structure is computed. In Fig. 2.3 we depict the root of Eq. (2.8) along with the one predicted for the homogenized Cauchy continuum in Eq. (2.6).

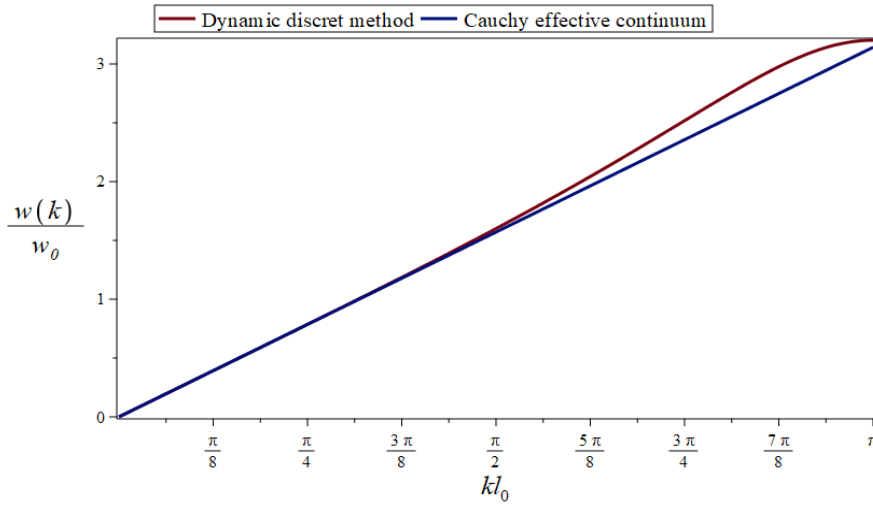


Figure 2.3 : Longitudinal dispersion curve obtained for the Cauchy effective continuum (in blue) and by the dynamic discrete method (in Red).

Fig. 2.3 suggests a separation of the two solutions obtained by the Cauchy continuum and by the DDM after a certain wavenumber magnitude or accordingly frequency value. In particular, in the low frequency regime, the band diagram corresponding to wavelengths that are very large compared to the unit cell size (Fig. 2.1), the Cauchy and the dynamic discrete solution of (2.8) coincide. More specifically, noting that  $w \ll w_0 \Rightarrow kl_0 \rightarrow 0$  which corresponds to long wavelengths (in the high wave modulation region) for which the separation of scales well applies, the following condition is satisfied:

$$w \rightarrow 0, u_{n+1} = U \cdot e^{i(-k(n+1)l_0)} = U = u_n \quad (2.9)$$

This low frequency domain corresponds to low wave numbers (Fig. 2.3) and it is non-dispersive. Therefore, two successive nodes admit identical displacements, so that the periodicity and the separation of scales in the  $(w-k)$  space are satisfied. In this range, the Cauchy predictions are sufficient to describe the wave propagation characteristics of the media. Beyond this limit, thus at higher frequencies, the Cauchy medium is no longer sufficient to describe the effective behavior of the system, as the latter becomes dispersive. We subsequently determine the scale separation condition in terms of both the frequency  $w$  and wavenumber  $k$ , based on the dispersion relation of Fig. 2.3.

### 2.3.1.1 Accounting for the effect of the wave frequency on the periodicity attributes of the medium

We extend the previous analysis which neglects the propagating wave frequency, beyond the non-dispersive region of the dispersion diagram of Fig. 2.3. To that scope, we employ as a limiting point for our analysis the wavenumber  $kl_0 = \pi / 2$ , which corresponds to the frequency  $w = \sqrt{3} \cdot w_0$ , beyond which the Cauchy and discrete solution deviate, as shown in Fig. 2.3. For this value, the longitudinal displacement of an intermediate node  $n$  (Fig. 2.2c) becomes:

$$u_n = \text{Re}(U \cdot e^{i\sqrt{3}w_0t - i\frac{n\pi}{2}}) = \text{Re}(U \cdot e^{i\sqrt{3}w_0t} \cdot (-i)^n) \quad (2.10)$$

Eq. (2.10) can be simplified discerning two cases for the order of the exponent  $n$ . In particular:

if  $n = 2q$  (even integer) then the displacement at the corresponding node is

$$u_{2q} = (-1)^q \cdot U \cdot \cos(\sqrt{3}w_0t)$$

if  $n = 2q + 1$  (odd integer) then the displacement at the corresponding node is

$$u_{2q+1} = (-1)^q \cdot U \cdot \sin(\sqrt{3}w_0t)$$

As a result, when the frequency ( $w = \sqrt{3} \cdot w_0$ ) of the propagating wave is taken into consideration, the assumption of the displacement periodicity on the nodes is lost. A total of four successive cells is required for the displacements of the initial node to be recovered, thus the periodicity now holds for a set of four unit cells:

$$\begin{aligned} u_1 &= U \cdot \sin(\sqrt{3}w_0t), \quad u_2 = -U \cdot \cos(\sqrt{3}w_0t), \\ u_3 &= -U \cdot \sin(\sqrt{3}w_0t), \quad u_4 = U \cdot \cos(\sqrt{3}w_0t) \end{aligned} \quad (2.11)$$

The displacements of the successive nodes defined in Eq. (2.11) are shown in Fig. 2.4, while the displacement of the 5<sup>th</sup> node, which is identical to the one of the first node is provided in the middle.

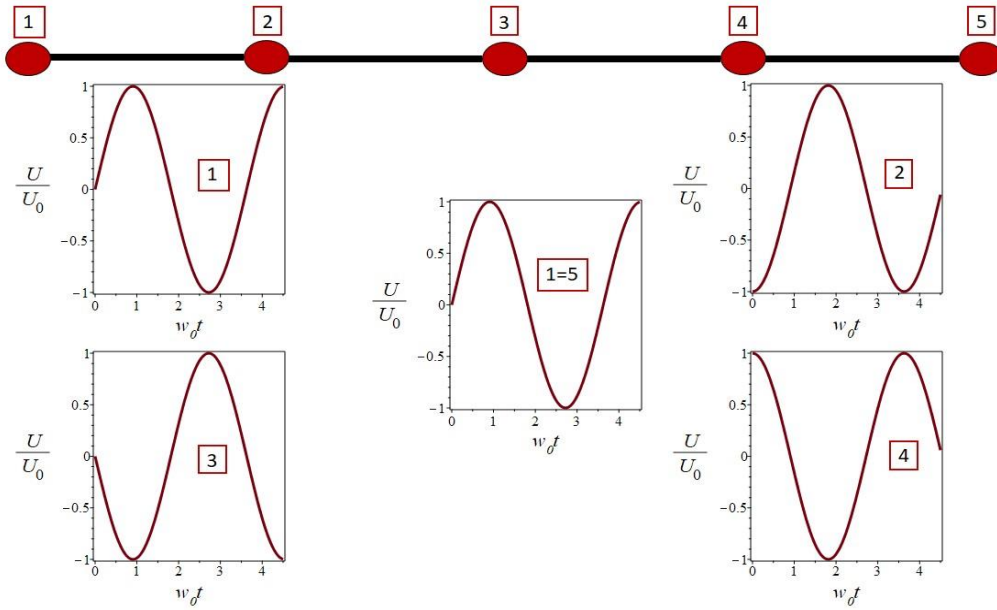


Figure 2.4 : Displacement of a series of 5 nodes in the 1D space, when the wave frequency is accounted for in the periodic solution.

Fig. 2.4 indicates that when the frequency of the propagating waves is accounted for in the system's periodic solution ( $w = \sqrt{3}w_0$ ), the displacement of the 5<sup>th</sup> node is identical to that of the first node. As a result, the periodicity condition at the limit of the non-dispersive region is four cells -rather than one cell- and cannot be satisfied for two neighboring nodes. The same applies to different wave number values with a non-negligible  $w$ . Indicatively, for a wave number double the one previously considered, that is for  $kl_0 = \pi$ , corresponding to a frequency  $w = 2\sqrt{3}w_0$  (Eq. (2.8)), the following set of nodal displacements for the two unit cells system are obtained:

$$u_n = \text{Re}(U \cdot e^{iwt - izn}) = \text{Re}(U \cdot e^{iwt}) \cdot (-1)^n = (-1)^n \cdot U \cdot \cos(2\sqrt{3} \cdot w_0 t) \quad (2.12)$$

Eq. (2.12) corresponds to a two-cell periodicity of the nodal displacement components. The previous analysis highlights the fact that for a Cauchy medium periodicity is not satisfied for any wave number and frequency that are away from the origin of the dispersion curve of Fig. 2.3.

### 2.3.2 Two-cell systems $\Omega_2$

We subsequently consider a system comprised of two equal unit-cells (Fig. 2.5a), which contains an internal node  $v$  in addition to the two extremity nodes (Fig. 2.5a). The length of the period becomes accordingly  $l = 2 \cdot l_0$ , while the system's minimum repetition consists of a total of 4 unit-cells (Fig. 2.5b).

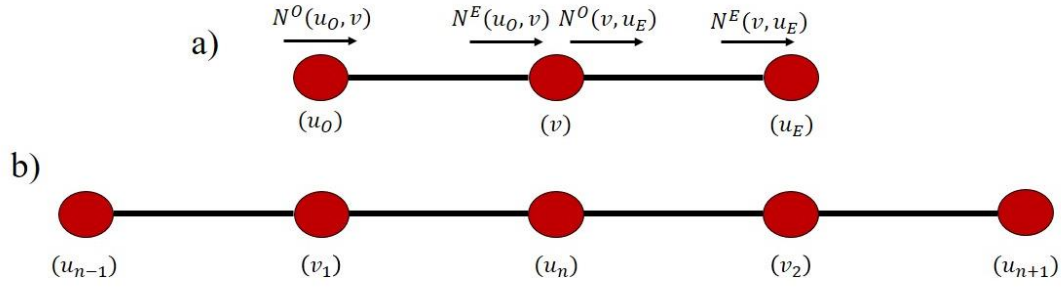


Figure 2.5 : A basic system of two-cells with an internal node  $v$  considered as the basic material unit (a). Two adjacent material units comprising a total of 4 unit-cells (b).

We initially express the displacement of the internal node of Fig. 2.5a as a function of its end nodes  $u_O, u_E$ . To that scope we write the balance of forces for the internal node  $v$  of Fig. 2.5a. For the equilibrium, we make use of the second order approximation of the normal forces of Eq. (2.2), upon which we obtain:

$$N^O(v, u_E) - N^E(u_O, v) = 0$$

$$\Rightarrow v(X^2 - 3) + (u_E + u_O) \left( \frac{X^2}{4} + \frac{3}{2} \right) = 0 \Rightarrow v = \frac{(u_O(X^2 + 6) + u_E(X^2 + 6))}{(4(3 - X^2))} \quad (2.13)$$

Eq. (2.13) can be used to analyze the limiting states of the two-cell system kinematics. In particular, the internal displacement noted  $v$  tends to infinity for the resonance wave frequency  $w = \sqrt{3} \cdot w_0$ . For lower wave frequency values  $w$ , the motion of the internal mass  $v$  is in the same direction as to the motion of the reference nodes (variables  $u_O$  and  $u_E$ ), as the denominator of Eq. (2.13) is positive. For  $w > \sqrt{3}w_0$  the internal node is out of phase with the respect to the motion of the extremity nodes of the two-cell system. Eq. (2.13) can be used to write the longitudinal forces of the extremity nodes of the two-cell system of Fig. 2.5a as a sole function of  $u_O$  and  $u_E$ , inserting Eq. (2.13) in Eq. (2.2), as follows:

$$N^E(v, u_E) = -N(u_E, v) = E \cdot A \cdot \frac{(u_O(X^4 + 12X^2 + 36) + u_E(-7X^4 + 60X^2 - 36))}{(24 \cdot l_0(3 - X^2))} \quad (2.14)$$

$$N^O(u_O, v) = EA \frac{(u_O(7X^4 - 60X^2 + 36) + u_E(-X^4 - 12X^2 - 36))}{(24 \cdot l_0(3 - X^2))} \quad (2.15)$$

Eqs. (2.14) and (2.15) can be subsequently used to compute the equilibrium at the node  $n$  of two adjacent material units (Fig. 2.5b), each of them comprised of two basic unit-cell systems, as follows:

$$N^O(u_n, v_2) - N^E(v_1, u_n) = 0 \Rightarrow u_n \left( X^4 - \frac{60}{7} X^2 + \frac{36}{7} \right) + u_{n-1} \left( -\frac{X^4}{14} - \frac{6}{7} X^2 - \frac{18}{7} \right) + u_{n+1} \left( -\frac{X^4}{14} - \frac{6}{7} X^2 - \frac{18}{7} \right) = 0 \quad (2.16)$$

Inserting the harmonic plane wave solution  $u_{n-1} = Ue^{i(\omega t - k \cdot (n-1) \cdot 2l_0)}$ ,  $u_n = Ue^{i(\omega t - k \cdot n \cdot 2l_0)}$   $u_{n+1} = Ue^{i(\omega t - k \cdot (n+1) \cdot 2l_0)}$  into Eq. (2.16) allows to compute the dispersion characteristics of the two-cell system, as the solution of the following equation:

$$(7 - \cos(2kl_0))X^4 + (-60 - 12 \cos(2kl_0))X^2 - 36(\cos(2kl_0) - 1) = 0 \quad (2.17)$$

The latter are presented in Fig. 2.6 in the interval of the Brillouin zone (Brillouin & Parodi, 1956), thus for  $k \cdot (2l_0) \in [-\pi, \pi] \rightarrow kl_0 \in \left[ -\frac{\pi}{2}, \frac{\pi}{2} \right]$ .

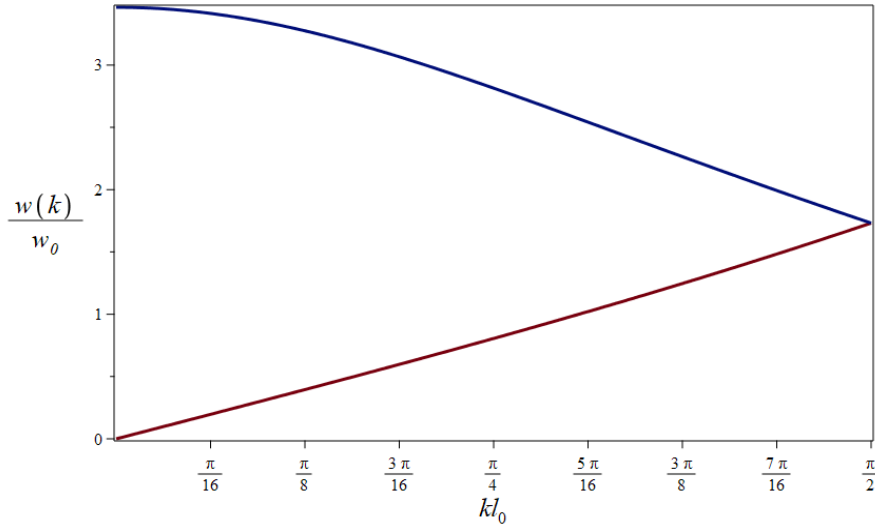


Figure 2.6: Dispersion curves for a two-cell system that includes an optical branch (blue line) and an acoustic branch (red line).

We can then provide the following classification of the different branches of the dispersion diagram according to the values of the ratio  $w/w_0$  referring also to Eq. (2.17). The first lower frequency branch starting from the origin constitutes the acoustic branch, which can be captured by the homogenized Cauchy medium for low  $k$  values. The second branch at higher frequencies constitutes the optical branch, which cannot be captured by a conventional homogenized Cauchy medium description or by the single scale equilibrium presented in Fig. 2.3. The point of transition between these two branches corresponds to the value of the resonance frequency  $w = \sqrt{3} \cdot w_0$ .

We subsequently analyze the periodicity of the system in high wavelength region where  $kl_0 \rightarrow 0$ . By writing the continuity equations between the neighboring cells (Eq. (2.16)), without replacing the displacement of the internal nodes by their values in terms of the extremity nodes. Thereupon, using the equilibrium of the internal node (Eq. (2.13)), we formulate the following system of equations:

$$\begin{cases} N^O(v, u_E = u) - N^E(u_O = u, v) = 0 \\ N^O(u_n = u, v_2 = v) - N^E(v_1 = v, u_n = u) = 0 \end{cases}$$

$$\Rightarrow \begin{bmatrix} -1 - \frac{X^2}{6} & 1 - \frac{X^2}{3} \\ 1 - \frac{X^2}{3} & -1 - \frac{X^2}{6} \end{bmatrix} \cdot \begin{bmatrix} u \\ v \end{bmatrix} = \begin{bmatrix} 0 \\ 0 \end{bmatrix} \Rightarrow X^2(X^2 - 12) = 0 \quad (2.18)$$

For the first solution ( $w \rightarrow 0$ ) of Eq. (2.18), the periodicity of neighboring nodes is satisfied, as we have shown in Eq. (2.9). At higher frequencies, the second solution of Eq. (2.18) is  $w = 2\sqrt{3}w_0$  (defining the starting point of the descending optical branch on Fig. 2.6), the previous linear system of equations writes  $-3u - 3v = 0$  for both equations of motion in Eq. (2.18). This indicates that the displacement of the internal nodes is in phase opposition with the displacement of the external nodes. Therefore, the periodicity is lost on  $\Omega_1$ , but is kept on  $\Omega_2$ , so that the separation of scales is satisfied over the period  $\Omega_2$  in the high wavelength region ( $kl_0 \rightarrow 0$ ). As a result, moving to the two-cells system extends the range of validity of the separation of scales to higher frequencies. In the sequel, we consider the three-cell period  $\Omega_3$  to analyze whether the choice of a larger period allows to further extend the range of frequencies for which scales can be separated.

### 2.3.3 Three-cells system $\Omega_3$

We subsequently consider the period  $\Omega_3$  composed of three cells of identical length, the driving external mode kinematic variables are  $u_o$  and  $u_E$  for the principal cell with internal variables  $v_1$  and  $v_2$  as schematically depicted in Fig. 2.7a:

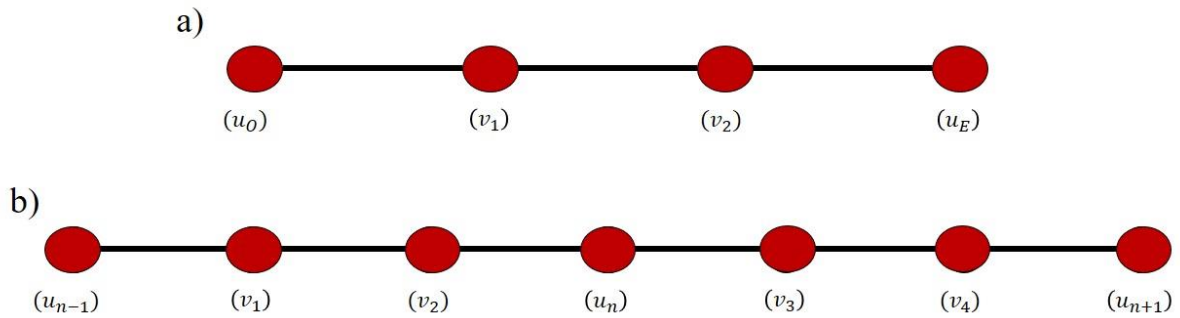


Figure 2.7 : Three-cells system  $\Omega_3$  with two internal nodes  $v_1$  and  $v_2$  considered as the basic material unit (a). Two adjacent material units comprised of a total of 6 unit-cells (b).

We first express the displacement of the two internal nodes, writing the equilibrium equations for the nodes  $v_1$  and  $v_2$  of Fig. 2.7a. Inserting the expression of the dynamic longitudinal forces defined in Eq. (2.2) up to the second order, we obtain:

$$\begin{cases} N(v_1, v_2) + N(v_1, u_D) = 0 \Rightarrow -\frac{E \cdot A}{6 \cdot l_0} (u_O (X^2 + 6) + v_1 (4X^2 - 12) + v_2 (X^2 + 6)) = 0 \\ N(v_2, v_1) + N(v_2, u_F) = 0 \Rightarrow -\frac{E \cdot A}{6 \cdot l_0} (u_E (X^2 + 6) + v_1 (X^2 + 6) + v_2 (4X^2 - 12)) = 0 \end{cases} \quad (2.19)$$

Solving the system of Eqs. (2.19) allows us to express the internal variables versus the driving external variables, namely the displacements of the extremity nodes  $u_E$  and  $u_O$ , as follows:

$$v_1 = \frac{-4(X^2 + 6) \left( u_O (X^2 - 3) + u_E \left( -\frac{X^2}{4} - \frac{3}{2} \right) \right)}{15(X^2 - 6) \left( X^2 - \frac{6}{5} \right)}, \quad v_2 = \frac{(X^2 + 6) u_O \left( (X^2 + 6) + u_E (-4X^2 + 12) \right)}{15 \left( (X^2 - 6) \left( X^2 - \frac{6}{5} \right) \right)} \quad (2.20)$$

The frequencies  $w = w_0 \sqrt{6}$ ,  $w = w_0 \sqrt{6/5}$  set the denominator of Eq. (2.20) to zero and are the resonance frequencies of the system, for which the displacement tends to infinity. Applying the continuity of forces on node  $n$  between two neighboring cells  $\Omega_3$  (Fig 2.7b) and using Eq. (2.20) along with the equilibrium equation of the common node between the two cells leads to the following dispersion relation:

$$N(u_n, v_2) + N(u_n, v_3) = 0 \Rightarrow \left( u_n (52X^6 - 684X^4 + 1728X^2 - 432) + u_{n-1} (X^6 + 18X^4 + 108X^2 + 216) + u_{n+1} (X^6 + 18X^4 + 108X^2 + 216) \right) = 0 \quad (2.21)$$

After inserting the harmonic planar wave Ansatz into Eq. (21), we obtain a solution of order  $w^6$  (three real roots), which is defined in a normalized  $X$  form as follows:

$$X^6 (52 + 2 \cos(3kl_0)) - X^4 (684 + 36 \cos(3kl_0)) + X^2 (1728 + 216 \cos(3kl_0)) - 432(1 - \cos(3kl_0)) = 0 \quad (2.22)$$

The solution of Eq. (2.22) provides the dispersion relation of the 3-cells system, which is plotted in the Brillouin zone  $kl_0 \in \left[ -\frac{\pi}{3}, \frac{\pi}{3} \right]$  in Fig. 2.8.

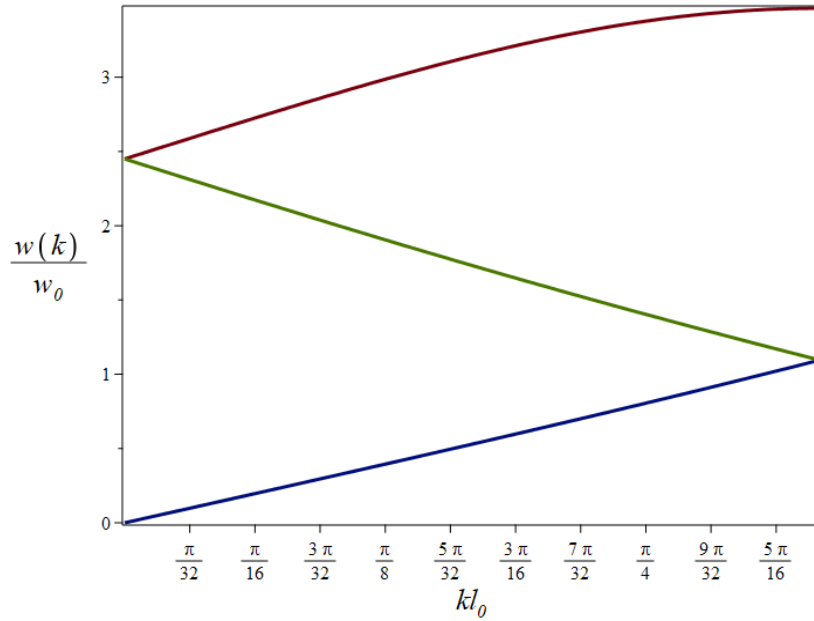


Figure 2.8 : Dispersion curve of the three-cells system including an acoustic (blue) and two optimal branches (green and red).

The dispersion diagram for  $\Omega_3$  is composed of three different branches with the transition points between the different branches to correspond to the eigenfrequencies of the system ( $w = w_0\sqrt{6}$ ,  $w = w_0\sqrt{6/5}$ ). The first branch is the acoustic branch passing through the origin while the second and third branches are optical branches, which can be no longer described by Cauchy continuum mechanics. Note that the group velocity changes its sign when moving across the transition points of Fig. 2.8.

In the high wavelength region ( $L_c \rightarrow \infty$ , Fig. 2.1) for which  $kl_0 \rightarrow 0$ , periodicity is obtained for a single unit cell, thus already in the  $\Omega_1$  analysis space (Section 2.3.1), so that two neighboring nodes have the same displacements. In the non-zero frequency region ( $X \neq 0$ ), the displacements of the internal variables are expressed versus the displacements of the driving variables  $u_{n+1}$  and  $u_n$ , as follows:

$$v_{1n} = \frac{-4(X^2 + 6)\left(u_n(X^2 - 3) + u_{n+1}\left(-\frac{X^2}{4} - \frac{3}{2}\right)\right)}{15(X^2 - 6)\left(X^2 - \frac{6}{5}\right)}, \quad v_{2n} = \frac{(X^2 + 6)u_n\left((X^2 + 6) + u_{n+1}(-4X^2 + 12)\right)}{15\left((X^2 - 6)(X^2 - \frac{6}{5})\right)} \quad (2.23)$$

By developing these expressions at low frequencies ( $X \rightarrow 0$ ), we obtain:

$$v_{1n} = \frac{1}{3}(2u_n + u_{n+1}) = u_n, \quad v_{2n} = \frac{1}{3}(u_n + 2u_{n+1}) = u_n \quad (2.24)$$

Thus, at low frequencies, the periodicity for a three-cell system is maintained, as a consequence of the one-cell periodicity in this frequency domain. At higher frequencies, taking the resonance frequency  $\omega = \sqrt{6} \omega_0$  based on the dispersion relation (2.22), the displacements are unbounded according to Eq. (2.23). In order to study the periodicity of a three-cell system, we impose identical displacements over neighboring super cells:  $\begin{cases} u_{n+1} = u_n = u \\ v_1 = v_3, v_2 = v_4 \end{cases}$ . We write the equilibrium equations for the internal nodes, and the equation of continuity between the two neighboring cells, condensed in the following system:

$$\begin{cases} N(v_1, v_2) + N(v_1, u_{n-1} = u) = 0 \\ N(v_2, v_1) + N(v_2, u_n = u) = 0 = 0 \\ N(u_n = u, v_2) + N(u_n, v_3 = v_1) = 0 = 0 \end{cases} \Rightarrow \begin{bmatrix} -1 - \frac{X^2}{6} & 2\left(1 - \frac{X^2}{3}\right) & -1 - \frac{X^2}{6} \\ -1 - X^2 & -1 - \frac{X^2}{6} & 2\left(1 - \frac{X^2}{3}\right) \\ 2\left(1 - \frac{X^2}{3}\right) & -1 - \frac{X^2}{6} & -1 - \frac{X^2}{6} \end{bmatrix} \cdot \begin{bmatrix} u \\ v_1 \\ v_2 \end{bmatrix} = \begin{bmatrix} 0 \\ 0 \\ 0 \end{bmatrix} \Rightarrow X^2 (X^2 - 6)^2 = 0 \quad (2.25)$$

This leads to distinguish two cases, for  $X=0$ , the internal nodes have the same displacements  $v_1 = v_2 = u$ , so that the periodicity is recovered for the single unit cell system  $\Omega_1$ . The frequency  $\omega = \omega_0 \sqrt{6}$  is a double root of Eq. (2.25), so that leads to the single equation  $u + v_1 + v_2 = 0$ , which admits an infinity of solutions represented by a basis of two vectors, so that the periodicity is not satisfied on  $\Omega_1$ , neither in  $\Omega_2$  (since  $v_1 \neq u$  and  $v_2 \neq u$ ) but instead it is satisfied in  $\Omega_3$ . Therefore the separation of scales is now fulfilled on  $\Omega_3$ . As a result, in the wavenumber zone which fulfills the condition  $kl_0 \rightarrow 0$ , we shall distinguish different behaviors depending on the frequency of interest, which corresponds to the three branches of the dispersion diagram (Fig. 2.8). We subsequently extend the discrete dynamical analysis to the two-dimensional situation.

## 2.4 Dynamical response of a 2D network material

In the current section, we compute the dispersion characteristics of two-dimensional media subjected to an incident horizontal wave with wave vector  $k(w) = \cos(n) / l_0$  using the discrete force and moment asymptotic expansions of Section 2.2. To that scope, we employ a square lattice with identical horizontal and vertical elements as depicted in Fig. 2.9a. Each beam element is assigned a length  $l = l_0$ , density  $\rho$  and modulus  $E$ , while the beam thickness is set to  $t = 0.1 \cdot l_0$ . Each node has three degrees of freedom, namely two in-plane displacement components  $(u, v)$  and a rotation  $\theta$ , as elaborated in Section 2.3. In order to study the dispersion properties of the periodic 2D network, we need to consider all neighboring elements attached to the lattice's principal node, as depicted in Fig. 2.9b (in black). For the square lattice in Fig. 2.9a, a total of 4 elements are attached to this central node (Fig. 2.9b).

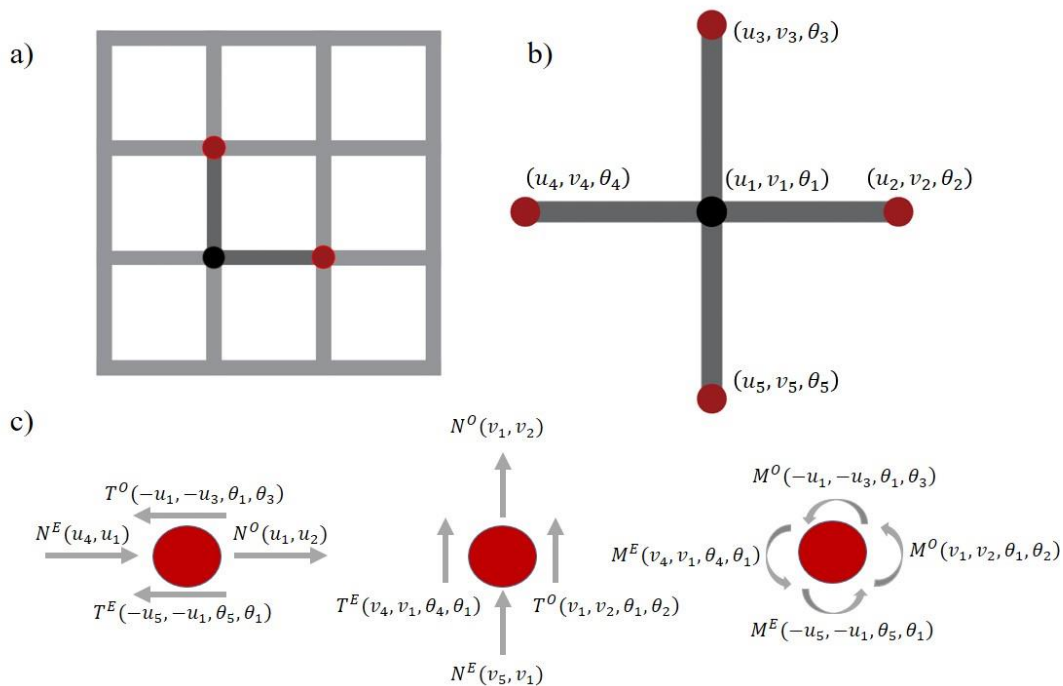


Figure 2.9 : Square lattice along with its basic elements (dark grey) in each material direction (a). The principal node 1, along with the four elements required for the description of its discrete equilibrium (b). The equilibrium of the normal, shear and moments for the principal node 1 is pictured in (c).

In order to compute the systems dispersion characteristics, we write the horizontal and vertical force equilibrium equations for the principal node 1 (Fig. 2.9b), as well as the moment

equilibrium for the same node. The corresponding forces and moments are schematically depicted in Fig. 2.9c. We number the displacement components of each node  $(u_i, v_i, \theta_i)$ , as depicted in Fig. 2.9b, upon which we derive:

$$N(u_1, u_2) + N(u_1, u_4) - T(-u_1, -u_3, \theta_1, \theta_3) - T(-u_1, -u_5, \theta_5, \theta_1) = 0 \quad (2.26)$$

$$N(v_1, v_3) + N(v_1, v_5) - T(-v_1, -v_4, \theta_4, \theta_1) + T(v_1, v_2, \theta_1, \theta_2) = 0 \quad (2.27)$$

$$M(v_1, v_2, \theta_1, \theta_2) + M(-u_1 - u_3, \theta_1, \theta_3) - M(v_1, v_4, -\theta_1, -\theta_4) - M(-u_1 - u_5, -\theta_1, -\theta_5) = 0 \quad (2.28)$$

The normal  $N$ , shear forces  $T$  and moments  $M$  entering Eqs. (2.26-2.28) are written in their asymptotic expansion form, summarized in Section 2. Eqs. (2.26-2.28) contain a total of 15 unknowns. Accounting for the periodicity of the nodal displacement components  $(n_1 l_0 \vec{e}_1 + n_2 l_0 \vec{e}_2)$  in the horizontal and vertical material direction  $((u_n, v_n, \theta_n) = (u, v, \theta) e^{-i(\omega t - n_1 k_x l_0 - n_2 k_y l_0)})$ , allows us to reduce the set of equations to 3 making use of the transformation matrix  $T$  (Phani et al., 2006) as follows:

$$q = T \tilde{q}, q = [u_1 \ v_1 \ \theta_1 \ u_2 \ v_2 \ \theta_2 \ u_3 \ v_3 \ \theta_3 \ u_4 \ v_4 \ \theta_4 \ u_5 \ v_5 \ \theta_5]^T, \tilde{q} = [u_1 \ v_1 \ \theta_1] \quad (2.29)$$

$$T^T = \begin{bmatrix} 1 & 0 & 0 & e^{-l k_x l} & 0 & 0 & e^{-l k_y l} & 0 & 0 & e^{-l k_x l} & 0 & 0 & e^{-l k_y l} & 0 & 0 \\ 0 & 1 & 0 & 0 & e^{-l k_x l} & 0 & 0 & e^{-l k_y l} & 0 & 0 & e^{-l k_x l} & 0 & 0 & e^{-l k_y l} & 0 \\ 0 & 0 & 1 & 0 & 0 & e^{-l k_x l} & 0 & 0 & e^{-l k_y l} & 0 & 0 & e^{-l k_x l} & 0 & 0 & e^{-l k_y l} \end{bmatrix}$$

The transformed 3x3 matrix with unknown displacement components  $\tilde{q}$  of the principal node 1 (Fig. 2.9b) is used to compute the dispersion characteristics of the lattice structure (Fig. 2.9a), setting its determinant to zero. A total of three roots arise, equal to the number of degrees of freedom of the principal node, corresponding to the shear, longitudinal and torsional mode.

For comparison purposes, we evaluate the dispersion diagram using the Bloch's theorem (Phani et al., 2006), using the basic unit cell depicted in Fig. 2.9b. Given the three degrees of freedom per node, a total of 15 degrees of freedom (named  $q$ ) are necessary for the construction of the unit-cell's total mass  $M$  and stiffness  $K$  matrices (Fig. 2.9b) as in the discrete case, with relevant details for the stiffness and mass matrix assembly process provided in (Phani et al., 2006; Reda et al., 2018; Karathanasopoulos et al., 2019). The dynamic equilibrium under the action of zero external forces then writes as follows:

$$(K - \omega^2 M)q = 0 \quad (2.30)$$

$$T^T (K - \omega^2 M) T \tilde{q} = 0 \quad (2.31)$$

We can reduce the set of equations defined in (2.30), using the periodicity transformation matrix  $T$  of Eq. (2.29) to a system of order 3 equal to the number of degrees of freedom of the primal node (1).

In Fig. 2.10a, we provide the dispersion characteristics of the square lattice using a low order approximation of the forces and moments entering Eqs. (2.2-2.4) in Eqs. (2.26-2.28). More specifically, in Fig. 2.10a, the normal force is expanded up to the 2<sup>nd</sup> order, while the shear force and moments up to the 4<sup>th</sup> order (which correspond to the same order of frequency). Contrariwise, in Fig. 2.10b, we provide the result upon a higher order expansion of the forces and moments (4<sup>th</sup> order for the normal force and 8<sup>th</sup> order for the shear forces and moments). The Bloch theorem results are depicted in Figs. 2.10a and 2.10b with dashed lines.

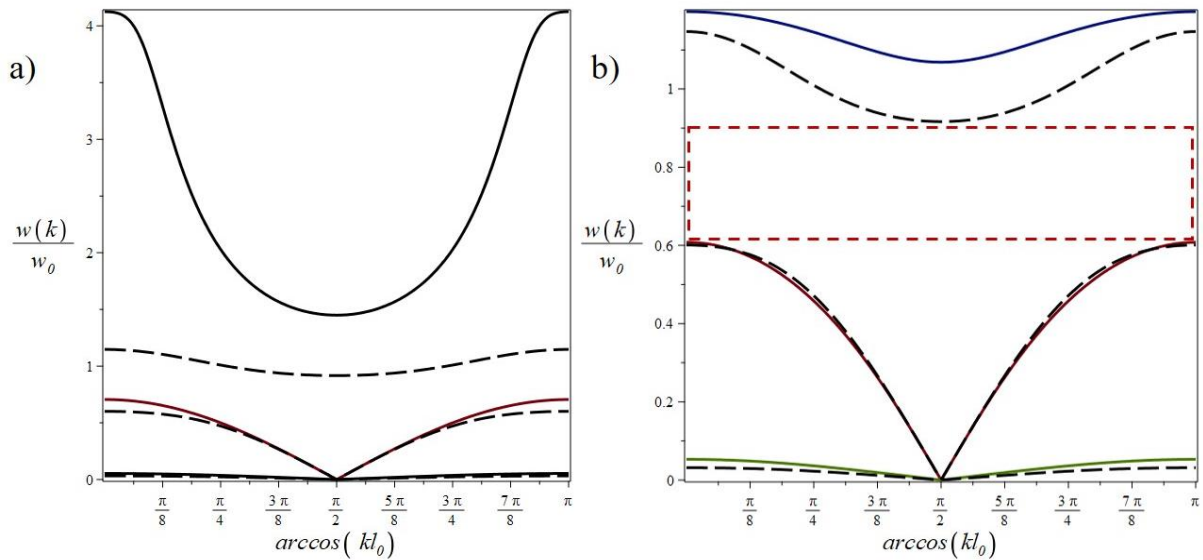


Figure 2.10 : Dispersion curves for a square lattice structure of Fig. 2.9b using the dynamic expression of the inner forces and moments up to the fourth order for the inner shear and moments along with the Bloch theorem solution (dashed lines) (a). Dispersion curves of same lattice for a higher order expansion (8<sup>th</sup> order) of the inner shear and moments (continuous lines) along with the Bloch theorem solution (dashed lines) (b).

Fig. 2.10 suggests that the effect of the order of the asymptotic expansion is more prominent for the accuracy of the higher modes and more specifically for the torsional mode. In particular, while the Bloch theorem formulation predicts a normalized frequency value of 1.14 for the extreme wave number values of  $\arccos(kl_0) = 0, \pi$  for the third mode, the low order discrete dynamics asymptotic solution is a clear multiple of it (Fig 2.10a). However, using its higher, height order formulation a value of 1.19 is obtained, which differs less than 5% higher than the Bloch solution predictions. The same tendency is observed on the

longitudinal mode, where the Bloch theorem solution gives a normalized frequency value of 0.6, while the fourth order DDM solution overestimates its value to 0.7, a difference that becomes practically negligible for the case where higher order expansions are used, as in Fig. 10b. The wave number of interest accordingly affects the accuracy of the discrete dynamics solution, so that for low wavelengths  $kl \rightarrow 0$ , the low order expansion of the inner dynamic forces and moments suffices to accurately capture the Bloch results for the first two modes (shear and longitudinal mode of Fig. 2.10a). However, for the higher torsional modes, differences which are up to 15% with respect to the Bloch wave solution are obtained using the higher order expansion of the lattices' inner forces and moments, with the actual difference value to depend on the propagating wave number.

## 2.5 Discussion

The analysis of Section 2.3, indicates that the acoustic, low frequency branch of one-dimensional periodic systems can be well captured, using a single nodal dynamic equilibrium of the structural system. In the low frequency range, the beam discrete dynamics method yields dispersion attributes which can be well compared to the ones computed upon a simplified effective Cauchy medium formulation (Fig. 2.3). In such a space, no additional information is obtained for the system dynamics with respect to classical approaches. However, when multi-scale equilibria are used, considering internal dynamic degrees of freedom for the system analyzed, higher frequency optical branches can be captured (Figs. 2.6 and 2.8). Such branches cannot be obtained by Cauchy or low frequency based mechanical formulations. Therefore, the frequency based, asymptotic expansion of the internal normal forces can allow for the description of higher-frequency dynamics, separating low and high frequency modes and characterizing the corresponding frequency transition points (Section 2.3.2, 2.3.3). The normalized scale separation frequency values in the high wavelength region, as elaborated in Sections 2.3.2 and 2.3.3 are summarized in Table 2.2.

Table 2.2 : Frequency values that satisfy the separation of scales as a function of the number of unit-cells considered within the basic period of the structural system.

Period	Scale separation frequency values $\left( X = \frac{w}{w_0} \right)$
One unit cell $\Omega_1$	$X \rightarrow 0$
Two unit cells $\Omega_2$	$X \rightarrow 0, X \rightarrow 2\sqrt{3}$
Three unit cells $\Omega_3$	$X \rightarrow 0, X \rightarrow \sqrt{6}^{+,-}$

The discrete dynamics asymptotic expansion method has been further employed to compute the band diagram structure of architected square lattice materials. It has been shown that the low order (up to the fourth order, **Appendix 1.A**) dynamic asymptotic expansion of the lattice's inner forces and moments well suffices to capture only the low frequency modes (shear and longitudinal mode) of the structure (Fig. 2.10a). However, for its higher modes to be sufficiently represented, a higher order expansion of its internal dynamic shear forces and moments is required (Section 2.4). In particular, the discrete dynamics results of Fig. 2.10b suggest that the difference of the Bloch results and the discrete beam dynamics computations differ by at most 15% for all wave numbers for the highest torsional mode when an 8<sup>th</sup> order approximation of the structure's internal forces and moments is used; a value that becomes almost an order of magnitude higher for low order asymptotic approximations of the structures' inner dynamics (Fig. 2.10a). Note however that the shear and longitudinal modes converge to the Bloch results in the long wavelength regime ( $kl_0 \rightarrow 0 \Rightarrow \arccos(kl_0) \rightarrow \pi/2$ ), already for a low order dynamic expansion of the structures' inner forces and moments (Fig. 2.10a).

## 2.6 Conclusion

Overall, in the current chapter, a higher order, discrete dynamics method has been elaborated to compute the dispersion attributes of periodic structures. The proposed methodology has been based on the higher order dynamic asymptotic expansion of the structure's inner forces and moments. Thereupon, analytical expressions for the normal, shear and bending moments developed within beam element structures have been provided, as a function of the propagating frequency. The methodology has been employed to compute the

## Chapter 2: Dispersion characteristics of periodic structural systems using higher order beam element dynamics

dispersion characteristics of one and two-dimensional periodic media. It has been shown that within the one-dimensional space, the discrete dynamics approach can capture, not only the acoustic branch, but also higher, optical frequency branches of the dispersion diagram, which are not accessible for methods restrained to low frequencies, such as Cauchy media formulations. What is more, the method inherently describes the dependence of the wavelength on the propagating frequency ( $w(k)$ ), separating the frequency regions for which optical, rather than acoustic branches are expected. In the two-dimensional space, it has been demonstrated that the eighth order asymptotic expansion of the system dynamics yields high accuracy solutions for the lower order modes of architected lattice materials, with the discrete dynamics dispersion predictions to deteriorate for the higher order modes of the Floquet-Bloch spectrum. This work can provide the basis for the dynamic, discrete element-based computation of the dispersion characteristics of periodic material structures and constitutes a reference in the development of enhanced formulations of higher accuracy within and beyond the upper limits of the Floquet-Bloch theorem of two and three-dimensional media.

### References

- [1] Antonakakis, T., Craster, R.V. (2012). High frequency asymptotics for microstructured thin elastic plates and platonics, *Proc. R. Soc.* 468, 1408-1427. <https://doi.org/10.1098/rspa.2011.0652>
- [2] Auriault, J.L., Bonnet, G., (1985). Dynamique des composites élastiques périodiques. *Arch Mech.* 37, 269–284 (in French).
- [3] Auriault, J.L., Boutin, C. (2012). Long wavelength inner-resonance cut-off frequencies in elastic composite materials. *Int. J. solid. Struct.* 49, 3269-3281. <https://doi.org/10.1016/j.ijsolstr.2012.07.002>.
- [4] Bacigalupo, A., & Gambarotta, L. (2017). Wave propagation in non-centrosymmetric beam-lattices with lumped masses: Discrete and micropolar modeling. *International Journal of Solids and Structures*, 118–119, 128–145. <https://doi.org/10.1016/J.IJSOLSTR.2017.04.010>
- [5] Bacigalupo, A., & Gambarotta, L. (2019). Generalized micropolar continualization of 1D beam lattices. *International Journal of Mechanical Sciences*, 155, 554–570. <https://doi.org/10.1016/J.IJMECSCI.2019.02.018>.
- [6] Bakhvalov, N.S., Panasenko, G. (1989). *Homogenisation: Averaging Processes in Periodic Media*, Springer Netherlands.
- [7] Bensoussan, A., Lions, J.L., Papanicolaou, G., (1987). *Asymptotic analysis for periodic structures*, North-Holland, Amsterdam.
- [8] Boutin, C., Auriault, J.L. (1993). Rayleigh scattering in elastic composite materials. *Int. J. Eng. Sci.* 31,1669–1689. [https://doi.org/10.1016/0020-7225\(93\)90082-6](https://doi.org/10.1016/0020-7225(93)90082-6).
- [9] Boutin, C., Rallu, A., & Hans, S. (2012). Large scale modulation of high frequency acoustic waves in periodic porous media. *The Journal of the Acoustical Society of America*, 132(6), 3622–3636. <https://doi.org/10.1121/1.4763553>.

- [10] Boutin, C., Rallu, A., Hans, S. (2014). Large scale modulation of high frequency waves in periodic elastic composites. *J. Mech. Phys. Solid*, 70, 362 – 381. <https://doi.org/10.1016/j.jmps.2014.05.015>.
- [11] Brillouin, L., Parodi, M. (1956). *Propagation des ondes dans les milieux périodiques*, Masson, Paris.
- [12] Caillerie, D., Trompette, P., Verna, P. (1989) Homogenisation of periodic trusses, IASS Symposium, Shell and Spatial Structures. Madrid.
- [13] Chesnais, C., Boutin, C., Hans, S. (2015). Wave propagation and non-local effects in periodic frame materials: Generalized continuum mechanics. *Mathematics and Mechanics of Solids*, 20(8), 929–958. <https://doi.org/10.1177/1081286513511092>
- [14] Colquitt, D. J. (2018). Composite dynamic models for periodically heterogeneous media. 14–16. <https://doi.org/10.1177/1081286518776704>
- [15] Craster, R.V., Kaplunov, J., Pichugin, A.V. (2010). High frequency homogenization for periodic media, *Proc. R. Soc. A*. 466, 2341-2362. <https://doi.org/10.1098/rspa.2009.0612>
- [16] Deymier, P.A. (2013). *Acoustic Metamaterials and Phononic Crystals*, Springer Series in Solid-State Sciences, Berlin.
- [17] Gonella, S., & Ruzzene, M. (2008). Homogenization and equivalent in-plane properties of two-dimensional periodic lattices. *International Journal of Solids and Structures*, 45(10), 2897–2915. <https://doi.org/10.1016/J.IJSOLSTR.2008.01.002>
- [18] Guenneau, S., Craster, R., Antonakakis, T., Cherednichenko, K., Cooper, S. (2012). Homogenization Techniques for Periodic Structures. *Theo. Num. Appli. AMU (PUP)*, 11, 1-31. <https://hal.archives-ouvertes.fr/hal-00785718>.
- [19] Hans, S., Boutin, C. (2008). Dynamics of discrete framed structures: a unified homogenized description. *J. Mech. Mat. Struct. Mathematical Sciences Publishers*, 3, 1709-1739. 10.2140/jomms.2008.3.1709. <https://doi.org/10.2140/jomms.2008.3.1709>.
- [20] Hu, J., Chang, Z., Hu, G. K. (2011). Approximate method for controlling solid elastic waves by transformation media. *Phys. Rev. B* 84.
- [21] Hussein, M.I., Leamy, M.J., Ruzzene, M. (2014). Dynamics of Phononic Materials and Structures: Historical Origins, Recent Progress and Future Outlook. *ASME Appl. Mech. Rev.* 66, 040802.
- [22] Kaina, N., Lemoult, F., Fink, M., Lerosey, G. (2015). Negative refractive index and acoustic superlens from multiple scattering in single negative metamaterials. *Nature* 525, 77–81.
- [23] Karathanasopoulos, N., Reda, H., Ganghoffer, J.-F. (2017). Designing two-dimensional metamaterials of controlled static and dynamic properties, *Comput. Materials Sci.* 138, 323-332. <https://doi.org/10.1016/j.commatsci.2017.06.035>.
- [24] Karathanasopoulos, N., Reda, H., Ganghoffer, J.-F. (2019). The role of non-slender inner structural designs on the linear and non-linear wave propagation attributes of periodic, two-dimensional architected materials, *J. Sound & Vibr.*, 445, 312-323, <https://doi.org/10.1016/j.jsv.2019.05.011>.
- [25] Lombardo, M., & Askes, H. (2012). Higher-order gradient continuum modelling of periodic lattice materials. *Computational Materials Science*, 52(1), 204–208. <https://doi.org/10.1016/j.commatsci.2011.05.025>.
- [26] Mace, B.R., Duhamel, D., Brennan, M.J., Hinke, L. (2005). Finite element prediction of wave motion in structural waveguides, *J. Acoust. Soc. Am*, 117, 2835-2842.
- [27] Ma, G.C., Sheng, P. (2016). Acoustic metamaterials: from local resonances to broad horizons. *Sci. Adv.* 2.
- [28] Mencik, J.M., Ichchou, M.N. (2008). A substructuring technique for finite element wave propagation in multi-layered systems. *Comp. Meth. App. Mech. Eng.* 197, 502-523. <https://doi.org/10.1016/j.cma.2007.08.002>.

- [29] Mencik, J.M., Duhamel, D.A. (2015). Wave-based model reduction technique for the description of the dynamic behavior of periodic structures involving arbitrary-shaped substructures and large-sized finite element models. *Finite Elements in Analysis and Design*, Elsevier, 101,1-14. <https://doi.org/10.1016/j.finel.2015.03.003>
- [30] Mitchell, S.J., Pandolfi, A., Ortiz, M. (2014). Metaconcrete: designed aggregates to enhance dynamic performance. *J. Mech. Phys. Solids* 65 (2014) 69–81. <https://doi.org/10.1016/j.jmps.2014.01.003>.
- [31] Nassar, H., He, Qi-C., Auffray, N. (2016). On asymptotic elastodynamic homogenization approaches for periodic media. *J. Mech. Phys. Solids*, Elsevier, 88, 274-290.
- [32] Panasenko, G. (2005). *Multi-scale Modelling for Structures and Composites*, Springer Netherlands.
- [33] Pasternak, E., Mühlhaus, H.B., Dyskin, A.V. (2006). Finite deformation model of simple shear of fault with microrotations: apparent strain localisation and en-echelon fracture pattern. *Philosophical Magazine*. 86, 3339–3371. <https://doi.org/10.1080/14786430500270392>.
- [34] Parnell, W.J., Abrahams, I.D. (2008). Homogenization for wave propagation in periodic fibre-reinforced media with complex microstructure. I - Theory. *J. Mech. Phys. Solids* 56, 2521–2540. <https://doi.org/10.1016/j.jmps.2008.02.003>.
- [35] Pasternak, E., Mühlhaus, H.B. (2005) Generalised homogenisation procedures for granular materials. *J. Eng. Maths*. 52, 199-229.
- [36] Phani, A.S., Woodhouse, J., Fleck, N.A. (2006). Wave propagation in two-dimensional periodic lattices, *J. Acoust. Soc. Am*. 119, 1995-2005. <https://doi.org/10.1121/1.2179748>.
- [37] Rallu, A., Hans, S., Boutin, C. (2017). High frequency reduced models for repetitive beams, *Procedia Engineering* 199, 1501–1506. <https://doi.org/10.1016/j.proeng.2017.09.487>.
- [38] Reda, H., Karathanasopoulos, N., Elnady, K., Ganghoffer, J.-F., Lakiss, H. (2018). The role of anisotropy on the static and wave propagation characteristics of two-dimensional architected materials under finite strains, *Materials & Design*, 147: 134-145. <https://doi.org/10.1016/j.matdes.2018.03.039>.
- [39] Reda, H., Karathanasopoulos, N., Ganghoffer, J.-F., Lakiss, H. (2018). Wave propagation characteristics of periodic structures accounting for the effect of their higher order inner material kinematics. *J. Sound & Vibr.* 431, 265-275. <https://doi.org/10.1016/j.jsv.2018.06.006>.
- [40] Sanchez-Palencia, E. (1980). *Nonhomogeneous media and Vibration Theory*, Lecture Notes in Physics 127, Springer, Berlin. <https://doi.org/10.1007/3-540-10000-8>.
- [41] Silva, P.B., Mencik, J.M., Arruda, J.R.F. (2015). Wave finite element-based superelements for forced response analysis of coupled systems via dynamic substructuring. *Int. J. Num. Meth. Eng.* 107, 453-476. <https://doi.org/10.1002/nme.5176>
- [42] Sridhar, A., Liu, L., Kouznetsova, V.G., Geers, M.G.D. (2018). Homogenized enriched continuum analysis of acoustic metamaterials with negative stiffness and double negative effects. *J. Mech. Phys. Solids*. 119, 104-117. <https://doi.org/10.1016/j.jmps.2018.06.015>
- [43] Suiker, A. S. J., Metrikine, A. V., & de Borst, R. (2001). Comparison of wave propagation characteristics of the Cosserat continuum model and corresponding discrete lattice models. *International Journal of Solids and Structures*, 38(9), 1563–1583. [https://doi.org/10.1016/S0020-7683\(00\)00104-9](https://doi.org/10.1016/S0020-7683(00)00104-9)
- [44] Wang, J., & Chen, W. (2019). Abnormal wave propagation behaviors in two-dimensional mass – spring structures with nonlocal effect. <https://doi.org/10.1177/1081286519853606>
- [45] Wen, J.H., Zhao, H., Lv, L., Yuan, B., Wang, G., Wen, X. (2011). Effects of locally resonant modes on underwater sound absorption in viscoelastic materials. *J. Acoust. Soc. Am*. 130, 1201–1208. <https://doi.org/10.1121/1.3621074>.
- [46] Willis, J.R. (1983). The overall elastic response of composite materials, *J. Appl. Mech*. 50, 1202-1209. doi:10.1115/1.3167202.

## Chapter 2: Dispersion characteristics of periodic structural systems using higher order beam element dynamics

[47] Willis, J.R. (1984). Variational principles and operator equations for electromagnetic waves in inhomogeneous media, *Wave Motion*, 6, 127-139. [https://doi.org/10.1016/0165-2125\(84\)90009-X](https://doi.org/10.1016/0165-2125(84)90009-X).

[48] Willis, J.R. (1997). *Continuum Micromechanics*, Springer-Verlag, New York, 265–290.

# **Chapter 3**

## **On the role of second gradient constitutive parameters in the static and dynamic analysis of heterogeneous media with micro-inertia effects**

### **Chapter 3: On the role of second gradient constitutive parameters in the static and dynamic analysis of heterogeneous media with micro-inertia effects**

#### **Summary**

In the current chapter, we develop a higher gradient dynamic homogenization method with micro-inertia effects. To that scope, we compute the macroscopic constitutive parameters up to the second gradient, using two distinct approaches, namely the Hamilton's principle and the total internal energy formulation. Thereupon, we analyze the sensitivity of the second gradient constitutive terms on the inner material and geometric parameters for the case of composite materials with a periodic, layered microstructure. The results suggest that the significance of the second gradient terms highly depend on the differences in the geometric and material properties of the underlying microstructural phases, as well as on the deformation mode of interest. What is more, the wave propagation study indicates that different higher gradient results are obtained, depending on the formulation used and on the wavenumber range of interest. In particular, Hamilton based, second gradient models perform poorly in the low wavenumber range, compared to first gradient or to analytic, exact solutions. Contrariwise, second gradient macroscopic constitutive formulations derived using the total higher gradient internal energy outperform first gradient approaches, better approximating the wave propagation characteristics of the effective medium, as the corresponding comparison in between the frequency diagrams and phase and group velocities suggest.

### 3.1 Introduction

It is experimentally proven that materials with a heterogeneous microstructure exhibit a dispersive wave propagation behavior, that is, each wavenumber travels with a different phase velocity (Erofejev, 2003). However, homogenization models based on the classical, Cauchy-type elasticity theory are not able to reproduce different aspects of the physical behavior of heterogeneous media, such as wave dispersion.

The impact of the heterogeneous microstructure on the wave propagation characteristics of materials was first recognized and analyzed by Mindlin (1964), who proposed several non-local continuum models to capture the dispersion relation of planar waves. Since the early works in the 1960s by Toupin (1962) and Koiter (1969), there has been several literature contributions to the topic, recently summarized in (Askes and Aifantis, 2009). Generalized continuum theories offer an attractive alternative for capturing dynamic behaviors overlooked by classical elasticity, especially dispersion relations (Lombardo and Askes, 2012). In order to study low frequency wave propagation in effective continuum media, enriched second gradient elasticity descriptions have been developed which account for microstructural effects descriptive of the dispersive wave behavior (Aifantis, 1998). Gradient-enriched theories can sufficiently capture dynamic behaviors overlooked by classical elasticity, in which second gradient terms are neglected. Different theories based on an enrichment of the classical elasticity framework by higher order gradients have been proposed in the past to overcome deficiencies of classical elasticity (see Aifantis, 1992,1998;Askes and Aifantis 2009, Reda et al. 2018a) and plasticity (see Askes et al., 2002; Askes et al., 2008; Askes and Aifantis, 2011; Askes et al.,2012). Their formulation has aimed at describing both static and dynamic phenomena (Gutkin and Aifantis, 1999; Gourgiotis and Georgiadis, 2009; Gonella and Ruzzene, 2010; Gonella et al., 2011).

Applications of gradient elasticity in dynamics have fostered extensive research (Ostoja-Starzewski, 2002; Papargyri-Beskou, 2004; Andrianov, 2010; Askes and Aifantis, 2011). Gradient elasticity models are useful to predict the wave dispersion characteristics in heterogeneous or discrete systems (see Mindlin, 1964; Muhlhaus and Oka, 1996; Gonella et al., 2011, Gonella and Ruzzene, 2010, Alibert, 2015). A thorough analysis of the effects brought about by gradient elasticity models can be found in (Papargyri-Beskou et al., 2009; Fafalis et al., 2012), especially the impact of the higher-order inertial terms (see Metrikine and

Askes, 2002; Askes and Aifantis, 2009; Askes et al., 2002). A detailed comparison between the dispersive characteristics of various simplified models of gradient elasticity can be found in (Askes et al., 2008). Accordingly, differences in between classical elasticity considerations and formulations that account for the role of higher order inner material kinematics or non-finite strains can be found in (Reda et al. 2018b, Karathanasopoulos et al., 2019, Reda et al. 2018c).

The descriptions of microstructural effects analyzed in wave propagation are most of the time phenomenological in nature, following either the line of micromorphic models (see Berezovski et al., 2013) or second gradient continuum models (see Fafalis et al., 2012). The phenomenological nature of these models entails that the material parameters involved in the wave propagation formulations need to be calibrated to experiments, and consequently such models are not predictive. The large number of intrinsic parameters to be identified requires a somewhat difficult measurement protocol; this issue is addressed especially in (Polyzos et al., 2015; Iliopoulos et al., 2016; Réthoré et al., 2015).

In order to circumvent this drawback, multiscale methods have been developed to link the dispersive aspects of wave propagation to the microstructure of the material. Amongst these, homogenization techniques derive the dynamical macroscopic behavior by upscaling the microscopic one, so obtaining a more coarse description of the dispersive wave propagation features, but still reflecting in a predictive manner the impact of the underlying material microstructure.

Amongst the employed micromechanical methods, asymptotic homogenization is quite appealing and has developed importantly in the field of wave propagation over the last decade, (see Fish and Chen., 2001; Guenneau et al., 2013; Bacigalupo and Gambarotta, 2010, 2012, 2014 a,b ). Boutin and Auriault (1993), extending the approach developed by Bensoussan et al. (1978), Sanchez-Palencia (1980) and Bakhvalov and Panasenko (1984), have proposed the long wave propagation in periodic media based on homogenization. The asymptotic expansion of the displacement field includes terms up to the third order to describe wave scattering. Homogenization in the time domain has also been proposed by several authors, see e.g. (Chen and Fish, 2000; Vivar-Pérez et al., 2009), considering both fast and slow time scales. In many studies, gradient elasticity theories have been derived from the continualisation of the response of a discrete lattice consisting of discrete masses and springs, see for example the early work of Mindlin (1972). Note that one of the biggest challenges of gradient elasticity theories is a

### Chapter 3: On the role of second gradient constitutive parameters in the static and dynamic analysis of heterogeneous media with micro-inertia effects

physical interpretation of the involved length-scale parameters as a function of the given microstructure (Askes and Aifantis, 2011).

Resorting to computational approaches, finite element computations over the unit cell with periodic Bloch boundary conditions have been performed to model acoustic waves scattering and to evaluate the band structure (Hussein, 2009; Huang, 2011). As an alternative strategy for the solution of the Floquet-Bloch problem, plane wave expansions of the displacement vector, elastic moduli and mass are done in Fourier series with respect to the periodicity vectors (Nemat-Nasser et al., 2011-2012).

Since the aforementioned approaches restrict to the low frequency range, they cannot describe the high frequency features encountered for microstructured periodic materials, like the presence of band gaps or negative refraction. High frequency behaviors were investigated in both discrete materials and composites with a high contrast of their elastic properties using asymptotic expansion methods (Andrianov et al., 2008, 2011; Craster et al., 2010; Zhikov (2000), Smyshlyaev (2009), Auriault and Boutin, 2012). First strain gradient formulations such as the ones elaborated in Mindlin (Mindlin 1964,1965) have further interest due to the possibility of associating them to higher order inertia terms, where the kinetic energy depends on the velocity gradient. These effects allow to better describe strain singularities at sharp crack tips and to capture size effects within the dynamic material behavior (dispersion relations) manifested by real materials such as porous materials, polymer foams (see Mindlin, 1964; Askes and Aifantis,2011). In the same spirit, a continuum model of Cauchy type including micro-inertia terms in the kinetic and potential energy was proposed in Wang and Sun (2002) and Sun and Huang (2007) with applications to the computation of the dispersion diagram for laminates which is compared with the exact solution for laminated media (Sun et al., 1968) obtained by the elasticity theory. The exact solution has been proved experimentally in (Robinson and al., 1974), where the existence of propagating bands and gaps in layered media was experimentally demonstrated.

A homogenization method for the analysis of wave propagation in materials with a periodic microstructure has been developed in Bacigalupo and Gambarotta (2012). The method is based on suitable micro-fluctuation functions which represent the material microstructure, incorporated in a variational-asymptotic approach. This approach has been recently extended in (Bacigalupo and Gambarotta, 2014a,b) to a higher order asymptotic expansion of the inner inertia terms, based on the mathematical convergence of the asymptotic solution (Smyshlyaev

and Cherednichenko, 2000), though with first order macroscopic constitutive parameters. However, up to now, the significance of higher order macroscopic terms in the static and wave propagation analysis of microstructured media with micro-inertia effects has not been analyzed. As a result, the corresponding macroscopic higher gradient internal length parameters have not been evaluated, while their effect on the wave propagation attributes of microstructured media remains unknown.

In this chapter, we develop a dynamic second gradient constitutive formulation for the analysis of the static and dynamic properties of heterogeneous media with micro-inertia effects. To that scope, we make use of the Hill-Mandel principle to relate macroscopic to microscopic parameters (Section 3.2), which we use as a basis for the derivation of the macroscopic equation of motion using separately the Hamilton's principle (Section 3.2.2) and the higher gradient description of the media's total internal energy (Section 3.2.3). We subsequently identify the micromechanical constants relating micro-scale attributes with macro-scale mechanics in the case of longitudinal and transverse deformations of layered two-phase composite materials (Sections 3.3.1). Thereafter, we analyze the significance of the higher gradient constitutive parameters as a function of the geometric and material properties of the underlying microstructure in the static case (Section 3.3.2). We extend our analysis in the wave propagation regime, computing phase and group velocities and comparing the Hamilton and the higher gradient energy method results with already available literature results in Sections 3.3.3.1 and 3.3.3.2 accordingly. We discuss on the obtained results as a function of the method and wave number interest region in Section 3.4 and conclude in Section 3.5.

## 3.2 Homogenization methods

### 3.2.1 Second gradient mechanics and Hill-Mandel principle

We consider a representative volume element (RVE) of a heterogeneous medium occupying a domain  $\Omega$ . The RVE is assumed to be small compared to the overall dimensions of the medium. We write the dynamic equilibrium of motion, as follows:

$$\sigma_{ij,j} = \rho \ddot{u}_i \quad (3.1)$$

Where  $\sigma$  in Eq. (3.1) stands for the micro-stress developed within the RVE and  $u$  for the micro-displacement.

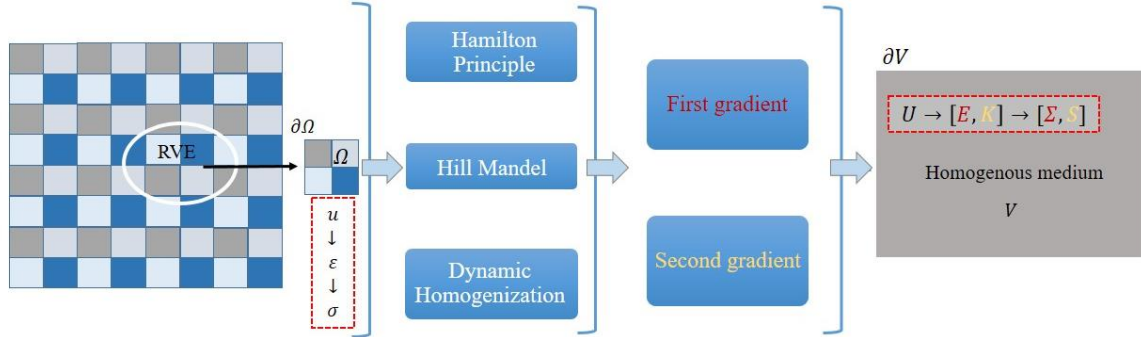


Figure 3.1: Homogenization concept from micro to macro model

We subsequently define the first and second order macro strain tensors  $E_{ij}$  and  $K_{ijk}$  and the first and second order stress tensors  $\Sigma_{ij}$  and  $S_{ijk}$  in component format accordingly, as follows (Trinh, 2011):

$$\begin{aligned}
 E_{ij} &= \frac{1}{|\Omega|} \int_{\Omega} \varepsilon_{ij} d\Omega = \langle \varepsilon_{ij} \rangle = E_{ij} = \frac{1}{2} \left( \frac{\partial U_i}{\partial X_j} + \frac{\partial U_j}{\partial X_i} \right) \\
 K_{ijk} &= \frac{1}{|\Omega|} \int_{\Omega} (\varepsilon_{ij} \otimes \nabla_k) d\Omega = \langle \varepsilon_{ij} \otimes \nabla_k \rangle = \frac{1}{2} \left( \frac{\partial^2 U_i}{\partial X_j \partial X_k} + \frac{\partial^2 U_j}{\partial X_i \partial X_k} \right) \\
 \Sigma_{ij} &= \frac{1}{|\Omega|} \int_{\Omega} \sigma_{ij} d\Omega = \langle \sigma_{ij} \rangle, \quad S_{ijk} = \langle \sigma_{ij} \otimes x_k \rangle
 \end{aligned} \tag{3.2}$$

Where the bracket notation  $\langle \cdot \rangle$  used in Eq. (3.2) denotes volume averages over the RVE of volume  $|\Omega|$ . The micro and macro scale position vectors are denoted with labels  $x$  and  $X$  respectively, while the lower and upper scale notations  $u$  and  $U$  are used for the micro and macro displacement components. We write the micro-displacement on the domain boundary as a function of the first and of the second order strain gradient terms of Eq. (3.2), as follows (Trinh et al., 2012):

$$u_i = x_j E_{ij} + \frac{1}{2} K_{ijk} x_j x_k \text{ on } \partial\Omega \tag{3.3}$$

Chapter 3: On the role of second gradient constitutive parameters in the static and dynamic analysis of heterogeneous media with micro-inertia effects

We subsequently compute the difference between the average of the microscopic energy and macroscopic strain energy by writing the following identity resulting from (3.3):

$$\int_{\partial\Omega} \left( u_i - x_j E_{ij} - \frac{1}{2} K_{ijk} x_j x_k \right) (\sigma_{mi} - \Sigma_{mi}) n_m ds = 0 \quad (3.4)$$

Using the divergence theorem, we simplify Eq. (3.4) (the calculation is detailed in **Appendix 2.A**), relating macroscopic and averaged microscopic energy terms with micro-inertia components as follows:

$$E_{ij} \Sigma_{ij} + K_{ijk} S_{ijk} = \left\langle \varepsilon_{ij} \sigma_{ij} \right\rangle + \left\langle \rho \ddot{u}_i \left( u_i - E_{ij} x_j - \frac{1}{2} K_{ijk} x_j x_k \right) \right\rangle \quad (3.5)$$

The linearity of the problem allows to introduce the localization operators relating the microscopic displacement  $u_i(X, x)$  and strain  $\varepsilon_{ij}(X, x)$  to the macro-strain components, as follows:

$$\begin{aligned} u_i(X, x) &= H^E_{ijk}(x) E_{jk}(X) + H^K_{ijkl}(x) K_{jkl}(X) \\ \varepsilon_{ij}(X, x) &= A^E_{ijkl}(x) E_{kl}(X) + A^K_{ijklm}(x) K_{klm}(X) \end{aligned} \quad (3.6)$$

Where  $H^E(x), H^K(x)$  in Eq. (3.6) stand for the localizations tensors relating micro displacements to the first and second gradient strain tensors  $E(X)$  and  $K(X)$  respectively. Accordingly,  $A^E(x), A^K(x)$  represent the localizations tensors relating the micro strains to the first and second gradient strain tensors  $E(X)$  and  $K(X)$ . By definition of the homogenized constitutive law, the average stress and hyper stress tensors are evaluated as the variation of the internal energy in function of first and second gradient macro-deformation to obtain the following:

$$\begin{aligned} \Sigma_{ij}^{dyn} &= C_{ijdl}^{\text{hom}} E_{dl} + B_{ijrst}^{\text{hom}} K_{rst} \\ S_{ijk}^{dyn} &= D_{ijkdl}^{\text{hom}} E_{dl} + A_{ijkrst}^{\text{hom}} K_{rst} \end{aligned} \quad (3.7)$$

### Chapter 3: On the role of second gradient constitutive parameters in the static and dynamic analysis of heterogeneous media with micro-inertia effects

Where  $C_{ijkl}^{\text{hom}}$ ,  $B_{ijst}^{\text{hom}}$ ,  $D_{ijkl}^{\text{hom}}$  and  $A_{ijklst}^{\text{hom}}$  are the first order, the coupling between the first and the second order stiffness tensors respectively, while  $\Sigma_{ij}$  and  $S_{ijk}$  stand accordingly for the Cauchy and for the hyperstress tensor.

In the sequel, we use Eq. (3.5) along with the Hamilton's principle to derive the dynamic equation of motion accounting for micro inertia terms.

#### 3.2.2 Hamilton principle based second gradient mechanics

In order to derive the macro equation of motion we use Hamilton's principle, as follows:

$$\delta \iint_{V,t} (T - P) dV dt = \iint_{\partial V,t} Q_i \delta U_i dS dt \quad (3.8)$$

Where  $V$  in Eq. (3.8) stands for the volume,  $Q_i$  for the traction exerted on the boundary of the volume  $V$ , and  $P$  and  $T$  are the deformation and kinetic energy densities respectively. The deformation energy density is defined as:

$$P = \frac{1}{2} \langle \varepsilon_{ij} \sigma_{ij} \rangle, T = \frac{1}{2} \langle \rho \dot{u}_i \dot{u}_i \rangle \quad (3.9)$$

Using Eq. (3.5) we write the expressions of deformation energy as a function of the macroscopic strains and of the micro-inertia components, as follows:

$$P = \frac{1}{2} E_{ij} \Sigma_{ij} + \frac{1}{2} K_{ijk} S_{ijk} + P' \quad (3.10)$$

$$P' = -\frac{1}{2} \left\langle \rho \dot{u}_i \left( u_i - E_{ij} x_j - \frac{1}{2} K_{ijk} x_j x_k \right) \right\rangle = P'(E, \dot{E}, K, \dot{K}) = P'(E, \dot{E}, \nabla E)$$

Where  $P'$  represents the deformation energy part related to micro-inertia terms. Accordingly, we write the kinetic energy part as a function of the macro-displacement components and mixed macroscopic displacement and microscopic fluctuation displacement term  $\hat{u}_i$  terms contained in  $T'$ , as follows:

$$T = \frac{1}{2} \langle \rho \dot{u}_i \dot{u}_i \rangle = \frac{1}{2} \langle \rho \dot{U}_i \dot{U}_i \rangle + T' \quad (3.11)$$

Where  $T'$  in Eq. (3.11) relates to microscopic and higher gradient strain terms, as shown in the sequel. In particular, in order to derive an explicit form of  $T'$ , we decompose the local displacement in the RVE into a displacement linear in the imposed macroscopic strain  $U_i^0$  as in Eq. (3.3) and a microscopic fluctuation term  $\hat{u}_i$  as follows :

Chapter 3: On the role of second gradient constitutive parameters in the static and dynamic analysis of heterogeneous media with micro-inertia effects

$$\begin{aligned} u_i &= U_i^0 + \hat{u}_i \quad \forall x \in \Omega \\ u_i &= U_i^0 = E_{ij}x_j + \frac{1}{2}K_{ijk}x_jx_k \quad \forall x \in \partial\Omega \end{aligned} \quad (3.12)$$

By substituting the displacement field of Eq. (3.12) in the kinetic energy expression of Eq. (3.11) we get the macro and the micro part of the kinetic energy, as follows:

$$T = \frac{1}{2} \langle \rho \dot{U}_i^0 \dot{U}_i^0 \rangle + \langle \rho (\dot{\hat{u}}_i) \dot{U}_i^0 \rangle + \frac{1}{2} \langle \rho (\dot{\hat{u}}_i) (\dot{\hat{u}}_i) \rangle \quad (3.13)$$

The first part in the kinetic energy definition, Eq. (3.13), defines the macroscopic kinetic energy and the second part the coupling between the macroscopic and microscopic components, while the last term stands for purely microscopic energy contributions. Note that, according to the micromechanics assumption, tensors  $E_{ij}$  and  $K_{ijk}$  are constant over the RVE.

As a result, the average density of the kinetic energy of the region  $\frac{1}{2} \langle \rho \dot{U}_i^0 \dot{U}_i^0 \rangle$  and the density of the macro kinetic energy, scalar  $\frac{1}{2} \langle \rho \rangle \dot{U}_i \dot{U}_i$  are equal. Therefore, it follows from (3.13) the expansion of the macro and micro kinetic energy terms successively as:

$$\begin{aligned} T &= \frac{1}{2} \langle \rho \rangle \dot{U}_i \dot{U}_i + \langle \rho (\dot{\hat{u}}_i) E_{ij} x_j \rangle + \frac{1}{2} \langle \rho (\dot{\hat{u}}_i) K_{ijk} x_j x_k \rangle + \frac{1}{2} \langle \rho (\dot{\hat{u}}_i) (\dot{\hat{u}}_i) \rangle \\ T' &= \langle \rho (\dot{\hat{u}}_i) \dot{E}_{ij} x_j \rangle + \frac{1}{2} \langle \rho (\dot{\hat{u}}_i) \dot{K}_{ijk} x_j x_k \rangle + \frac{1}{2} \langle \rho (\dot{\hat{u}}_i) (\dot{\hat{u}}_i) \rangle = T'(\dot{E}_{ij}, \dot{K}_{ijk}) \end{aligned} \quad (3.14)$$

We next substitute into Eq. (3.8) the expression of deformation and kinetic energy to obtain the macro equation of motion:

$$\delta \iint_{V,t} \left( \frac{1}{2} \langle \rho \rangle \dot{U}_i \dot{U}_i + T' - \left( \frac{1}{2} E_{ij} \Sigma_{ij} + \frac{1}{2} K_{ijk} S_{ijk} + P' \right) \right) dV dt = 0 \quad (3.15)$$

We simplify Eq. (3.15) using integration by parts of each component as detailed in Eqs. (2.A.3-2.A.18) of the **Appendix 2.A**. Thereupon, we obtain the equation of motion which contains surface ( $S$ ) and volume ( $V$ ) integrals as follows:

Chapter 3: On the role of second gradient constitutive parameters in the static and dynamic analysis of heterogeneous media with micro-inertia effects

$$\begin{aligned}
& \int \Sigma_{ij,j} \delta U_i \delta V - \int S_{ijk,jk} \delta U_i \delta V + \int \frac{\partial}{\partial X_j} \left( \frac{\partial P'}{\partial E_{ij}} \right) \delta U_i \delta V + \int \frac{\partial}{\partial X_j} \left( \frac{\partial^2}{\partial t^2} \left( \frac{\partial P'}{\partial \ddot{E}_{ij}} \right) \right) \delta U_i \delta V \\
& + \int \frac{\partial}{\partial X_j} \frac{\partial}{\partial t} \left( \frac{\partial T'}{\partial \dot{E}_{ij}} \right) \delta U_i \delta V - \int \frac{\partial^2}{\partial X_j \partial X_k} \left( \frac{\partial^2}{\partial t^2} \left( \frac{\partial P'}{\partial \ddot{K}_{ijk}} \right) \right) \delta U_i \delta V - \int \left( \frac{\partial^2}{\partial X_j \partial X_k} \left( \frac{\partial P'}{\partial K_{ij}} \right) \right) \delta U_i \delta V \\
& - \int \frac{\partial}{\partial X_j} \left( \frac{\partial}{\partial X_k} \left( \frac{\partial}{\partial t} \left( \frac{\partial T'}{\partial \dot{K}_{ijk}} \right) \right) \right) \delta U_i \delta V \\
& - S_1 - S_{2a} - S_{2b} + S_3 - S_{4a} - S_{4b} - S_{4c} - S_{4d1} - S_{4d2} + S_{5a} + S_{5b} = \int \langle \rho \rangle \delta U_i \ddot{U}_i \delta V
\end{aligned} \tag{3.16}$$

Where the scalars  $S_i$  therein are surface integrals, detailed in the **Appendix 2.A**.

Separating the volume integrals from the surface integrals ( $S$ ) in Eq. (3.16), we obtain the following macroscopic equation of motion:

$$\Sigma_{ij,j} - S_{ijk,jk} + F_i = \langle \rho \rangle \ddot{U}_i \tag{3.17}$$

Where in Eq. (3.17) the Cauchy and the hyperstress tensors are calculated in the static situation (following the Hamilton principle formulation [Wang and Sun, 2006]), as follows:

$$\begin{aligned}
\Sigma_{ij} &= \frac{1}{2} \langle A_{krj}^E C_{krmn} A_{mndl}^E + A_{rsdl}^E C_{rsmn} A_{mnij}^E \rangle E_{dl} + \frac{1}{2} \langle A_{klj}^E C_{klmn} A_{mnrst}^K + A_{klrst}^K C_{klmn} A_{mnij}^E \rangle K_{rst} \\
S_{ijk} &= \frac{1}{2} \langle A_{rsdl}^E C_{rsmn} A_{mnijk}^K + A_{rsijk}^K C_{rsmn} A_{mndl}^E \rangle E_{dl} + \frac{1}{2} \langle A_{pfijk}^K C_{pfmn} A_{mnrst}^K + A_{dlrst}^K C_{dlnm} A_{mnijk}^K \rangle K_{rst}
\end{aligned} \tag{3.18}$$

In the Hamilton formulation of Eq. (3.17), the dynamic part is contained in the effective body force term  $F_i$  defined as follows (it does not depend on the constitutive law):

$$F_i = \frac{\partial}{\partial X_j} \left( \left( \frac{\partial P'}{\partial E_{ij}} \right) + \frac{\partial^2}{\partial t^2} \left( \frac{\partial P'}{\partial \ddot{E}_{ij}} \right) + \frac{\partial}{\partial t} \left( \frac{\partial T'}{\partial \dot{E}_{ij}} \right) + \frac{\partial}{\partial X_k} \left( - \left( \frac{\partial^2}{\partial t^2} \left( \frac{\partial P'}{\partial \ddot{K}_{ijk}} \right) \right) - \frac{\partial}{\partial t} \left( \frac{\partial T'}{\partial \dot{K}_{ijk}} \right) - \left( \frac{\partial P'}{\partial K_{ijk}} \right) \right) \right) \tag{3.19}$$

The micro-inertia force of Eq. (3.19) is calculated as a function of the displacement and strain localization operators introduced in Eq. (3.6) detailed in the **Appendix 2.A.3** as follows:

$$\begin{aligned}
F_i &= \frac{\partial}{\partial X_j} \left( \frac{1}{2} \ddot{E}_{mn} \langle \rho (H_{inn}^E x_j + H_{mij}^E x_n - 2\delta_i^m x_j x_n) \rangle + \frac{1}{2} \ddot{K}_{rsk} \langle \rho \left( H_{irsk}^K x_j + \frac{1}{2} H_{rij}^E x_s x_k - \delta_i^r x_s x_j x_k \right) \rangle \right) \\
&- \frac{\partial^2}{\partial X_j \partial X_k} \left( \ddot{E}_{rs} \left\langle \frac{\rho}{2} \left( H_{rij}^K x_s + \frac{1}{2} H_{irs}^E x_j x_k - \delta_i^r x_s x_j x_k \right) \right\rangle + \frac{1}{4} \ddot{K}_{rst} \langle \rho (H_{rij}^K x_s x_t + H_{irst}^K x_j x_k - \delta_i^r x_s x_j x_t) \rangle \right)
\end{aligned} \tag{3.20}$$

In the sequel, we derive the dynamic equilibrium based on the total higher gradient potential energy in the presence of micro-inertia effects.

### 3.2.3 Dynamic higher gradient energy formulation of the constitutive law

In the Dynamic Higher Gradient Energy (DHGE) formulation, we compute the effective dynamic constitutive law by deriving the expression of the internal energy. Inserting the localization tensors of Eq. (3.6) back into Eq. (3.5) enables to write the total internal energy as a function of the macro-strain parameters in Eq. (3.21), as follows:

$$\begin{aligned}
 2.W^{\text{int}}(E, K) &= (E_{ij} \cdot \Sigma_{ij} + K_{ijk} \cdot S_{ijk}) = \langle \varepsilon_{ij} \sigma_{ij} \rangle + \left\langle \rho \ddot{u}_i \left( u_i - E_{ij} x_j - \frac{1}{2} K_{ijk} x_j x_k \right) \right\rangle \\
 &= \left\langle A_{ijkl}^E E_{kl} \cdot C_{ijmn} \cdot A_{mnpq}^E E_{rs} + A_{ijkl}^E \cdot E_{kl} C_{ijmn} A_{mnpq}^K K_{rst} + A_{ijkl}^K K_{klf} C_{ijmn} A_{mnpq}^E E_{rs} + A_{ijkl}^K K_{klf} C_{ijmn} A_{mnpq}^K K_{rst} \right\rangle \\
 &+ \left\langle \rho \left( \begin{aligned} &H_{ijk}^E \ddot{E}_{jk} H_{iqr}^E E_{qr} + H_{ijk}^E \ddot{E}_{jk} H_{irst}^K K_{rst} - H_{ijk}^E \ddot{E}_{jk} E_{iq} x_q - \frac{1}{2} H_{ijk}^E \ddot{E}_{jk} K_{iqr} x_q x_r \\ &+ H_{ijkl}^K \ddot{K}_{jkl} H_{iqr}^E E_{qr} + H_{ijkl}^K \ddot{K}_{jkl} H_{irst}^K K_{rst} - H_{ijkl}^K \ddot{K}_{jkl} E_{iq} x_q - \frac{1}{2} H_{ijkl}^K \ddot{K}_{jkl} K_{iqr} x_q x_r \end{aligned} \right) \right\rangle \quad (3.21)
 \end{aligned}$$

The first order macro stress tensor and the second gradient tensor are obtained by deriving the expression of the energy (Eq. (3.21)) with respect to the macro-deformation of the first and of the second gradient respectively (the derivations are detailed in **Appendix 2.B**):

$$\begin{aligned}
 \Sigma_{ij}^{\text{dyn}} &= \frac{\partial W^{\text{int}}(E, K, \ddot{E}, \ddot{K})}{\partial E_{ij}} + \frac{\partial^2}{\partial t^2} \left( \frac{\partial W^{\text{int}}(E, K, \ddot{E}, \ddot{K})}{\partial \ddot{E}_{ij}} \right) \\
 &= E_{dl} \left\langle \frac{1}{2} (A_{krij}^E C_{krmn} A_{mndl}^E + A_{rsdl}^E \cdot C_{rsmn} \cdot A_{mnij}^E) \right\rangle + K_{rst} \left\langle \frac{1}{2} (A_{klj}^E C_{klmn} A_{mnrst}^K + A_{klrst}^K C_{klmn} A_{mnij}^E) \right\rangle \\
 &+ \ddot{E}_{dl} \left\langle \frac{\rho}{2} (H_{qdl}^E H_{qij}^E + H_{kij}^E H_{kdl}^E - H_{idl}^E x_j - H_{dij}^E x_l) \right\rangle + \\
 &\quad \ddot{K}_{rst} \left\langle \frac{\rho}{2} (H_{qrst}^K H_{qij}^E + H_{krst}^K H_{kij}^E - H_{irst}^K x_j - \frac{1}{2} H_{rij}^E x_s x_t) \right\rangle \quad (3.22) \\
 S_{ijk} &= \frac{\partial W^{\text{int}}(E, K, \ddot{E}, \ddot{K})}{\partial K_{ijk}} + \frac{\partial^2}{\partial t^2} \frac{\partial W^{\text{int}}(E, K, \ddot{E}, \ddot{K})}{\partial \ddot{K}_{ijk}} \\
 &= \left\langle \frac{1}{2} A_{rsdl}^E C_{rsmn} A_{mnijk}^K + \frac{1}{2} A_{rsijk}^K C_{rsmn} A_{mndl}^E \right\rangle \cdot E_{dl} + \left\langle \frac{1}{2} A_{pfijk}^K C_{pfmn} A_{mnrst}^K + \frac{1}{2} A_{dlrst}^K C_{dlmn} A_{mnijk}^K \right\rangle \cdot K_{rst} \\
 &+ \left\langle \frac{\rho}{2} (H_{qdl}^E H_{qijk}^K + H_{rdl}^E H_{rijk}^K - \frac{1}{2} H_{idl}^E x_k x_j - H_{dijk}^K x_l) \right\rangle \cdot \ddot{E}_{dl} + \\
 &\quad \left\langle \frac{\rho}{2} (H_{lrst}^K H_{lijk}^K + H_{drst}^K H_{dijk}^K - \frac{1}{2} H_{rijk}^K x_s x_t - \frac{1}{2} H_{irst}^K x_j x_k) \right\rangle \cdot \ddot{K}_{rst}
 \end{aligned}$$

We note that the dynamic part in the macroscopic constitutive expressions in Eq. (3.22) arises from the derivation of the micro-inertia terms with respect to the tensors  $\ddot{E}$  and  $\ddot{K}$ .

Considering a plane harmonic wave solution ( $U = U_0 e^{I \cdot (k \cdot X_1 - wt)}$ ), the second time derivative of the strain and strain gradient are expressed as follows:

$$\begin{pmatrix} \ddot{E} \\ \ddot{K} \end{pmatrix} = -w^2 \begin{pmatrix} E \\ K \end{pmatrix} \quad (3.23)$$

Where  $w$  in Eq. (3.23) is the frequency of the propagating waves. Using Eq. (3.22), we express the homogenized dynamic constitutive tensors in Eq. (3.7), as follows (**Appendix 2.B**):

$$\begin{aligned} C_{ijkl}^{\text{hom,dyn}} &= \left\langle \frac{1}{2} \left( A_{krj}^E C_{krmn} A_{mndl}^E + A_{rsdl}^E C_{rsmn} A_{mnij}^E \right) \right\rangle - w^2 \left\langle \frac{\rho}{2} \begin{pmatrix} H_{qdl}^E H_{qij}^E + H_{kij}^E H_{kdl}^E \\ -H_{idl}^E x_j - H_{dij}^E x_l \end{pmatrix} \right\rangle \\ B_{ijrst}^{\text{hom,dyn}} &= \left\langle \frac{1}{2} \left( A_{klj}^E C_{klmn} A_{mnrst}^K + A_{klrst}^K C_{klmn} A_{mnij}^E \right) \right\rangle - w^2 \left\langle \frac{\rho}{2} \begin{pmatrix} H_{qrst}^K H_{qij}^E + H_{krst}^K H_{kij}^E \\ -H_{irst}^K x_j - \frac{1}{2} H_{rij}^E x_s x_t \end{pmatrix} \right\rangle \\ D_{ijkl}^{\text{hom,dyn}} &= \left\langle \frac{1}{2} A_{rsdl}^E C_{rsmn} A_{mnijk}^K + \frac{1}{2} A_{rsijk}^K C_{rsmn} A_{mndl}^E \right\rangle - w^2 \left\langle \frac{\rho}{2} \begin{pmatrix} H_{qdl}^E H_{qijk}^K + H_{rdl}^E H_{rijk}^K \\ -\frac{1}{2} H_{idl}^E x_k x_j - H_{dijk}^K x_l \end{pmatrix} \right\rangle = B_{dijk}^{\text{hom,dyn}} \\ A_{ijkrst}^{\text{hom,dyn}} &= \left\langle \frac{1}{2} A_{pfjk}^K C_{pfmn} A_{mnrst}^K + \frac{1}{2} A_{dlrst}^K C_{dlmn} A_{mnijk}^K \right\rangle - w^2 \left\langle \frac{\rho}{2} \begin{pmatrix} H_{lrst}^K H_{lijk}^K + H_{drst}^K H_{dijk}^K \\ -\frac{1}{2} H_{rijk}^K x_s x_t - \frac{1}{2} H_{irst}^K x_j x_k \end{pmatrix} \right\rangle \end{aligned} \quad (3.24)$$

### 3.3 Results

#### 3.3.1 Composite laminated media

We apply the previously elaborated methodologies to the case of composite materials with a periodic, layered microstructure. To that scope, we define below the attributes of the unit-cell structure, its total length set to  $L = 1m$ . Fig. 3.2 summarizes the geometric parameters characterizing the unit-cell, as well as the material parameters for both two phases.

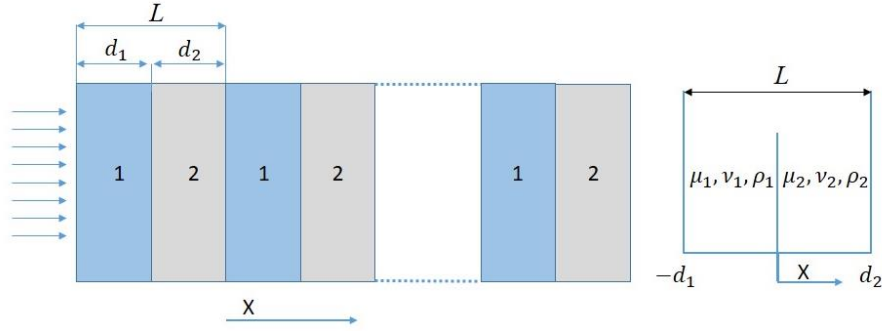


Figure 3.2: Periodic layered composite material geometry (left) and its unit cell material parameters (right).

In Fig. 3.2,  $\mu_1, \mu_2$  and  $\nu_1, \nu_2$  stand for the shear moduli and for the Poisson's ratio;  $\rho_1, \rho_2$  and  $d_1, d_2$  represent the mass density and the thickness of the first and of the second layers. The micro-displacement field is represented with superscripts for each medium and subscripts for the direction of each displacement component, as follows:

$$u^1 = \begin{bmatrix} u_1^1 \\ u_2^1 \end{bmatrix}, u^2 = \begin{bmatrix} u_1^2 \\ u_2^2 \end{bmatrix} \quad (3.25)$$

### 3.3.1.1 Identification of micromechanical constants upon normal deformations

We subsequently determine the expressions of the localization operators of Eq. (3.6) for the case of normal macroscopic deformations. In such a deformation mode, the macro displacement field is along the  $X$  direction, so that it holds:

$$U_1 = f(X_1) \Rightarrow E_{11} \neq 0, K_{111} \neq 0 \quad (3.26)$$

The micro-displacements follow the definition of Eq. (3.25) and (3.6), where the coefficients of the localization tensors are denoted with  $a_i$  and  $b_i$  for the first and second layer successively, as follows:

Chapter 3: On the role of second gradient constitutive parameters in the static and dynamic analysis of heterogeneous media with micro-inertia effects

$$\begin{aligned}
 u_1^1(x) &= \begin{bmatrix} H_{111}^{E\ 1} & H_{1111}^{K\ 1} \end{bmatrix} \cdot \begin{bmatrix} E_{11} \\ K_{111} \end{bmatrix} = \begin{bmatrix} a_0 + a_1x & a_2 + a_3x + a_4 \frac{x^2}{2} \end{bmatrix} \cdot \begin{bmatrix} E_{11} \\ K_{111} \end{bmatrix} \\
 \Rightarrow \left\{ \begin{aligned} \varepsilon_{11}^1(x) &= \begin{bmatrix} A_{1111}^{E\ 1} & A_{11111}^{K\ 1} \end{bmatrix} \cdot \begin{bmatrix} E_{11} \\ K_{111} \end{bmatrix} = \begin{bmatrix} a_1 & a_3 + a_4x \end{bmatrix} \cdot \begin{bmatrix} E_{11} \\ K_{111} \end{bmatrix} \\
 u_1^2(x) &= \begin{bmatrix} H_{111}^{E\ 2} & H_{1111}^{K\ 2} \end{bmatrix} \cdot \begin{bmatrix} E_{11} \\ K_{111} \end{bmatrix} = \begin{bmatrix} b_0 + b_1x & b_2 + b_3x + b_4 \frac{x^2}{2} \end{bmatrix} \cdot \begin{bmatrix} E_{11} \\ K_{111} \end{bmatrix} \\
 \Rightarrow \left\{ \begin{aligned} \varepsilon_{11}^2(x) &= \begin{bmatrix} A_{1111}^{E\ 2} & A_{11111}^{K\ 2} \end{bmatrix} \cdot \begin{bmatrix} E_{11} \\ K_{111} \end{bmatrix} = \begin{bmatrix} b_1 & b_3 + b_4x \end{bmatrix} \cdot \begin{bmatrix} E_{11} \\ K_{111} \end{bmatrix}
 \end{aligned} \right. \quad (3.27)
 \end{aligned}$$

Eq. (3.27) contains a total of 10 unknown parameters  $a_i$  and  $b_i$ . The micro-stress developed in each inner material phase is given as a function of the micro-strains of Eq. (3.27), as follows:

$$\left\{ \begin{aligned} \sigma_{11}^1(x) &= (\lambda_1 + 2\mu_1) \cdot \varepsilon_{11}^1(x) = (\lambda_1 + 2\mu_1) \cdot \begin{bmatrix} a_1 & a_3 + a_4x \end{bmatrix} \cdot \begin{bmatrix} E_{11} \\ K_{111} \end{bmatrix} \\
 \sigma_{11}^2(x) &= (\lambda_2 + 2\mu_2) \cdot \varepsilon_{11}^2(x) = (\lambda_2 + 2\mu_2) \cdot \begin{bmatrix} b_1 & b_3 + b_4x \end{bmatrix} \cdot \begin{bmatrix} E_{11} \\ K_{111} \end{bmatrix}
 \end{aligned} \right. \quad (3.28)$$

Where  $\lambda$  in Eq. (3.28) defines the first Lamé coefficient, equal to  $2\mu\nu/(1-2\nu)$ . Using Eq. (3.2) we get  $E_{11} = \frac{\partial U_1}{\partial x}$ ,  $K_{111} = \frac{\partial^2 U_1}{\partial x^2}$  for the first and second gradient macro strains. We use the interface continuity condition for the displacements, upon which we obtain two equations. Accordingly, using the boundary conditions for the displacement field, we retrieve four additional equilibrium equations, noting that first and second gradient terms  $E_{ij}$  and  $K_{ijk}$  can be treated independent. The body forces are null within the cell, so that the continuity of stresses and stress gradients provides us with a total of three additional equations (two and one respectively). The boundary and interface conditions are summarized as follows:

$$\left\{ \begin{aligned} u_1^1(0) &= u_2^1(0) \\ u_1^1(-d_1) &= -E_{11}d_1 + K_{111} \frac{d_1^2}{2}, u_2^1(d_2) = E_{11}d_2 + K_{111} \frac{d_2^2}{2} \\ \sigma_{11}^1(0) &= \sigma_{11}^2(0), \frac{\partial \sigma_{11}^1}{\partial x}(0) = \frac{\partial \sigma_{11}^2}{\partial x}(0)
 \end{aligned} \right. \quad (3.29)$$

### Chapter 3: On the role of second gradient constitutive parameters in the static and dynamic analysis of heterogeneous media with micro-inertia effects

The 9 equations in the set of Eqs. (3.29) do however not suffice to calculate the 10 coefficients appearing in Eq. (3.27). As an additional condition, we require the average of the microscopic deformations for the first and second gradient to be equal to the corresponding macroscopic deformations, as follows:

$$\langle \varepsilon_{11} \rangle_{\Omega} = E_{11}, \langle \nabla \varepsilon_{11} \rangle_{\Omega} = K_{111} \quad (3.30)$$

**Remark:** note that we impose the quadratic displacement only to the RVE boundary and not in the entire volume; this entails that the average (in the volume sense) of the fluctuating displacement does vanish only on the RVE boundary but not necessarily within the whole volume. We use the condition that the average microscopic strains  $\varepsilon_{ij}$  and their gradient  $\nabla_k(\varepsilon_{ij})$  are equal to the macroscopic strain  $E_{ij}$  and strain gradient  $K_{ijk}$  components respectively similarly to (Boutin, 1996), so that the fluctuation of the strain and strain gradient has zero mean values.

Note that Eq. (3.30) provides solely one additional dependent condition, as the average of micro-strains leads to a condition that is a linear combination of the ones contained in Eq. (3.29). Solving the system of Eqs. (3.29, 3.30) with the use of Eq. (3.27) and (3.28), we obtain the following expressions of the microscopic coefficients  $a_i$  and  $b_i$ :

$$\begin{aligned}
 a_0 &= -\frac{d_1 d_2 ((\lambda_1 + 2\mu_1) - (\lambda_2 + 2\mu_2))}{(\lambda_1 + 2\mu_1) d_2 + d_1 (\lambda_2 + 2\mu_2)}, a_1 = \frac{(\lambda_2 + 2\mu_2)(d_1 + d_2)}{(\lambda_1 + 2\mu_1) d_2 + d_1 (\lambda_2 + 2\mu_1)}, \\
 a_2 &= \frac{d_2 d_1 ((\lambda_1 + 2\mu_1)^2 d_2 d_1 + (\lambda_1 + 2\mu_1)(\lambda_2 + 2\mu_2)(d_1^2 - d_2 d_1 + L d_1) + d_1 d_2 (\lambda_2 + 2\mu_2)^2)}{2((\lambda_1 + 2\mu_1) d_2 + d_1 (\lambda_2 + 2\mu_2))^2}, \\
 a_3 &= -\frac{(\lambda_2 + 2\mu_2)(d_1 (\lambda_2 + 2\mu_2)(d_1^2 - d_2^2 + L d_1) + d_2 (\lambda_1 + 2\mu_1)(d_1^2 + d_2 d_1))}{2((\lambda_1 + 2\mu_1) d_2 + d_1 (\lambda_2 + 2\mu_2))^2}, \\
 a_4 &= \frac{(\lambda_2 + 2\mu_2) L}{(\lambda_1 + 2\mu_1) d_2 + d_1 (\lambda_2 + 2\mu_2)} \\
 b_0 &= -\frac{d_1 d_2 ((\lambda_1 + 2\mu_1) - (\lambda_2 + 2\mu_2))}{(\lambda_1 + 2\mu_1) d_2 + d_1 (\lambda_2 + 2\mu_2)}, b_1 = \frac{(\lambda_1 + 2\mu_1)(d_1 + d_2)}{(\lambda_1 + 2\mu_1) d_2 + d_1 (\lambda_2 + 2\mu_2)}, \\
 b_2 &= \frac{d_2 d_1 ((\lambda_1 + 2\mu_1)^2 d_2 d_1 + (\lambda_1 + 2\mu_1)(\lambda_2 + 2\mu_2)(d_1^2 - d_2 d_1 + L d_1) + d_1 d_2 (\lambda_2 + 2\mu_2)^2)}{2((\lambda_1 + 2\mu_1) d_2 + d_1 (\lambda_2 + 2\mu_2))^2}, \\
 b_3 &= -\frac{(\lambda_1 + 2\mu_1)(d_1 (\lambda_2 + 2\mu_2)(L d_1 - d_2^2 + d_1^2) + d_2 (\lambda_1 + 2\mu_1)(d_1^2 + d_2 d_1))}{2((\lambda_1 + 2\mu_1) d_2 + d_1 (\lambda_2 + 2\mu_2))^2}, \\
 b_4 &= \frac{(\lambda_1 + 2\mu_1) L}{(\lambda_1 + 2\mu_1) d_2 + d_1 (\lambda_2 + 2\mu_2)}
 \end{aligned} \tag{3.31}$$

### 3.3.1.2 Identification of micromechanical constants upon transverse deformations

In the transverse deformation case, the displacement field is parallel to the direction of the layers, so that  $U_2 = f(X_1) \Rightarrow E_{21} \neq 0, K_{211} \neq 0$ . Writing the micro-displacements as a function of the macro-strain in each layer through the localization operators of Eq. (3.6), we obtain:

$$\begin{aligned}
 u_2^1(x_1) &= \begin{bmatrix} H_{212}^{E \ 1} & H_{2121}^{K \ 1} \end{bmatrix} \cdot \begin{bmatrix} E_{21} \\ K_{211} \end{bmatrix} = \begin{bmatrix} a_0 + a_1 x_1 & a_2 + a_3 x_1 + a_4 \frac{x_1^2}{2} \end{bmatrix} \cdot \begin{bmatrix} E_{21} \\ K_{211} \end{bmatrix} \\
 u_2^2(x_1) &= \begin{bmatrix} H_{212}^{E \ 2} & H_{2121}^{K \ 2} \end{bmatrix} \cdot \begin{bmatrix} E_{21} \\ K_{211} \end{bmatrix} = \begin{bmatrix} b_0 + b_1 x_1 & b_2 + b_3 x_1 + b_4 \frac{x_1^2}{2} \end{bmatrix} \cdot \begin{bmatrix} E_{21} \\ K_{211} \end{bmatrix} \\
 u_1^1(x_2) &= u_1^2(x_2) = A x_2 E_{21} + C \frac{x_2^2}{2} K_{211} = \begin{bmatrix} H_{121}^E & H_{1211}^K \end{bmatrix} \cdot \begin{bmatrix} E_{21} \\ K_{211} \end{bmatrix}
 \end{aligned} \tag{3.32}$$

Eq. (3.32) contains a total of 12 unknowns. The micro-strains field and its gradient are computed using Eq. (3.32), as follows:

Chapter 3: On the role of second gradient constitutive parameters in the static and dynamic analysis of heterogeneous media with micro-inertia effects

$$\begin{aligned}
\varepsilon_{21}^1(x_1, x_2) &= \frac{1}{2} \left( \frac{\partial u_2^1}{\partial x_1}(x_1) + \frac{\partial u_1^1}{\partial x_2}(x_2) \right) = \begin{bmatrix} A_{2121}^E & A_{21211}^K \end{bmatrix} \begin{bmatrix} E_{21} \\ K_{211} \end{bmatrix} \\
&= \begin{bmatrix} \frac{1}{2}(a_1 + A) & \frac{1}{2}(a_3 + a_4 x_1 + Cx_2) \end{bmatrix} \begin{bmatrix} E_{21} \\ K_{211} \end{bmatrix} \\
\varepsilon_{21,1}^1 &= \frac{1}{2}(a_4 K_{211}), \varepsilon_{21,2}^1 = \frac{1}{2}(CK_{211}) \\
\varepsilon_{21}^2(x_1, x_2) &= \frac{1}{2} \left( \frac{\partial u_2^2}{\partial x_1}(x_1) + \frac{\partial u_1^2}{\partial x_2}(x_2) \right) = \begin{bmatrix} A_{2121}^E & A_{21211}^K \end{bmatrix} \begin{bmatrix} E_{21} \\ K_{211} \end{bmatrix} \\
&= \begin{bmatrix} \frac{1}{2}(b_1 + A) & \frac{1}{2}(b_3 + b_4 x_1 + Cx_2) \end{bmatrix} \begin{bmatrix} E_{21} \\ K_{211} \end{bmatrix} \\
\varepsilon_{21,1}^2 &= \frac{1}{2}(b_4 K_{211}), \varepsilon_{21,2}^2 = \frac{1}{2}(CK_{211})
\end{aligned} \tag{3.33}$$

Since the first and second gradient micro-strains in Eq. (3.33) are symmetric tensors, we require that the localization tensors of Eq. (3.6) enjoy the following symmetry properties:

$$\begin{aligned}
H_{212}^E &= H_{221}^E, H_{112}^E = H_{121}^E \\
A_{2121}^E &= A_{1221}^E, A_{21211}^K = A_{12211}^K
\end{aligned} \tag{3.34}$$

Using Eq. (3.33), we compute the micro-stress developed in each of the inner material phases, as follows:

$$\begin{aligned}
\sigma_{21}^1(x_1, x_2) &= 2\mu_1 \cdot \varepsilon_{21}^1(x_1, x_2) = 2\mu_1 (a_1 E_{21} + a_3 K_{211} + a_4 x_1 K_{211} + A E_{21} + C x_2 K_{211}) \\
\sigma_{21}^2(x_1, x_2) &= 2\mu_2 \cdot \varepsilon_{21}^2(x_1, x_2) = 2\mu_2 (b_1 E_{21} + b_3 K_{211} + b_4 x_1 K_{211} + A E_{21} + C x_2 K_{211})
\end{aligned} \tag{3.35}$$

Where the first and second gradient macro-strain components entering Eq. (3.33) are defined as follows (Eq. (3.2)):

$$\begin{aligned}
E_{21} &= \frac{1}{2} \left( \frac{\partial U_2}{\partial X_1} + \frac{\partial U_1}{\partial X_2} \right), E_{11} = 0, E_{22} = 0 \\
K_{211} &= \frac{\partial E_{12}}{\partial X_1}, K_{122} = 0, K_{112} = 0
\end{aligned} \tag{3.36}$$

In order to calculate the constants  $a_i$  and  $b_i$ , we use the continuity conditions for the displacement at the interface, which provide two equations; the boundary conditions for the displacements provide 4 equations and the continuity of stress and stress gradients at the interface provide two and one equilibrium equation respectively. What is more, we use the

average of the microscopic first gradient deformations and the average of the microscopic second gradient deformations to be equal to the corresponding macroscopic ones, as follows:

$$\begin{aligned}
 u_2^1(0) &= u_2^2(0) \\
 u_2^1(-d_1) &= -E_{21}d_1 + K_{211} \frac{d_1^2}{2}, u_2^2(d_2) = E_{21}d_2 + K_{211} \frac{d_2^2}{2} \\
 \sigma_{21}^1(0) &= \sigma_{21}^2(0), \frac{\partial \sigma_{21}^1}{\partial x_1}(0) = \frac{\partial \sigma_{21}^2}{\partial x_1}(0) \\
 \langle \varepsilon_{21} \rangle &= E_{21}, \langle \varepsilon_{21,1} \rangle = K_{211}, \langle \varepsilon_{12,2} \rangle = K_{122}
 \end{aligned} \tag{3.37}$$

Solving the system of Eq. (3.37) using Eq. (3.33)-(3.36), we obtain the following constants  $a_i$  and  $b_i$  for the transverse deformation mode:

$$\begin{aligned}
 a_0 &= \frac{d_1 d_2 (\mu_1 - \mu_2) (d_1 + d_2 - 3L)}{L(d_1 \mu_2 + d_2 \mu_1)}, a_1 = \frac{(\mu_1 - \mu_2) d_2^2 + ((-d_1 + 3L)\mu_2 + \mu_1(d_1 - 2L))d_2 + Ld_1 \mu_2}{L(d_1 \mu_2 + d_2 \mu_1)} \\
 a_2 &= \frac{d_2 d_1 \left( \frac{d_2 d_1 \mu_1^2}{2} + \left( \frac{d_1^2}{2} + Ld_1 - d_2 \left( L - \frac{d_2}{2} \right) \right) \mu_1 \mu_2 + \frac{d_2 d_1 \mu_2^2}{2} \right)}{(d_1 \mu_2 + d_2 \mu_1)^2}, \\
 a_3 &= -\frac{\mu_2 \left( -d_2^3 \mu_1 + (2L\mu_1 - d_1)d_2^2 + \mu_1 d_1^2 d_2 + 2 \left( L + \frac{d_1}{2} \right) d_1^2 \mu_2 \right)}{2(d_1 \mu_2 + d_2 \mu_1)^2} \\
 a_4 &= \frac{2\mu_2 L}{(d_1 \mu_2 + d_2 \mu_1)}, b_0 = \frac{d_1 d_2 (\mu_1 - \mu_2) (d_1 + d_2 - 3L)}{L(d_1 \mu_2 + d_2 \mu_1)}, \\
 b_1 &= \frac{(-\mu_1 + \mu_2) d_1^2 + ((-d_2 + 3L)\mu_1 + \mu_2(d_2 - 2L))d_2 + Ld_2 \mu_1}{(d_1 \mu_2 + d_2 \mu_1)}, \\
 b_2 &= \frac{d_2 d_1 \left( \frac{d_2 d_1 \mu_1^2}{2} + \left( \frac{d_1^2}{2} + Ld_1 - d_2 \left( L - \frac{d_2}{2} \right) \right) \mu_1 \mu_2 + \frac{d_2 d_1 \mu_2^2}{2} \right)}{(d_1 \mu_2 + d_2 \mu_1)^2}, \\
 b_3 &= -\frac{-d_2^3 \mu_1^2 + (2L\mu_1^2 - d_1 \mu_2 \mu_1) d_2^2 + \mu_1^2 d_1^2 d_2 + (2L + d_1) d_1^2 \mu_2 \mu_1}{2(d_1 \mu_2 + d_2 \mu_1)^2}, \\
 b_4 &= \frac{2\mu_1 L}{(d_1 \mu_2 + d_2 \mu_1)}, A = \frac{2L - d_1 - d_2}{L}, C = 0
 \end{aligned} \tag{3.38}$$

### 3.3.2 Homogenized higher gradient static effective properties

We subsequently analyze the higher gradient static effective properties of the layered media. The latter are independent of the method used for their derivation, as it can be observed

by comparing the Hamilton principle expanded in section 3.2.2 (Eqs. (3.17-3.18)) and the internal energy method in section 3.2.3 (Eqs. (3.22)-(3.24)),  $w = 0$ ).

### 3.3.2.1 Longitudinal mode

We compute the higher gradient constitutive properties of the layered composite of Section 3.3.1 for the case of identical elastic material properties ( $\lambda_1 = \lambda_2 = \lambda, \mu_1 = \mu_2 = \mu$ ), namely Lamé coefficient and shear modulus values used in the elastic law ( $\sigma_{11}^{1,2}(x) = (\lambda_{1,2} + 2\mu_{1,2}) \cdot \varepsilon_{11}^{1,2}(x)$ ). After calculating the constants of the displacement vectors in each layer, we use Eq. (3.18) or the static part of Eq. (3.24) to calculate the homogenized tensors of first gradient elasticity,  $C^{\text{hom}}$  (in  $MPa$ ), the coupling tensor  $B^{\text{hom}}, D^{\text{hom}}$  (in  $MPa \cdot m$ ) and the second gradient tensor  $A^{\text{hom}}$  (in  $MPa \cdot m^2$ ) respectively, as a function of the geometric attributes of the unit-cell. In Eq. (3.39), we provide the corresponding expressions as a function of the layers thickness ratio  $\alpha = d_1 / d_2$  and of the total unit-cell length  $L$  of the cell, as follows:

$$\begin{aligned}
 C_{1111}^{\text{hom}} &= \lambda + 2\mu \\
 B_{1111}^{\text{hom}} = D_{1111}^{\text{hom}} &= \frac{(\lambda + 2\mu)}{2} \left( -\frac{(3\alpha^2 - 1)}{(\alpha + 1)^2} \right) \cdot L \\
 A_{111111}^{\text{hom}} &= \frac{(\lambda + 2\mu)}{3} \left( \frac{(7\alpha^4 + \alpha^3 - 3\alpha^2 + \alpha + 1)}{(\alpha + 1)^4} \right) \cdot L^2
 \end{aligned} \tag{3.39}$$

For layers of identical properties, the set of Eqs. (3.39) provides a first gradient tensor  $C_{1111}^{\text{hom}}$  which is identical to the constitutive tensor of both layers. In Fig. 3.3a, we depict the homogenized tensors as a function of the geometrical ratio  $\alpha = d_1 / d_2$  for equal material moduli in each inner material phase.

What is more, we explore the sensitivity of the second gradient terms on the discrepancies of the inner material properties in the layered composite medium for the case of equal inner layer thickness ( $d_1 = d_2$ ). Thereupon, we calculate the characteristic second gradient length  $l_{e11}(m)$  as a function of the elastic modulus ratio  $\phi = E_2 / E_1$ , plotted in Fig. 3.4a.

$$l_{e_{111}} = \sqrt{\frac{A_{111111}^{\text{hom}}}{C_{1111}^{\text{hom}}}} = 0.72 \cdot L \sqrt{\frac{(\phi^2 + 1.12\phi + 0.322)(\phi^2 + 0.033\phi + 0.041)}{(\phi + 0.67)^3 \phi}} \quad (3.40)$$

The characteristic length of Eq. (3.40) for equal layers thickness and for the first layer being 1.5 times the thickness of the second ( $d_1 = 1.5d_2$ ) is recorded in Fig. 3.4a as a function of the elastic modulus ratio  $\phi$ . The results indicate that the effect of second gradient terms increase when the contrast in the material attributes of the microstructural phases increases.

### 3.3.2.2 Transverse mode

For the case of transverse deformations, we calculate the homogenized constitutive tensors for equal micro-scale material properties using Eq. (3.18) or Eq. (3.24) ( $w=0$ ), as a function of the layers thickness ratio  $\alpha = d_1 / d_2$ , to be:

$$\begin{aligned} C_{2121}^{\text{hom}} &= 2\mu \\ B_{21211}^{\text{hom}} &= D_{21121}^{\text{hom}} = -\frac{\mu}{2} \left( \frac{(5\alpha^2 - 1)}{(\alpha + 1)^2} \right) \cdot L \\ A_{211211}^{\text{hom}} &= \frac{\mu}{24} \left( \frac{(79\alpha^4 + 16\alpha^3 - 6\alpha^2 + 16\alpha + 7)}{(\alpha + 1)^4} \right) \cdot L^2 \end{aligned} \quad (3.41)$$

We depict the dependence of the coupling and second gradient stiffness term of Eq. (3.41) in Fig. 3.3b.

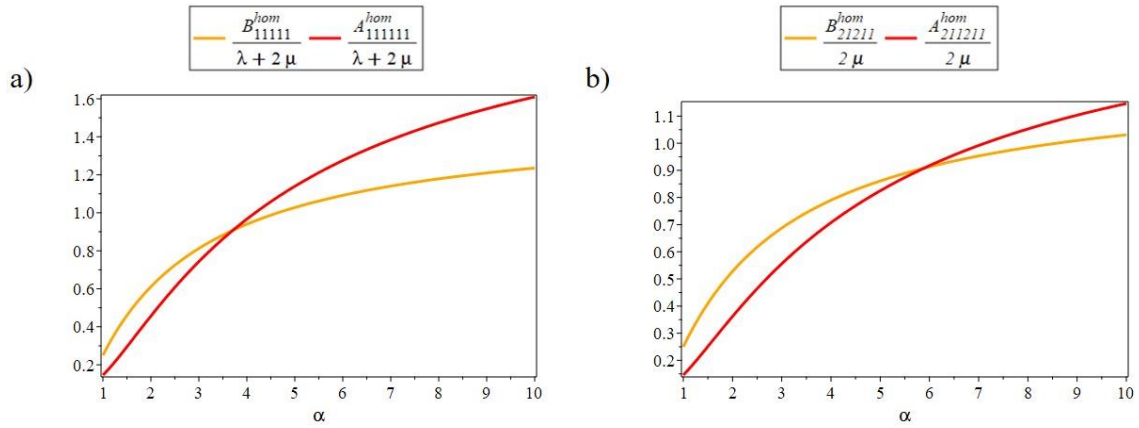


Figure 3.3: Homogenized second gradient and coupling tensors in function of layers thickness ratio  $d_1/d_2$  for longitudinal (a) and for transverse (b).

Fig. 3.3 indicates that upon increasing geometric discrepancies of the layers within the unit-cell, the higher gradient contributions become more significant. We subsequently analyze the sensitivity of the second gradient terms on the moduli ratio value  $\phi = E_2 / E_1$  for the case of equal layer thickness ( $d_1 = d_2$ ). We calculate the characteristic second gradient length  $l_{e_{211}}$  to be:

$$l_{e_{211}} = \sqrt{\frac{A_{211211}^{hom}}{C_{2121}^{hom}}} = 0.175 \cdot L \sqrt{\frac{\phi(\phi + 0.67)(\phi + 0.49)(\phi + 0.031)}{(\phi + 0.67)^2 (1.15 \cdot 10^{-21} + 0.0455 \cdot \phi + 0.0682\phi^2)}} \quad (3.42)$$

The characteristic length  $l_{e_{211}}$  of Eq. (3.42) corresponding to equal layer thickness ( $d_1 = d_2$ ) is depicted in Fig. 3.4b as a function of  $\phi$  along with the case where the thickness of the first layer is 1.5 times the thickness of the second layer.

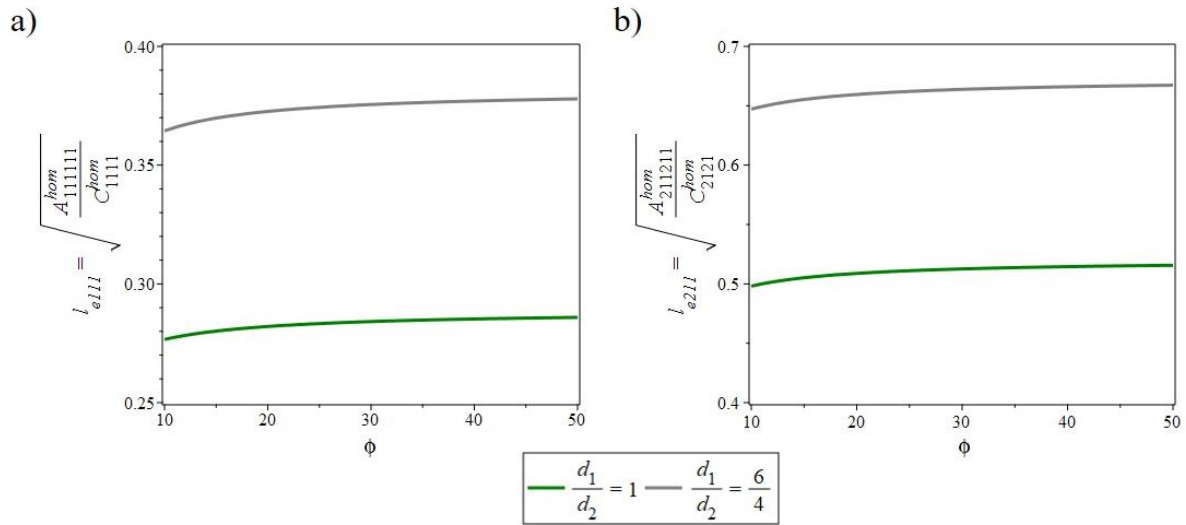


Figure 3.4 : Second gradient characteristic length as a function of the elastic modulus ratio  $\phi$  for the case of longitudinal and b) for transverse deformations (b) for different thickness ratio values.

Fig. 3.4b suggests that as the contrast of the microscale material properties increases, the corresponding significance of second gradient effects increases for the transverse propagation mode. Thereupon, the first gradient is increasingly insufficient to describe the behavior of the medium as the inner contrast of the micro-scale material properties increases, whereas the second gradient significance increases.

### 3.3.3 Wave propagation in layered, periodic media

In the current section, we use the second gradient macroscopic dynamic equation of motion with micro-inertia effects to study the wave propagation characteristics of periodic, composite layered media. For the study, we use both the Hamilton formulation of Section 3.2.2 and the higher gradient energy method of Section 3.2.3 upon longitudinal and transverse deformations. We determine the dispersion characteristics of the propagating longitudinal and shear waves, as function of the propagating wave numbers ( $k$ ). In particular, we compute the phase velocity ( $c$ ), describing the velocity at which the phase of any given frequency ( $\omega$ ) travels within the

Chapter 3: On the role of second gradient constitutive parameters in the static and dynamic analysis of heterogeneous media with micro-inertia effects

medium and the group velocity ( $v_g$ ), which describes the velocity of the envelope shape of the wave amplitudes. The phase and group velocity are defined as follows:

$$c = \frac{w}{k}, v_g = \frac{\partial w}{\partial k} \quad (3.43)$$

For the present study, we consider different material properties for each of the phases within the unit-cell structure of the periodic medium. The material properties of both phases are listed in Table 3.1.

Table 3.1: Geometric and mechanical layers properties the laminate layers.

Properties	First layer	Second layer
Thickness	50%	50%
Poisson's ration	$\nu = 0.3$	$\nu = 0.3$
Shear modulus	$\mu_1 = 80760 \text{ MPa}$	$\mu_2 = 8076 \text{ MPa}$
Mass density	$\rho_1 = 8000 \text{ Kg/m}^3$	$\rho_2 = 800 \text{ Kg/m}^3$

For the computation of the wave propagation attributes, a harmonic wave propagation Ansatz is considered, with a displacement  $U_d$  being a function of the propagating wave numbers and frequency components, as follows:

$$U_d = U_0 e^{i \frac{\xi}{L} (X_1 - ct)} \quad (3.44)$$

In Eq. (3.44),  $U_0$  stands for the displacement amplitude,  $k$  for the wave number and  $c$  for the phase velocity. The wave number is described in a normalized form  $\xi = kL$ , while  $i$  stands for the imaginary number, such that  $i^2 = -1$ . The subscript  $d$  is used to denote the direction of propagation, taking the values one for the longitudinal and two for the transverse.

### 3.3.3.1 Hamilton principle up to second gradient in dynamic state

In the current section, we use the second gradient Hamilton principle formulation of Section 3.2.2 to derive the macro equation of motion and the wave propagation characteristics of the laminated media, using the material properties in Table 3.1. To that purpose, we compute

the homogenized first order stress tensor  $\left( \Sigma_{d1} = \frac{\partial W}{\partial E_{ij}} \right)$ , using Eq. (3.18) for the longitudinal and transverse mode, along with the constants calculated in Eqs. (3.31, 3.38). Thereupon, we obtain:

$$\Sigma_{d1} = U_0 \cdot \xi e^{-I(ct-X1)\xi} (H_1^d \cdot \xi + H_2^d \cdot I) \quad (3.45)$$

Wherein the parameters  $H_1^d$  and  $H_2^d$  are constants summarized in Table 3.2. We compute accordingly the hyper-stress using Eq. (3.18) as the following expression:

$$S_{d1} = \frac{\partial W}{\partial K_{ijk}} = U_0 \xi e^{-I(ct-X1)\xi} (H_3^d \cdot \xi + H_4^d \cdot I) \quad (3.46)$$

Wherein the parameters  $H_3^d$  and  $H_4^d$  are constants summarized in Table 3.2. Using Eq. (3.20), we calculate the homogenized macro-inertia forces on the laminated medium as follows:

$$\begin{aligned} F_d &= \frac{\partial}{\partial X_1} \left( \frac{1}{2} \ddot{E}_{d1} \left\langle \rho (H_{dd1}^E x_1 + H_{dd1}^E x_1 - 2x_1^2) \right\rangle + \frac{1}{2} \ddot{K}_{d11} \left\langle \rho \left( H_{dd11}^K x_1 + \frac{1}{2} H_{dd1}^E x_1^2 - x_1^3 \right) \right\rangle \right) \\ &- \frac{\partial^2}{\partial X_1 \partial X_1} \left( \frac{1}{2} \ddot{E}_{d1} \left\langle \frac{\rho}{2} \left( H_{dd11}^K x_1 + \frac{1}{2} H_{dd1}^E x_1^2 - x_1^3 \right) \right\rangle + \frac{1}{4} \ddot{K}_{d11} \left\langle \rho (H_{dd11}^K x_1^2 + H_{dd11}^K x_1^2 - x_1^4) \right\rangle \right) \\ &= \frac{\partial}{\partial X_1} \left( \frac{1}{2} \ddot{E}_{d1} \left\langle \rho (H_{dd1}^E x_1 + H_{dd1}^E x_1 - 2x_1^2) \right\rangle \right) - \frac{\partial^2}{\partial X_1 \partial X_1} \left( \frac{1}{4} \ddot{K}_{d11} \left\langle \rho (H_{dd11}^K x_1^2 + H_{dd11}^K x_1^2 - x_1^4) \right\rangle \right) \\ &= (H_5^d + H_6^d \cdot \xi^2) c^2 \xi^4 U_0 e^{(I\xi(-ct+X1))} \end{aligned} \quad (3.47)$$

Where the parameters  $H_5^d$  and  $H_6^d$  in Eq. (3.47) are constants summarized in Table 3.2; we note that the coupling terms in the micro-inertia force cancel out. We substitute the expressions of the first, second order stress and micro inertia forces back into Eq. (3.17) and using the homogenized properties of the media (Eqs. (3.45-3.47)), we obtain the macro-equations of motion both for the longitudinal and the transverse mode, as follows:

$$\left( H_1^d (H_7) + H_4^d \right) \xi \cdot I - H_2^d (H_7) + H_3^d \cdot \xi^2 + H_5^d \cdot \xi^2 c^2 (H_7)^3 + H_6^d \cdot \xi^4 c^2 (H_7)^3 + \rho^H \cdot c^2 = 0 \quad (3.48)$$

Restricting the kinematics to the first gradient, we obtain the following macro-equations of motion:

$$-H_2^d (H_7) + H_3^d \cdot \xi^2 c^2 (H_7)^3 + \rho^H \cdot c^2 = 0 \quad (3.49)$$

Chapter 3: On the role of second gradient constitutive parameters in the static and dynamic analysis of heterogeneous media with micro-inertia effects

Equation of motion Eq. (3.49) coincides with the one derived in [Wang and Sun, 2007]. The constants entering Eqs. (3.48) and (3.49) and used in subsequent computations are summarized in Table 3.2.

Table 3.2: Constant values obtained by the Hamilton principle based on second gradient mechanics

Mode constants	Longitudinal wave	Transverse wave
$H_1^d$	2336 MPa / m	1334 Mpa / m
$H_2^d$	51392.72 Mpa / m	29367.27 Mpa / m
$H_3^d$	-2238 Mpa	-1279 Mpa
$H_4^d$	-2336 Mpa	-1334 Mpa
$H_5^d$	122.72 kg / m <sup>5</sup>	122.72 kg / m <sup>5</sup>
$H_6^d$	13.7 kg / m <sup>5</sup>	9.12 kg / m <sup>5</sup>
$H_7$	1 m	1 m

We depict in Fig. 3.5 the dispersion characteristics of the laminated media using Eqs. (3.48) and (3.49) for the longitudinal mode in Fig. 3.5a and for the transverse mode in Fig. 3.5b. The second gradient Hamilton principle based results are shown with a cyan color, while the first gradient results in green. The latter have been already presented in (Wang and Sun, 2002). We further compare the results with the ones provided in (Bacigalupo and Gambarotta, 2014b) depicted in yellow, and with the exact solution of (Sun et al., 1968) in black. We make use of the periodicity of the medium along the X direction to obtain a better approximation of the dispersion curves, translating the wave vector for  $k > \pi$  by  $2\pi$ . The results in Fig. 3.5 are normalized with respect to the phase velocities at zero frequency for both modes,  $\hat{c}_1 = 3.417 \cdot 10^3$  m / s and  $\hat{c}_2 = 2.58 \cdot 10^3$  m/s accordingly.

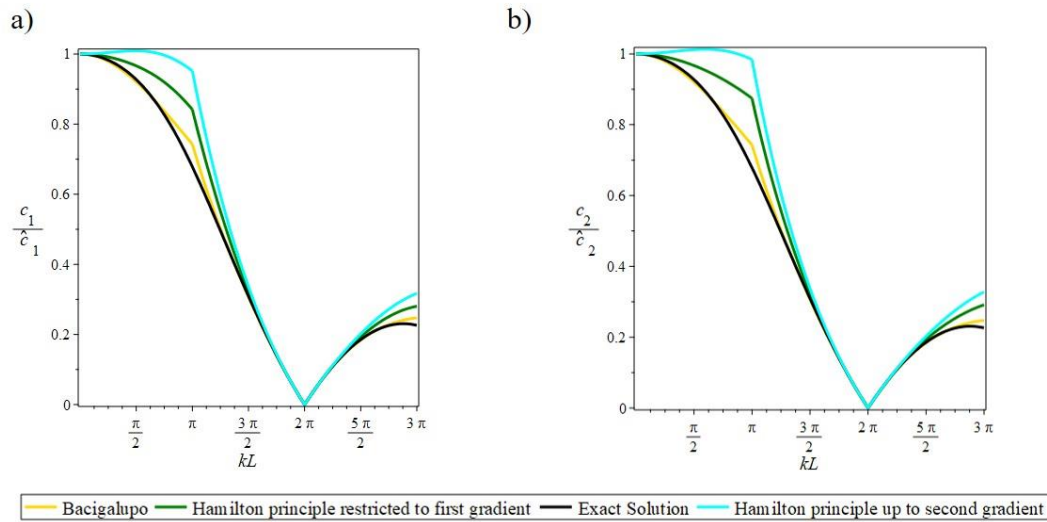


Figure 3.5: Phase velocity curves obtained by Hamilton principle up to second order (Cyan), for first gradient (green), first gradient with higher order micro-inertia effects (yellow) in (Bacigalupo & Gambarotta, 2014b) and the exact solution (red) provided by (Sun et al., 1968) (Appendix 2.C).

The results of Fig. 3.5 show that the extension of Hamiltonian principle into second gradient doesn't provide an improvement with respect to first gradient results, yielding phase velocities which deviate from the exact solution to a greater extent than first order methods for wave number values close to  $kL = \pi$ . However, all methods converge to the exact solution predictions for higher wave number values.

In the next section, we develop the dynamic higher gradient energy homogenization method (DHGE) as an alternative approach for the computation of the effective behavior of the composite medium.

### 3.3.3.2 Higher gradient dynamic homogenization method

In the current section we use the DHGE method developed in Section 3.2.3 to study the wave propagation characteristics of laminated media upon both longitudinal and transverse deformations. Using the dynamic first and second gradient stress tensors evaluated in Section 3.2.3 (Eq. (3.22)) we compute the dispersion characteristics of the heterogeneous laminated medium when imposing a longitudinal harmonic wave normal to the layering. In this part we

use the homogenized expressions of the dynamic tensors in function of the frequency, Eq. (3.24), for both longitudinal ( $d = 1$ ) and transverse ( $d = 2$ ) modes as follows:

$$\begin{aligned}
 C_{d1d1}^{\text{hom,dyn}} &= \left\langle \frac{1}{2} \left( A_{1dd1}^E C_{1dd1} A_{1dd1}^E + A_{d1d1}^E C_{d1d1} A_{d1d1}^E \right) \right\rangle - w^2 \left\langle \frac{\rho}{2} \left( H_{dd1}^E H_{dd1}^E + H_{dd1}^E H_{dd1}^E \right) \right\rangle \\
 &= C_1^d - C_2^d \cdot \xi^2 c^2 \\
 B_{d1d11}^{\text{hom,dyn}} &= \left\langle \frac{1}{2} \left( A_{d1d1}^E C_{d1d1} A_{d1d1}^K + A_{1dd1}^E C_{1dd1} A_{d1d1}^K \right) \right\rangle - w^2 \left\langle \frac{\rho}{2} \left( H_{dd11}^K H_{dd1}^E + H_{dd11}^K H_{dd1}^E \right) \right\rangle \\
 &= C_3^d - C_4^d \cdot \xi^2 c^2 \\
 D_{d11d1}^{\text{hom,dyn}} &= \left\langle \frac{1}{2} \left( A_{d1d1}^E C_{d1d1} A_{d1d1}^K + A_{1dd1}^E C_{1dd1} A_{d1d1}^K \right) \right\rangle - w^2 \left\langle \frac{\rho}{2} \left( H_{dd1}^E H_{dd11}^K + H_{dd1}^E H_{dd11}^K \right) \right\rangle \\
 &= C_3^d - C_4^d \cdot \xi^2 c^2 \\
 A_{d11d11}^{\text{hom,dyn}} &= \left\langle \frac{1}{2} \left( A_{d1d1}^K C_{d1d1} A_{d1d1}^K + A_{1dd1}^E C_{1dd1} A_{d1d1}^K \right) \right\rangle - w^2 \left\langle \frac{\rho}{2} \left( H_{dd11}^K H_{dd11}^K + H_{dd11}^K H_{dd11}^K \right) \right\rangle \\
 &= C_5^d - C_6^d \cdot \xi^2 c^2
 \end{aligned} \tag{3.51}$$

**Remark:** we checked that the dynamical second gradient moduli vanish for a homogeneous laminate.

The constants  $C_1^d$  to  $C_6^d$  entering Eq. (3.51) are summarized in Table 3.3 for the case of the material properties listed in Table 3.1. Using the expressions of Eq. (3.51), we compute the sensitivity of the second gradient characteristics lengths ( $l_{e111}, l_{e211}$ ) as a function of the normalized wavenumber ( $kL$ ) for different values of the phase velocity, for the case of longitudinal (Fig. 3.6a,  $c_1 / \hat{c}_1$ ) and transverse deformations (Fig. 3.6b,  $c_2 / \hat{c}_2$ ).

Chapter 3: On the role of second gradient constitutive parameters in the static and dynamic analysis of heterogeneous media with micro-inertia effects

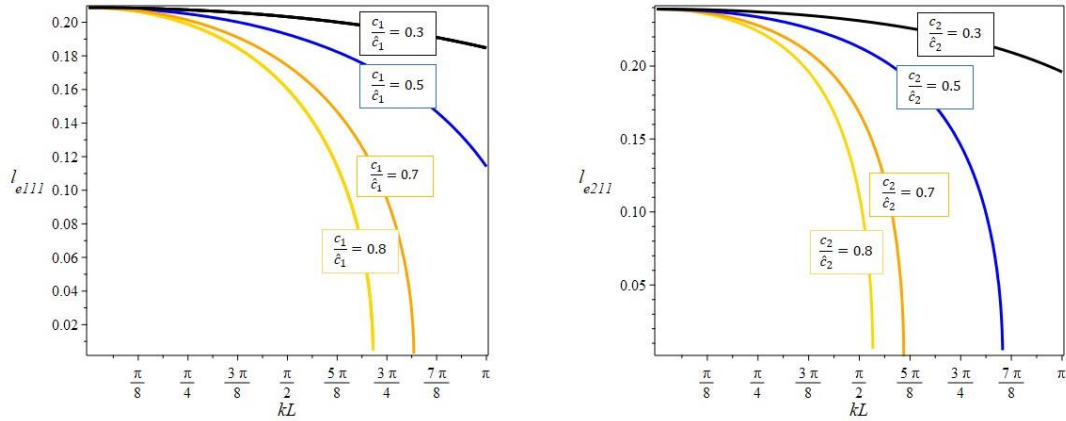


Figure 3.6 : Variation of dynamic second gradient characteristic length as a function of the normalized wavenumber for different values of the phase velocity for the case of longitudinal (a) and transverse (b) deformation mode.

The tensors in Eq. (3.51) are used to calculate the homogenized stress and hyper-stress constitutive expressions of Eq. (3.7), presented in Eq. (3.52) with modified index notation:

$$\begin{aligned}\Sigma_{d1}^{dyn} &= C_{d1d1}^{hom,dyn} E_{d1} + B_{d1d11}^{hom,dyn} K_{d11} \\ S_{d11}^{dyn} &= D_{d1d11}^{hom,dyn} E_{d1} + A_{d11d11}^{hom,dyn} K_{d11}\end{aligned}\quad (3.52)$$

Using the homogenized constitutive expressions of Eq. (3.52), we write the equilibrium equation of motion as follows:

$$\nabla_{x_1} \left( \Sigma_{d1}^{dyn} - \nabla_{x_1} S_{d11}^{dyn} \right) = \rho \ddot{U}_d \quad (3.53)$$

Inserting Eq. (3.51) and Eq. (3.52) into Eq. (3.53) the wave equation of motion is retrieved to determine the dispersion relation of the wave in the two modes (longitudinal and transverse), as follows:

$$\frac{1}{d} \left( (C_1^d - C_2^d \cdot \xi^2 c^2) \xi^2 \cdot (C_7)^3 + (C_5^d - C_6^d \cdot \xi^2 c^2) \xi^4 C_7 \right) - \rho^{hom} (C_7)^3 \xi^2 c^2 = 0 \quad (3.54)$$

Restricting the kinematics to the first gradient we obtain the following macro-equation of motion:

Chapter 3: On the role of second gradient constitutive parameters in the static and dynamic analysis of heterogeneous media with micro-inertia effects

$$\frac{1}{d} \left( (C_1^d - C_2^d \cdot \xi^2 c^2) \xi^2 \cdot (C_7)^3 \right) - \rho^{\text{hom}} (C_7)^3 \xi^2 c^2 = 0 \quad (3.55)$$

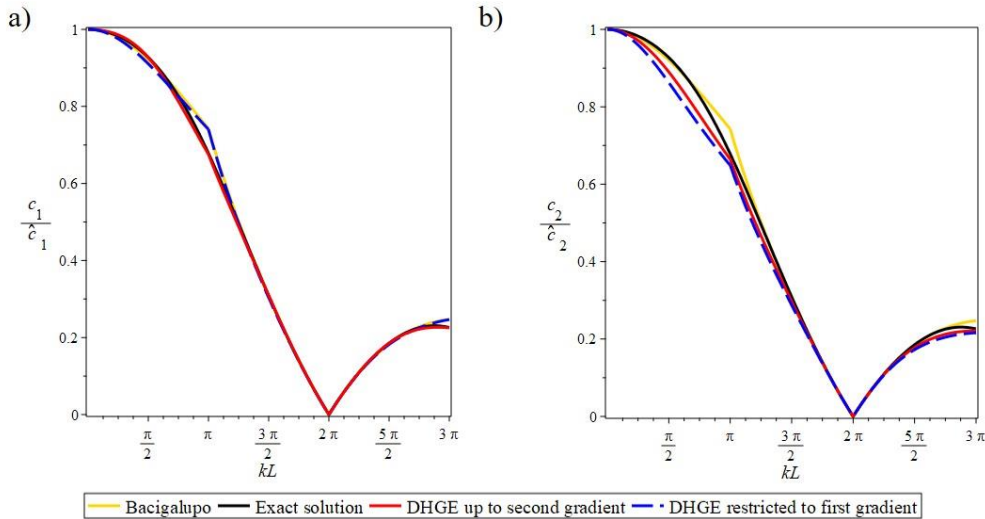
All constants entering Eqs. (3.54) and (3.55) are summarized in Table 3.3.

Table 3.3: Constants value obtained by the DHGE method.

Mode constants	Longitudinal mode	Transverse mode
$C_1^d$	51392.72 MPa	58734.54 MPa
$C_2^d$	368.1 kg / m <sup>3</sup>	1227.27 kg / m <sup>3</sup>
$C_3^d$	-2336 MPa · m	-2669 MPa · m
$C_4^d$	-152 kg / m <sup>2</sup>	-289 kg / m <sup>2</sup>
$C_5^d$	2238 MPa · m <sup>2</sup>	2558 MPa · m
$C_6^d$	59 kg / m	78 kg / m
$C_7$	1 m	1 m
$\hat{c}_d$	3.417 · 10 <sup>3</sup> m / s	2.58 · 10 <sup>3</sup> m/s

The first gradient wave equation restricts to the second power of the normalized wave vector ( $\xi^2$ ). We subsequently compare the second gradient homogenization results with the analytical solution provided by (Sun et al., 1968) and the results in (Bacigalupo & Gambarotta, 2014a). In Fig. 3.7, we plot the normalized phase velocity ( $c_d / \hat{c}_d$ ) where the phase velocities of the longitudinal mode  $\hat{c}_1$  and of the shear mode  $\hat{c}_2$  are calculated using the homogenized first gradient tensor of Eq. (3.24) in the static analysis case ( $\hat{c}_d = \sqrt{C_{d1d1}^{\text{hom,Static}} / \rho^{\text{hom}}}, w = 0$ ), using material properties summarized in Table 3.1. The phase velocity computed by the DHGE method (Eq. (3.54, 3.55)) is depicted in red, while a blue dashed line is used for the first gradient computations. The asymptotic homogenization results are depicted in yellow and the

exact solution (**Appendix 2.C**) in black. Fig. 3.7a provides the longitudinal mode results, while Fig. 3.7b the ones corresponding to the transverse mode.



*Figure 3.7: Normalized phase velocity curves for longitudinal wave (a) and for transverse wave (b) obtained by the DHGE method with first and second gradient constitutive parameters (blue and red respectively). The exact solution is presented in black (Sun et al., 1968), while the yellow color curves correspond to the first gradient constitutive formulation with higher gradient inner micro-inertia terms provided in (Bacigalupo & Gambarotta, 2014).*

Fig. 3.7 indicates that the DHGE method provides a very good agreement with the exact solution (black) over the entire range of normalized wave number values both for the longitudinal and for the transverse mode. The first gradient results (blue) are very close to the first gradient constitutive modeling results with higher gradient micro-inertia terms (yellow curves) in the left plot of Fig. 3.7a.

We subsequently compute the normalized frequency  $w/w_0$  in Fig. 3.8a,b, the normalization being carried out with respect to the natural frequency, defined as  $w_0 = \hat{c}_d / L$  which is equal to the wave velocity since we deal with a laminated cell of unit length; the normalized frequency together with the group velocity (Fig. 3.8c,d) are recorded versus the wavenumber.

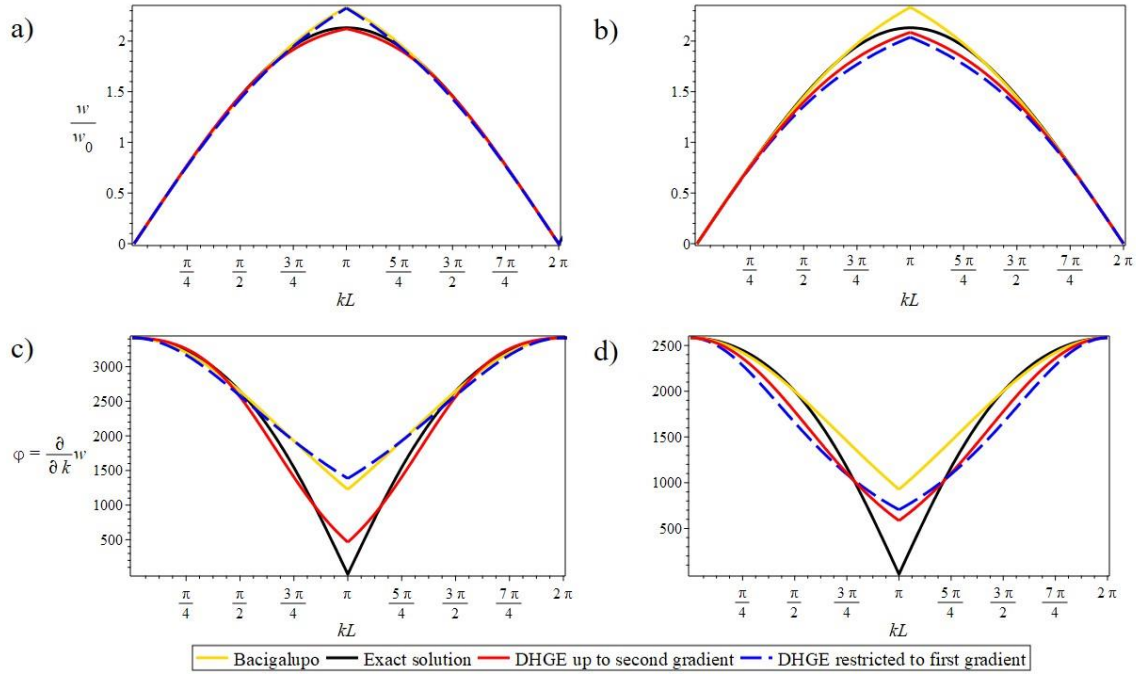


Figure 3.8: Frequency of the longitudinal (a) and transverse waves (b) and group velocity for the longitudinal (c) and transverse waves (d) for both dynamic homogenization methods as a function of the propagating wave number value.

Figures 3.8a and 3.8b indicate that the exact solution predicts a maximum frequency value for a propagating wave number  $kL = \pi$ , with a continuous frequency gradient, so that  $w'(\pi^-) = w'(\pi^+)$ . The near zero slope applies for the second gradient homogenization method of Section 3.2.3, while all other approaches lead to a more prominent discontinuity point for a normalized wavenumber value of  $kL = \pi$ . The continuous frequency plots at  $kL = \pi$  require a zero group velocity at the same point, as indicated by the black curves of Fig. 3.8c and 3.8d. The dynamic, second gradient constitutive formulation is closer to the minimum group velocity for both the longitudinal and the transverse mode, with first gradient formulations to predict notably higher values (Figs. 3.8c, 3.8d).

### 3.4. Discussion

The results of Section 3.3 suggest that the significance of higher gradient constitutive terms in the presence of micro-inertia effects depends both on the geometric and on the material properties of the underlying microstructure. In particular, the coupling and second gradient terms increase upon increasing difference of the relative fraction ( $d_1/d_2$ ) of the phases

### Chapter 3: On the role of second gradient constitutive parameters in the static and dynamic analysis of heterogeneous media with micro-inertia effects

contained within the unit-cell architecture, as shown in Fig. 3.3. What is more, the evolution of the second gradient characteristic lengths indicate that higher order effects become more prominent upon increasing differences in the moduli of the phases contained within the unit cell ( $\phi$ ) for the longitudinal mode (Fig. 3.4a) and for the transverse mode (Fig. 3.4b), with the most prominent changes to take place upon geometric rather than material differences in the underlying microstructural phases.

The second gradient effects depend, not only on the geometric and material parameters of the underlying unit-cell architecture, but also on the propagating wave-number of interest. This can be observed in Fig. 3.7, where the addition of second gradient effects improves the consistency of the computed results (red curve in Fig. 3.7a) for wavenumbers close to  $kL = \pi$  with respect to the Floquet-Bloch, elasticity-based solution. The differences observed for moderate wavenumbers vanish in the higher wavenumber regime of  $kL = 2\pi$ , where all formulations yield the same predictions with the one provided by the elasticity solution (**Appendix 2.C**).

The higher gradient constitutive modelling results are considerably sensitive to the formulation used for their derivation. In particular, using the Hamilton's principle which involves the static Cauchy and hyperstress tensors (the second gradient formulation in Section 3.2.2) leads to phase velocity predictions which substantially differ from the ones predicted by the elasticity-based, Floquet-Bloch results or from first gradient constitutive modelling approximations in the wavenumber region close to  $kL = \pi$ , both for the longitudinal (Fig. 3.5a) and for the transverse mode (Fig. 3.5b). The recorded differences can be primarily attributed to the fact that the dynamic, micro-inertia terms of Eq. (3.5) contribute solely to the potential energy part  $P'$  and not to the kinetic energy part  $T'$  of Eq. (3.11), in which only higher strain gradient terms appear (Eqs. (3.11)-(3.13)). The overestimation of the phase velocity for Hamilton-based methods in the wavenumber region  $kL = \pi$  is already visible for first gradient constitutive modeling results (green curves in Fig. 3.5), an observation made in previous contributions (Wang and Sun 2002, Sun and Huang 2007). In this wavenumber space and upon the Hamilton formulation, the Floquet-Bloch results are best approximated by higher asymptotic expansion contributions of the micro-inertia terms with the macroscopic constitutive parameters retained to their first-order approximation (Bacigalupo & Gambarotta, 2014b). However, the dispersion curves retain a discontinuous rate of change at  $kL = \pi$ , contrary to the continuous elasticity theory predictions.

The dynamic, second gradient constitutive modeling results obtained based on the Hamilton's principle in Section 3.2.2, fundamentally differ from the ones obtained with the use of the dynamic higher gradient energy method of Section 3.2.3, for which the Hill-Mandel expression is directly used to compute the total internal energy stored in the medium (Section 3.2.3). Thereupon, the derived macro-stress and hyperstress are frequency dependent (Section 3.2.3) and not static as in the Hamilton principle based derivations (Section 3.2.2). In the energy based method, the micro-inertia effects related to each of the constitutive tensors can be directly assessed, contrary to the Hamilton formulation, where the constitutive terms are static and not dynamic, with the micro-inertia effects to be assimilated in the  $F_i$  term of Eq. (3.19).

The DHGE method yields high consistency results throughout the entire wavenumber range, as it can be observed from the dispersion curves of Fig. 3.7 and from the frequency and group velocity curves of Fig. 3.8. More specifically, first order gradient based methods lead to an inflection point at  $kL = \pi$  (Fig. 3.7), a discontinuity which is not present for the Floquet-Bloch solution or nearly disappears for the higher gradient based homogenization method results in Fig. 3.7 (red). For normalized wavenumbers equal to  $kL = \pi$ , the frequency does not depend on position – as the Floquet-Bloch results suggest –, so that a transition from planar to standing waves takes place (frequency depends only on time and not on position). This is expressed in the frequency plots of Fig. 3.8a and 3.8b, where the first gradient constitutive results (yellow and blue curves) do not provide continuous frequencies, while their corresponding group velocities are far from zero. Contrariwise, the second gradient formulation elaborated in Section 3.2.3 yields a nearly continuous frequency curve slope, with a group velocity value that approaches zero at the maximum frequency point (Fig. 3.8c, 3.8d).

### 3.5 Conclusion

Overall, in the current chapter, a dynamic higher gradient constitutive model with micro-inertia effects has been developed for the computation of the static and dynamic attributes of heterogeneous materials with an inner microstructure. The method has been used to compute the macroscopic static and dynamic second gradient constitutive parameters of two-phase composite layered materials, using both the Hamilton's principle and the total internal higher gradient energy. The sensitivity of the second gradient constitutive parameters has been

analyzed as a function of the inner material and geometric microstructural parameters for the case of layered two-phase composite structure. It has been noted that the significance of second gradient terms increases, upon increasing differences in the volumetric ratio and in the material properties of the microstructural phases for both longitudinal and transverse deformation patterns. What is more, evidence has been provided that the incorporation of higher gradient macroscopic constitutive parameters can well describe the wave propagation characteristics of the micro-structured media when formulated using the Hill-Mandel equality in the context of its total, dynamic higher gradient deformation energy. The latter yields high accuracy results for the propagating phase and group velocities over the entire wave-number space, outperforming first order constitutive formulations.

## References

- [1] Alibert, J.J., Della Corte, A., (2015). Second-gradient continua as homogenized limit of pantographic microstructured plates: a rigorous proof. *Zeitschrift für angewandte Mathematik und Physik*. 66(5), 2855-2870.
- [2] Andrianov, I.V., Bolshakov, V.I., Danishevs'kyi, V.V., Weichert, D., (2008). Higher order asymptotic homogenization and wave propagation in periodic composite materials. *Proceedings of the Royal Society A*, 464(2093), 1181–1201. <https://doi.org/10.1098/rspa.2007.0267>.
- [3] Andrianov, I.V., Awrejcewicz, J., Danishevs'kyi, V.V., Weichert, D., (2011). Wave propagation in periodic composites: higher-order asymptotic analysis versus plane-wave expansion method. *Journal of Computational and Nonlinear Dynamics* 6(1), 011015-1 - 011015-8. DOI: 10.1115/1.4002389.
- [4] Andrianov, I., Awrejcewicz, J., Weichert, D., (2010). Improved Continuous Models for Discrete Media. *Mathematical Problems in Engineering*, <http://dx.doi.org/10.1155/2010/986242>.
- [5] Aifantis, E., (1992). *International Journal of Engineering Science* 30(10):1279-1299. doi: 10.1016/0020-7225(92)90141-3.
- [6] Aifantis, E., (1998). Strain gradient interpretation of size effects. *International Journal of Fracture*, 95(1), 299-314. doi: 10.1023/A:1018625006804.
- [7] Askes, H., Aifantis, E., (2009). Gradient elasticity and flexural wave dispersion in carbon nanotubes. *Phys. Rev. B* 80, 195412.
- [8] Askes, H., Aifantis, E., (2011). Gradient elasticity in statics and dynamics: An overview of formulations, length scale identification procedures, finite element implementations and new results. *International Journal of Solids and Structures*, 48(13), 1962-1990.
- [9] Askes, H., Calik-Carakose, U., Susmel, L., (2012). Gradient elasticity length scale validation using static fracture experiments of PMMA and PVC. *International Journal of Fracture*, 176(2), 223–227. doi:10.1007/s10704-012-9735-x.
- [10] Askes, H., Metrikine, A., (2002). One-dimensional dynamically consistent gradient elasticity models derived from a discrete microstructure: Part 2: Static and dynamic response.

European Journal of Mechanics - A/Solids, 21(4), 573-588. [doi.org/10.1016/S0997-7538\(02\)01217-2](https://doi.org/10.1016/S0997-7538(02)01217-2).

[11] Askes, H., Metrikine, A., Pichugin, A., Bennett, T., (2008). Four simplified gradient elasticity models for the simulation of dispersive wave propagation. *Journal Philosophical Magazine*, 88(28-29) 3415-3443. [doi.org/10.1080/14786430802524108](https://doi.org/10.1080/14786430802524108).

[12] Auriault, J.L., Boutin, C., (2012). Long wavelength inner-resonance cut-off frequencies in elastic composite materials. *International Journal of Solids and Structures*, 49(23–24), 3269-3281.

[13] Bacigalupo, A., Gambarotta, L., (2010). Strain-gradient computational homogenization of heterogeneous materials with periodic microstructure. *ZAMM Z. Angew. Math. Mech.* 90, 796–811. <https://doi.org/10.1016/j.ijsolstr.2012.07.002>.

[14] Bacigalupo, A., Gambarotta, L., (2012). Computational two-scale homogenization of periodic masonry: characteristic lengths and dispersive waves. *Computer Methods in Applied Mechanics and Engineering*, 213–216, 16-28. [doi.org/10.1016/j.cma.2011.11.020](https://doi.org/10.1016/j.cma.2011.11.020).

[15] Bacigalupo, A. (2014a). Second-order homogenization of periodic materials based on asymptotic approximation of the strain energy: formulation and validity limits. *Materials Science (cond-mat.mtrl-sci)*. arXiv:1401.7855.

[16] Bacigalupo, A., Gambarotta, L., (2014b). Second-gradient homogenized model for wave propagation in heterogeneous periodic media. *International Journal of Solids and Structures*, 51(5) 1052-1065. <https://doi.org/10.1016/j.ijsolstr.2013.12.001>.

[17] Bakhvalov, N.S., Panasenko, G.P., (1984). *Homogenization, Averaging process in periodic Media*. Kluwer Academic Publishers. Moscow.

[18] Bensoussan, A., Lions, J.L., Papanicolaou, G., (1978). *Asymptotic Analysis for periodic structures*. Amsterdam, New York, North-Holland Pub. [www.ams.org/bookpages/chel-374](http://www.ams.org/bookpages/chel-374).

[19] Berezovski, A., Engelbrecht, J., Salupere, A., Tamm, K., Peets, T., Berezovski, M., (2013). Dispersive waves in microstructured solids. *International Journal of Solids and Structures*, 50(11–12) 1981-1990. doi: <https://doi.org/10.1016/j.ijsolstr.2013.02.018>.

[20] Boutin, C., Auriault, J.L., (1993). Rayleigh scattering in elastic composite materials. *International Journal of Engineering Science*, 31(12) 1669-1689. [https://doi.org/10.1016/0020-7225\(93\)90082-6](https://doi.org/10.1016/0020-7225(93)90082-6).

[21] Chen, W., Fish, J., (2000). A dispersive model for wave propagation in periodic heterogeneous media based on homogenization with multiple spatial and temporal scales. *Journal of Applied Mechanics*, 68(2), 153-161. doi:10.1115/1.1357165.

[22] Claude Boutin, (1996). Microstructural effects in elastic composites. *International Journal of Solids and Structures*, 33 (7) 1023-105.

[23] Craster, R.V., Kaplunov, J., Pichugin, A.V., (2010). High-frequency homogenization for periodic media. *Proceedings of the Royal Society A*, 466, 2341–2362. <https://doi.org/10.1098/rspa.2009.0612>.

[24] Erofejev, V. I., (2003). *Wave Processes in Solids with Microstructure*. World Scientific, 2003.

[25] Fafalis, D., Filopoulos, S., Tsamasphyros, G., (2012). On the capability of generalized continuum theories to capture dispersion characteristics at the atomic scale. *European Journal of Mechanics - A/Solids*, 36, 25–37. doi:10.1016/j.euromechsol.2012.02.004.

[26] Fish, J., Chen, W., (2001). Higher-order homogenization of initial/boundary-value problem, *J. Eng. Mech.* 127, 1223-1230.

[27] Gonella, S., Steven Greene, M., & Liu, W. K. (2011). Characterization of heterogeneous solids via wave methods in computational microelasticity. *Journal of the Mechanics and Physics of Solids*, 59(5), 959-974. <https://doi.org/10.1016/j.jmps.2011.03.003>.

- [28] Gonella, S., Ruzzene, M., (2010). Multicell homogenization of one-dimensional periodic structures. *Journal of Vibration and Acoustics*, 132(1). <https://doi:10.1115/1.4000439>.
- [29] Gourgiotis, P., Georgiadis, H., (2009). Plane-strain crack problems in microstructured solids governed by dipolar gradient elasticity. *Journal of the Mechanics and Physics of Solids* 57(11) 1898-1920. Doi: 10.1016/j.jmps.2009.07.005.
- [30] Guenneau, S., Craster, R., Antonakakis, T., Cherednichenko, K., Cooper, S., (2013). *Homogenization Techniques for Periodic Structures*. E. Popov. Gratings: Theory and Numeric Applications, AMU (PUP), pp.11.1-11.31. <https://hal.archives-ouvertes.fr/hal-00785718>.
- [31] Gutkin, M., Aifantis, E., (1999). Dislocations in the theory of gradient elasticity. *Scripta Mater* 40, 559-566.
- [32] Huang, Z.G., 2011. Analysis of Acoustic Wave in Homogeneous and Inhomogeneous Media Using Finite Element Method. *Acoustic Waves - From Microdevices to Helioseismology*, Marco G. Beghi, IntechOpen. DOI: 10.5772/18792.
- [33] Hussein, M.I., (2009). Reduced Bloch mode expansion for periodic media band structure calculations. *Proceedings of the Royal Society A*, 465, 2825–2848. <https://doi.org/10.1098/rspa.2008.0471>.
- [34] Iliopoulos, S., Aggelis, D., Polyzos, D., (2016). Wave dispersion in fresh and hardened concrete through the prism of gradient elasticity, *International Journal of Solids and Structures*, 78–79, 149-159. <https://doi.org/10.1016/j.ijsolstr.2015.09.005>.
- [35] Karathanasopoulos, N., Reda, H., & Ganghoffer, J. F. (2019). The role of non-slender inner structural designs on the linear and non-linear wave propagation attributes of periodic, two-dimensional architected materials. *Journal of Sound and Vibration*, 455, 312–323. <https://doi.org/10.1016/J.JSV.2019.05.011>.
- [36] Koiter, W.T., (1969). Couple-stresses in the theory of elasticity: I and II. *Philosophical transactions of the royal society of London OF LONDON B*, 67 ,17-44.
- [37] Lombardo, M., Askes, H., (2012). Higher-order gradient continuum modelling of periodic lattice materials. *Computational Materials Science*, 52(1), 204-208. <https://doi.org/10.1016/j.commatsci.2011.05.025>.
- [38] Metrikine, A.V., Askes, H., (2002). [One-dimensional dynamically consistent gradient elasticity models derived from a discrete microstructure: Part 1: Generic formulation](#). *European Journal of Mechanics - A/Solids* 21(4), 555-572. DOI: 10.1016/S0997-7538(02)01218-4.
- [39] Mindlin, R.D., (1964). Micro-structure in linear elasticity. *Archive for Rational Mechanics and Analysis*, 16(1), 51–78. <https://doi.org/10.1007/BF00248490>.
- [40] Mindlin, R., (1965). Second gradient of strain and surface-tension in linear elasticity. *International Journal of Solids and Structures*, 1(4), 417-438. [https://doi.org/10.1016/0020-7683\(65\)90006-5](https://doi.org/10.1016/0020-7683(65)90006-5).
- [41] Mindlin, R.D., (1972). Elasticity, piezoelectricity and crystal lattice dynamics. *Journal of Elasticity*, 2(4), 217–282. <https://doi.org/10.1007/BF00045712>.
- [42] Mühlhaus, H., Oka, F., (1996). [Dispersion and wave propagation in discrete and continuous models for granular materials](#). *International Journal of Solids and Structures*, 33(19), 2841-2858. Doi: 10.1016/0020-7683(95)00178-6.
- [43] Nemat-Nasser, S., Srivastava, A., (2011). Overall dynamic constitutive relations of layered elastic composites. *Journal of the Mechanics and Physics of Solids* 59(10),1953-1965. Doi: 10.1016/j.jmps.2011.07.008.
- [44] Nemat-Nasser, S., Srivastava, A., (2012). Overall dynamic properties of three-dimensional periodic elastic composites. *Proceedings of the Royal Society A Mathematical Physical and Engineering Sciences*, 468(2137), 269-287. Doi: 10.1098/rspa.2011.0440.

- [45] Ostoja-Starzewki, M., (2002). [Lattice models in micromechanics](#). Applied Mechanics Reviews, 55(1), 35-60. doi:10.1115/1.1432990.
- [46] Papargyri-Beskou, S., Polyzos, D., Beskos, D.E., (2009). [Wave dispersion in gradient elastic solids and structures: a unified treatment](#). International Journal of Solids and Structures 46 (21), 3751-3759. <https://doi.org/10.1016/j.ijsolstr.2009.05.002>.
- [47] Papargyri-Beskou, S., Beskos, D.E., (2004). Response of gradient-viscoelastic bar to static and dynamic axial load. Acta Mechanica, 170(3-4), 199-212. <https://doi.org/10.1007/s00707-004-0106-1>.
- [48] Polyzos, D., Huber, G., Mylonakis, G., Triantafyllidis, T., Papargyri-Beskou, S., Beskos, D.E., (2015). Torsional vibrations of a column of fine-grained material: A gradient elastic approach. Journal of the Mechanics and Physics of Solids, 76, 338-358. <https://doi.org/10.1016/j.jmps.2014.11.012>.
- [49] Reda, H., Karathanasopoulos, N., Rahali, Y., Ganghoffer, J. F., & Lakiss, H. (2018a). Influence of first to second gradient coupling energy terms on the wave propagation of three-dimensional non-centrosymmetric architected materials. International Journal of Engineering Science, 128, 151-164. <https://doi.org/10.1016/J.IJENGSCI.2018.03.014>.
- [50] Reda, H., Karathanasopoulos, N., Ganghoffer, J. F., & Lakiss, H. (2018b). Wave propagation characteristics of periodic structures accounting for the effect of their higher order inner material kinematics. Journal of Sound and Vibration, 431, 265-275. <https://doi.org/10.1016/J.JSV.2018.06.006>
- [51] Reda, H., Karathanasopoulos, N., Elnady K., Ganghoffer, J. F., & Lakiss, H. (2018c), The role of anisotropy on the static and wave propagation characteristics of two-dimensional architected materials under finite strains, Materials and design, 147, 134-145, 2018, <https://doi.org/10.1016/j.matdes.2018.03.039>
- [52] Réthoré, J., Kaltenbrunner, C., Dang, T., Chaudet, P., Kuhn, M., (2015). Gradient-elasticity for honeycomb materials: Validation and identification from full-field measurements. International Journal of Solids and Structures, 72, 108-117. <https://doi.org/10.1016/j.ijsolstr.2015.07.015>.
- [53] Robinson, C. W., Leppelmeier, G. W., (1974). Experimental Verification of Dispersion Relations for Layered Composites. Journal of Applied Mechanics, 41(1). Doi: 10.1115/1.3423280.
- [54] Sanchez Palencia, E., (1980). Non-Homogeneous Media and Vibration Theory. Lecture Notes in Physics, 127, Springer, Berlin.
- [55] Smyshlyaev, V.P., Cherednichenko, K.D., (2000). On rigorous derivation of strain gradient effects in the overall behaviour of periodic heterogeneous media. Journal of the Mechanics and Physics of Solids 48(6):1325-1357. DOI: 10.1016/S0022-5096(99)00090-3.
- [56] Smyshlyaev, V.P., (2009). Propagation and localization of elastic waves in highly anisotropic periodic composites via two-scale homogenization. Mechanics of Materials, 41(4), 434-447. <https://doi.org/10.1016/j.mechmat.2009.01.009>.
- [57] Sun, C.T., Achenbach, J.D., Herrmann, G., (1968). Time-harmonic waves in a stratified medium propagating in the direction of the layering. Journal of Applied Mechanics, 35(2), 408-411. doi:10.1115/1.3601212.
- [58] Sun, C.T., Huang, G.L., (2006). Modeling Heterogeneous Media with Microstructures of Different Scales. Journal of Applied Mechanics, 74(2), 203-209. doi:10.1115/1.2188536.
- [59] Toupin, R.A., (1962). Elastic materials with couple-stresses. Archive for Rational Mechanics and Analysis, 11(1), 385-414. <https://doi.org/10.1007/BF00253945>.
- [60] Trinh, D.K., (2011). Méthodes d'homogénéisation d'ordre supérieur pour les matériaux architecturés. École nationale supérieure des Mines de Paris.

### Chapter 3: On the role of second gradient constitutive parameters in the static and dynamic analysis of heterogeneous media with micro-inertia effects

- [61] Trinh D.K., Janicke R., Auffray N., (2012). Evaluation of generalized continuum substitution models for heterogeneous materials. *Journal for Multiscale Computational Engineering*, 10 (6): 527–549. DOI: 10.1615/IntJMultCompEng.2012003105.
- [62] Vivar-Perez, J.M., Gabbert, U., Berger, H., Rodriguez-Ramos, R., Bravo-Castillero, J., Guinovart-Diaz, R., Sabina, F.J., (2009). [A dispersive nonlocal model for wave propagation in periodic composites](#). *European Journal of Mechanics - A/Solids* 82(3). DOI: 10.1016/j.euromechsol.2014.05.009.
- [63] Wang, Z.-P., Sun, C.T., (2002). Modelling micro-inertia in heterogeneous materials under dynamic loading. *Wave Motion*, 36(4), 473–485. DOI: 10.1016/S0165-2125(02)00037-9.
- [64] Zhikov, V.V., (2000). On an extension of the method of two-scale convergence and its applications. *Sbornik: Mathematics*, 191(7), 973-1014. DOI:10.1070/SM2000v191n07ABEH000491.

## **Chapter 4**

Higher-gradient and micro-inertia contributions on the mechanical response of composite beam structures

## **Chapter 4: Higher-gradient and micro-inertia contributions on the mechanical response of composite beam structures**

### **Summary**

In the current work, we study the role of higher-order and micro-inertia contributions on the mechanical behavior of composite structures. To that scope, we compute the complete set of the effective static and dynamic properties of composite beam structures using a higher-order dynamic homogenization method which incorporates micro-inertia effects. We consider different inner composite element designs, with material constituents that are of relevance for current engineering practice. Thereupon, we compute the effective static longitudinal higher-gradient response, quantifying the relative difference with respect to the commonly employed, Cauchy-mechanics formulation. We observe that within the static analysis range, higher-order effects require high internal length values and highly non-linear strain profile distributions for non-negligible higher-order effects to appear. We subsequently analyze the longitudinal, higher-gradient eigenfrequency properties of composite structural members, accounting for the role of micro-inertia contributions. Thereupon, we derive analytical expressions that relate the composite material's effective constitutive parameters with its macroscale vibration characteristics. We provide for the first-time evidence that micro-inertia contributions can counteract the effect of second-gradient properties on the eigenfrequencies of the structure, with their relative significance to depend on the mode of interest. What is more, we show that the internal length plays a crucial role in the significance of micro-inertia contributions, with their effect to be substantial for low, rather than for high internal length values, thus for a wide range of materials used in engineering practice.

## 4.1 Introduction

In the case of materials with a non-homogeneous microstructure, the classical, first order formulation of linear elasticity does not typically suffice to fully describe the effective macroscopic material behavior (Mindlin & Eshel, 1968). Higher gradient formulations are required, which take into account not only the local strain of the material, but also the variation of the strain field, thus nonlocal information (Lim et al., 2015).

A wide range of enhanced continuum theories has been up to now developed to circumvent the limitations of classical, first order models. The formulation of the generalized continua has been based on either top-down or bottom-up approaches. In the first case, the macroscale energy functions are assumed to contain higher order contributions that relate to inner microstructural parameters (Engelbrecht et al., 2007; Berezovski et al., 2013; Dingreville et al., 2013, 2014). The latter need to be calibrated on available macroscopic data, such as experimental non-destructive tests (Dontsov et al., 2013; Engelbrecht & Berezovski, 2015), but cannot distinguish between the different microstructural contributions as of their very nature. In the bottom-up approach, a continualization or a homogenization scheme needs to be applied. For the former, the higher-order interactions between the different microstructural phases have to be appropriately described (Metrikine & Askes, 2002, Pichugin et al., 2008); so that choices for the discretization of the higher-order parameters need to be made (Hermitian, Element-Free Galerkin formulations). By that means, certain postulations for the micro-scale mechanical behavior are introduced (Polyzos & Fotiadis, 2012). Accordingly, homogenization schemes have been mainly based on asymptotic formulations, which rely on the expansion of the spatial and temporal parameters to fast and slow varying components (Andrianov et al., 2008; Brito-Santana et al., 2015; Hui & Oskay, 2014). Thereupon, different models have been elaborated and used to characterize the dispersion properties of media with an underlying periodic, layered microstructure (Wautier & Guzina, 2015; Bennett et al., 2007; De Domenico & Askes, 2016).

The modeling approach is crucial both for the accurate characterization of the effective static macroscale properties and for the sufficient representation of its wave propagation characteristics (Chen & Fish, 2001; Reda et al., 2018). In particular, the incorporation of higher gradient contributions can eliminate singularities or discontinuities that may appear for first order formulations (Exadaktylos & Vardoulakis, 1998; Chang, 1997). What is more, higher-order models can capture wave dispersion phenomena over a wide range of wave numbers and

## Chapter 4: Higher-gradient and micro-inertia contributions on the mechanical response of composite beam structures

more importantly in the high wave number region, where typically low-order methods are insufficient (Bennett et al., 2007; M. Şimşek, 2016).

Apart from the sufficient description of the wave propagation characteristics of engineering materials, the design of structures with optimized vibration properties (Shimoda et al., 2016) requires artificial material designs with extra-ordinary attributes. It has been observed that certain lattice material designs allow for an increase of the basic eigenfrequency, reducing structural weights while retaining specific stiffness characteristics for cantilever and doubly supported artificial beam structures (Cheng et al., 2018). What is more, different regular and irregular lattice patterns have been shown to allow for a substantial shift of the primal eigenmode to a higher frequency value, isolating lower range frequencies (Syam et al., 2018; Andresen et al., 2020).

Higher gradients contributions have been shown to affect the structural vibration properties (Altan et al., 1996; Salehian & Inman, 2008; Bisegna & Caruso, 2011). In particular, evidence has been provided that the incorporation of higher-order terms leads to increased natural frequency values, with the value of the internal length to be crucial for the relative differences recorded (Li et al., 2016). Analytical solutions for the natural frequencies of strain-gradient rod structures verify the previous conclusions (Altan et al., 1996). It should be noted that higher-gradient terms can affect both the primal and the higher order modes, with the higher order frequencies to be more sensitive to gradient effects (Altan et al., 1996). Furthermore, in the case of forced-vibrations, it has been noted that higher-gradient contributions may not-only modify the form of the time-displacement curves, but also the maximum values of the recorded deformations (Tsepoura et al., 2002). Analogous conclusions have been reported for the role of higher-gradient strain contributions on the vibration response of plate structures (Yin et al., 2010).

Up to now, the higher-gradient strain constitutive parameters have been characterized either through asymptotic homogenization approaches or postulated to lie within a certain range. However, no exact second gradient homogenization method has been used to characterize the static and dynamic response of micro-structured materials upon a direct correlation of micro and macro-scale parameters. What is more, the effect of micro-inertia has been typically disregarded. As a result, the significance of micro-inertia contributions on the dynamic characteristics of structural members remains non-quantified along with its relative importance with respect to the eigenmode of interest.

In the current work, we make use of a higher-gradient homogenization scheme, which avoids the need to postulate the form of the non-local interactions, while it accounts for the

effect of micro-inertia contributions. In Section 4.2, we elaborate on the computation of the effective first and second-gradient static and dynamic properties of the materials used for the design of the composite representative unit-cell hereby studied. Subsequently, we compute the static response of a beam structure architected with different inner microstructural material phases, quantifying the effect of higher-gradient stiffness attributes (Section 4.3.1). Thereafter, we compute the eigenfrequencies of the composite beam structure using the Cauchy mechanics assumptions which we compare with the use of dedicated finite element models (Section 4.3.2.1). We extend the Cauchy mechanics framework to the higher-gradient and micro-inertia analysis space, providing analytical solutions for the dependence of the eigenfrequencies on the first, second-gradient and micro-inertia parameters (Section 4.3.2.2). We subsequently compute the eigenfrequency properties for the second-gradient and micro-inertia constitutive modeling case which we compare with the Cauchy mechanics predictions for different modes and for different inner material designs within (Section 4.3.2.2) and beyond (Section 4.3.3) the range of commonly used engineering materials. We discuss the obtained results in Section 4.4 and conclude in Section 4.5.

## 4.2 Materials and methods

### 4.2.1 Composite beams

We consider a composite laminated beam structure of length  $L$  (Fig. 4.1a), with a two-phase unit-cell material design of length  $l$ . The unit-cell contains materials with different elastic moduli values  $E_1$  and  $E_2$  as well as density values  $\rho_1$  and  $\rho_2$  with thickness  $d_1$  and  $d_2$  (Fig. 4.1a). The static and dynamic characteristics of the structure (Fig. 4.1b) related to the Cauchy (C), second-gradient (SG) and micro-inertia ( $\mu l$ ) properties are computed using the framework elaborated in Section 4.2.2. The dependence of the effective static (Fig. 4.1c) and dynamic (Fig. 4.1d) structural properties on the microstructural design parameters and modeling order are analyzed in Section 4.3.

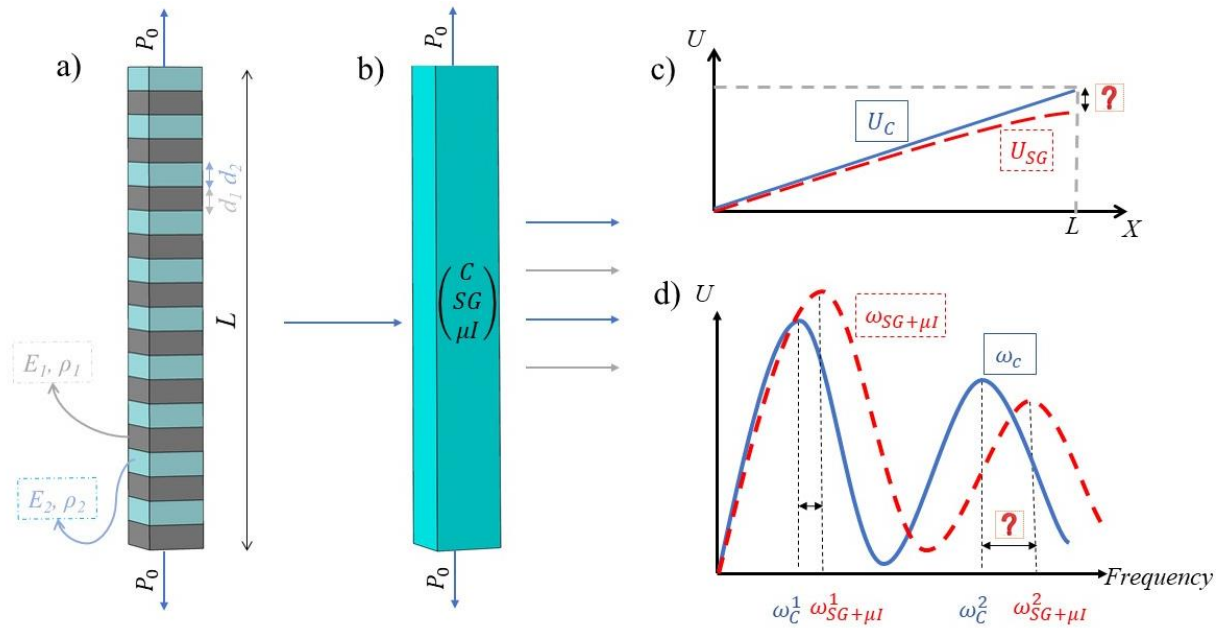


Figure 4.1: A two-phase composite beam structure (a) with effective Cauchy (C), Second-Gradient (SG) and micro-inertia ( $\mu I$ ) properties (b) which depend on its micro-scale material parameters. Upon loading, the obtained static (c) and dynamic (d) characteristics directly depend on the modeling formulation employed for the assessment of its structural response at the effective continuum scale.

For the unit-cell design, different material combinations are considered, with material constituents typically used in composite structures (Mallick, 2007). More specifically, carbon, epoxy and glass-based unit-cell material designs are considered, their elastic moduli ( $E$ ), density ( $\rho$ ) and lame coefficient values ( $\lambda = E\nu / (1+\nu) / (1-2\nu)$ ,  $\mu = E / (2(1+\nu))$ ) summarized in Table 4.1:

Table 4.1 : Mechanical properties of the materials used in the design of the microstructure of the composite beam of Fig. 4.1a.

Material	$E$ (GPa)	$\rho$ (kg/m <sup>3</sup> )	$\lambda$ (GPa)	$\mu$ (GPa)
Silicon Carbide	400	3000	346	148
Borosilicate Glass	60	2300	16.6	25
E-Glass	72	2500	23	29.5
Epoxy	3.4	1250	2.48	1.28
Carbon	250	1800	115.5	98.4

For the computation of the Lamé coefficients provided in Table 4.1, the Poisson's ratio value was set to 0.35, 0.2, 0.22, 0.33, 0.27 for the Silicon Carbide, Borosilicate Glass, E-Glass, Epoxy, and Carbon accordingly (Mallick, 2007).

#### 4.2.2 Higher gradient and micro-inertia constitutive material modeling

In the current work, we base our developments on the generalized Hill-Mandel lemma to express the energy stored in the deformed domain for an adopted strain gradient effective continuum (Chapter 3), as follows:

$$E_{ij}\Sigma_{ij} + K_{ijk}S_{ijk} = \left\langle \varepsilon_{ij}\sigma_{ij} \right\rangle + \left\langle \rho\ddot{u}_i \left( u_i - E_{ij}x_j - \frac{1}{2}K_{ijk}x_jx_k \right) \right\rangle \quad (4.1)$$

Where in Eq. (4.1),  $\Sigma_{ij}$  and  $S_{ijk}$  represent the homogenized stress and hyperstress tensors while  $E_{ij}$  and  $K_{ijk}$  are their conjugate first and second gradient strain tensors. Accordingly,  $\varepsilon_{ij} = \frac{1}{2}(u_{i,j} + u_{j,i})$  and  $\sigma_{ij}$  stand respectively for the micro-strain and micro-stress developed within the microscale of the material. The dynamic energy part contains the micro-inertia contributions generated by the microscale inertia terms. Thereupon, the density  $\rho$  and the micro-displacement field  $u_i$  appear.

For the derivation of the homogenized stress and hyperstress constitutive behavior based on Eq. (4.1), the expression of the material's total deformation energy is used, as elaborated in (Chapter 3). In the corresponding constitutive formulation, the homogenized stress and hyperstress tensors include both the static and dynamic, time-dependent strain components denoted with  $\ddot{E}_{dl}$  and  $\ddot{K}_{rst}$  accordingly for the first and for the second gradient strain tensors. The complete set of constitutive equations writes in terms of the dynamical stress tensor expressions:

$$\begin{aligned} \Sigma_{ij}^{\text{hom,dyn}} &= \begin{bmatrix} C_{ijdl}^{\text{hom,stat}} & C_{ijdl}^{\text{hom,dyn}} \end{bmatrix} \begin{bmatrix} E_{dl} \\ \ddot{E}_{dl} \end{bmatrix} + \begin{bmatrix} B_{ijrst}^{\text{hom,stat}} & B_{ijrst}^{\text{hom,dyn}} \end{bmatrix} \begin{bmatrix} K_{rst} \\ \ddot{K}_{rst} \end{bmatrix} \\ S_{ijk}^{\text{hom,dyn}} &= \begin{bmatrix} D_{ijkdl}^{\text{hom,stat}} & D_{ijkdl}^{\text{hom,dyn}} \end{bmatrix} \begin{bmatrix} E_{dl} \\ \ddot{E}_{dl} \end{bmatrix} + \begin{bmatrix} A_{ijkrst}^{\text{hom,stat}} \end{bmatrix} \begin{bmatrix} K_{rst} \end{bmatrix} \end{aligned} \quad (4.2)$$

Where in Eq. (4.2), the coefficients  $C_{ijkl}^{\text{hom}}$  stand for the first order constitute stiffness component, while the coefficients  $B_{ijrst}^{\text{hom}}$  and  $D_{ijkl}^{\text{hom}}$  for the coupling stiffness terms between the first and second order stress and kinematic parameters, which are non-zero for non centrosymmetric microstructures. The coefficients  $A_{ijklst}^{\text{hom}}$  represent the purely second gradient constitutive moduli.

For the calculation of each constitutive stiffness parameter of Eq. (4.2), localization operators need to be employed, relating micro-displacements and micro-strains with the corresponding macro-strain and strain gradient tensors  $E_{dl}$  and  $K_{rst}$ . The localization operators relating the micro-displacements to the strain components are denoted with  $H^E$  and  $H^K$  respectively, while the localization operators relating micro and macro strains are  $A^E$  and  $A^K$  accordingly. The constants included in the displacement and strain localization operators (Eq. 3.A2) are identified using the boundary and continuity conditions for the first and the second gradient terms (Eq. 3.A4). They are functions of the individual material parameters contained in the different material phases of the unit-cell structure (Eq. 3.A5), as elaborated in **Appendix 3.A**. For the case of longitudinal loading, the stiffness coefficients of Eq. (4.2) express in a simplified form as a function of the localization operators as follows:

$$\begin{aligned}
 \begin{bmatrix} C_{1111}^{\text{hom,stat}} \\ C_{1111}^{\text{hom,dyn}} \end{bmatrix} &= \begin{bmatrix} C_1^1 \\ C_2^1 \end{bmatrix} = \begin{bmatrix} \langle 2A_{1111}^{E(i)} (\lambda_i + 2\mu_i) A_{1111}^{E(i)} \rangle \\ \langle \rho (H_{111}^E H_{111}^E - H_{111}^E x) \rangle \end{bmatrix} \\
 \begin{bmatrix} B_{11111}^{\text{hom,stat}} \\ B_{11111}^{\text{hom,dyn}} \end{bmatrix} &= \begin{bmatrix} D_{11111}^{\text{hom,stat}} \\ D_{11111}^{\text{hom,dyn}} \end{bmatrix} = \begin{bmatrix} C_3^1 \\ C_4^1 \end{bmatrix} = \begin{bmatrix} \langle 2A_{1111}^{E(i)} (\lambda_i + 2\mu_i) A_{11111}^{K(i)} \rangle \\ \langle \frac{\rho}{2} \left( 2H_{1111}^{K(i)} H_{111}^{E(i)} - H_{1111}^{K(i)} x - \frac{1}{2} H_{111}^{E(i)} x \cdot x \right) \rangle \end{bmatrix} \quad (4.3) \\
 \begin{bmatrix} A_{1111111}^{\text{hom,stat}} \end{bmatrix} &= \begin{bmatrix} C_5^1 \end{bmatrix} = \begin{bmatrix} \langle 2A_{1111}^{K(i)} (\lambda_i + 2\mu_i) A_{1111111}^{K(i)} \rangle \end{bmatrix}
 \end{aligned}$$

Where in Eq. (4.3),  $\lambda_i$  and  $\mu_i$  are the Lamé constants of each material phase contained in the unit-cell design with the subscript  $i \in \{1,2\}$  to denote the corresponding phase. Using a

simplified notation for the constants  $C_i^1$ , the dynamic stress and hyperstress definitions in Eq. (4.2) can be re-written as follows:

$$\begin{aligned}\Sigma_{11}^{\text{hom,dyn}} &= \begin{bmatrix} C_1^1 & C_2^1 \end{bmatrix} \begin{bmatrix} E_{11} \\ \ddot{E}_{11} \end{bmatrix} + \begin{bmatrix} C_3^1 & C_4^1 \end{bmatrix} \begin{bmatrix} K_{111} \\ \dot{K}_{111} \end{bmatrix} \\ S_{111}^{\text{hom,dyn}} &= \begin{bmatrix} C_3^1 & C_4^1 \end{bmatrix} \begin{bmatrix} E_{11} \\ \ddot{E}_{11} \end{bmatrix} + [C_5^1][K_{111}]\end{aligned}\quad (4.4)$$

The stiffness coefficients  $C_i^1$  are calculated based on the unit-cell constituent material properties of Table 4.1, with the localization operator expressions defined by Eq. (3.A2) and (3.A5). For the computations to follow, equal phase thickness properties ( $d_1 = d_2$ ) are employed.

### 4.2.3 Static and dynamic equilibrium of the homogenized structure

The dynamic equilibrium equation of motion along the longitudinal axis of the composite beam structure in Fig. 4.1b writes as follows:

$$\nabla_x (\Sigma_{11} - \nabla_x S_{111}) = \rho^{\text{hom}} \frac{\partial^2 U}{\partial t^2} \quad (4.5)$$

Where in Eq. (4.5),  $\rho^{\text{hom}}$  stands for the homogenized density of the beam microstructure. Using the stress and hyperstress definitions of Eq. (4.4) and after substitution into the dynamic equilibrium Eq. (4.5), we obtain the following dynamical equilibrium equation:

$$C_1^1 \frac{\partial^2 U}{\partial X^2} + C_2^1 \frac{\partial^2}{\partial t^2} \left( \frac{\partial^2 U}{\partial X^2} \right) - C_5^1 \frac{\partial^4 U}{\partial X^4} = \rho^{\text{hom}} \frac{\partial^2 U}{\partial t^2} \quad (4.6)$$

Where in Eq. (4.6), the coupling stiffness terms  $C_3^1$  and  $C_4^1$  entering Eq. (4.4) cancel out. In Eq. (4.6), the root of the ratio of the second to first gradient coefficients  $C_5^1$  and  $C_1^1$  defines the longitudinal internal length parameter  $l_e = \sqrt{C_5^1 / C_1^1}$ . Accordingly, the stiffness coefficient  $C_2^1$  characterizes the micro-inertia contribution part, represented by the second term on the left hand side of Eq. (4.6). We note that Eq. (4.6) simplifies to the classical Cauchy mechanics description of the medium, once the micro-inertia and second gradient contribution terms are neglected, as follows:

$$C_1^1 \frac{\partial^2 U}{\partial X^2} = \rho^{\text{hom}} \frac{\partial^2 U}{\partial t^2} \quad (4.7)$$

By eliminating the time-dependent derivatives in Eq. (4.7), we obtain the Cauchy mechanics, static equilibrium of the structure. Similarly, the higher gradient static equilibrium is obtained by eliminating the time-dependent derivatives from Eq. (4.6), as follows:

$$C_1^1 \frac{\partial^2 U}{\partial X^2} - C_5^1 \frac{\partial^4 U}{\partial X^4} = 0 \quad (4.8)$$

## 4.3 Results

### 4.3.1 Static response

In the current section, we compute the longitudinal static response of a composite beam structure (Fig. 4.1a) based on the higher-gradient equilibrium definition of Eq. (4.8). For the computation of the Cauchy and higher-gradient stiffness parameters ( $C_1^1$  and  $C_5^1$  accordingly), we make use of the constitutive expressions of Eq. (4.3). Different unit-cell material designs are employed relevant to engineering praxis (Tan & Poh, 2018). In particular, Borosilicate Glass and Silicon Carbide, E-Glass and epoxy, as well as Carbon and Epoxy unit-cell designs are used in equal volumetric proportions within the unit-cell structure (Tan & Poh, 2018). Each of them leads to different first and second gradient ( $C_1^1$  and  $C_5^1$  accordingly) stiffness coefficients, as well as effective internal length values  $l_e$ , as summarized in Table 4.2:

*Table 4.2 : Homogenized stiffness coefficients and internal length values for different Carbon and Glass-based unit-cell material designs using the material properties of Table 4.1 and the definitions of Eq. (4.3).*

Materials	Unit-cell	$C_1^1$ (MPa)	$C_5^1$ (MPa · mm <sup>2</sup> )	$l_e$ (mm)
1	Borosilicate Glass- Silicon Carbide	120761.54	5088.52	0.205
2	E-Glass- Epoxy	9491.49	326.86	0.186
3	Carbon- Epoxy	9913.36	245.23	0.157

We note that the internal length values obtained using the homogenization method of Section 4.2.2 lie in close agreement to the ones provided in (Tan & Poh, 2018), where a 0.193mm, 0.163mm and 0.15mm value has been accordingly computed for the Borosilicate Glass- Silicon Carbide, E-Glass- Epoxy and Carbon- Epoxy unit-cell designs.

We compute the higher-gradient static structural response by solving Eq. (4.8), which requires a total of four boundary conditions, as of its fourth-order nature. We employ two classical, one non-classical and a symmetry boundary condition for the strain at the middle of the beam structure. In particular, we set the displacement at the start equal to zero ( $u(0)=0$ ) and the stress at the other end equal to the area-normalized applied force ( $\sigma(L)=P_0 / A$ ). Accordingly, we set the rate of strain change at the middle of the beam structure equal to zero ( $\varepsilon'(L/2)=0$ ) and the strain value at the start of the beam equal to a non-classical, non-Cauchy-mechanics value  $\varepsilon_{SG}$  that can be in general different from the constant strain profile corresponding to the Cauchy-mechanics solution of the problem ( $\varepsilon_0=(P_0 / A) / C_1^I$ ).

$$\begin{cases} u(0) = 0, & \sigma(L) = P_0 / A \\ \varepsilon(0) = \varepsilon_{SG}, & \varepsilon'(L/2) = 0 \end{cases} \quad (4.9)$$

Solving the equilibrium of Eq. (4.8) with the boundary conditions of Eq. (4.9), we directly obtain the strain and displacement field along the length of the beam structure. In Fig. 4.2, we provide the strain and displacement profile for the case of a microscale material design with Borosilicate Glass and Silicon Carbide, with an internal length value of  $l_e = 0.2mm$  (the effective properties summarized in Table 4.2). For the strain-related end boundary condition, we employ the limiting case of a zero end-strain ( $\varepsilon_{SG} = 0$ ), leading to a highly non-linear strain profile evolution, as depicted in Fig. 4.2a.

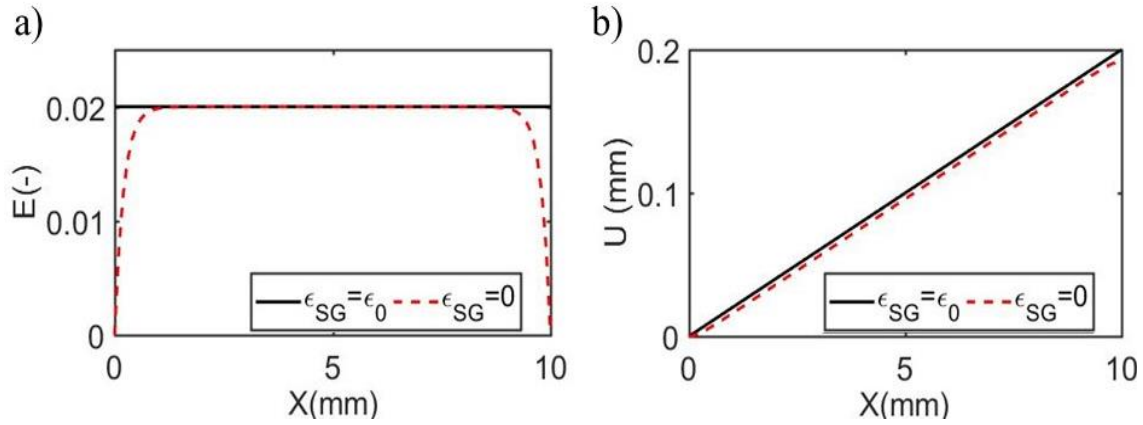


Figure 4.2 : Strain and displacement along the beam using the second gradient formulation for  $\epsilon_{SG} = 0$  (Red), and the linear solution for  $\epsilon_{SG} = \epsilon_0$  (Black) for a loading  $P_0 / A = 0.02C_1^I$  at the loaded extremity of the beam.

Fig. 4.2 highlights a strong boundary layer effect occurring at both domain edges, since the local strains for the boundary condition  $\epsilon_{SG} = 0$  are incompatible with the Cauchy-type, pure first-gradient solution. This strain heterogeneity reflects the importance of second gradient effects to capture such boundary layers. On the other hand, Fig. 4.2 indicates that the effect of the higher-gradient on the displacement profile of the beam is rather small for an internal length value of  $l_e = 0.2mm$  obtained for the unit-cell with Borosilicate Glass and Silicon Carbide, its properties summarized in Table 4.2. The difference in the end-tip displacement is in the order of 4%, a value which reflects the maximum difference for all practice-relevant composite material designs of Table 4.2. In particular, a tip-displacement difference of 3.7% is computed for the E-Glass and Epoxy unit-cell material design of Table 4.2 and a 3.1% for the Epoxy and Carbon unit-cell material design. We note that analogous results are obtained for the case of a variable beam length, where the higher-gradient end-tip displacement of a beam structure with a length  $L = 15mm$  and  $L = 20mm$  differs accordingly by 2.7% and 2% with respect to the Cauchy mechanics solution for Borosilicate Glass and Silicon Carbide.

In Fig. 4.3, we analyze the sensitivity of the longitudinal static response on the internal length value of the material, employing  $l_e$  values that way exceed the range of internal length values computed for the common engineering material designs of Table 4.2.

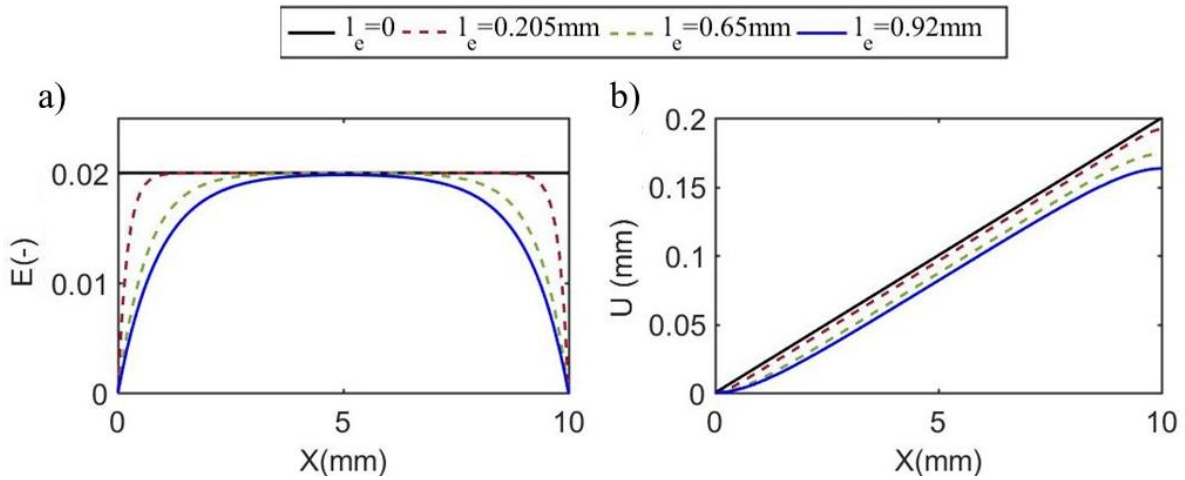


Figure 4.3 : Macroscopic strain (a) and displacement (b) profiles for a total of four internal length values, starting from the Cauchy-mechanics case ( $l_e = 0$ ) up to a substantially high internal length value of  $l_e = 0.92$  mm . The loading is kept constant to  $P_0 / A = 0.02C_1^I$  as in the results of Fig. 4.2.

The results of Fig. 4.3 elucidate the influence of the internal length value  $l_e$  on the macroscopic displacement field of the structure. Using the Cauchy (black curve,  $l_e = 0$ ) and Borosilicate Glass and Silicon Carbide case (red curve,  $l_e = 0.205$  mm) as a reference (also depicted in Fig. 4.2), we observe that as we increase the internal length values, the difference in the higher-gradient and Cauchy mechanics predictions of the end-tip displacement of the structure are increasing. In particular, the difference in the end-tip displacement between the higher-gradient and the Cauchy mechanics predictions become 13% (green curve) and 18.4% (blue curve) for the artificial material designs with internal length values of  $l_e = 0.65$  mm and  $l_e = 0.92$  mm accordingly.

### 4.3.2 Micro-inertia effects on the higher-gradient, eigenfrequency properties

In the sequel, we analyze the eigenfrequency properties of the composite structure accounting both for micro-inertia and higher-gradient effects on its dynamic characteristics. For completeness, in Section 4.3.2.1, we compute the eigenfrequency properties in the simplified, Cauchy-mechanics case, where micro-inertia and higher-gradient effects are neglected. Subsequently, in Section 4.3.2.2, we quantify the effect of micro-inertia contributions on the effective dynamic properties for composite materials used in praxis, while in Section 4.3.3 we carry out a general-case, sensitivity study on the internal-length and relative density values.

#### 4.3.2.1. Cauchy mechanics eigenfrequency attributes

We hereby compute the eigenfrequency properties of the composite beam structure of Fig. 1a using the dynamic Cauchy mechanics formulation of Eq. (4.7). For the eigenfrequency computation, we insert the general waveform solution  $U(X,t) = U_0 e^{i(kX \pm \omega t)}$  in the differential equilibrium of Eq. (4.7), where  $k$  stands for the propagating wavenumber and  $\omega$  for the corresponding frequency. After simplifications, we obtain:

$$\omega^2 = k^2 \cdot \left( \frac{C_1^1}{\rho^{\text{hom}}} \right) \quad (4.10)$$

The static displacement field profile  $Z(X)$  is obtained using the method of separation of variables for the macro-displacement field  $U(X,t)$ . The time-dependent response  $T(t)$  is thus decoupled from the spatial displacement profile, as follows:

$$U(X,t) = Z(X) \cdot T(t) \quad (4.11)$$

Inserting the definition of Eq. (4.11) to the dynamic equilibrium of Eq. (4.7), we obtain for the time-dependent and the following two equations:

$$T''(t) = -\omega^2 \cdot T(t) = -k^2 \cdot \left( \frac{C_1^1}{\rho^{\text{hom}}} \right) \cdot T(t) \quad (4.12a)$$

$$C_1^1 \cdot Z''(X) + k^2 \cdot (C_1^1) \cdot Z(X) = 0 \quad (4.12b)$$

The general solution form of Eq. (4.12b) writes:

$$Z(X) = R_1(k) \cdot \cos(k \cdot X) + R_2(k) \cdot \sin(k \cdot X) \quad (4.13)$$

Where in Eq. (4.13) the constant parameters  $R_1$  and  $R_2$  can be directly determined by the boundary conditions of the structure. For the case of zero end displacements ( $Z(0|L) = 0$ ), we determine the values of  $k$  which give a unique solution of the constants  $R_1$  and  $R_2$ , leading to a solution of the following form:

$$\sin(\xi) = 0 \quad (4.14)$$

Where  $\xi = kL$  in Eq. (4.14) stands for the normalized wavenumber. We insert the roots of Eq. (4.14) into the frequency expression of Eq. (4.10) to obtain the eigenfrequency values for the different modes. In Eq. (4.15), we provide the first three eigenmodes for all unit-cell from Table 4.1 as follows:

$$\begin{aligned} \omega_{c1}^{Mat1} &= \frac{\pi}{L} \sqrt{\frac{C_1^1}{\rho^{\text{hom}}}} = 2.1 \cdot 10^6 \text{ Hz}, \omega_{c2}^{Mat1} = \frac{2\pi}{L} \sqrt{\frac{C_1^1}{\rho^{\text{hom}}}} = 4.2 \cdot 10^6 \text{ Hz}, \omega_{c3}^{Mat1} = \frac{3\pi}{L} \sqrt{\frac{C_1^1}{\rho^{\text{hom}}}} = 6.3 \cdot 10^6 \text{ Hz} \\ \omega_{c1}^{Mat2} &= \frac{\pi}{L} \sqrt{\frac{C_1^1}{\rho^{\text{hom}}}} = 7 \cdot 10^5 \text{ Hz}, \omega_{c2}^{Mat2} = \frac{2\pi}{L} \sqrt{\frac{C_1^1}{\rho^{\text{hom}}}} = 1.4 \cdot 10^6 \text{ Hz}, \omega_{c3}^{Mat2} = \frac{3\pi}{L} \sqrt{\frac{C_1^1}{\rho^{\text{hom}}}} = 2.12 \cdot 10^6 \text{ Hz} \\ \omega_{c1}^{Mat3} &= \frac{\pi}{L} \sqrt{\frac{C_1^1}{\rho^{\text{hom}}}} = 8 \cdot 10^5 \text{ Hz}, \omega_{c2}^{Mat3} = \frac{2\pi}{L} \sqrt{\frac{C_1^1}{\rho^{\text{hom}}}} = 1.6 \cdot 10^6 \text{ Hz}, \omega_{c3}^{Mat3} = \frac{3\pi}{L} \sqrt{\frac{C_1^1}{\rho^{\text{hom}}}} = 2.4 \cdot 10^6 \text{ Hz} \end{aligned} \quad (4.15)$$

We compare the computed eigenfrequencies of Eq. (4.15) with the ones obtained out of the dynamic, finite element analysis (Abaqus) of the composite beam structure for the case of a micro-scale design composed by Borosilicate Glass and Silicon Carbide, as summarized in Table 4.1, using the same boundary conditions of Section 4.3.2.1. We provide the mesh and the displacement profiles for the first three eigenmodes along with the corresponding frequency values in Fig. 4.4:

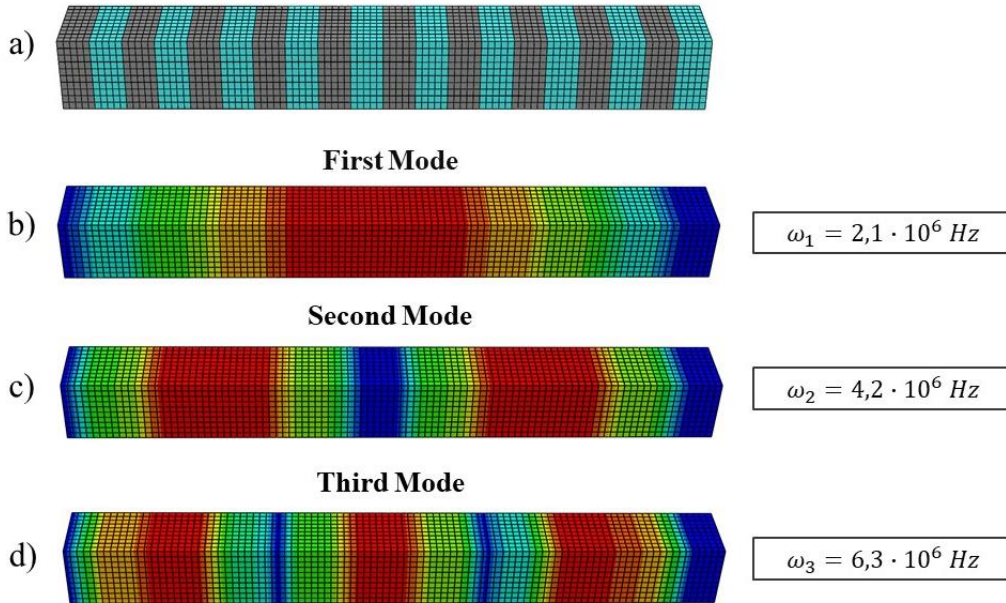


Figure 4.4: Mesh (a) and longitudinal displacement profiles for the first three eigenfrequency values (b, c and d accordingly) along with the corresponding eigenfrequency value for the Borosilicate Glass and Silicon Carbide unit-cell design of Table 4.2.

The eigenfrequency values obtained by the finite element based eigenfrequency analysis match the results obtained by the use of the homogenized structural properties. In particular,

the relative difference lies below 1% for all micro-scale material attributes of Table 4.2 for all eigenfrequency values of Eq. (4.15). We below extend the eigenfrequency analysis to quantify the effect of higher-gradient and micro-inertia contributions..

#### 4.3.2.2 Micro-inertia effects on the higher-gradient dynamic attributes

We subsequently analyze the effect of micro-inertia contributions on the longitudinal eigenfrequencies of different composite beam designs in the presence of higher-gradient effects. To that scope, we consider the complete form of the dynamic equilibrium equation provided in Eq. (4.6), for which we obtain the following expression for the eigenfrequency values  $\omega$ , proceeding in a complete analogy to Section 4.3.2.1:

$$\omega^2 = k^2 \cdot \left( \frac{C_5^1 \cdot k^2 + C_1^1}{k^2 \cdot C_2^1 + \rho^{\text{hom}}} \right) \quad (4.16)$$

The eigenfrequency definition of Eq. (4.16) depends, not only on the static stiffness term attribute  $C_1^1$  as in the Cauchy mechanics formulation case (Eq. (4.10)), but also on the second-gradient stiffness  $C_5^1$  and on the micro-inertia coefficient  $C_2^1$  term. Applying the separation of variables process (Eq. (4.11)) for the dynamic equilibrium Eq. (4.6), we obtain the following set of decoupled space and time differential equations in complete analogy to Section 4.3.2.1:

$$T''(t) = -\omega^2 \cdot T(t) = -k^2 \cdot \left( \frac{C_5^1 \cdot k^2 + C_1^1}{k^2 \cdot C_2^1 + \rho^{\text{hom}}} \right) \cdot T(t) \quad (4.17a)$$

$$Z'''' \cdot (-C_5^1) + Z'' \cdot (C_1^1 - C_2^1 \cdot \omega^2) + Z \cdot \rho^{\text{hom}} \omega^2 = 0 \quad (4.17b)$$

Eq. (4.17b) contains not only the forth-order, higher-gradient term related to the stiffness coefficient  $C_5^1$ , but also the effect of the micro-inertia term  $C_2^1$  encompassed in the modified coefficient of the second order spatial derivative. Its effect is frequency-dependent, as it can be directly observed out of the multiplying frequency term. The general solution of the differential Eq. (4.17b) takes the form:

$$Z(X) = C_1'(k) \cdot e^{\Psi \cdot X} + C_2'(k) \cdot e^{-\Psi \cdot X} + C_3'(k) \cdot \cos(k \cdot X) + C_4'(k) \cdot \sin(k \cdot X) \quad (4.18)$$

Where in Eq. (4.18),  $\Psi' = \frac{\sqrt{C_1^1 \rho^{\text{hom}} + C_5^1 k^2 \rho^{\text{hom}}}}{\sqrt{C_2^1 C_5^1 k^2 + C_3^1 \rho^{\text{hom}}}}$  is a constant parameter that depends on all effective material parameters entering Eq. (4.6), as well as on the propagating wavenumber  $k$ . The constants  $C_i'(k)$  are computed for the case of zero end-displacements and displacement gradients ( $Z(0|L) = Z'(0|L) = 0$ ), in complete analogy to Section 4.3.2.1. Thereupon, the characteristic equation of Eq. (4.19) is obtained for the wavenumber to get a unique solution for the constants  $C_i'(k)$ , as follows:

$$\begin{aligned} & \sin(kL) \cdot (e^{-\Psi' L} - e^{\Psi' L}) \cdot (k^2 - \Psi'^2) + 2\Psi' \cdot k \cdot \cos(kL) \cdot (-e^{-\Psi' L} - e^{\Psi' L}) \\ & + 2k \cdot \Psi' (1 + e^{-\Psi' L} \cdot e^{\Psi' L}) = 0 \end{aligned} \quad (4.19)$$

After the computation of the roots of Eq. (4.19), the eigenfrequencies can be directly computed using Eq. (4.16), which can be re-written in a non-dimensional form as follows:

$$\Omega' = \frac{\omega'}{\sqrt{\frac{C_1^1}{\rho^{\text{hom}}}}} \cdot L = \frac{kL}{\sqrt{\frac{C_1^1}{\rho^{\text{hom}}}}} \cdot \left( \sqrt{\frac{C_5^1 \cdot k^2 + C_1^1}{k^2 \cdot C_2^1 + \rho^{\text{hom}}}} \right) \quad (4.20)$$

For the eigenfrequencies' computation, the complete set of effective material parameters needs to be calculated. The effective relative density  $\rho^{\text{hom}}$  and micro-inertia  $C_2^1$  parameters for each of the composite material designs of Table 4.2 are provided in Table 4.3. The computations are based on the mechanical definitions of Section 4.2.2.

Table 4.3 : Homogenized static and dynamic properties of the composite unit-cell material designs of Tables 1 and 2 for equal micro-scale layer thickness  $d_i$  in Fig. 4.1a.

Material	Unit-cell		$C_2^1$ (tonne/mm)	$\rho^{\text{hom}}$ (tonne/mm <sup>3</sup> )
1	Borosilicate Glass	Silicon Carbide	$1.57 \cdot 10^{-10}$	$2.65 \cdot 10^{-9}$
2	E-Glass	Epoxy	$1.45 \cdot 10^{-10}$	$1.875 \cdot 10^{-9}$
3	Carbon	Epoxy	$1.3 \cdot 10^{-10}$	$1.525 \cdot 10^{-9}$

Chapter 4: Higher-gradient and micro-inertia contributions on the mechanical response of composite beam structures

We subsequently compute the first three eigenfrequencies of the composite beam structure of Fig. 4.1b ( $L=10mm$ ), considering the different unit-cell material property combinations of Tables 4.2 and 4.3. In Table 4.4, we provide the normalized eigenfrequency values for a unit-cell structure composed of Borosilicate Glass and Silicon Carbide. For each mode, the Cauchy mechanics eigenfrequency ( $\Omega_c$ , Section 4.3.2.1) is computed, along with the second-gradient eigenfrequency value ( $\Omega_{SG}$ ) for which the micro-inertia effects are disregarded ( $c_2^1$  is set to zero in Eq. (4.20)) and the eigenfrequency value where both second-gradient and micro-inertia contributions are considered ( $\Omega_{SG+\mu I}$ ).

Table 4.4 : Eigenfrequency values of the composite Silicon Carbide-Borosilicate Glass (Tables 4.2, 4.3) beam structure upon a Cauchy (C), Second-Gradient (SG) and Second-Gradient with micro-inertia (SG+ $\mu I$ ) modeling formulation.

Mode	Cauchy		SG			SG + $\mu I$		
	$\xi$	$\Omega_c$	$\xi$	$\Omega_{SG}$	$\%(\Omega_{SG} - \Omega_c) / \Omega_c$	$\xi$	$\Omega_{SG+\mu I}$	$\%(\Omega_{SG+\mu I} - \Omega_c) / \Omega_c$
1	$\pi$	3.14	3.28	3.28	4.6	3.28	3.27	4.1
2	$2\pi$	6.28	6.55	6.61	5.3	6.55	6.53	4
3	$3\pi$	9.42	9.82	10.01	6.3	9.83	9.75	3.5

Table 4.4 indicates that the eigenfrequency values computed with the incorporation of second-gradient effects are higher than the ones obtained by the classical, Cauchy-mechanics based formulation. The difference for the Borosilicate Glass-Silicon Carbide material case is in the order of 4-6% for the second-gradient modeling formulation, with the actual value to depend on the mode of interest, upon a uniquely increasing relative difference for the higher modes. The corresponding relative difference for the case where micro-inertia contributions are accounted for is lower compared to the second-gradient modeling case. The numerical result reflects the definition of Eq. (4.20), where the micro-inertia terms contribute to the denominator of the frequency expression.

For the higher modes, the second-gradient formulation with micro-inertia contributions provides results which are closer to the Cauchy mechanics predictions, with the purely second-gradient formulation to substantially overestimate the eigenfrequency values. In Table 4.5, we provide the corresponding results for the case of a composite material design with a lower internal length value ( $l_e = 0.185mm$ ) and a lower relative density value.

Table 4.5 : Eigenfrequency values of the composite E-Glass and Epoxy (Tables 4.2, 4.3) beam structure upon a Cauchy (C), Second-Gradient (SG) and Second-Gradient with micro-inertia contributions (SG+ $\mu I$ ) modeling formulation.

Mode	Cauchy		SG			SG + $\mu I$		
	$\xi$	$\Omega_c$	$\xi$	$\Omega_{SG}$	$\%(\Omega_{SG} - \Omega_c) / \Omega_c$	$\xi$	$\Omega_{SG+\mu I}$	$\%(\Omega_{SG+\mu I} - \Omega_c) / \Omega_c$
1	$\pi$	3.14	3.26	3.27	4.1	3.26	3.26	3.8
2	$2\pi$	6.28	6.52	6.57	4.6	6.53	6.47	3
3	$3\pi$	9.42	9.78	9.94	5.52	9.79	9.6	1.9

Table 4.5 provides relative differences in the eigenfrequency values that increase upon increasing mode for the second-gradient modeling formulation, as in the case of the composite material design of Table 4.4, though lower in magnitude, as of the lower internal length value. However, when micro-inertia effects are considered in the eigenfrequency computation, the eigenfrequency values computed are closer to the Cauchy-mechanics predictions.

While for the first mode the eigenfrequency values for the second-gradient and second-gradient with micro-inertia formulations are rather close, the corresponding difference for the third mode becomes substantial. In particular, neglecting the micro-inertia effects leads to a substantial overestimation of the third eigenfrequency with respect to the higher-gradient with micro-inertia dynamic model (SG+ $\mu I$ ). More specifically, a nearly three times higher relative eigenfrequency difference is obtained for the third mode (5.52 vs 1.9% in Table 4.5).

In Table 4.6, we summarize the eigenfrequency values for the third composite material combination of Table 4.3, with the lowest internal length value ( $l_e = 0.157mm$ ) and the most lightweight material design of Table 4.3.

Table 4.6 : Eigenfrequency values of the composite Carbon and Epoxy (Tables 4.2, 4.3) beam structure upon a Cauchy (C), Second-Gradient (SG) and Second-Gradient with micro-inertia effects (SG+ $\mu I$ ).

Mode	Cauchy		SG			SG + $\mu I$		
	$\xi$	$\Omega_c$	$\xi$	$\Omega_{SG}$	$\%(\Omega_{SG} - \Omega_c) / \Omega_c$	$\xi$	$\Omega_{SG+\mu I}$	$\%(\Omega_{SG+\mu I} - \Omega_c) / \Omega_c$
1	$\pi$	3.14	3.24	3.25	3.5	3.24	3.23	2.9
2	$2\pi$	6.28	6.49	6.52	3.8	6.49	6.41	2
3	$3\pi$	9.42	9.73	9.84	4.5	9.74	9.47	0.5

Table 4.6 reveals the same pattern with the ones observed for the inner composite material designs of Tables 4.4 and 4.5. In particular, the second-gradient formulation yields higher eigenfrequency values with respect to the Cauchy-mechanics predictions for all modes, with the relative differences to increase upon increasing mode value. However, in the higher-gradient with micro-inertia contributions case ( $SG+\mu I$ ), an inverse pattern is obtained. More specifically, while the  $SG+\mu I$  modeling formulation yields an eigenfrequency value that is very close to the Cauchy mechanics predictions for the third mode, the use of a merely second-gradient formulation overestimates the eigenfrequency value by an additional 4% (4.5% in Table 4.6).

### 4.3.3 Sensitivity of the dynamic properties on the micro-inertia contributions for different second-gradient material designs

The results of Section 4.3.2.2 provide evidence that the role of micro-inertia on the effective structural dynamic properties depends both on the magnitude of the internal length parameter, as well as on the mode of interest. We subsequently analyze the sensitivity of the three primal longitudinal eigenfrequency values on the value of the internal length parameter  $l_e$ . To that scope, we use the Cauchy mechanics stiffness  $c_1^I$  and relative density value  $\rho^{\text{hom}}$  computed for the composite Silicon Carbide and Borosilicate Glass material case in Tables 4.2 and 4.3. In Fig. 4.5, we compute the sensitivity of the eigenfrequency values of Eq. (4.16) on the micro-inertia contributions  $c_2^I$ , for the three primal structural modes for different values of the internal length  $l_e$ .

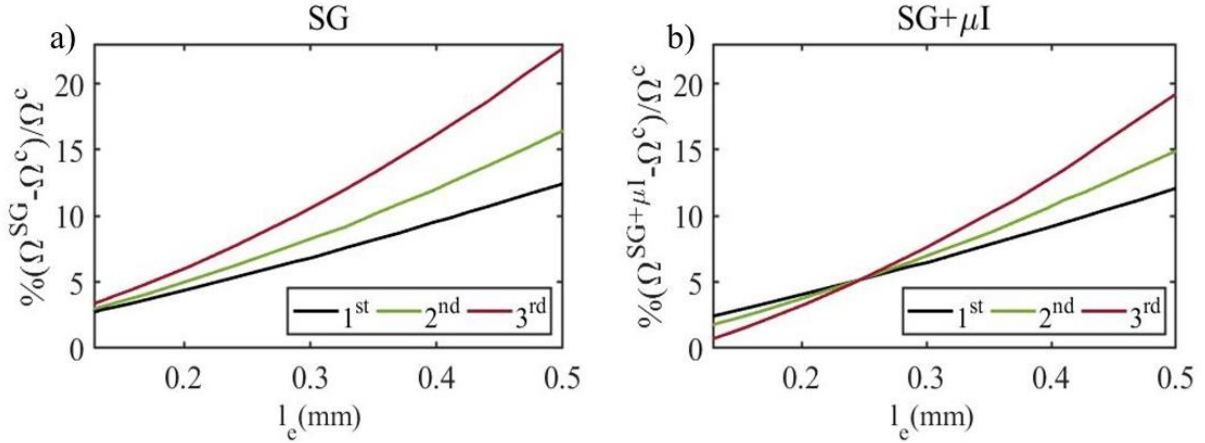


Figure 4.5 : Relative difference of the eigenfrequency values computed for the second-gradient ( $SG$ ) and the second-gradient with micro-inertia ( $SG+\mu I$ ) formulation (subplots (a) and (b) accordingly) for the first three eigenmodes for different values of the internal length

$$l_e.$$

Comparing the relative eigenfrequency differences of Fig. 4.5a and Fig. 4.5b we can directly deduce that the significance of micro-inertia contributions highly depends on the internal length value and mode of interest. More specifically, in the low range of internal length values, micro-inertia contributions reduce the difference between the complete modeling formulation ( $SG+\mu I$ ) and the Cauchy-mechanics predictions (Fig. 4.5b), with the effect to be more prominent for the second and third mode. Contrariwise, for high internal length values ( $l_e > 0.25mm$ ) the differences in-between the results of the higher-gradient with micro-inertia formulation ( $SG+\mu I$ ) and the purely second-gradient ( $SG$ ) results are substantially reduced, as the comparison between the curves of Figs. 4.5a and 4.5b suggest.

We subsequently explore the sensitivity of the eigenfrequency values on the density values of the material phases contained in the unit-cell of the underlying microstructure. The latter affect the micro-inertia coefficient  $C_2^1$  entering the definition of Eq. (4.6). To that scope, we consider different internal length values, namely  $l_e$  values of 0.153 mm, 0.205 mm, 0.25 mm and 0.29 mm, while we vary the ratio of the micro-scale material density to lie in-between 1 and 16. In Fig. (4.6), we compare the eigenfrequency results computed by the higher-gradient with micro-inertia formulation ( $SG+\mu I$ ) with the Cauchy-mechanics predictions using the normalized eigenfrequency form of Eq. (4.20). We note that for the purely second-gradient case, the relative differences arising with respect to the Cauchy-mechanics predictions do not depend on the density ratio variations of the material phases contained in the unit-cell design,

as solely the relative density value  $\rho^{\text{hom}}$  affects the eigenfrequency value computations of Eq. (4.20), a term that cancels out for  $C_2^1 = 0$  in Eq. (4.20).

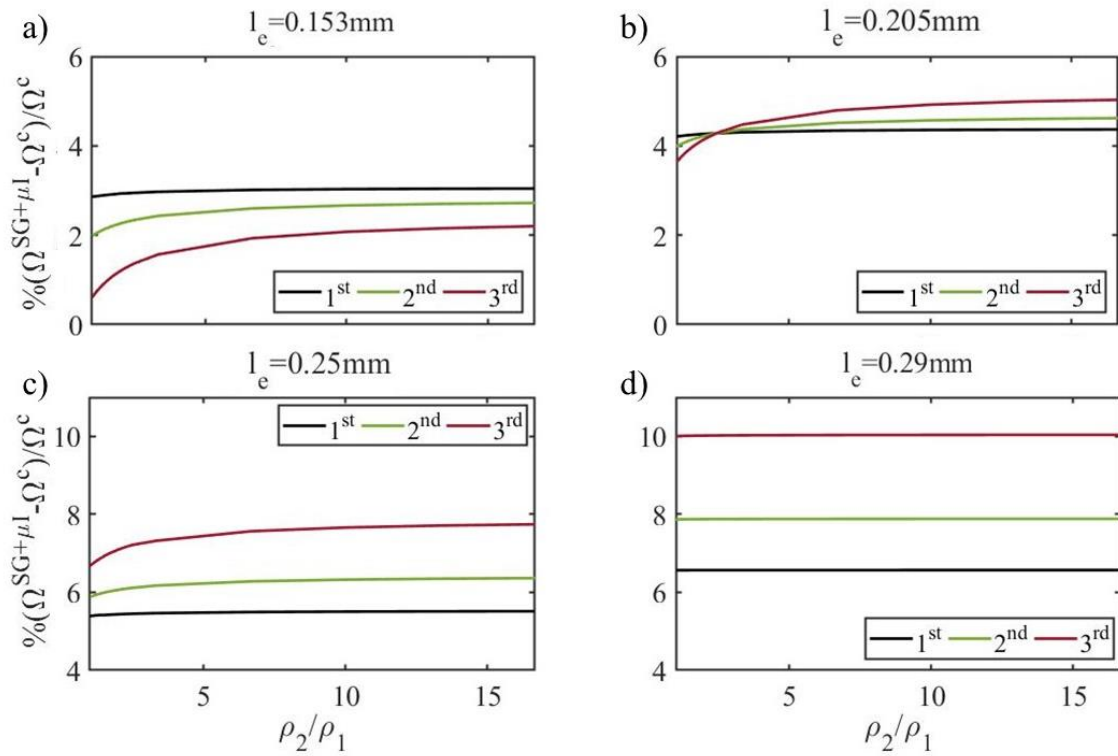


Figure 4.6 : Relative difference of the  $SG + \mu I$  response with respect to the Cauchy-mechanics (C) predictions as a function of the variation of the density ratio of the individual material phases contained in the unit-cell for different internal lengths values  $l_e = 0.153\text{mm}$  (a),  $l_e = 0.205\text{mm}$  (b),  $l_e = 0.25\text{mm}$  (c) and  $l_e = 0.29\text{mm}$  (d).

Fig. 4.6 indicates that the differences observed in between the second-gradient and micro-inertia formulation ( $SG + \mu I$ ) and the Cauchy-mechanics (C) results depend, not only on the value of the internal length parameter  $l_e$ , but also on the ratio of the density values of the material phases contained in the microstructure of the material. Figs. 4.6a, 4.6b and 4.6c reveal the nature of the dependence for a given internal length value: Upon increasing ratios of the density values, the difference to the Cauchy mechanics predictions increase. The effect appears in the low range of  $l_e$  values ( $l_e < 0.25\text{mm}$ ) and is more prominent for low values of the  $\rho_2 / \rho_1$  ratio. As the internal length values increase ( $l_e > 0.25\text{mm}$ ), the second-gradient and micro-inertia modeling predictions ( $SG + \mu I$ ) become insensitive to the ratio of the density values contained in the unit-cell within the microscale, yielding a  $\rho_2 / \rho_1$  insensitive response for  $l_e = 0.29\text{mm}$

(Fig. 4.6d), thus emulating the second-gradient modeling response predictions of Eq. (4.20) for  $C_2^1 = 0$ .

#### 4.4 Discussion

The selection of the proper modeling formulation is of crucial importance for the accurate characterization of the mechanical response of multiscale structures. From a constitutive modeling perspective, the internal length is sufficient to assess the importance of higher-gradient stiffness contributions on the static macroscale mechanical response of beam structures. However, for the dynamic structural properties, not only the complete spectrum of the available static-related attributes need to be accounted for, but also all dynamics-related characteristics, micro-inertia contributions included.

The bottom-up static analysis of Section 4.3.1 indicates that the relative importance of higher-gradient contributions on the longitudinal static response is rather low for typical composite element designs with low internal length values ( $l_e \in [0..0.25mm]$ , Fig. 4.2). In particular, using the utterly non-linear strain profile distribution of Fig. 4.2a corresponding to a highly inhomogeneous element strain evolution, the difference of the higher-gradient end-tip displacement solution from the Cauchy mechanics results is below 5%. Substantial differences can occur (>10%) only for internal length values that way exceed ( $l_e > 0.5mm$ ) the range computed for the composite material designs of Table 4.1 as in Fig. 4.3. The framework provided in Section 4.2 allows for a direct, multiscale computation of the relevant higher-gradient parameters for micro-scale material constituents beyond the ones summarized in Table 4.1, providing a generic means of quantifying the magnitude and significance of the microscale parameters.

While the effective static displacements of Figs. 4.2 and 4.3 are reduced upon the incorporation of the higher-gradient stiffness contributions, the corresponding dynamic eigenfrequency attributes are increased (Sections 4.3.2, 4.3.3). Considering a purely second-gradient constitutive modeling formulation, without the effect of micro-inertia parameters leads solely to higher eigenfrequency values for all structural modes, an effect that can be explained using Eq. (4.16) upon a zero value of the micro-inertia coefficient term ( $C_2^1 \rightarrow 0$  in Eq. (4.16)). However, when micro-inertia effects are accounted for, the structural eigenfrequency values can be either closer to or quasi-identical to the Cauchy mechanics predictions, depending on the mode of interest and on the internal length value. The

significance of the micro-inertia parameters increases for low internal length values ( $l_e \in [0 \dots 0.25 \text{mm}]$ , Fig. 4.5), thus within the range of internal lengths expected for typical composite inner material designs, as the ones provided in Tables 4.1 and 4.2. Thereupon, the frequency space separating the higher eigenmodes can decrease, instead of systematically increasing as in the case of a purely second-gradient formulation.

Moreover, Fig. 4.6 provides evidence that for low internal length values ( $l_e \in [0 \dots 0.25 \text{mm}]$ , Fig. 4.6), the micro-inertia contributions introduce a sensitivity to the density ratio of the materials contained within the microscale of the structure, an effect that is more prominent for the higher-order modes (Figs. 4.6a, 4.6b). Effects of the kind cannot be captured by purely second-gradient formulations, as they restrain to the dependence on the relative density value  $\rho^{\text{hom}}$ , which simplifies in the normalized frequency form expression of Eq. (4.20) for  $C_2^1 = 0$ .

## 4.5 Conclusion

Overall, the current chapter has analyzed for the first time the role of micro-inertia and higher-gradient material parameters on the dynamic behavior of structural members in a combined manner. Evidence has been provided that the static response can be well-separated from the dynamic behavior where not-only higher-gradient, but also micro-inertia contributions appear. More specifically, it has been shown that while high internal length values are a prerequisite for non-negligible, higher-gradient effects to appear both in statics and dynamics, this is not the case for micro-inertia contributions. In particular, it has been demonstrated that micro-inertia terms can be significant in the low range of internal length values that is relevant for a wide range of commonly-used engineering materials. Thereupon, micro-inertia contributions can counteract the effect of higher-gradient stiffness terms, so that a mere consideration of higher-gradient terms may lead to a substantial overestimation of the computed eigenfrequencies, in particular for the higher-order modes. We aspire that the provided results serve as a reference for the computation of the longitudinal vibration properties, not only of composite structures, but also of general-form structural systems, providing a fundamental basis for the assessment of the relative significance of micro-inertia and higher-gradient material parameters.

## References

- [1] Andrianov, I. V., Bolshakov, V. I., Danishevskiy, V. V., and Weichert, D. (2008). Higher order asymptotic homogenization and wave propagation in periodic composite materials. *Proc. R. Soc. A.*, 464(2093). <https://doi.org/10.1098/rspa.2007.0267>.
- [2] Andresen, S., Bäger, A., Hamm, C. (2020). Eigenfrequency maximisation by using irregular lattice structures, *Journal of Sound and Vibration*, 465 (115027). <https://doi.org/10.1016/j.jsv.2019.115027>.
- [3] Altan, B. S., Evensen, H. A., Aifantis, E.C. (1996). Longitudinal vibrations of a beam: a gradient elasticity approach, *Mechanics Research Communications*, 23(1), 35-40. [https://doi.org/10.1016/0093-6413\(95\)00074-7](https://doi.org/10.1016/0093-6413(95)00074-7).
- [4] Bennett, T., Gitman, I. M., and Askes, H. (2007). Elasticity theories with higher-order gradients of inertia and stiffness for the modelling of wave dispersion in laminates. *Int. J. Fract.*, 148, 185–193. <https://doi.org/10.1007/s10704-008-9192-8>.
- [5] Berezovski, A., Engelbrecht, J., Salupere, A., Tamm, K., Peets, T., Berezovski, M. (2013). Dispersive waves in microstructured solids. *Int. J. Solids Struct.*, 50(11-12) 1981–1990. <https://doi.org/10.1016/j.ijsolstr.2013.02.018>.
- [6] Bisegna, P., Caruso, G. (2011). Dynamical behavior of disordered rotationally periodic structures: A homogenization approach, *Journal of Sound and Vibration*, Volume 330 (11), 2608-2627. <https://doi.org/10.1016/j.jsv.2010.12.009>.
- [7] Brito-Santana, H., Wang, Y. S., Rodriguez-Ramos, R., Bravo-Castillero, J., Guinovart-Daz, R., Tita, V. (2015). A dispersive nonlocal model for shear wave propagation in laminated composites with periodic structures. *Eur. J. Mech. A. Solids*, 49, 35–48. <https://doi.org/10.1016/j.euromechsol.2014.05.009>.
- [8] Chang, C.S. (1997). Wave propagation in granular rod using high-gradient theory. *J Eng Mech*, ASCE, 123 (1). [https://doi.org/10.1061/\(ASCE\)0733-9399\(1997\)123:1\(52\)](https://doi.org/10.1061/(ASCE)0733-9399(1997)123:1(52)).
- [9] Chen, W. and Fish, J. (2001). A dispersive model for wave propagation in periodic heterogeneous media based on homogenization with multiple spatial and temporal scales. *J. Appl. Mech.* 68(2), 153–161. <https://doi.org/10.1115/1.1357165>.
- [10] Cheng, L., Liang, X., Belski, E., Wang, X., Sietins, J.M., Ludwick, S., To, A. (2018). Natural Frequency Optimization of Variable-Density Additive Manufactured Lattice Structure: Theory and Experimental Validation, *J. Manuf. Sci. Eng.* 140(10): 105002 (16 pages). <https://doi.org/10.1115/1.4040622>.
- [11] De Domenico, D. and Askes, H. (2016). A new multi-scale dispersive gradient elasticity model with micro-inertia: Formulation and C0-finite element implementation. *Int. J. Numer. Meth. Eng.*, 108(5), 485–512. <https://doi.org/10.1002/nme.5222>.
- [12] Dingreville, R., Robbins, J., Voth, T. E. (2013). Multiresolution modeling of the dynamic loading of metal matrix composites. *JOM*, 65, 203–214. <https://doi.org/10.1007/s11837-012-0508-9>.
- [13] Dingreville, R., Robbins, J., Voth, T. E. (2014). Wave propagation and dispersion in elasto-plastic microstructured materials. *International Journal of Solids and Structures*, 51(11–12) 2226-2237. <https://doi.org/10.1016/j.ijsolstr.2014.02.030>.
- [14] Dontsov, E. V., Tokmashev, R. D., and Guzina, B. B. (2013). A physical perspective of the length scales in gradient elasticity through the prism of wave dispersion. *International Journal of Solids and Structures*, 50(22–23) 3674-3684. <https://doi.org/10.1016/j.ijsolstr.2013.07.012>.
- [15] Engelbrecht, J., Berezovski, A., Pastrone, F., and Braun, M. (2007). Waves in microstructured materials and dispersion. *Philos. Mag.*, 85(33-35), 4127–4141. <https://doi.org/10.1080/14786430500362769>.

- [16] Engelbrecht, J. and Berezovski, A. (2015). Reflections on mathematical models of deformation waves in elastic microstructured solids. *Mathematics and Mechanics of Complex Systems*, 3 (1) 43-82. <https://doi.org/10.2140/memocs.2015.3.43>.
- [17] Exadaktylos, G.E. & Vardoulakis, I. (1998). Surface instability in gradient elasticity with surface energy. *Int J Solids Struct* 35 (18) 2251–2281. [https://doi.org/10.1016/S0020-7683\(97\)89945-3](https://doi.org/10.1016/S0020-7683(97)89945-3).
- [18] Hui, T. & Oskay, C. (2014). A high order homogenization model for transient dynamics of heterogeneous media including micro-inertia effects. *Comput. Method. Appl. Mech. Eng.*, 273, 181–203. <https://doi.org/10.1016/j.cma.2014.01.028>.
- [19] Lim, C. W., Zhang, G., Reddy, J. N. (2015). A higher-order nonlocal elasticity and strain gradient theory and its applications in wave propagation. *Journal of the Mechanics and Physics of Solids*, 78, 298–313. <https://doi.org/10.1016/j.jmps.2015.02.001>.
- [20] Li, L., Hu, Y., Li, X. (2016). Longitudinal vibration of size-dependent rods via nonlocal strain gradient theory, *International Journal of Mechanical Sciences*, 115–116, 135-144, <https://doi.org/10.1016/j.ijmecsci.2016.06.011>.
- [21] Mallick, P. K. (2007). *Fibre-Reinforced Composites - Materials, Manufacturing and Design*. 536. CRC Press, Boca Raton, Florida.
- [22] Metrikine, A. V. and Askes, H. (2002). One-dimensional dynamically consistent gradient elasticity models derived from a discrete microstructure: Part 1: Generic formulation. *European Journal of Mechanics - A/Solids*, 21(4), 555-572. [https://doi.org/10.1016/S0997-7538\(02\)01218-4](https://doi.org/10.1016/S0997-7538(02)01218-4).
- [23] Mindlin, R.D., Eshel, N.N. (1968). On first strain-gradient theories in linear elasticity. *Int J Solids Struct*, 4(1) 109-124. [https://doi.org/10.1016/0020-7683\(68\)90036-X](https://doi.org/10.1016/0020-7683(68)90036-X).
- [24] Pichugin, A. V., Askes, H., and Tyas, A. (2008). Asymptotic equivalence of homogenisation procedures and fine-tuning of continuum theories. *Journal of Sound and Vibration*, 313(3–5), 858-874. <https://doi.org/10.1016/j.jsv.2007.12.005>.
- [25] Polyzos, D. and Fotiadis, D. I. (2012). Derivation of Mindlin's first and second strain gradient elastic theory via simple lattice and continuum models. *International Journal of Solids and Structures*, 49(3–4), 470-480. <https://doi.org/10.1016/j.ijsolstr.2011.10.021>.
- [26] Reda, H., Karathanasopoulos, N., Rahali, Y., Ganghoffer, J. F., & Lakiss, H. (2018). Influence of first to second gradient coupling energy terms on the wave propagation of three-dimensional noncentrosymmetric architected materials. *International Journal of Engineering Science*, 128, 151–164. <https://doi.org/10.1016/J.IJENGSCI.2018.03.014>.
- [27] Salehian, A., Inman, D.J. (2008). Dynamic analysis of a lattice structure by homogenization: Experimental validation, *Journal of Sound and Vibration*, 316 (1–5) 180-197. <https://doi.org/10.1016/j.jsv.2008.02.031>.
- [28] Shimoda, M., Nagano, T., Morimoto, T., Liu, Y., Shi, J.X. (2016). Non-parametric free-form optimal design of frame structures in natural frequency problem, *Int. J. Mech. Sci.* 117, 334–345, <https://doi.org/10.1016/j.ijmecsci.2016.08.024>.
- [29] Şimşek, M. (2016). Nonlinear free vibration of a functionally graded nanobeam using nonlocal strain gradient theory and a novel Hamiltonian approach, *International Journal of Engineering Science*, 105, 12-27. <https://doi.org/10.1016/j.ijengsci.2016.04.013>.
- [30] Syam, P.W., Jianwei, W., Zhao, B., Maskery, I., Elmadih, W., Leach, R. (2018). Design and analysis of strut-based lattice structures for vibration isolation, *Precision Engineering*, 52, 494-506. <https://doi.org/10.1016/j.precisioneng.2017.09.010>.
- [31] Tan, S.H. & Poh, L.H. (2018). Homogenized Gradient Elasticity Model for Plane Wave Propagation in Bilaminate Composites. *Journal of Engineering Mechanics*, 144 (9). [https://doi.org/10.1061/\(ASCE\)EM.1943-7889.0001496](https://doi.org/10.1061/(ASCE)EM.1943-7889.0001496).

#### Chapter 4: Higher-gradient and micro-inertia contributions on the mechanical response of composite beam structures

- [32] Tsepoura, K., Papargyri-Beskou, S., Polyzos, D., Beskos, D.E. (2002). Static and dynamic analysis of a gradient-elastic bar in tension, *Archive of Applied Mechanics*, 72, 483–497. <https://doi.org/10.1007/s00419-002-0231-z>.
- [33] Wautier, A. & Guzina, B. B. (2015). On the second-order homogenization of wave motion in periodic media and the sound of a chessboard. *J. Mech. Phys. Solids*, 78, 382–414. <https://doi.org/10.1016/j.jmps.2015.03.001>.
- [34] Yin, L., Qian, Q., Wang, L., Xia, W. (2010). Vibration analysis of microscale plates based on modified couple stress theory, *Acta Mechanica Solida Sinica*, 23 (5), 386-393, [https://doi.org/10.1016/S0894-9166\(10\)60040-7](https://doi.org/10.1016/S0894-9166(10)60040-7).

**Chapter 5**  
Wave Propagation in 2D  
composites Structure using  
Higher Gradient Size  
Independent Homogenization

## **Chapter 5: Wave Propagation in 2D composites Structure using Higher Gradient Size Independent Homogenization**

### **Summary**

In the current chapter, we study the role of higher gradient contributions on the static and wave propagation characteristics of composite structures. To that scope, we use a higher gradient energy formulation to compute the complete set of effective higher gradient properties. We use both a unit-cell size-dependent and size-independent modeling formulation which is based on correction terms that include quadratic inertia tensor terms. Thereupon, we compute the homogenized properties of composites with internal inclusion for which we computed the internal lengths parameters for different unit cell material and geometric properties. We show that the higher gradient effect is limited for low material contrast and strongly depends on the volumetric fraction of the material phases included. We provide evidence that the selection of the higher gradient modeling formulation is crucial for the computed wave propagation characteristics. In particular, the dispersion attributes computed using size-independent models are close to Cauchy mechanics prediction for small volumetric inclusion, while size-dependent models are overestimating the computed frequencies by a substantial amount. What is more, we show that frequencies computed depend on the propagation mode of interest, with the shear frequency mode to be more affected than the longitudinal mode irrespective of the formulation employed.

## 5.1 Introduction

Predictive micromechanical models aiming at understanding the impact of the geometry and properties of reinforcement and matrix on the macro scale composite response witness a significant development, as the experimental determination of the mechanical properties of composites is delicate due to the number of independent moduli that have to be measured in 3D situation. Hence, predictive approaches prove convenient in order to bridge the scales and to provide a constitutive law at a continuum scale, whereby the equivalent continuum properties can be related to both the geometrical and mechanical microstructural parameters of the composite constituents. Furthermore, designing such kind of materials in an optimal way requires understanding the relation between the internal architecture and physical properties, and suitable ways to evaluate these properties.

The mechanics of generalized continua can be defined as the mechanics of matter for circumstances in which the conventional continuum mechanics cannot offer a promising approach (Kröner, 1968). In order to keep a continuum description, one has to consider a generalized continuum to model the substitution material resulting from the homogenization process. As known, classical homogenization techniques limited to small loading or deformation field wavelength comparing to the microstructure size (Trinh et al., 2012). The objective of homogenization towards generalized continua is to remedy to these limitations and to extend the range of validity of the continuum approach beyond the strict assumption of the scale separation (Mindlin, 1964; Eringen and Suhubi, 1964). The incorporation of the microstructural scale within enhanced continuum formulations involves the relaxation of the local action hypothesis and the introduction of a spatial interaction and typical length scales to account for the influence of neighboring points in the formulation of constitutive equations. There are essentially two ways to generalize the classical definition of a continuum, classified into higher-order and higher-gradient continua. Higher-order continua involves additional degrees of freedom like the Cosserat medium promoted by the Cosserat brothers (Cosserat and Cosserat, 1909) and the micromorphic medium (Eringen and Suhubi, 1964; Mindlin, 1964; Germain, 1973). In Cosserat elasticity (Cosserat and Cosserat, 1909) local rotations are added as degrees of freedom. In higher-gradient continua, one keeps the same degrees of freedom but to higher gradients of the displacement field are added as arguments of the strain energy density.

In classical continuum mechanics (Truesdell and Noll, 1965), all higher order displacement gradients are neglected and only the first order displacement gradient is involved in measuring

the deformations of a body. Such kinematic framework turns out not to be rich enough to describe a variety of important mechanical and physical phenomena (Auffray, 2010). Especially, the classical continuum mechanics proves to be intrinsically size independent, as reported by in (Truesdell and Noll, 1992). Particularly, size effects and a non-local behavior may arise due to the discrete nature of matter at a sufficiently small-scale level. The lack of a material length scale parameter in the classical continuum elasticity theory leads to an inaccurate description of the structural behaviors with microstructure (Goda et al., 2015).

The development of additive manufacturing has indeed allowed for the engineering of a new class of materials that obtain their effective mechanical attributes by their inner topological design rather than from their chemical composition, and generate exceptional material performances far beyond those of the base material (Cheng et al., 2018). Artificial materials of the kind deserve the wording architected materials or metamaterials, as of their potential to yield effective static and dynamic attributes that can well extend the design space of the base material used. Architected materials designed with a quasi-periodic inner topology have witnessed a rapid expansion in the recent period, the complex internal topology of architected materials prohibits the use of direct numerical simulations or full-field computations of macrostructures made of architected materials, which become numerically too expensive. While, the mechanical response of periodic architected materials can be analyzed at the macroscopic level at the scale of a unit cell that is repeated to build a regular lattice.

Amongst the possible a priori choices of the effective substitution medium mentioned previously (Cosserat, micromorphic, strain-gradient ...). The strain gradient elastic continuum introduced in (Mindlin, 1964) and (Mindlin & Eshel, 1968) offers several advantages as underlined in (Yvonnet et al., 2020). Since it is rich enough to represent emergent properties without having recourse to the micromorphic medium that has many more inherent parameters (Auffray et al., 2015) and such a model can be constructed using asymptotic homogenization (Boutin, 1996; Bacigalupo and Gambarotta, 2010, 2014; Tran et al., 2012).

A large body of works has been devoted to strain gradient homogenization in the literature since more than 40 years (Ben-Amoz, 1976; Forest and Sab, 1998; Forest, 1998; Forest et al., 2001; Trinh et al., 2012; Tran et al., 2012; Rahali et al., 2015; Bacigalupo and Gambarotta, 2010). For both composites with periodic or random microstructures (Goda & Ganghoffer, 2016), auxetic architected materials (Bacigalupo & Gambarotta, 2014) or random fibrous media (Berkache et al., 2017). Different approaches have been employed in the literature for

## Chapter 5: Wave Propagation in 2D composites Structure using Higher Gradient Size Independent Homogenization

the derivation of the effective mechanical properties of strain gradient models of heterogeneous microstructures.

Periodic homogenization methods rely on the asymptotic expansion of the searched solution versus a small parameter representative of the relative scale of the unit cell (with respect to the macroscale of the overall structure ( $\varepsilon = l/L$ )) have been developed in (Bensoussan et al., 1978; Sanchez-Palencia, 1980) considering the main proponents. Expansion of the series up to second order leads to the formulation of an effective strain gradient continuum whereby the local solution depends on the macroscopic strain gradient (Gambin and Kröner, 1989; Boutin, 1996; Triantafyllidis and Bardenhagen, 1996; Smyshlyaev and Cherednichenko, 2000; Tran, 2012). The strain gradient elastic moduli are computed by solving in a sequential manner two unit cell boundary value problems, a classical one leading to the Cauchy moduli and a higher order BVP associated with the macroscopic strain gradient as a kinematic source term.

Pure asymptotic expansion methods (Boutin, 1996; Smyshlyaev and Cherednichenko, 2000) are sometimes combined with a Fast Fourier Transform FFT method to compute the effective properties (Tran et al., 2012; Li and Zhang, 2013). A quite common strategy to compute the strain gradient moduli is to use suitable quadratic boundary conditions over the RVE as the minimum kinematic loading capturing a gradient of the strain at the macroscopic level. An approach followed by many authors (Gologanu et al., 1997; Forest, 1998; Forest et al., 2001; Kanit et al., 2003; Geers et al., 2001; Kouznetsova et al., 2004; Auffray et al., 2010; Barboura and Li, 2018). This method extends the classical kinematic uniform boundary conditions employed in Cauchy type homogenization (Huet, 1990). The method however suffers from two major flaws, since the effective strain gradient moduli remain non-zero for homogeneous materials or under conditions of scale separation (Forest and Trinh, 2011). Corrections to these spurious effects were recently proposed (Yvonnet et al., 2020), where they added a body force field to the quadratic boundary conditions together with a correction of the localization tensor to get a convergence effective strain gradient moduli for big number of cells. Very recently, (Monchiet et al., 2020) made a correction to the employed quadratic boundary conditions, thereby getting rid of the strain gradient effects (the effective medium remains of Cauchy type). Furthermore, the computed strain gradient effects converge asymptotically with the number of periods. Note that this asymptotic homogenization method avoid the spurious effect since the source term in the second order unit cell problem vanishes for a homogeneous medium. Moreover, another type of correction provided in (Li, 2011)

## Chapter 5: Wave Propagation in 2D composites Structure using Higher Gradient Size Independent Homogenization

where second gradient moduli are independent of periods number, the correction terms used the first gradient moduli and the quadratic inertia of the structure. Furthermore, the author provides an analytical solution of the higher gradient constitutive parameters for 1D and 2D composites structures.

The homogenization method is crucial for both the static analysis of composites and for its wave dispersion characteristics. Classical elasticity based on Cauchy continuum mechanics assumptions lead to linear dispersion relations (Chapter 2), so it proves unable to describe the dispersion relations occurring in microstructured materials. On the other hand, enriched continua like strain gradient medium prove able to capture the dispersive nature of propagating waves, as shown e.g. in (Rosi & Auffray, 2016). What is more, the validity range of higher gradient formulations is broader than that of classical homogenization formulations (Rosi & Auffray, 2016).

The main objective and novel aspect of this chapter is the setting up of a homogenization method towards strain gradient effective media, as an extension of the methodology used in 1D heterogeneous media (Chapter 3), relying on variational principles articulated with Hill macrohomogeneity lemma. As will be evidenced, the method is able to deliver effective strain gradient moduli that are size independent and is thus able to capture effective properties that are intrinsic to the microstructure, and their influence on the wave dispersion characteristics are analyzed in function of the microstructure contrast between the composite constituents.

In this work, we propose theoretical developments for the derivation of the effective strain gradient properties of composite materials including corrections terms accounting for higher gradient terms, and wave propagation analysis using the homogenized properties in Section 5.2.2. In Section 5.3, we elaborate on the computation of the effective second gradient effective moduli for 2D composites structures, which we compare to analytical results (Section 5.3.2.1), while in Section 5.3.2.2, we analyze the size effects on the high gradient effective moduli with and without corrections terms. Furthermore, we analyze the variation of the higher gradient internal length (a second order tensor) for different contrasts of microstructure volume fraction and moduli, and assess the importance of correction terms (Section 5.3.2.3). In addition to the static analysis, we derive the wave propagation of the composite structure for classic continua, which we compare with the use of dedicated finite element models (Section 5.3.3.2). We subsequently compute the wave propagation properties for such composites using the higher gradient moduli with the corrections terms in Section 5.3.3.3, which we compare to Cauchy mechanics prediction for different microstructure properties in Section 5.3.3.4. We discuss the obtained results in Section 5.4 and conclude in Section 5.5.

The following notations are used throughout the present work. The gradient of a scalar or tensor field with respect to the position is denoted with the nabla operator and the position as a subscript, viz.  $\nabla_X E(X)$  represents the gradient of the tensor field  $E(X)$  with respect to  $X$ . The transpose of a tensor is written with a superscript notation, for instance  $B^T$ . The symmetrized dyadic product is denoted  $\otimes^s$ . The dot product therein represents the internal product in the space of Cartesian tensors. The simple, double and triple contractions of tensors are written  $:$ ,  $::$ , respectively. The vector product of two vectors or tensors  $U, V$  is denoted  $U \times V$ .

## 5.2 Materials and methods

### 5.2.1 Theoretical formulation

We impose a macroscopic strain  $E(X)$  and a strain gradient  $K(X)$  to a unit cell, the displacement will be decomposed to a quadratic form linear to the imposed parameters, and a fluctuation displacement  $\tilde{u}_i(y)$ , nil on the unit cell boundaries. Therefore, the displacement will be as follows:

$$u_i = E_{ij} \cdot y_j + \frac{1}{2} K_{ijk} : (y_j \otimes y_k) + \tilde{u}_i(y) \quad (5.1)$$

Where  $K_{ijk}$  is the second gradient of macro-displacement  $U(X)$  tensor, here defined as the second displacement gradient corresponding to Mindlin (Mindlin, 1964) form I of strain gradient elasticity. Similar to first gradient homogenization, the fluctuating part of the displacement corrects for the existing discrepancies between the macroscopic imposed displacement and the real displacement field of the media.

Deriving the micro-displacement in Eq. (5.1), we get the micro-strain as function of the macroscopic strains  $(E(X), K(X))$  as follows:

$$\varepsilon_{ij} = E_{ij} + \frac{1}{2} K_{ijk} y_k + \tilde{\varepsilon}_{ij}(y) \quad (5.2)$$

Wherein  $\tilde{\varepsilon}_{ij}(y) = \frac{1}{2} (\tilde{u}_{i,j} + \tilde{u}_{j,i})(y)$  is the strain fluctuation. The strain energy of the effective strain gradient continuum,  $W_M(E, K)$ , writes as a bilinear form of the kinematic measures,

adopting in the sequel a small strains formulation (so energies are expressible as quadratic functions of their kinematic arguments):

$$\begin{aligned} W_M(E, K) &= \frac{1}{2} \left( E_{ij} : C_{ijkl}^{\text{hom}} : E_{kl} + E_{ij} : (B_{ijkl}^{\text{hom}} + B_{ijkl}^{\text{hom,T}}) : K_{klm} + K_{ijk} : A_{ijklmn}^{\text{hom}} : K_{lmn} \right) \\ &= \langle w_m(\varepsilon) \rangle_Y = \langle \varepsilon_{ij}(y) : c_{ijkl}(y) : \varepsilon_{kl}(y) \rangle_Y \end{aligned} \quad (5.3)$$

Where  $c_{ijkl}(y)$  is the elasticity tensor of the material at the microscale,  $A_{ijklmn}^{\text{hom}}$  therein the sixth order tensor of strain gradient moduli, and  $B_{ijklm}^{\text{hom}}$  a fifth order tensor of coupling moduli between first and second gradient effects; the presence in Eq. (5.3) of the sum  $(B_{ijklm}^{\text{hom}} + B_{ijklm}^{\text{hom,T}})$  is a consequence of the existence of a strain energy potential which guarantees the symmetry of the effective overall stiffness matrix, by Schwarz relation.

The macroscopic strain gradient energy density entails the following strain gradient constitutive law at the macroscopic level, relating the average Cauchy stress  $\Sigma_{ij}$  and hyperstress  $S_{ijk}$  to the strain and strain gradient tensors  $(E_{ij}(X), K_{ijk}(X))$  as follows:

$$\begin{aligned} \Sigma_{ij} &= \frac{\partial W}{\partial E_{ij}} = C_{ijqt}^{\text{hom}} : E_{qt} + B_{ijqtw}^{\text{hom}} K_{qtw} \\ S_{ijk} &= \frac{\partial W}{\partial K_{ijk}} = D_{ijkqt}^{\text{hom}} : E_{qt} + A_{ijkqtw}^{\text{hom}} K_{qtw} \end{aligned} \quad (5.4)$$

An extended minimization principle over all periodic fluctuations holds for the strain energy in Eq. (5.3) using the micro-strain expression, Eq. (5.2), so that one can write:

$$\begin{aligned} W_M(E, K) &\stackrel{H-M}{=} \underset{\tilde{u}}{\text{Min}} \langle w_m(\varepsilon) \rangle = \underset{\tilde{u}}{\text{Min}} \frac{1}{2} \int_Y \varepsilon_{ij}(y) : c_{ijkl}(y) : \varepsilon_{kl}(y) \\ &= \underset{\tilde{u}}{\text{Min}} \frac{1}{2} \int_Y \left( E_{ij} + K_{ijk} y_k + \nabla_{y_j} \tilde{u}_i \right) : c_{ijmn}(y) : \left( E_{mn} + K_{mnp} y_p + \nabla_{y_n} \tilde{u}_m \right) \end{aligned} \quad (5.5)$$

The stationarity condition of the functional on the right-hand side of (5.5) delivers as a necessary condition a BVP to be satisfied by the optimal fluctuation associated to the real displacement field (in the absence of body forces) as follows:

$$\text{div} \left\{ c_{ijkl}(y) : \left( E_{kl} + K_{klm} y_m + \nabla_{y_l} \tilde{u}_k \right) \right\} = 0 \quad (5.6)$$

The linearity of the fluctuating displacement with respect to the kinematic loading in Eq. (5.6), tensors  $(E_{kl}, K_{klm})$ , allows writing:

$$\tilde{u}_i(y) = H_{ijk}^E(y) : E_{jk} + H_{ijkl}^K(y) : \cdot K_{jkl} \quad (5.7)$$

Wherein  $H^E(x), H^K(x)$  in Eq. (5.7) stand for the displacement localization tensors relating the fluctuating displacements to the first and second gradient strain tensors  $E(X)$  and  $K(X)$  accordingly.

Inserting into Eq. (5.6) the fluctuating displacement as in Eq. (5.7), we get the 1<sup>st</sup> and 2<sup>nd</sup> gradient unit cell BVP's as the stationarity conditions of the functional on the left hand side of Eq. (5.5):

$$\begin{aligned} & -\text{div} \left\{ c_{ijkl}(y) : \left( E_{kl} + K_{klm} y_m + \nabla_{y_l} \left( H_{kmn}^E(y) : E_{mn} + H_{klmn}^K : \cdot K_{lmn} \right) \right) \right\} = 0 \\ \Rightarrow & \text{BVP1: } -\text{div} \left\{ c_{ijkl}(y) : \left( E_{kl} + \nabla_{y_l} \left( H_{kmn}^E(y) : E_{mn} \right) \right) \right\} = 0 \quad \text{1<sup>st</sup> gradient unit cell problem} \end{aligned} \quad (5.8a)$$

$$\Rightarrow \text{BVP2: } -\text{div} \left\{ c_{ijkl}(y) : \left( K_{klm} y_m + \nabla_{y_l} \left( H_{klmn}^K : \cdot K_{lmn} \right) \right) \right\} = 0 \quad \text{2<sup>nd</sup> gradient unit cell pb} \quad (5.8b)$$

These unit-cell BVP's lead to the expressions of the micro-displacement, these latter being used to evaluate the homogenized properties of the unit-cell. Deriving the internal energy in Eq. (5.3) with respect to the imposed first gradient macro-strain  $E_{ij}$  as mentioned in Eq. (5.4), we get the first gradient macro-stress as follows:

$$\begin{aligned} \Sigma_{ij} &= \frac{\partial w}{\partial E_{ij}} = C_{ijqt}^{\text{hom}} : E_{qt} + B_{ijqtw}^{\text{hom}} K_{qtw} \\ &= \frac{1}{2} \frac{\partial}{\partial E_{ij}} \int_Y \left( \left( E_{mn} + K_{mnp} y_p + \nabla_{y_n} \left( H_{mrv}^E(y) : E_{rv} + H_{mrvd}^K : K_{rvd} \right) \right) : C_{mnqt}(y) : \right. \\ & \quad \left. \left( E_{qt} + K_{qtw} y_w + \nabla_{y_t} \left( H_{qwd}^E(y) : E_{wd} + H_{qwdx}^K : K_{wdx} \right) \right) \right) d\Omega \\ &= \left( E_{qt} \int_Y \left( C_{ijqt} + C_{ijwd} \nabla_{y_d} \left( H_{wqt}^E \right) + C_{mnqt} \nabla_{y_n} \left( H_{mij}^E \right) + C_{mnwd} \nabla_{y_n} \left( H_{mij}^E \right) \nabla_{y_d} \left( H_{wqt}^E \right) \right) d\Omega \right) \\ &+ \left( K_{qtw} \int_Y \left( C_{ijqt} y_w + C_{ijkl} \nabla_{y_l} \left( H_{kqtw}^K \right) + y_w C_{mnqt} \nabla_{y_n} \left( H_{mij}^E \right) + C_{mnkl} \nabla_{y_n} \left( H_{mij}^E \right) \nabla_{y_l} \left( H_{kqtw}^K \right) \right) d\Omega \right) \end{aligned} \quad (5.9)$$

The same holds for the second order macroscopic stress tensor, so we derive the energy from Eq. (5.3) with respect to the second gradient imposed macroscopic-strain  $K_{ijk}$  as

mentioned in Eq. (5.4) to get the following expression of the hyperstress tensor in component form:

$$\begin{aligned}
 S_{ijk} &= \frac{\partial w}{\partial K_{ijk}} = D_{ijkqt}^{\text{hom}} : E_{qt} + A_{ijkqtw}^{\text{hom}} K_{qtw} \\
 &= \frac{1}{2} \frac{\partial}{\partial K_{ijk}} \int_Y \left( \left( E_{mn} + K_{mnp} y_p + \nabla_{y_n} (H_{mrv}^E(y) : E_{rv} + H_{mrvd}^K : K_{rvd}) \right) : C_{mnqt}(y) : \right. \\
 &\quad \left. \left( E_{qt} + K_{qtw} y_w + \nabla_{y_t} (H_{qwd}^E(y) : E_{wd} + H_{qwdx}^K : K_{wdx}) \right) \right) d\Omega \\
 &= E_{qt} \int_Y \left( C_{ijqt} y_k + y_k C_{ijwd} \nabla_{y_d} (H_{wqt}^E) + C_{mnqt} \nabla_{y_n} (H_{mijk}^K) + C_{mnwd} \nabla_{y_n} (H_{mijk}^K) \nabla_{y_d} (H_{wqt}^E) \right) d\Omega \\
 &\quad + K_{qtw} \int_Y \left( C_{ijqt} y_k y_w + y_k C_{ijsd} \nabla_{y_d} (H_{sqtw}^K) + y_w C_{mnqt} \nabla_{y_n} (H_{mijk}^K) + C_{mnsd} \nabla_{y_n} (H_{mijk}^K) \nabla_{y_d} (H_{sqtw}^K) \right) d\Omega
 \end{aligned} \tag{5.10}$$

By identification, we simply get the first and the second gradient elasticity tensors  $C^{\text{hom}}$  and  $A^{\text{hom}}$  respectively, and the coupling between them encapsulated in tensors  $B^{\text{hom}}$  and  $D^{\text{hom}}$  as the following integrals:

$$\begin{aligned}
 C_{ijqt}^{\text{hom}} &= \int_Y \left( \left( C_{ijqt} + C_{ijwd} \nabla_{y_d} (H_{wqt}^E) + C_{ijwd} \nabla_{y_d} (H_{wqt}^E) + C_{mnqt} \nabla_{y_n} (H_{mij}^E) + C_{mnwd} \nabla_{y_n} (H_{mij}^E) \nabla_{y_d} (H_{wqt}^E) \right) \right) d\Omega \\
 B_{ijkqw}^{\text{hom}} &= \int_Y \left( C_{ijqt} y_w + C_{ijkl} \nabla_{y_l} (H_{kqtw}^K) + y_w C_{mnqt} \nabla_{y_n} (H_{mij}^E) + C_{mnkl} \nabla_{y_n} (H_{mij}^E) \nabla_{y_l} (H_{kqtw}^K) \right) d\Omega \\
 D_{ijqkt}^{\text{hom}} &= \int_Y \left( C_{ijqt} y_k + y_k C_{ijwd} \nabla_{y_d} (H_{wqt}^E) + C_{mnqt} \nabla_{y_n} (H_{mijk}^K) + C_{mnwd} \nabla_{y_n} (H_{mijk}^K) \nabla_{y_d} (H_{wqt}^E) \right) d\Omega = B_{qtijk}^{\text{hom}} \\
 A_{ijkqtw}^{\text{hom}} &= \int_Y \left( C_{ijqt} y_k y_w + y_k C_{ijsd} \nabla_{y_d} (H_{sqtw}^K) + y_w C_{mnqt} \nabla_{y_n} (H_{mijk}^K) + C_{mnsd} \nabla_{y_n} (H_{mijk}^K) \nabla_{y_d} (H_{sqtw}^K) \right) d\Omega
 \end{aligned} \tag{5.11}$$

Using these effective tensors, we further write the tensor form of the stress and hyper-stress accounting for their symmetric (Auffray et al., 2010) as follows:

$$\begin{pmatrix} \Sigma_{11} \\ \Sigma_{22} \\ \sqrt{2}\Sigma_{12} \end{pmatrix} = \begin{pmatrix} C_{1111}^{\text{hom}} & C_{1122}^{\text{hom}} & \sqrt{2}C_{1112}^{\text{hom}} \\ C_{2211}^{\text{hom}} & C_{2222}^{\text{hom}} & \sqrt{2}C_{2212}^{\text{hom}} \\ \sqrt{2}C_{1211}^{\text{hom}} & \sqrt{2}C_{1222}^{\text{hom}} & 2C_{1212}^{\text{hom}} \end{pmatrix} \begin{pmatrix} E_{11} \\ E_{22} \\ \sqrt{2}E_{12} \end{pmatrix} \tag{5.12a}$$

$$\begin{pmatrix} S_{111} \\ S_{221} \\ \sqrt{2}S_{122} \\ S_{222} \\ S_{112} \\ \sqrt{2}S_{121} \end{pmatrix} = \begin{pmatrix} A_{111111}^{\text{hom}} & A_{111221}^{\text{hom}} & \sqrt{2}A_{111222}^{\text{hom}} & A_{111222}^{\text{hom}} & A_{111112}^{\text{hom}} & \sqrt{2}A_{111121}^{\text{hom}} \\ A_{221111}^{\text{hom}} & A_{221221}^{\text{hom}} & \sqrt{2}A_{221222}^{\text{hom}} & A_{221222}^{\text{hom}} & A_{221112}^{\text{hom}} & \sqrt{2}A_{221121}^{\text{hom}} \\ \sqrt{2}A_{122111}^{\text{hom}} & \sqrt{2}A_{122221}^{\text{hom}} & 2A_{122122}^{\text{hom}} & \sqrt{2}A_{122222}^{\text{hom}} & \sqrt{2}A_{122112}^{\text{hom}} & 2A_{122121}^{\text{hom}} \\ A_{222111}^{\text{hom}} & A_{222221}^{\text{hom}} & \sqrt{2}A_{222122}^{\text{hom}} & A_{222222}^{\text{hom}} & A_{222112}^{\text{hom}} & \sqrt{2}A_{222121}^{\text{hom}} \\ A_{112111}^{\text{hom}} & A_{112221}^{\text{hom}} & \sqrt{2}A_{112122}^{\text{hom}} & A_{112122}^{\text{hom}} & A_{112112}^{\text{hom}} & \sqrt{2}A_{112121}^{\text{hom}} \\ \sqrt{2}A_{121111}^{\text{hom}} & \sqrt{2}A_{121221}^{\text{hom}} & 2A_{121112}^{\text{hom}} & \sqrt{2}A_{121122}^{\text{hom}} & \sqrt{2}A_{121112}^{\text{hom}} & 2A_{121121}^{\text{hom}} \end{pmatrix} \begin{pmatrix} K_{111} \\ K_{221} \\ \sqrt{2}K_{122} \\ K_{222} \\ K_{112} \\ \sqrt{2}K_{121} \end{pmatrix} \tag{5.12b}$$

We calculate the correction terms of the second gradient as described in **Appendix 4.B**. We identify the first and second gradient corrected constitutive tensors as follows:

$$\begin{aligned} C_{ijlm}^{\text{hom}*} &= C_{ijlm}^{\text{hom}} \\ A_{ijklmn}^{\text{hom}*} &= A_{ijklmn}^{\text{hom}} - C_{ijlm}^{\text{hom}} I_{kn} \end{aligned} \quad (5.13)$$

Wherein the quadratic moments of inertia are components of the second order tensor

$$I_{km} = \int_{\Omega} y_k \cdot y_m d\Omega.$$

We quantify the importance of second gradient constitutive parameters by the internal length parameters, elaborated as the ratio of the second gradient constitutive parameters to the classical Cauchy tensor. We use the internal length formula from (Goda & Ganghoffer, 2016) with simplified Voigt notation as follows, in which the free Greek indices vary from 1 to 3:

$$le_{\alpha\beta} = \sqrt{\frac{\sum_{r=1}^{r=2} A_{\alpha r \beta r}^{\text{hom}}}{C_{\alpha\beta}^{\text{hom}}}} \quad (5.14)$$

## 5.2.2 Homogenization modeling

In this work, we implement the previous computation of the effective first and second gradient moduli in the 2D case using the finite element code FreeFem, where we use the BVP for first and second gradient from Eqs. (5.8a, 5.8b) in order to compute the displacement within the unit cell domain. Each elasticity tensor is written in 2D case using the general formula derived in Eq. (5.11) as function of the materials parameters and the localization variables  $(H^E, H^K)$ . In the sequel, we describe the methodology used in the finite element study to calculate the homogenized properties of the heterogeneous structures for the longitudinal case, and then other cases will be derived using the same methodology.

### 5.2.2.1 First gradient modeling

We start imposing a longitudinal macroscopic strain to the unit-cell  $\Omega$   $(E_{11} = 1, E_{12} = E_{21} = 0, E_{22} = 0)$ , using microscopic expression of the strain as in Eq. (5.2) and fluctuation terms as in Eq. (5.7), we express the micro-strain as function of the first gradient longitudinal displacement localizations  $H_{i11}^E$  as follows:

$$\begin{aligned} \varepsilon_{11} &= E_{11} + \nabla_x (H_{111}^E) E_{11}, \varepsilon_{22} = \nabla_y (H_{211}^E) E_{11} \\ \varepsilon_{12} &= \nabla_y (H_{111}^E) E_{11}, \varepsilon_{21} = \nabla_x (H_{211}^E) E_{11} \end{aligned} \quad (5.15)$$

The weak form of the BVP1 for the first gradient formulation writes from Eq. (8a) as follows:

$$\int_{\Omega} \left[ \begin{aligned} & \left( \lambda_i \left( E_{11} + \nabla_x \left( H_{111}^E \right) E_{11} + \nabla_y \left( H_{211}^E \right) E_{11} \right) + 2\mu_i \left( E_{11} + \nabla_x \left( H_{111}^E \right) E_{11} \right) \right) \nabla_x v_x \\ & + \left( \lambda_i \left( E_{11} + \nabla_x \left( H_{111}^E \right) E_{11} + \nabla_y \left( H_{211}^E \right) E_{11} \right) + 2\mu_i \left( \nabla_y \left( H_{211}^E \right) E_{11} \right) \right) \nabla_y v_y + \\ & \mu_i \cdot \left( \nabla_y \left( H_{111}^E \right) E_{11} + \nabla_x \left( H_{211}^E \right) E_{11} \right) \cdot \left( \nabla_x v_x + \nabla_y v_y \right) \end{aligned} \right] d\Omega = 0 \quad (5.16)$$

Where  $(v_x, v_y)$  are the test function components.

Using FreeFem, we carry out the unit cell problems of Eq. (5.16) on the composite structure (Fig. 5.1), we generate a triangular mesh with 15628 triangles and 8115 vertices. Solving the first gradient unit-cell problem leads to identify the first gradient longitudinal localizers  $H_{i11}^E$ , which are inserted in Eq. (5.11) to evaluate the rigidity tensors of first gradient and coupling between first and second gradient  $(C_{ijqt}^{\text{hom}}, B_{ijqtw}^{\text{hom}})$  accordingly.

### 5.2.2.2 Second gradient modeling

Extending previous writings to the second order formulation, we express the micro-strain from Eq. (5.2) as function of the second gradient longitudinal displacement localizers  $H_{i11}^K$  as in Eq. (5.7), by imposing a longitudinal strain gradient to the unit cell  $\Omega$   $(K_{111} = 1, K_{221} = 0, K_{122} = 0, K_{222} = 0, K_{112} = 0, K_{121} = 0)$  as follows:

$$\begin{aligned} \varepsilon_{11} &= K_{111}x + \nabla_x \left( H_{1111}^K \right) K_{111}, \varepsilon_{22} = \nabla_y \left( H_{2111}^K \right) K_{111} \\ \varepsilon_{12} &= \nabla_y \left( H_{1111}^K \right) K_{111}, \varepsilon_{21} = \nabla_x \left( H_{2111}^K \right) K_{111} \end{aligned} \quad (5.17)$$

Using the last expression of the micro-strain in Eq. (5.8b), we write the weak form of BVP 2 for the second gradient as follows:

$$\int_{\Omega} \left[ \begin{aligned} & \left( \lambda_i \left( K_{111}x + \nabla_x \left( H_{1111}^K \right) K_{111} + \nabla_y \left( H_{2111}^K \right) K_{111} \right) + 2\mu_i \left( K_{111}x + \nabla_x \left( H_{1111}^K \right) K_{111} \right) \right) \nabla_x v_x \\ & + \left( \lambda_i \left( K_{111}x + \nabla_x \left( H_{1111}^K \right) K_{111} + \nabla_y \left( H_{2111}^K \right) K_{111} \right) + 2\mu_i \left( \nabla_y \left( H_{2111}^K \right) K_{111} \right) \right) \nabla_y v_y + \\ & \mu_i \cdot \left( \nabla_y \left( H_{1111}^K \right) K_{111} + \nabla_x \left( H_{2111}^K \right) K_{111} \right) \cdot \left( \nabla_x v_x + \nabla_y v_y \right) \end{aligned} \right] d\Omega = 0 \quad (5.18)$$

Solving the BVP in Eq. (5.18) on the same mesh generated for the first gradient unit-cell problem in section 5.2.2.1, we calculate the second gradient displacement localizations tensors  $H_{i11}^K$  over the unit cell, which are used to compute the homogenized second gradient rigidity

tensor and the coupling tensor  $(A_{ijkqlw}^{\text{hom}}, D_{ijkql}^{\text{hom}})$  accordingly, as described in Eq. (5.11). The computed effective properties form the basis for the analysis of wave propagation features in heterogeneous materials.

The next section is devoted to the study of wave propagation within 2D composites on the basis of the formulated strain gradient effective continuum.

### 5.2.3 Wave dispersion for 2D structures

For the homogenized 2D continuum model, the equations of motion using the derived second gradient formulation express for the longitudinal and transverse parts as the two following partial differential equations along the  $(X_1, X_2)$  directions of a Cartesian coordinates system:

$$\begin{bmatrix} \left( \frac{\partial \Sigma_{11}}{\partial X_1} + \frac{\partial \Sigma_{12}}{\partial X_2} \right) - \frac{\partial^2 S_{111}}{\partial X_1 \partial X_1} - \frac{\partial^2 S_{112}}{\partial X_1 \partial X_2} - \frac{\partial^2 S_{121}}{\partial X_2 \partial X_1} - \frac{\partial^2 S_{122}}{\partial X_2 \partial X_2} \\ \left( \frac{\partial \Sigma_{21}}{\partial X_1} + \frac{\partial \Sigma_{22}}{\partial X_2} \right) - \frac{\partial^2 S_{211}}{\partial X_1 \partial X_1} - \frac{\partial^2 S_{212}}{\partial X_1 \partial X_2} - \frac{\partial^2 S_{221}}{\partial X_2 \partial X_1} - \frac{\partial^2 S_{222}}{\partial X_2 \partial X_2} \end{bmatrix} = \rho^{\text{hom}} \begin{bmatrix} \ddot{U} \\ \ddot{V} \end{bmatrix} \quad (5.19)$$

Here,  $\ddot{U}$  and  $\ddot{V}$  are the horizontal and vertical components of the acceleration vector, the overhead dot denoting the time derivative. The homogenized effective density therein is given by  $\left( \rho^{\text{hom}} = \sum_i \rho_i A_i / \sum_i A_i \right)$  where  $(\rho_i, A_i)$  are the density and surface for each constituent within the heterogeneous structure (each constituent having a homogeneous density and properties), which follows the mixture rules, and the homogenized stress and hyper-stress are calculated using Eq. (5.12a) and (5.12b).

In order to obtain the dispersion relation for the propagating waves through the structure, we consider a harmonic wave propagating along an axis in the infinite planar second gradient effective medium, so the generalized displacement field with components  $U, V$  at a point  $(X_1, X_2)$  is assumed in the following form:

$$\begin{bmatrix} U(X_1, X_2) \\ V(X_1, X_2) \end{bmatrix} = \begin{bmatrix} U_0 \\ V_0 \end{bmatrix} e^{I(\omega t - k_x X_1 - k_y X_2)} \quad (5.20)$$

Where  $(U_0, V_0)$  is the displacement amplitude,  $(k_x, k_y)$  are the wave vector components,  $\omega$  is the frequency, and  $I$  is the imaginary number such that  $I^2 = -1$ . The wave vector is a complex number: its real part represents the attenuation in the  $X_1$ - $X_2$  plane, and its imaginary part defines the phase constants. In this study, we consider the wave vector without attenuation.

Substituting the ansatz of Eq. (5.20) in the equation of motion Eq. (5.19) delivers the following algebraic equation:

$$D(k_1, k_2, \omega) \cdot \begin{pmatrix} U_0 \\ V_0 \end{pmatrix} = 0 \quad (5.21)$$

The dispersion relation will be derived by imposing a unique solution to the last characteristics equation (5.21) as the frequency  $\omega$  as function of the wave vector components  $(k_x, k_y)$ .

### 5.3 Application to inclusion based composite materials

#### 5.3.1 Overview of inclusion based composite models

Inclusion architectures are considered as the most significant feature in composite design due to their numerous practical applications and they spread across many industrial areas. They provide an excellent compromise between lightness and stiffness, and often for a low cost of production. Introducing such inclusions where they are needed is an efficient method of using inclusions to improve composite performances. Mechanical properties of composites containing inclusions have become a topic of great interest in recent years because of the manifest technological importance of such materials. Their excellent mechanical properties are largely because their microstructure can be adjusted to achieve controlled mechanical properties at the mesoscopic or macroscopic levels. In view of exploiting the full potential of these solids, their constitutive mechanical response has clearly to be entirely understood and modeled based on the available microstructural information.

Based on loading conditions and structural requirements, shape of inclusions in a composite may vary: it can be for instance particles, continuous fibers, and short fibers. In the

## Chapter 5: Wave Propagation in 2D composites Structure using Higher Gradient Size Independent Homogenization

last years, composites composed of inclusions with various shapes have become popular in a wide range of applications, especially through fabrication techniques such as injection molding, bulk molding compound, and three-dimensional weaving and braiding. Since inclusions reinforced composites made of a base material with stronger inclusions are attractive due to their increased usage in structural and noise control engineering, the need for understanding of the composites are growing up. The assessment of the intrinsic mechanical properties of such composites is a critical issue since experimental measurements may be difficult and costly. We address in this section the issue of constructing first and second order grade effective constitutive models as substitutes of the initial structure of such composites reinforced with inclusions.

There is a long history in the evaluation of the effective elastic properties of such heterogeneous materials, which remains one of the most tangible problems of micromechanics. A wide diversity of approaches have been developed to predict the overall mechanical responses of predicting the effective elastic properties of composite materials containing inclusion, based on the knowledge of the mechanical properties, geometries, and distributions of their inherent phases (Torquato, 2001; Milton, 2002), and (Goda et al., 2016). Starting from the pioneering papers of Eshelby who introduced the celebrated Eshelby's tensor (Eshelby, 1957) for isotropic ellipsoidal inclusions, analytical predictions of the effective properties of such inclusion-based composites have been provided in the dilute regime. Mori-Tanaka (Tanaka, 1973) method that proves efficient for the study of the overall behavior of composite materials containing non-dilute concentration of reinforcements. This scheme further enjoys the property (Weng, 1990 and 1992) that the elastic moduli of identical shaped multiphase composites predicted by the Mori-Tanaka mean-field theory systematically coincide with Hashin-Shtrikman's bounds (Hashin and Shtrikman, 1962). Computational homogenization for reinforced composites define a third set of methods to evaluate the effective properties from the work of (Guedes and Kikuchi, 1990) devoted to linear elasticity problems.

Finite element methods constitute a powerful technique widely used to evaluate the local stress and strain states for complex microstructures, see (Goda et al., 2016) and references therein. Based on the equivalent strain energy approach, based on the relationship established between the strain energy of the considered microstructures and that of the homogenized equivalent model, FE analyses have been developed over the past years to compute the first and second order grade continuum models equivalent to such reinforced composites. In this method, boundary conditions based on combinations of imposed quadratic displacements and nil tractions applied along the outer boundaries of an identified representative volume element

are formulated (Goda et al., 2016), leading to the determination of both classical and strain gradient effective constitutive elastic moduli.

In the current section, we use the second gradient modeling described in section 5.2.2 for the higher gradient energy (HGE) formulation derived in section 5.2.1 for 2D composites structures in order to compute their static properties. In Section 5.3.2.1, we compare the provided results of the higher gradient constitutive parameters with previous studies for the same composites structure. Subsequently, in Section 5.3.2.2, we study the impact of correction terms defined in Eq. (5.13) on the size effects as for 1\*1, 2\*2 and 3\*3 unit-cells. For completeness, we analyze the effect of microstructure contrast on the internal length parameters in Section 5.3.2.3.

### 5.3.2 Static properties of 2D composite microstructures

We consider a unit size ( $l = 1mm$ ) square matrix with an elasticity coefficient and Poisson's ratio ( $E_1 = 100MPa, \nu_1 = 0.3$ ), including a circular hole or an inclusion with radius  $R$  at the matrix center as in Fig. 5.1. According to (Auffray et al., 2015) coupling tensors will be negligible for such centrosymmetric structures, so we focus in this study on the first and second gradient constitutive tensors.

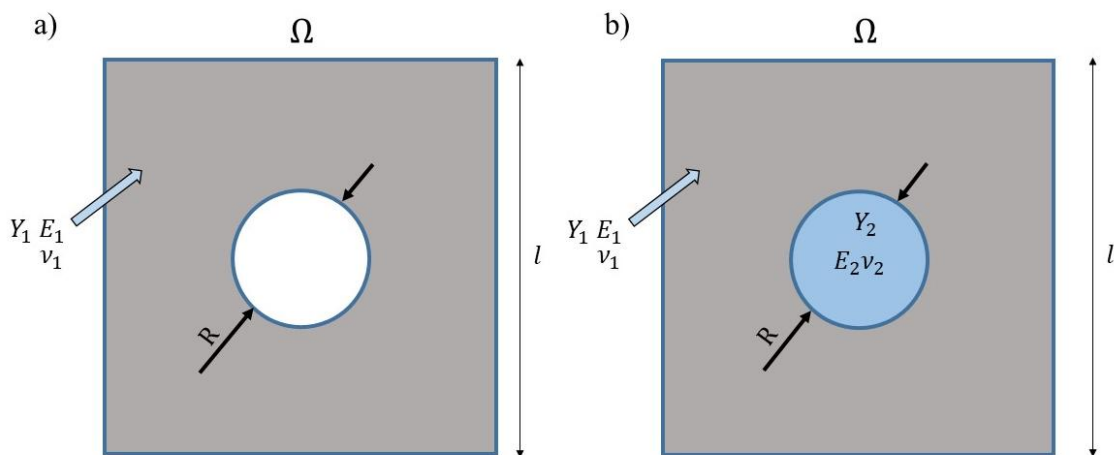


Figure 5.1: Centrosymmetric matrix and central hole (a) and reinforcement material (b).

#### 5.3.2.1 Validation with analytical second gradient formulation

We use the second gradient formulation described in Section 5.2.1, to compute the higher gradient elastic properties of the composite structure as in Fig. 5.1a for the case where the

second phase is a hole, which we compare to the analytical higher gradient constitutive parameters (Li, 2011) in Table 5.1.

In view of the tetragonal symmetry class of the chosen RVE in Fig. 5.1a as discussed in (Auffray et al., 2015), the higher gradient elasticity tensor will have the following structure:

$$A_{ijklmn}^{\text{hom}} = \begin{pmatrix} A_{111111}^{\text{hom}} & A_{111221}^{\text{hom}} & A_{111122}^{\text{hom}} & & & \\ A_{111221}^{\text{hom}} & A_{221221}^{\text{hom}} & A_{221122}^{\text{hom}} & & & \\ A_{111122}^{\text{hom}} & A_{221122}^{\text{hom}} & A_{122122}^{\text{hom}} & & & \\ & & & \text{Sym.} & & \\ & & & & A_{111111}^{\text{hom}} & A_{111221}^{\text{hom}} & A_{111122}^{\text{hom}} \\ & & & & A_{111221}^{\text{hom}} & A_{221221}^{\text{hom}} & A_{221122}^{\text{hom}} \\ & & & & A_{111122}^{\text{hom}} & A_{221122}^{\text{hom}} & A_{122122}^{\text{hom}} \end{pmatrix} \quad (5.22)$$

The analytical higher gradient constitutive parameters are calculated in (Li, 2011) as a function of the matrix properties for the higher gradient constitutive parameters with and without correction  $A_{ijklmn}^{\text{hom}}$  and  $A_{ijklmn}^{\text{hom}*}$  accordingly as follows:

$$A_{ijklmn}^{\text{hom}} = C_{ijlm}^0 \delta_{kn} \left( \frac{l^2}{12} - \frac{\pi R^4}{4l^2} \right) \quad (5.23a)$$

$$A_{ijklmn}^{\text{hom}*} = C_{ijlm}^0 \delta_{kn} \frac{\pi R^2}{12} \left( 1 - \frac{3R^2}{l^2} \right) \quad (5.23b)$$

Wherein  $\delta_{kn}$  is the Kronecker symbol (unity for  $k=n$ , and zero otherwise), and  $C_{ijlm}^0$  is the matrix elasticity tensor provided for completeness in **Appendix 4.C**.

Using the analytical higher gradient constitutive parameters from Eqs. (5.23a, b) for the 2D structure in Fig. 5.1a, we calculate the relative difference between the higher gradient homogenized properties without correction terms (SG) using the static higher gradient energy formulation (HGE in short) as described in section 5.2.1, and the analytical solution provided in (Li, 2011) as in Table 5.1.

Table 5.1: Relative difference between the homogenized second gradient constitutive parameters of the 2D composite structure in Fig. 1a using HGE without the correction terms and the analytical results of (Li, 2011).

$A_{ijklmn}^{\text{hom}} \left( \text{MPa} \cdot \text{mm}^2 \right)$	HGE method	Analytical solution (Li, 2011)	% relative difference
$A_{111111}$	10.23	10.36	1.25
$A_{111221}$	4.38	4.44	1.35
$A_{111122}$	0	0	0
$A_{221221}$	10.33	10.36	0.3
$A_{122122}$	2.95	2.96	0.3

From the Table 5.1 we see the very good accordance between the HGE and the analytical solution in (Li, 2011), with the maximum relative difference less than 1.35% for the homogenized higher gradient parameters.

Using the higher gradient formulation described in Section 5.2.1 and the correction terms from Eq. (5.13), we calculate the relative difference between the homogenized properties calculated using the HGE including correction terms (SG\*), and the analytical solution provided in (Li, 2011) as in Table 5.2.

Table 5.2: Relative difference between of the homogenized second gradient constitutive parameters of the 2D composite structure in Fig. 5.1a using HGE with corrections terms and the analytical results of (Li, 2011).

$A_{ijklmn}^{\text{hom}*} \left( \text{MPa} \cdot \text{mm}^2 \right)$	HGE method	Analytical solution (Li, 2011)	% relative difference
$A_{111111}^{\text{hom}*}$	2.22	2.3	3.47
$A_{111221}^{\text{hom}*}$	0.96	0.99	3
$A_{111122}^{\text{hom}*}$	0	0	0
$A_{221221}^{\text{hom}*}$	2.32	2.32	0
$A_{122122}^{\text{hom}*}$	0.66	0.66	0

From the comparison provided in Table 5.2, the maximum relative difference between the HGE formulation described in Section 5.2.1 and the analytical solution of (Li, 2011) is less than 3.5% for the homogenized higher gradient parameters including the correction terms.

### 5.3.2.2 Sensitivity of the homogenized properties to size effects

In this part, we analyze the size effects on the higher gradient constitutive parameters. To that scope, we study the variation of the higher gradient constitutive terms with and without the correction terms as described in Eq. (5.13) for different RVE sizes.

For the representative unit-cell of the limited plate of Fig. 5.2a, we choose one, two or three unit-cells as in Fig. 5.2b, 5.2c, and 5.2d accordingly. We note that  $l = 1mm$  is the dimension of one unit-cell. The composite is made of a linearly elastic matrix material with the following properties ( $E_1 = 1000MPa, \nu_1 = 0.3$ ), and a circular inclusion with properties ( $E_2 = 10MPa, \nu_2 = 0.3$ ) and a radius  $R = 0.3mm$ .

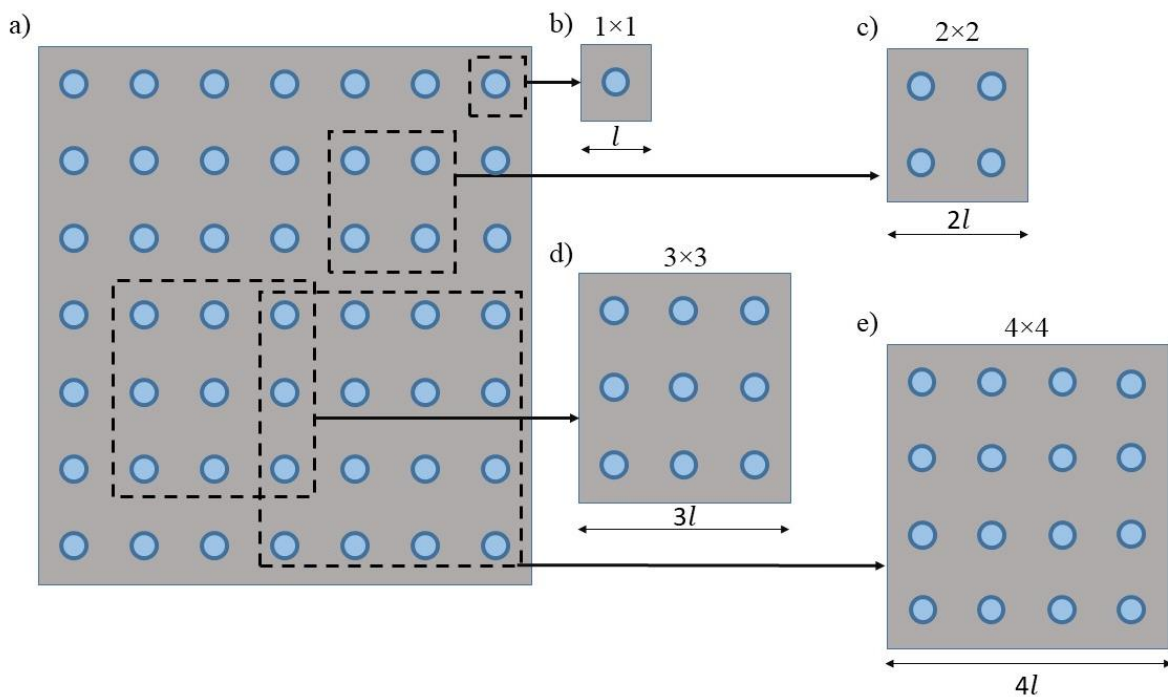


Figure 5.2: Square pattern (a) with three different square unit-cell choices (b, c, d and e) of dimension  $l, 2l, 3l$  and  $4l$  accordingly.

Using the first and second gradient model described in Section 5.2.2, we calculate the homogenized properties of different RVE sizes in Figs. 5.2b, 5.2c, 5.2d and 5.2e, where we verified that Cauchy tensor is size independent as mentioned in (Truesdell and Noll, 1992). We show the variation of second gradient effective properties without any correction in Fig. 5.3a, and with the correction provided in Eq. (5.13) in Fig. 5.3b as follows:

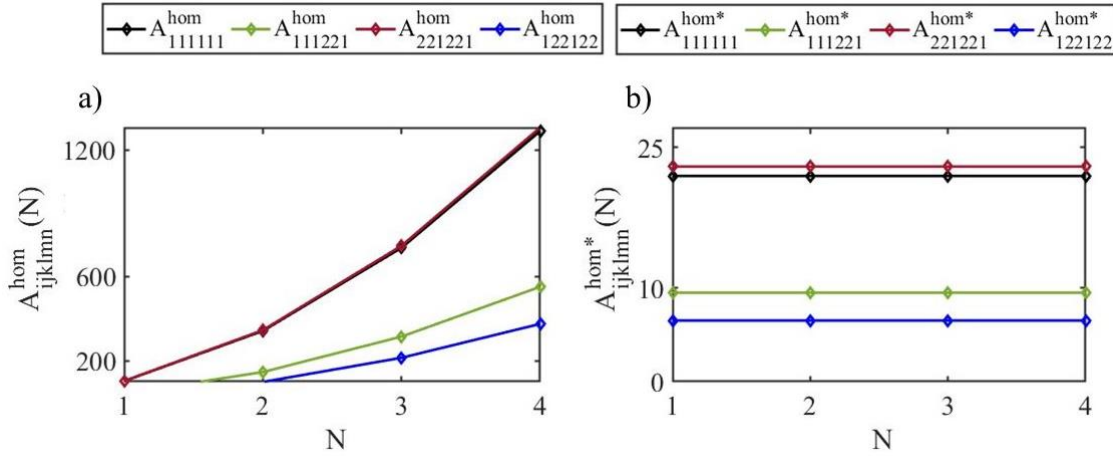


Figure 5.3 : Second gradient constitutive moduli variation for different RVE sizes without correction terms  $A_{ijklmn}^{\text{hom}}$  in (a) and with correction terms  $A_{ijklmn}^{\text{hom}*}$  in (b).

Fig. 5.3a shows that second gradient effective moduli without the correction are diverging for large RVE sizes. Contrariwise, when adding the correction terms of Eq. (5.13), the second gradient constitutive moduli are independent of the RVE size as shown in Fig. 5.3b.

### 5.3.2.3 Sensitivity of internal length parameters to the microstructure contrast

We evaluate the impact of higher gradient constitutive parameters on the macroscopic behavior of the structure by studying the internal length parameters  $le_{\alpha\beta}$  (mm) as defined in Eq. (5.14), elaborated as the ratio of second gradient to first gradient equivalent moduli. In the sequel, we analyze the influence of inclusion radius  $R$ , elasticity ratio of the matrix to the inclusion ( $E_1 / E_2$ ) on the internal length parameters, using the size dependent higher gradient constitutive parameters  $A_{ijklmn}^{\text{hom}}$  as defined in Eq. (5.11). To that scope, we use the developed formulation in Section 5.2.1 to compute the first and the second gradient constitutive parameters without correction for the composite structure in Fig. 5.1b, for different values of inclusion radius  $R$  for  $(E_1 / E_2) \in \{20, 100\}$  in Fig. 4a and 4b accordingly and for different elasticity ratio ( $E_1 / E_2$ ) for  $R = 0.25\text{mm}, 0.4\text{mm}$  in Fig. 5.4c and 5.4d accordingly.

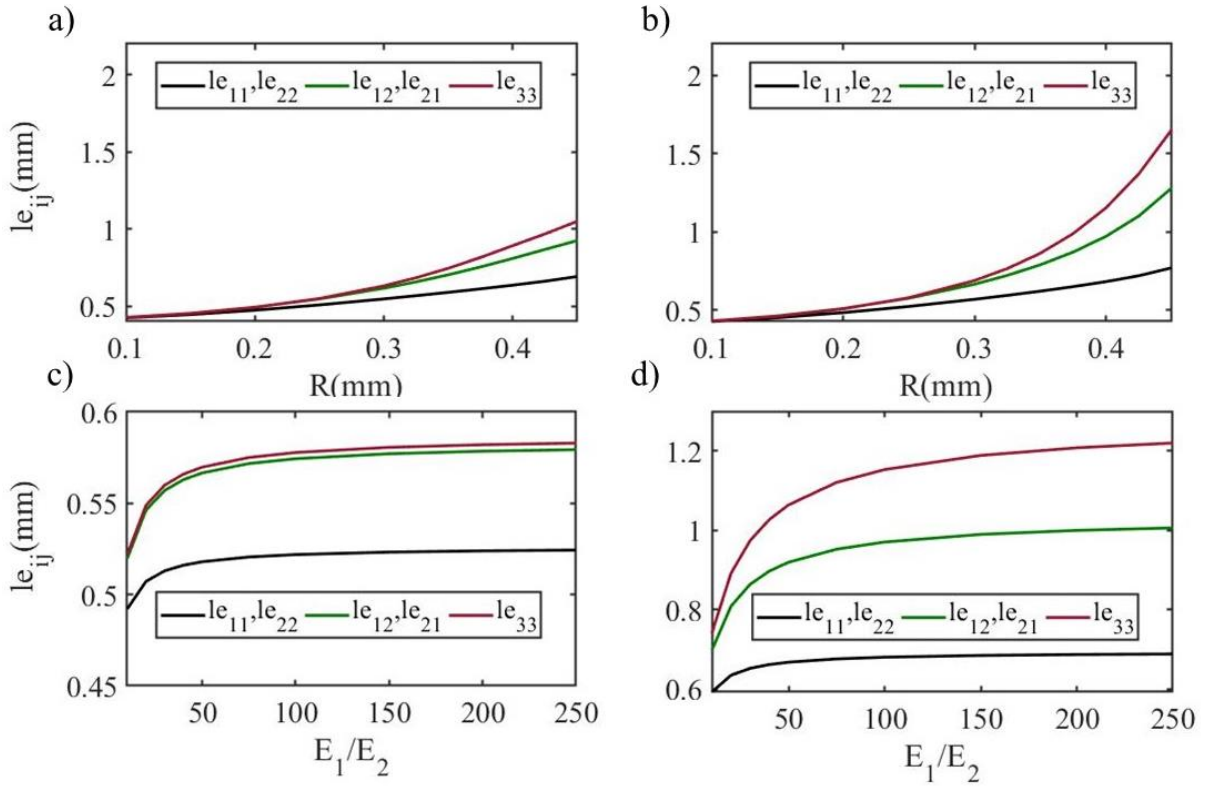


Figure 5.4 : Variation of internal length parameters  $le_{ij}$  (mm) as function of the inclusion radius  $R$  (mm) for  $(E_1/E_2) = 20, 100$  in (a) and (b) accordingly as function of the microscopic elasticity ratio  $(E_1/E_2)$  for  $R = 0.25$  mm,  $0.4$  mm in (c) and (d) accordingly.

Fig. 5.4 shows that higher gradient internal length parameters without the correction terms  $le_{\alpha\beta}$  (mm) are increasing for high inclusion radius as shown in Fig. 5.4a, 5.4b, where the maximum variation is observed for  $le_{33}$  (Red),  $0.62$  mm for  $(E_1/E_2) = 20$  in Fig. 5.4a and  $1.22$  mm for  $(E_1/E_2) = 100$  in Fig. 5.4b. Moreover, the internal length parameters are also increasing for different values  $(E_1/E_2)$  but they converge at high values of the elasticity ratio  $(E_1/E_2)$ . The maximum variation for different values of  $(E_1/E_2)$  occurs for  $le_{33}$  (Red) which is  $0.061$  mm for  $R = 0.25$  mm in Fig. 5.4c and  $0.48$  mm for  $R = 0.4$  mm in Fig. 5.4d.

In the sequel, we use the higher gradient constitutive moduli size independent  $A_{ijklmn}^{\text{hom}*}$  which includes the correction terms of Eq. (5.13) to the same analysis we applied for the non-corrected higher gradient constitutive moduli in Fig. 5.4 as follows:

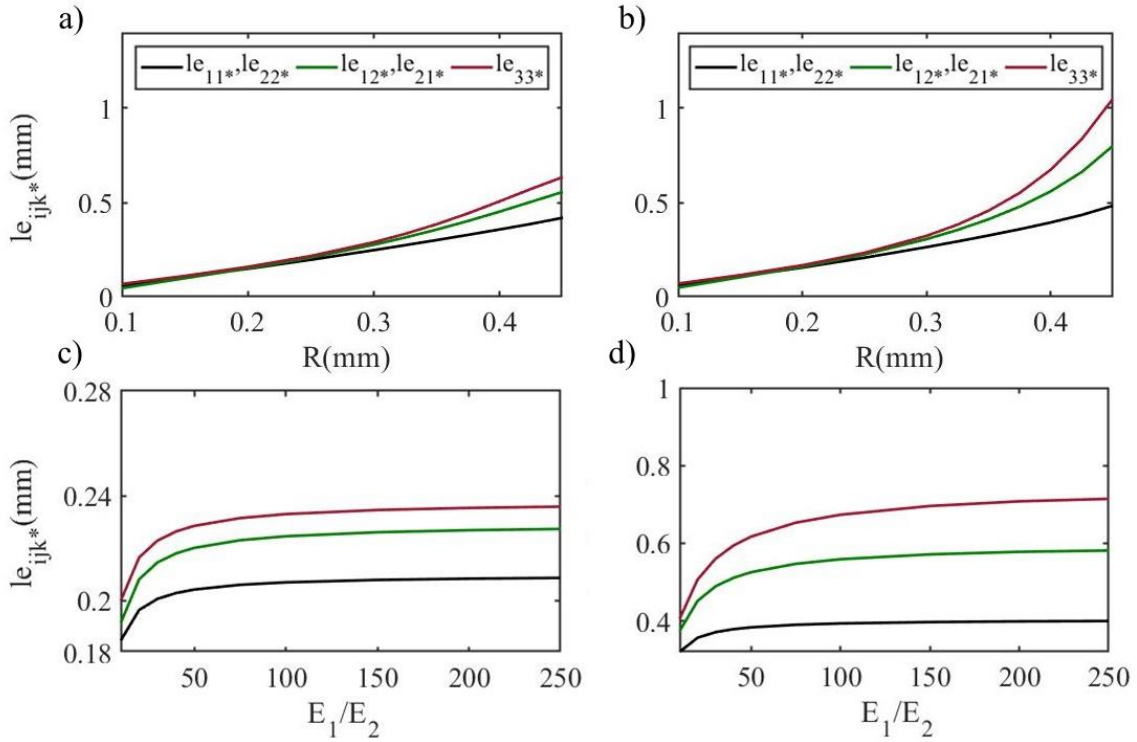


Figure 5.5 : Variation of internal length parameters  $le_{ij^*}$  (mm) as function of inclusion radius  $R$  (mm) for  $(E_1/E_2) = 20, 100$  in (a) and (b) accordingly, and as function of the elasticity ratio  $(E_1/E_2)$  for  $R = 0.2$  mm,  $0.4$  mm in (c) and (d) accordingly.

Fig. 5.5 shows that higher gradient internal length parameters with correction terms  $le_{\alpha\beta^*}$  (mm) are increasing for high inclusion radius as shows Fig. 5.5a, 5.5b, the maximum variation being observed for  $le_{33^*}$  (Red) which is 0.57mm for  $(E_1/E_2) = 20$  in Fig. 5.6a and 0.98mm for  $(E_1/E_2) = 100$  in Fig. 5.5b. Moreover, the internal length parameters are also increasing for different values  $(E_1/E_2)$  but converging at high values of elasticity ratio  $(E_1/E_2)$ . The maximum variation for different values of  $(E_1/E_2)$  lies in  $le_{33^*}$  (Red) which is 0.04mm for  $R = 0.25$  mm in Fig. 5.5c and 0.32mm for  $R = 0.4$  mm in Fig. 5.5d.

### 5.3.3 Wave propagation analysis within 2D second gradient media

Homogenization methods are crucial for both the static analysis of composites and for their wave dispersion characteristics. Classical elasticity based on Cauchy continuum mechanics assumptions lead to linear dispersion relations (Chapter 2), so it proves unable to describe the dispersion relations occurring in microstructured materials. On the other hand, enriched

continua like strain gradient medium prove able to capture the dispersive nature of propagating waves, as shown e.g. in (Rosi & Auffray, 2016). What is more, the validity range of higher gradient formulations is broader than that of classical homogenization formulations (Rosi & Auffray, 2016).

In this part, we study the wave propagation through the square matrix with circular inclusion of Fig. 5.1b, where the matrix made of linearly elastic material with an elasticity coefficient ( $E$ ), Poisson's ratio ( $\nu$ ) and density ( $\rho$ ) accordingly ( $E_1 = 100MPa, \nu_1 = 0.3, \rho_1 = 1000Kg / m^3$ ), and a circular inclusion with ( $E_2 = 10MPa, \nu_2 = 0.3, \rho_2 = 1000Kg / m^3$ ) and radius  $R = 0.4mm$ . Firstly, we use COMSOL to calculate the dispersion characteristics of the structure (Section 5.3.3.1). Then using the homogenized properties calculated using the HGE formulation from Section 5.2.1, We know that the validity range of homogenization-based dispersion relation will be restricted to the low wavenumber as discussed in (Rosi & Auffray, 2016). We compare COMSOL results with first gradient solution in Section 5.3.3.2. For completeness, in Section 5.3.3.3, we calculate the dispersion relations using the higher gradient formulation with and without the correction terms of Eq. (5.13), while in Section 5.3.3.4; we study the sensitivity of microstructure geometrical and mechanical contrast on the difference between first and second gradient with and without the correction terms.

### 5.3.3.1 COMSOL dispersion characteristics

We generate the following domain and FE mesh of the composite unit cell (Fig. 5.1b), showing the displacement shape for the longitudinal and the transverse mode (using COMSOL) as follows:

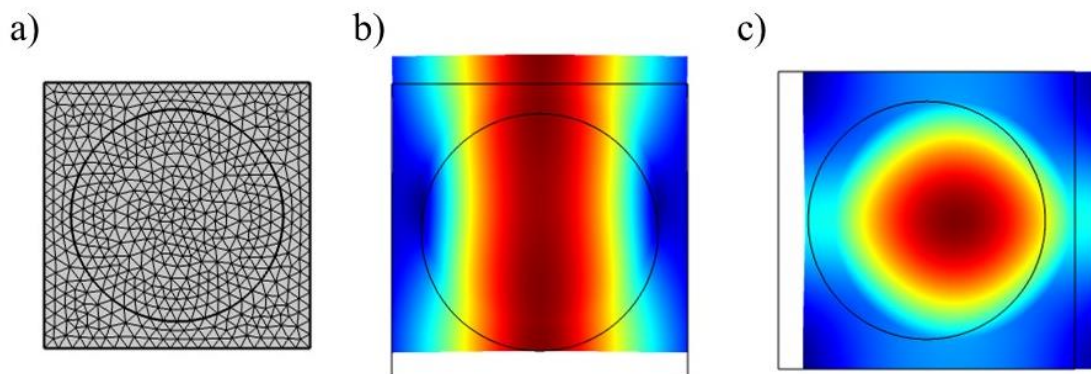


Figure 5.6 : Mesh of the composite structure (a), and displacement shape for the transverse (b) and longitudinal (c) propagating modes.

We compute the dispersion relation using COMSOL over the entire Brillouin zone of the square (Fig. 5.7a), for the transverse and longitudinal modes (Fig. 5.7b).

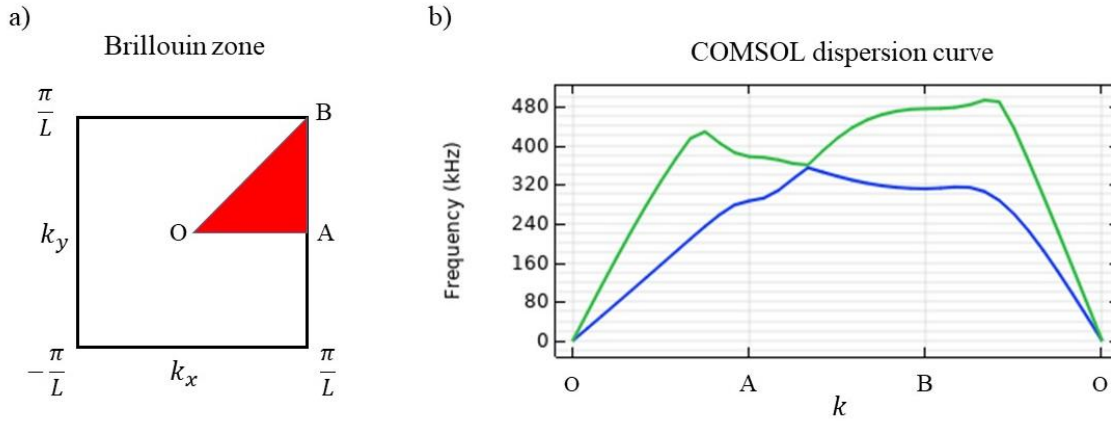


Figure 5.7 : Longitudinal (Green) and transverse (Blue) wave dispersion (b) through the 2D composite structure from Fig. 5.1b in Brillouin zone (a).

Fig. 5.7b shows the dispersion diagram for the shear (Blue) and longitudinal modes (Green) over the entire Brillouin zone (Fig. 5.7a) of the composite unit cell (Fig. 5.1b). According to (Rosi & Auffray, 2016), the homogenization-based dispersion curves are restrained in the low wavenumber range, therefore, we subsequently compute the dispersion curves in the range of wavenumbers  $k \in [0, 0.6]$ .

### 5.3.3.2 First gradient dispersion analysis

Starting with the classical Cauchy type homogenization relying on the homogenization method described in Section 5.2.1 restricted to the first gradient, we calculate the homogenized Cauchy tensor as defined in Eq. (5.12a) for the composite structures (Fig. 5.1b) as follows:

$$\begin{pmatrix} C_{1111}^{\text{hom}} = 48.6 & C_{1122}^{\text{hom}} = 14.8 & C_{1112}^{\text{hom}} = 0 \\ C_{2211}^{\text{hom}} = 14.8 & C_{2222}^{\text{hom}} = 48.6 & C_{2212}^{\text{hom}} = 0 \\ C_{1211}^{\text{hom}} = 0 & C_{1222}^{\text{hom}} = 0 & C_{1212}^{\text{hom}} = 9 \end{pmatrix} \text{MPa} \quad (5.24)$$

We calculate the dispersion relations using the methodology described in Section 5.2.3 but restricting to the first order approximation in Eq. (5.19) for the first two modes, and we compare this later with COMSOL results of Fig. 5.7b restricting to small wave numbers and to the low frequency domain. Therefore, we consider the expression of the wavenumber in zone (OA) of Fig. 5.7a ( $k_x = \pi k / l$ ) to get the following dispersion curves:

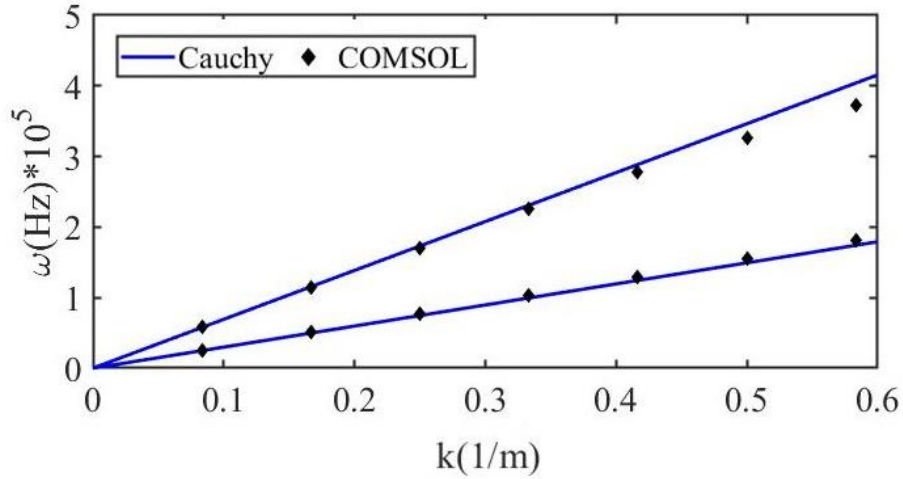


Figure 5.8: Dispersion relation of the composite structure (Fig. 5.1b) using Cauchy approximation (Blue), and COMSOL with the diamond points for the shear (lower band) and longitudinal modes (upper band).

Fig. 5.8 shows a good agreement between the first gradient dispersion solution (blue) and the one provided from COMSOL computations at small wavenumber; however, the first gradient is providing a non-dispersive relation.

### 5.3.3.3 Second gradient dispersion analysis

We subsequently analyze the effect of the higher gradient constitutive parameters on the wave dispersion characteristics. To that scope, we calculate the second gradient elasticity tensor from Eq. (5.11), without correction terms using the second gradient formulation described in Section 5.2.1 to get the following tensor:

$$A_{ijklmn}^{\text{hom}} = \left( \begin{array}{ccc|ccc} A_{111111}^{\text{hom}} = 8.6 & A_{111221}^{\text{hom}} = 3.7 & A_{111122}^{\text{hom}} = 0 & & & \\ A_{111221}^{\text{hom}} = 3.7 & A_{221221}^{\text{hom}} = 8.7 & A_{221122}^{\text{hom}} = 0 & & \text{Sym.} & \\ A_{111122}^{\text{hom}} = 0 & A_{221122}^{\text{hom}} = 0 & A_{122122}^{\text{hom}} = 2.5 & & & \\ \hline & & & A_{111111}^{\text{hom}} = 8.6 & A_{111221}^{\text{hom}} = 3.7 & A_{111122}^{\text{hom}} = 0 \\ & & & A_{111221}^{\text{hom}} = 3.7 & A_{221221}^{\text{hom}} = 8.7 & A_{221122}^{\text{hom}} = 0 \\ & & & A_{111122}^{\text{hom}} = 0 & A_{221122}^{\text{hom}} = 0 & A_{122122}^{\text{hom}} = 2.5 \end{array} \right) (N) \quad (5.25)$$

We calculate next the second gradient constitutive tensor including the correction terms as defined in Eq. (5.13) of the 2D matrix with the circular inclusion of Fig. 5.1b using as follows:

$$A_{ijklmn}^{\text{hom}*} = \left( \begin{array}{ccc|ccc} A_{111111}^{\text{hom}*} = 2.5 & A_{111221}^{\text{hom}*} = 1.1 & A_{111122}^{\text{hom}*} = 0 & & & \\ A_{111221}^{\text{hom}*} = 1.1 & A_{221221}^{\text{hom}*} = 2.6 & A_{221122}^{\text{hom}*} = 0 & & \text{Sym.} & \\ A_{111122}^{\text{hom}*} = 0 & A_{221122}^{\text{hom}*} = 0 & A_{122122}^{\text{hom}*} = 0.75 & & & \\ \hline & & & A_{111111}^{\text{hom}*} = 2.5 & A_{111221}^{\text{hom}*} = 1.1 & A_{111122}^{\text{hom}*} = 0 \\ & & & A_{111221}^{\text{hom}*} = 1.1 & A_{221221}^{\text{hom}*} = 2.6 & A_{221122}^{\text{hom}*} = 0 \\ & & & A_{111122}^{\text{hom}*} = 0 & A_{221122}^{\text{hom}*} = 0 & A_{122122}^{\text{hom}*} = 0.75 \end{array} \right) (N) \quad (5.26)$$

Using the second gradient tensors in Eq. (5.25, 5.26) we derive the dispersion relation proceeding in complete analogy to Section 5.3.3.2 but now incorporating the second gradient contribution to the wave dispersion in Eq. (5.19). In the figure below, we present the wave dispersion using both Cauchy first gradient approximation and the higher gradient behavior with and without the correction terms of Eq. (5.13) (SG and SG\* accordingly) for small wave numbers in the interval  $k \in [0, 0.6]$ .

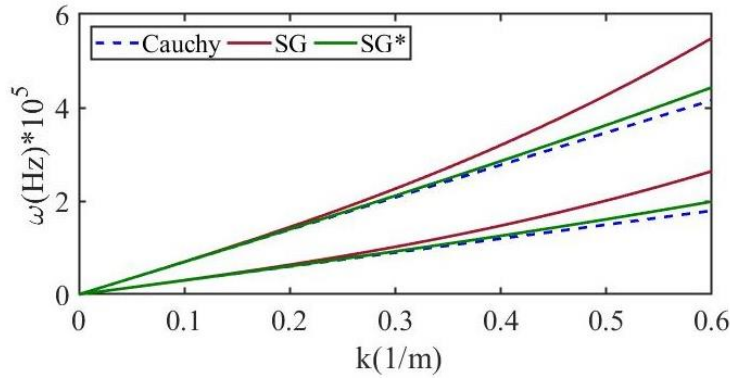


Figure 5.9: Wave dispersion diagram using the first gradient theory (Blue), the higher gradient approximation without correction terms (Red) and with correction terms (Green) for the shear mode (lower band) and the longitudinal mode (upper band).

As Fig. 5.9 shows, consideration of higher gradient terms for the longitudinal and transverse modes shows dispersive properties, which is not the case for the first gradient linear dispersion characteristics (in Blue). The relative difference between the higher gradient formulations without correction terms (Red) and the first gradient response (Blue) for the transverse mode (lower band) and for the longitudinal mode (upper mode) are 27% and 22% accordingly at  $k = 0.6m^{-1}$ , while introducing the correction terms (Green) this difference will decrease to 6% and 4% for the transverse and longitudinal modes accordingly.

### 5.3.3.4 Sensitivity of the dispersive frequency to the microstructure properties

We subsequently analyze the effect of microstructure geometrical and mechanical contrasts on the relative difference between the first (C) and the higher gradient approximations without and with corrections (SG and SG\* accordingly) at  $k = 0.6m^{-1}$  in Fig. 5.10. In Figs. 5.10a and 5.10b, we analyze the relative difference (% of the dispersive frequency) for different inclusion radius  $R$  with an elasticity ratio equal to 100 between the matrix and the inclusion ( $E_1 / E_2 = 100MPa$ ) for both transverse and longitudinal modes accordingly, and for different

elasticity ratio ( $E_1 / E_2$ ) for a radius  $R = 0.4mm$  in Figs. 5.10c and 5.10d for both transverse and longitudinal modes accordingly.

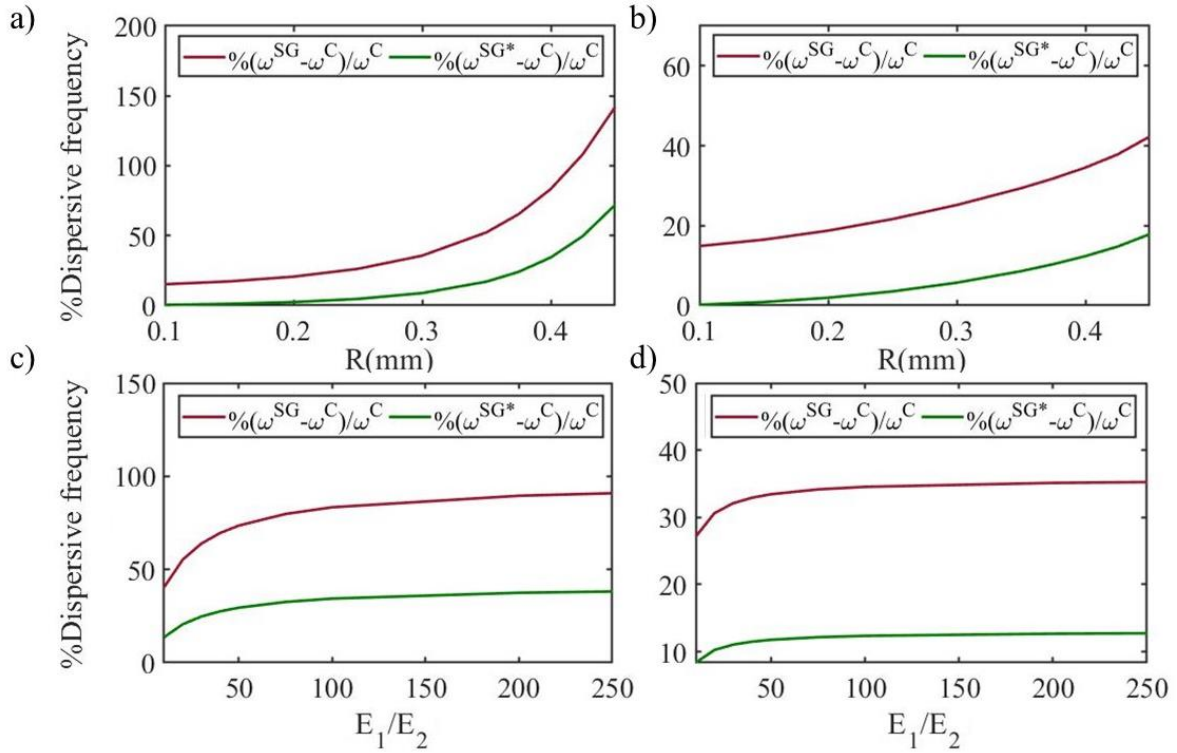


Figure 5.10 : Maximum relative difference in the dispersion curves at  $k = 0.6m^{-1}$  between the higher gradient formulation without correction terms (SG in Red) and with correction terms (SG\* in Green) for different inclusion radii  $R$  with a contrast of moduli ( $E_1 / E_2 = 100MPa$ ) for the transverse and longitudinal modes in (a) and (b) accordingly, and for different elasticity ratio ( $E_1 / E_2$ ) with  $R = 0.4mm$ , for the transverse and longitudinal modes in (c) and (d) accordingly.

Figs. 5.10a and 5.10b shows the effect of the inclusion radius ( $R$ ) on the % dispersive frequency at  $k = 0.6m^{-1}$  for the transverse and longitudinal modes. For the transverse mode (Fig. 10a), the % of dispersive frequency will vary by 127% with the radius for the higher gradient behavior without the correction terms (SG), while when considering the correction terms (SG\*) the variation with radius will decrease to a maximum of 72%. Meanwhile, the longitudinal mode variation is less important than for the first mode, while it is 27% for the SG approximation and 17% for SG\*.

As Figs. 5.10c and 5.10d show, the % of dispersive frequency changes by 50% and 25% for the transverse mode using SG and SG\* formulations versus the values of elasticity ratio between the matrix and the inclusion. Meanwhile, for the longitudinal mode it changes by 8%

and 4% for the SG and SG\* formulations accordingly. We should note that for high values of the elasticity ratio ( $E_1 / E_2$ ) the % of dispersive frequency converges to a constant value.

## 5.4 Discussion

The developed strain gradient proves to be size independent effects as analyzed in Section 5.3.2.2, due to introduced corrections terms in Eq. (5.13). Higher gradient constitutive parameters take a lesser value with the introduced correction, as shown by the analytical expression of higher gradient constitutive parameter in Eq. (5.13). This effect can also be seen in the values of the internal length analyzed in section 5.3.2.3: indeed, the internal length of the higher gradient constitutive size dependent parameters in Fig. 5.4 reaches bigger magnitude than the size independent higher gradients parameters (Fig. 5.5).

Furthermore, microstructure geometrical and mechanical properties of the square matrix with central circle inclusion (Fig. 5.1b) have a crucial effect on the higher gradient constitute parameters (with and without corrections terms). Fig. 5.4 and Fig. 5.5 showing successively the effects of the inclusion radius and elasticity ratio of the individual constituents ( $E_1 / E_2$ ), highlight that the internal length is more sensitive to the inclusion radius (R), over a wide range of variation of the elasticity ratio. For completeness, it has been shown that including higher gradient with correction terms for small geometric and mechanical contrast has no impact on the macroscopic static or dynamic behavior, whereby the classical first gradient is sufficient to describe the composite macroscopic behavior.

Moreover, the wave propagation analysis of Section 5.3.3.4 shows that the microstructural geometrical and mechanical parameters impact as a consequence the maximum frequency occurring at the wavenumber  $k = 0.6(1/m)$ , these dependency being related to the mode number. Fig. 5.10a and 5.10b show that for high volume fraction of inclusions (high inclusion radius), the maximum difference between the first and second gradient dispersive frequency is increasing for the second gradient formulation with or without correction terms (SG\*, SG) but this difference shows a smaller variation for the corrected formulation (SG\*). Moreover, the variation of the dispersive frequency is increasing with the elasticity ratio ( $E_1 / E_2$ ) and it shows an asymptotic convergence; this variation is less pronounced for the longitudinal mode or when the correction term is incorporated into the analysis. Fig. 5.10 also shows that this variation will depend on the mode under consideration: the transverse mode experiences a more significant variation than the longitudinal mode, the difference between modes resulting

from the transverse internal length  $l_{e_{33}}$  taking a higher value than the longitudinal length  $l_{e_{11}}$  as analyzed in section 5.3.2.3.

Higher strain gradient effects can be obtained using architected materials like pantographic structures (dell’Isola et al., 2019; Rahali et al, 2015) as the one shown in Fig. 5.11 , where the structures is made of a linear elastic isotropic material with an elasticity coefficient and Poisson’s ratio ( $E = 2500MPa, \nu = 0.3$ ) accordingly. Using the higher gradient formulation described in section 5.2.1 we calculate the following first and second gradient homogenized tensors (Eq. (5.27)) of the pantographic structure on the following mesh:

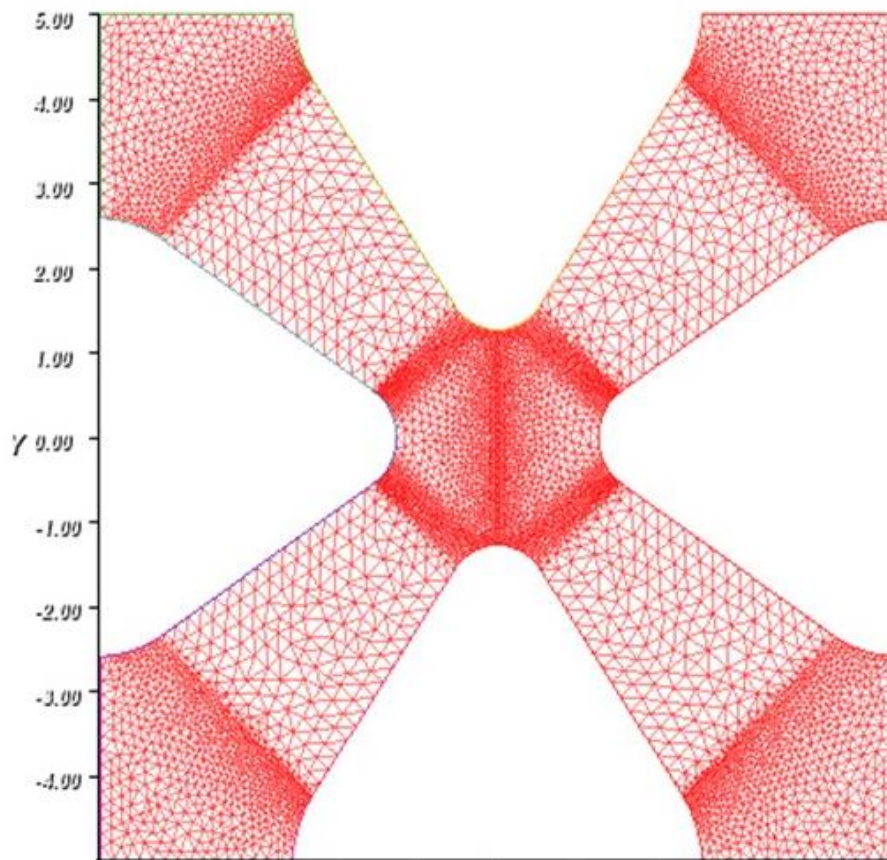


Figure 5.11: Pantographic structure with perpendicular diagonal.

$$\begin{pmatrix} \Sigma_{11} \\ \Sigma_{22} \\ \sqrt{2}\Sigma_{12} \end{pmatrix} = \begin{pmatrix} 1114 & 847 & 0 \\ 847 & 1114 & 0 \\ 0 & 0 & 1231 \end{pmatrix} \begin{pmatrix} E_{11} \\ E_{22} \\ \sqrt{2}E_{12} \end{pmatrix} MPa$$

$$\begin{pmatrix} S_{111} \\ S_{221} \\ \sqrt{2}S_{122} \\ S_{222} \\ S_{112} \\ \sqrt{2}S_{121} \end{pmatrix} = \begin{pmatrix} 28461 & 11940 & 213 & 0 & 0 & 0 \\ 11940 & 29177 & 211 & 0 & 0 & 0 \\ 213 & 211 & 16907 & 0 & 0 & 0 \\ 0 & 0 & 0 & 28461 & 11940 & 213 \\ 0 & 0 & 0 & 11940 & 29177 & 211 \\ 0 & 0 & 0 & 213 & 211 & 16907 \end{pmatrix} \begin{pmatrix} K_{111} \\ K_{221} \\ \sqrt{2}K_{122} \\ K_{222} \\ K_{112} \\ \sqrt{2}K_{121} \end{pmatrix} (N) \quad (5.27)$$

Using these homogenized properties, we calculate the higher gradient internal length using Eq. (5.14) to get ( $le_{11}=le_{22}=7.19mm; le_{12}=le_{21}=5.31mm; le_{33}=5.24mm$ ).

These internal lengths shows the important of higher gradient constitutive parameters comparing to Cauchy behavior for the pantographic structure (Fig. 5.11).

## 5.5 Conclusion

Overall, the current work has analyzed for the first time the role of correction terms and microstructure mechanical and geometrical contrast of the individual constituents of composites (inclusion and matrix) on their static and dynamic response. In the static situation, we have shown that higher gradient internal length characteristics decrease when adding corrections terms which provides size-independent higher gradient constitutive parameters. The internal length parameters are strongly dependent on the geometrical microstructure properties (the fraction of inclusion), whereas the microstructure mechanical properties (elasticity ratio between the matrix and the inclusion) have a lesser impact on the internal lengths which are converging at high contrast of elastic moduli. The sensitivity of the internal lengths to the microstructure properties is significant for the size-dependent higher gradient formulation, while adding corrections terms makes it less sensitive. Furthermore, the dispersive frequency obtained using the higher gradient formulation depends on the microstructure properties; this dependency is more prominent for the transverse mode than the longitudinal mode for the considered composite properties. We aspire that the provided results serve as a reference for the computation of the static and dynamic properties of composite structures and architected materials in the broad sense specially for the ones which provides a prominent higher gradients constitutive behavior (as the discussed pantograph), providing a fundamental theoretical and numerical basis for the assessment of the relative significance of higher-gradient material parameters.

## References

- [1] Auffray, N., Bouchet, R., Brechet, Y., (2010). Strain gradient elastic homogenization of bidimensional cellular media. *Int. J. Solids Struct.* 47 (13), 1698–1710. <https://doi.org/10.1016/j.ijsolstr.2010.03.011>.
- [2] Auffray, N., Dirrenberger, J., Rosi, G., (2015). A complete description of bi-dimensional anisotropic strain-gradient elasticity. *Int. J. Solids Struct.*, 69-70, 195–206 . <https://doi.org/10.1016/j.ijsolstr.2015.04.036>.
- [3] Bacigalupo, A., Gambarotta, L., (2010). Second-order computational homogenization of heterogeneous materials with periodic microstructure. *ZAMM-J. Appl. Math. Mech.*, 90 (10–11), 796–811. <https://doi.org/10.1002/zamm.201000031>.
- [4] Bacigalupo, A., Gambarotta, L., (2014). Homogenization of periodic hexa-and tetrachiral cellular solids. *Compos. Struct.* 116, 461–476. <https://doi.org/10.1016/j.compstruct.2014.05.033>.
- [5] Barboura, S., Li, J., (2018). Establishment of strain gradient constitutive relations by using asymptotic analysis and the finite element method for complex periodic microstructures. *Int. J. Solids Struct.* 136, 60–76. <https://doi.org/10.1016/j.ijsolstr.2017.12.003>.
- [6] Ben-Amoz, M., (1976). A dynamic theory for composite materials. *Z. Angew. Math. Phys.* 27 (1), 83–99. <https://doi.org/10.1007/BF01595244>.
- [7] Bensoussan, A., Lions, J. -L. and Papanicolaou, G. (1978). *Asymptotic Analysis of Periodic Structures*. North-Holland, Amsterdam.
- [8] Berkache, K., Deogekar, S., Goda, I., Picu, R., Ganghoffer, J.-F., (2017). Construction of second gradient continuum models for random fibrous networks and analysis of size effects. *Compos. Struct.* 181, 347–357. <https://doi.org/10.1016/j.compstruct.2017.08.078>.
- [9] Boutin, C., (1996). Microstructural effects in elastic composites, *International Journal of Solids and Structures*, 33(7) 1023-1051. [https://doi.org/10.1016/0020-7683\(95\)00089-5](https://doi.org/10.1016/0020-7683(95)00089-5).
- [10] Cheng, L., Liang, X., Belski, E., Wang, X., Sietins, J.M., Ludwick, S., To, A. (2018). Natural Frequency Optimization of Variable-Density Additive Manufactured Lattice Structure: Theory and Experimental Validation, *J. Manuf. Sci. Eng.* 140(10): 105002 (16 pages). <https://doi.org/10.1115/1.4040622>.
- [11] Cosserat E., Cosserat F., 1909. *Théorie des corps déformables*. Herman et Fils, Paris. <https://doi.org/10.1038/081067a0>.
- [12] Dell’Isola, F., Seppecher, P., Alibert, J.J. et al. Pantographic metamaterials: an example of mathematically driven design and of its technological challenges. *Continuum Mech. Thermodyn.* 31, 851–884 (2019). <https://doi.org/10.1007/s00161-018-0689-8>.
- [13] Eringen, A.C., Suhubi, E.S., (1964). Nonlinear theory of simple micro-elastic solids—I. *International Journal of Engineering Science*, 2 (2) 189–203, 389-40. [https://doi.org/10.1016/0020-7225\(64\)90004-7](https://doi.org/10.1016/0020-7225(64)90004-7).
- [14] Eshelby, J.D., (1997). The determination of the elastic field of an ellipsoidal inclusion, and related problems. *Proc. R. Soc. Lond.* A241 (1226) 376–396. <https://doi.org/10.1098/rspa.1957.0133>.
- [15] Forest, S., (1998). Mechanics of generalized continua: construction by homogenization. *Journal de Physique IV* (8), 39–48. <https://doi.org/10.1051/jp4:1998405>.
- [16] Forest, S., Pradel, F., Sab, K., (2001). Asymptotic analysis of heterogeneous Cosserat media. *Int. J. Solids Struct.* 38 (26-27), 4585–4608. [https://doi.org/10.1016/S0020-7683\(00\)00295-X](https://doi.org/10.1016/S0020-7683(00)00295-X)
- [17] Forest, S., Sab, K., (1998). Cosserat overall modelling of heterogeneous materials. *Mech. Res. Commun.* 25(4), 449–454. [https://doi.org/10.1016/S0093-6413\(98\)00059-7](https://doi.org/10.1016/S0093-6413(98)00059-7).

- [18] Forest, S., Trinh, D., (2011). Generalized continua and non-homogeneous boundary conditions in homogenisation methods. *ZAMM-J. Appl. Math.Mech.* 91 (2), 90–109. <https://doi.org/10.1002/zamm.201000109>.
- [19] Gambin, B., Kroner, E., (1989). High order terms in the homogenized stress-strain relation of periodic elastic media. *Phys. Stat. Sol. (b)* 151, 513–519. <https://doi.org/10.1002/pssb.2221510211>.
- [20] Geers, M., Kouznetsova, V., Brekelmans, W., (2001). Gradient-enhanced computational homogenization for the micro-macro scale transition. *Le J. Phys. IV* 11 (PR5), Pr5–145. <https://doi.org/10.1051/jp4:2001518>.
- [21] Germain, P. (1973). The method of virtual power in continuum mechanics. Part 2 : Microstructure. *SIAM J. Appl. Math.*, 25(3) 556–575, 1973. <https://doi.org/10.1137/0125053>.
- [22] Goda, I., Ganghoffer, J.-F., (2015). Identification of couple-stress moduli of vertebral trabecular bone based on the 3D internal architectures, *Journal of the Mechanical Behavior of Biomedical Materials*, 51, 99-118. <https://doi.org/10.1016/j.jmbbm.2015.06.036>.
- [23] Goda, I., Ganghoffer, J.-F., (2016). Construction of first and second order grade anisotropic continuum media for 3D porous and textile composite structures. *Compos. Struct.* 141, 292–327. <https://doi.org/10.1016/j.compstruct.2016.01.061>.
- [24] Gologanu, M., Leblond, J-B., Perrin, G., Devaux, J. (1997). Recent Extensions of Gurson’s Model for Porous Ductile Metals. In: Suquet P. (eds) *Continuum Micromechanics*. International Centre for Mechanical Sciences, 377. Springer, Vienna.
- [25] Guedes, J., Kikuchi, N., (1990). Preprocessing and postprocessing for materials based on the homogenization method with adaptive finite element methods. *Comput. Meth.Appl.Mech. Eng.* 83(2), 143–198. [https://doi.org/10.1016/0045-7825\(90\)90148-F](https://doi.org/10.1016/0045-7825(90)90148-F).
- [26] Hashin, Z., Shtrikman, S., (1962). A variational approach to the theory of the elastic behaviour of multiphase materials. *J. Mech. Phys. Solids*, 11 (2), 127-140. [https://doi.org/10.1016/0022-5096\(63\)90060-7](https://doi.org/10.1016/0022-5096(63)90060-7).
- [27] Huet, C., (1990). Application of variational concepts to size effects in elastic heterogeneous bodies. *J. Mech. Phys. Solids* 38 (6), 813–841. [https://doi.org/10.1016/0022-5096\(90\)90041-2](https://doi.org/10.1016/0022-5096(90)90041-2).
- [28] Kanit, T., Forest, S., Galliet, I., Mounoury, V., Jeulin, D., (2003). Determination of the size of the representative volume element for random composites: statistical and numerical approach. *Int. J. Solids Struct.* 40 (13-14), 3647–3679. [https://doi.org/10.1016/S0020-7683\(03\)00143-4](https://doi.org/10.1016/S0020-7683(03)00143-4).
- [29] Kouznetsova, V., Geers, M., Brekelmans, W., (2004). Multi-scale second order computational homogenization of multi-phase materials: a nested finite element solution strategy. *Comput. Methods Appl. Mech. Eng.* 193 (48-51), 5525–5550. <https://doi.org/10.1016/j.cma.2003.12.073>.
- [30] Kröner, E., (1968). Elasticity theory of materials with long range cohesive forces *International Journal of Solids and Structures*, 3(5), 731-742. [https://doi.org/10.1016/0020-7683\(67\)90049-2](https://doi.org/10.1016/0020-7683(67)90049-2).
- [31] Li, J., Zhang, X.-B., (2013). A numerical approach for the establishment of strain gradient constitutive relations in periodic heterogeneous materials. *Eur. J. Mech.-A/Solids* 41, 70–85. <https://doi.org/10.1016/j.euromechsol.2013.03.001>.
- [32] Milton, G., (2002). *The Theory of Composites* (Cambridge Monographs on Applied and Computational Mathematics), 1st ed. Cambridge University Press.
- [33] Mindlin, R.D., Eshel, N.N. (1968). On first strain-gradient theories in linear elasticity. *Int J Solids Struct*, 4(1) 109-124. [https://doi.org/10.1016/0020-7683\(68\)90036-X](https://doi.org/10.1016/0020-7683(68)90036-X).
- [34] Monchiet, V., Auffray, N., Yvonnet, J., (2020). Strain-gradient homogenization: a bridge between asymptotic expansion and quadratic boundary condition methods. *Mech. Mat.*, 143. <https://doi.org/10.1016/j.mechmat.2019.103309>.

- [35] Mori T., Tanaka K., (1973). Average stress in matrix and average energy of materials with misfitting inclusions. *Acta Metallurgica*, 21(5) 571-574. [https://doi.org/10.1016/0001-6160\(73\)90064-3](https://doi.org/10.1016/0001-6160(73)90064-3).
- [36] Rahali, Y., Giorgio, I., Ganghoffer, J.-F. , dell'Isola, F., (2015). Homogenization à la Piola produces second gradient continuum models for linear pantographic lattices. *Int. J. Eng. Sci.* 97, 148–172. <https://doi.org/10.1016/j.ijengsci.2015.10.003>.
- [37] Rosi, G., Auffray, N., (2016). Anisotropic and dispersive wave propagation within strain-gradient framework. *Wave Motion*, 63, 120-134. <https://doi.org/10.1016/j.wavemoti.2016.01.009>.
- [38] Sanchez-Palencia, E., (1980). *Non-Homogeneous Media and Vibration Theory*, Springer, Berlin. <https://doi.org/10.1007/3-540-10000-8>.
- [39] Smyshlyaev, V., Cherednichenko, K., (2000). On rigorous derivation of strain gradient effects in the overall behaviour of periodic heterogeneous media. *J. Mech. Phys. Solids* 48 (6-7), 1325–1357. [https://doi.org/10.1016/S0022-5096\(99\)00090-3](https://doi.org/10.1016/S0022-5096(99)00090-3).
- [40] Torquato, S., (2001). *Random Heterogeneous Materials*, corrected. Springer.
- [41] Tran, T.-H., Monchiet, V., Bonnet, G., (2012). A micromechanics-based approach for the derivation of constitutive elastic coefficients of strain-gradient media. *Int. J. Solids Struct.* 49, 783–792. <https://doi.org/10.1016/j.ijsolstr.2011.11.017>.
- [42] Triantafyllidis, N., Bardenhagen, S., (1996). The influence of scale size on the stability of periodic solids and the role of associated higher order gradient continuum models, *Journal of the Mechanics and Physics of Solids*, 44 (11), 1891-1928. [https://doi.org/10.1016/0022-5096\(96\)00047-6](https://doi.org/10.1016/0022-5096(96)00047-6).
- [43] Trinh, D. K., Janicke, R., Auffray, N., Diebels, S., Forest, S., (2012). EVALUATION OF GENERALIZED CONTINUUM SUBSTITUTION MODELS FOR HETEROGENEOUS MATERIALS, *International Journal for Multiscale Computational Engineering*, 10 (6), 527-549, DOI: 10.1615/IntJMCompEng.2012003105.
- [44] Truesdell, C. and Noll, W. (1965) *The Non-Linear Field Theories of Mechanics*. In: Flügge, S., Ed., *Encyclopedia of Physics*, Vol. 3, Springer-Verlag, Berlin. [http://dx.doi.org/10.1007/978-3-642-46015-9\\_1](http://dx.doi.org/10.1007/978-3-642-46015-9_1).
- [45] Truesdell, C. and Noll, W. (1992). *The Non-Linear Field Theories of Mechanics*, Springer-Verlag Berlin. <https://doi.org/10.1007/978-3-662-13183-1>.
- [46] Weng, G.J., (1990). The theoretical connection between Mori-Tanaka's theory and the Hashin-Shtrikman-Walpole bounds. *Int. J. Eng. Sci.*, 28 (11) 1111-1120. [https://doi.org/10.1016/0020-7225\(90\)90111-U](https://doi.org/10.1016/0020-7225(90)90111-U).
- [47] Weng, G.J., (1992). Explicit evaluation of Willis' bounds with ellipsoidal inclusions *Int. J. Eng. Sci.*, 30 (1) 83-92. [https://doi.org/10.1016/0020-7225\(92\)90123-X](https://doi.org/10.1016/0020-7225(92)90123-X).
- [48] Yvonnet, J., Auffray, N., Monchiet, V., (2020). Computational second-order homogenization of materials with effective anisotropic strain-gradient behavior, *International Journal of Solids and Structures*, 191–192, 434-448. <https://doi.org/10.1016/j.ijsolstr.2020.01.006>.

# Conclusions and Perspectives

### Conclusions and Perspectives

A higher gradient static and dynamic formulation has been developed to evaluate the classic and higher gradient constitutive parameters of heterogeneous structures, based on a dynamical homogenization method. To that scope, we made use of the Hill extended macro-homogeneity condition relating the macroscopic and microscopic strain energies. The calculated higher gradient constitutive parameters prove to be size-dependent, with strain gradient effective moduli increasing in a nonlinear manner with the unit cell number, but converging for a few repetitions of the unit cell. The incorporation into the formulation of correction terms based on the quadratic inertia tensor provides size-independent higher gradient constitutive parameters. This formulation has been used to analyze the static and dynamic mechanical response of composite structures.

As to dynamical aspects, the performed analyses evidence that a first gradient type behavior is not sufficient to describe the wave propagation features, since it is limited to a non-dispersive behavior. To the contrary, higher order formulations have the ability to describe the dispersive behavior encountered in such microstructures materials. To that scope, we elaborate a discrete dynamics method (DDM) to compute the dispersion attributes of periodic structures, with a proposed methodology based on the higher order dynamic asymptotic expansion of the structure's inner forces and moments; the higher order terms of the proposed formulation provide a dispersive frequency of propagating waves.

Another modeling strategy followed in the thesis consists in incorporating higher gradient dynamic macroscopic constitutive parameters, which proves able to model the wave propagation characteristics of microstructured media. The dispersion frequency proves to be strongly dependent on the microscopic mechanical and geometrical contrast through the influence of the higher gradient constitutive parameters. This dependency is related to the chosen formulation of size effects, where the largest frequency values stand for the size-independent higher gradient formulation. As a matter of completeness, it has been shown that for small geometric and mechanical contrasts the classical Cauchy mechanics type formulation is sufficient to describe the composite macroscopic behavior.

Secondly, we show that higher gradient contributions in statics depend on the selected non-classical boundary conditions, whereas higher-order effects require highly non-linear strain profile distributions. While higher gradient constitutive formulation predicts much higher eigenfrequencies of the heterogeneous structure compared to Cauchy response, the

## Conclusions and Perspectives

consideration of micro-inertia contributions may counteract the effect of higher-gradient stiffness terms. Moreover, our analyses show that higher gradient effects mostly appear in the low range of internal length values that is relevant for a wide range of commonly used engineering materials. Applications of this methodology have been done to the dynamical study of vibrating laminated heterogeneous beams.

Several open questions need to be investigated before higher order homogenization should be considered an established method. What are the adequate boundary conditions that should be used? As we know, dispersion properties homogenization-based analyses are limited to small wavenumbers. As such, it remains an open question how to analyze higher gradient contribution for large wavenumbers.

In terms of perspectives, we have established a platform of models and simulation tools for the higher gradient homogenization of composites structures. These tools can be used to determine the higher order effective static and dynamical response of architected materials, like the pantographic structure, which shows a prominent higher gradient contribution. Different applications can be envisaged on such structures using the tools provided in this thesis to study their vibration and acoustic properties. Some work has been recently initiated in this direction with the group of Pr. Francesco dell'Isola (Department of Structural and Geotechnical Engineering, Rome, Italy) in order to investigate from an experimental point of view the higher gradient constitutive behavior for pantographic structure and to compare it with the homogenized model.

Furthermore, an extension of the developed finite element model to 3D is planned to calculate the homogenized properties of different architecture materials. An application on non-centrosymmetric structures can be done using the developed formulation to analyze the coupling tensors, which form the acoustical gyrotropic tensor that is responsible for the so-called acoustical activity.

The 3D model can be used to analyze all resonance modes for architecture materials, and to find the geometric and mechanical properties, which can increase the first eigenfrequency values for isolation purpose. Numerical simulations have to be combined with experimental investigations to validate the choice of the more adequate homogenization formulation and dynamical constitutive model.

# Appendices

## Appendices

### Appendix 1.A: Expression of the dynamic forces and moments

#### 1.A.1 Dynamical expression of the Normal Force

We integrate the dynamical equations of a beam on each nodes in order to determine the dynamic expression of forces in terms of the nodes displacements and rotation.

The longitudinal force is related to the strain as follows:

$$N = -EA \frac{\partial u}{\partial x} \Rightarrow \frac{\partial N}{\partial x} = -EA \frac{\partial^2 u}{\partial x^2} = \rho A \ddot{u} \quad (1.A.1)$$

We assume the propagation of harmonic plane waves of the form:

$$u(x,t) = u(x).e^{i\omega t} \Rightarrow \ddot{u}(x,t) = \omega^2 .u(x,t) \quad (1.A.2)$$

Inserting the harmonic wave in (1.A.1) leads to:

$$-EA \frac{\partial^2 u}{\partial x^2} = \rho A \omega^2 u(x) \rightarrow EA \frac{\partial^2 u}{\partial x^2} + \rho A \omega^2 u(x) = 0 \quad (1.A.3)$$

The solution of previous differential equation writes:

$$u(x) = c_1 . \cos(\chi . x) + c_2 . \sin(\chi . x) \quad (1.A.4)$$

In which the coefficient  $\left(\chi = \sqrt{\rho \omega^2 / E}\right)$  is the compressional frequency coefficient expressed of units  $m^{-1}$ . We adopt the following boundary conditions:

$$\begin{aligned} u(0) &= c_1 = u_1 \\ u(l_0) &= c_1 . \cos(\chi . l_0) + c_2 . \sin(\chi . l_0) = u_2 \end{aligned} \quad (1.A.5)$$

It then holds:

$$c_2 = \frac{u_2 - u_1 . \cos(\chi . l_0)}{\sin(\chi . l_0)} \Rightarrow u(x) = u_1 . \cos(\chi . x) + \frac{u_2 - u_1 . \cos(\chi . l_0)}{\sin(\chi . l_0)} . \sin(\chi . x) \quad (1.A.6)$$

Inserting (1.A.6) in (1.A.1) we get the expression of the normal force:

$$\begin{aligned} N(x) &= -EA \left( -\chi u_1 . \sin(\chi . x) + \frac{u_2 - u_1 . \cos(\chi . l_0)}{\sin(\chi . l_0)} . \chi . \cos(\chi . x) \right) \\ &= \frac{EA \chi}{\sin(\chi . l_0)} (u_1 . \sin(\chi . x) . \sin(\chi . l_0) - u_2 \cos(\chi . x) + u_1 . \cos(\chi . l_0) . \chi . \cos(\chi . x)) \end{aligned} \quad (1.A.7)$$

We can now identify the values of forces at the extremities  $x=0$  and  $x=l_0$ :

$$N(0) = N_O(u_1, u_2) = \frac{EA\chi}{\sin(\chi l_0)} (-u_2 + u_1 \cdot \cos(\chi l_0) \cdot \chi) = N(u_1, u_2) \quad (1.A.8)$$

$$N(l) = N_E(u_1, u_2) = \frac{EA\chi}{\sin(\chi l_0)} (u_1 - u_2 \cos(\chi l_0)) = -N(u_2, u_1)$$

We assume that the compression wave length  $\lambda_c$  is much larger than the beam length, thus the compression coefficient  $(\chi l_0)$  is very small, so that the normal force can be developed in powers of  $(\chi l_0)$  using asymptotic expansion:

$$N(u_1, u_2) = \frac{EA}{l_0} \left( (u_1 - u_2) - \frac{(\chi l_0)^2}{6} (2u_1 + u_2) - \frac{(\chi l_0)^4}{360} (8u_1 + 7u_2) + o((\chi l_0)^5) \right) \quad (1.A.9)$$

### 1.A.2 Dynamical expression of the transverse force and bending moments

Following the same procedure, the expressions of the transversal force can be calculated by integrating the transverse equilibrium equation using the constitutive law:

$$\frac{dT}{dx} = \rho A \ddot{v}, \quad \frac{dM}{dy} + T = 0 \quad \text{and} \quad M = -EI \cdot \frac{d^2 v}{d^2 y} \quad (1.A.10)$$

We note that  $y$  represent the coordinates in the direction of the transverse motion of the beam  $v$ .

After deriving twice the moments respecting to  $y$  we get:

$$EI \cdot \frac{d^4 v}{d^4 y} = \rho A \omega^2 v \quad (1.A.11)$$

As a summary we obtain:

$$\begin{aligned} v(y) &= c_1 \cdot e^{\beta y} + c_2 \cdot e^{-\beta y} + c_3 \cdot e^{-i\beta y} + c_4 \cdot e^{i\beta y} \\ \theta(y) &= c_1 \cdot \beta \cdot e^{\beta y} - c_2 \cdot \beta \cdot e^{-\beta y} - c_3 \cdot i\beta \cdot e^{-i\beta y} + c_4 \cdot i\beta \cdot e^{i\beta y} \\ M(y) &= -EI(c_1 \cdot \beta^2 \cdot e^{\beta y} + c_2 \cdot \beta^2 \cdot e^{-\beta y} - c_3 \cdot \beta^2 \cdot e^{-i\beta y} - c_4 \cdot \beta^2 \cdot e^{i\beta y}) \\ T(y) &= EI(c_1 \cdot \beta^3 \cdot e^{\beta y} - c_2 \cdot \beta^3 \cdot e^{-\beta y} + c_3 \cdot i\beta^3 \cdot e^{-i\beta y} - c_4 \cdot i\beta^3 \cdot e^{i\beta y}) \end{aligned} \quad (1.A.12)$$

In which parameter  $\beta = \sqrt[4]{\rho A \omega^2 / EI}$  is defined as the bending coefficient with the unit  $m^{-1}$ . In order to determine the coefficients of Eq. (1.A.12) we adopt the following boundary conditions:

$$\begin{aligned} v(0) &= v_1 = c_1 + c_2 + c_3 + c_4 \\ v(l_0) &= v_2 = c_1 \cdot e^{\beta l_0} + c_2 \cdot e^{-\beta l_0} + c_3 \cdot e^{-i\beta l_0} + c_4 \cdot e^{i\beta l_0} \\ \theta(0) &= \theta_1 = c_1 \cdot \beta - c_2 \cdot \beta - c_3 \cdot i\beta + c_4 \cdot i\beta \\ \theta(l_0) &= \theta_2 = c_1 \cdot \beta \cdot e^{\beta l_0} - c_2 \cdot \beta \cdot e^{-\beta l_0} - c_3 \cdot i\beta \cdot e^{-i\beta l_0} + c_4 \cdot i\beta \cdot e^{i\beta l_0} \end{aligned} \quad (1.A.13)$$

After solving this system and inserting the constants in the previous expression of the transverse force and moment we get:

$$\begin{aligned}
 M(v_1, v_2, \theta_1, \theta_2) &= \frac{EI \cdot \beta^2}{(1 - \cos(\beta l_0) \cdot \cosh(\beta l_0))} \cdot \left[ \begin{array}{l} (\sin(\beta l_0) \cdot \sinh(\beta l_0)) \cdot v_1 + (\cos(\beta l_0) - \cosh(\beta l_0)) \cdot v_2 \\ + \frac{1}{\beta} (\cosh(\beta l_0) \cdot \sin(\beta l_0) - \cos(\beta l_0) \cdot \sinh(\beta l_0)) \cdot \theta_1 \\ - \frac{1}{\beta} \cdot (\sin(\beta l_0) - \sinh(\beta l_0)) \cdot \theta_2 \end{array} \right] \\
 T(v_1, v_2, \theta_1, \theta_2) &= \frac{EI \cdot \beta^3}{(1 - \cos(\beta l_0) \cdot \cosh(\beta l_0))} \cdot \left[ \begin{array}{l} (\sin(\beta l_0) \cdot \cosh(\beta l_0) + \sinh(\beta l_0) \cdot \cos(\beta l_0)) \cdot v_1 \\ - (\sin(\beta l_0) + \sinh(\beta l_0)) \cdot v_2 + \frac{\theta_1}{\beta} \cdot (\sin(\beta l_0) \cdot \sinh(\beta l_0)) \\ - \frac{\theta_2}{\beta} \cdot (\cos(\beta l_0) - \cosh(\beta l_0)) \end{array} \right]
 \end{aligned} \tag{1.A.14}$$

We assume that the bending wave length  $\lambda_j$  is much larger than the beam length, thus the compression coefficient  $(\beta l_0)$  is very small, so forces can be developed in power of  $(\beta l_0)$  using asymptotic expansion:

$$T(v_1, v_2, \theta_1, \theta_2) = \frac{12EI}{l_0^3} \left( \begin{array}{l} (v_1 - v_2) + \frac{l_0}{2} (\theta_1 + \theta_2) - \frac{(\beta l_0)^4}{840} (26v_1 + 9v_2) - \frac{(\beta l_0)^4 l_0}{5040} (22\theta_1 + 13\theta_2) - \\ \frac{(\beta l_0)^8}{240} (73 \cdot 10^{-4} v_1 + 66 \cdot 10^{-4} v_2) - \frac{(\beta l_0)^8 \cdot l_0}{846720} (65 \cdot \theta_1 - 61 \cdot \theta_2) + o((\beta l_0)^{10}) \end{array} \right) \tag{1.A.15}$$

$$M(v_1, v_2, \theta_1, \theta_2) = \frac{6EI}{l_0^2} \left( \begin{array}{l} (v_1 - v_2) + \frac{l_0}{3} (2\theta_1 + \theta_2) - \frac{(\beta l_0)^4}{2520} (22v_1 + 13v_2) - \frac{(\beta l_0)^4 l_0}{2520} (4\theta_1 - 3\theta_2) \\ - (\beta l_0)^8 \left( \frac{13}{6096384} v_1 + \frac{61}{5080320} v_2 \right) - (\beta l_0)^8 l_0 \left( \frac{17}{6350400} \theta_1 - 2.508 \times 10^{-6} \cdot \theta_2 \right) \\ + o((\beta l_0)^{10}) \end{array} \right) \tag{1.A.16}$$

## Appendix 2.A: Hamilton principle

### 2.A.1 Second gradient from surface to volume integration

To derive the energy equation which link the macro-energy with the micro-energy and displacement we start by the following integral:

$$\int_{d\Omega} \left( u_i - x_j E_{ij} - \frac{1}{2} K_{ijk} x_j x_k \right) (\sigma_{mi} - \Sigma_{mi}) \cdot n_m ds \tag{2.A.1}$$

Using the divergence theorem we get the new form of this integral which is equal to zero (using the assumption of displacement on the boundaries):

## Appendices

$$\begin{aligned}
& \int_{\Omega} \left( \varepsilon_{im} - \delta_{jm} E_{ij} - \frac{1}{2} K_{ijk} \delta_{jm} x_k - \frac{1}{2} K_{ijk} \delta_{km} x_j \right) (\sigma_{mi} - \Sigma_{mi}) + \\
& \left( u_i - x_j E_{ij} - \frac{1}{2} K_{ijk} x_j x_k \right) (\sigma_{mi,m}) d\Omega \\
0 = & \langle \varepsilon_{im} \sigma_{mi} \rangle - E_{im} \Sigma_{mi} - \frac{1}{2} K_{imk} \langle x_k \sigma_{mi} \rangle - \frac{1}{2} K_{ijm} \langle x_j \sigma_{mi} \rangle + \frac{1}{2} K_{imk} \langle x_k \rangle \Sigma_{mi} + \frac{1}{2} K_{ijm} \langle x_j \rangle \Sigma_{mi} \\
& + \langle u_i \rho \ddot{u}_i \rangle - E_{ij} \langle x_j \rho \ddot{u}_i \rangle - \frac{1}{2} K_{ijk} \langle x_j x_k \rho \ddot{u}_i \rangle \\
\Rightarrow & E_{ik} \Sigma_{ki} = \langle \varepsilon_{ik} \sigma_{ki} \rangle - \frac{1}{2} K_{ijk} \langle x_k \sigma_{ji} \rangle - \frac{1}{2} K_{ijk} \langle x_j \sigma_{ki} \rangle + \langle u_i \rho \ddot{u}_i \rangle - E_{ij} \langle \rho \ddot{u}_i x_j \rangle - \frac{1}{2} K_{ijk} \langle x_j x_k \rho \ddot{u}_i \rangle \\
\Rightarrow & E_{ij} \Sigma_{ij} = \langle \varepsilon_{ij} \sigma_{ij} \rangle - K_{ijk} S_{ijk} + \langle u_i \rho \ddot{u}_i \rangle - E_{ij} \langle \rho \ddot{u}_i x_j \rangle - \frac{1}{2} K_{ijk} \langle x_j x_k \rho \ddot{u}_i \rangle \\
\Rightarrow & E_{ij} \Sigma_{ij} + K_{ijk} S_{ijk} = \langle \varepsilon_{ij} \sigma_{ij} \rangle + \left\langle \rho \ddot{u}_i \left( u_i - E_{ij} x_j - \frac{1}{2} K_{ijk} x_j x_k \right) \right\rangle
\end{aligned} \tag{2.A.2}$$

### 2.A.2 Hamiltonian principle up to second gradient

$$\delta \int_{V,t} \left( \frac{1}{2} \langle \rho \rangle \dot{U}_i \dot{U}_i + T' - \left( \frac{1}{2} E_{ij} \Sigma_{ij} + \frac{1}{2} K_{ijk} S_{ijk} + P' \right) \right) dV dt = 0 \tag{2.A.3}$$

We start to calculate using the integration by parts of each integral:

$$Integral_1 = \delta \int_{V,t} \left( \frac{1}{2} E_{ij} \Sigma_{ij} \right) dV dt \tag{2.A.4}$$

We note that that the effective stress can be defined from the strain energy density  $w(E)$ :

$$\begin{aligned}
\Sigma_{ij} &= \frac{\partial w(E, K)}{\partial E_{ij}} \\
\delta \int w dV dt &= \int \delta w dV dt = \int \frac{\partial w}{\partial E_{ij}} \delta E_{ij} dV dt = \int \Sigma_{ij} \delta E_{ij} dV dt = \int \Sigma_{ij} \delta \left( \frac{U_{i,j} + U_{j,i}}{2} \right) dV dt = \int \Sigma_{ij} \delta U_{i,j} dV dt \\
\Rightarrow Integral_1 &= \delta \int \frac{1}{2} E_{ij} \Sigma_{ij} dV dt = \int \Sigma_{ij} \delta U_{i,j} dV dt = \int \Sigma_{ij} \delta U_{i,j} n_j dV dt - \int \Sigma_{ij,j} \delta U_i dV dt \\
&= S_1 - \int \Sigma_{ij,j} \delta U_i dV dt
\end{aligned} \tag{2.A.5}$$

Similarly, the hyperstress tensor derives from the same strain energy density as:

$$S_{ijk} = \frac{\partial w(E, K)}{\partial K_{ijk}} \tag{2.A.6}$$

Then, it holds due to Euler theorem for functions homogeneous of degree two:

## Appendices

$$K_{ijk} \frac{\partial Z}{\partial K_{ijk}} = 2Z \Rightarrow Z = \frac{1}{2} K_{ijk} S_{ijk} \quad (2.A.7)$$

This entails the following variation (we note that in the following variation we will neglect the time constant because we will derive the final equation with respect to t):

$$\begin{aligned} Integral_2 &= \delta \int w dV dt = \int \delta w dV dt = \int \frac{\partial w}{\partial K_{ijk}} \delta K_{ijk} dV dt = \int S_{ijk} \delta K_{ijk} dV dt = \int S_{ijk} \delta U_{i,jk} dV dt \\ &= \delta \int S_{ijk} K_{ijk} dV dt = \int (S_{ijk} \delta U_{i,j})_{,k} dV dt - \int S_{ijk,k} \delta U_{i,j} dV dt \\ &= \int (S_{ijk} \delta U_{i,j}) n_k dS dt - \int S_{ijk,k} \delta U_{i,j} dV dt \\ &= S_{2a} - \int S_{ijk,k} \delta U_{i,j} dV dt = S_{2a} - \left( \int (S_{ijk,k} \delta U_i)_{,j} dV dt - \int S_{ijk,kj} \delta U_i dV dt \right) \\ &= S_{2a} - \int (S_{ijk,k} \delta U_i)_{,j} dV dt + \int S_{ijk,kj} \delta U_i dV dt \\ &= S_{2a} - \int (S_{ijk,k} \delta U_i) n_j dS dt + \int S_{ijk,kj} \delta U_i dV dt = S_{2a} + S_{2b} + \int S_{ijk,kj} \delta U_i dV dt \end{aligned} \quad (2.A.8)$$

$$\begin{aligned} Integral_3 &= \frac{1}{2} \int \delta \langle \rho \rangle \dot{U}_i \dot{U}_i dV dt = \int \langle \rho \rangle \delta \dot{U}_i \dot{U}_i dV dt \\ &= \langle \rho \rangle \delta U_i \dot{U}_i \Big|_{\Delta T} - \int \langle \rho \rangle \delta U_i \ddot{U}_i dV dt = S_3 - \int \langle \rho \rangle \delta U_i \ddot{U}_i dV dt \end{aligned} \quad (2.A.9)$$

We next calculate the variation of the internal energy fluctuation:

$$\begin{aligned} Integral_4 &= \delta \int P'(E_{ij}, \ddot{E}_{ij}, K_{ijk}, \ddot{K}_{ijk}) dV dt = \int \frac{\partial P'}{\partial E_{ij}} \delta E_{ij} + \frac{\partial P'}{\partial \ddot{E}_{ij}} \delta \ddot{E}_{ij} + \frac{\partial P'}{\partial K_{ijk}} \delta \nabla E_{ij} + \frac{\partial P'}{\partial \ddot{K}_{ijk}} \delta \nabla \ddot{E}_{ij} dV dt \\ &= \int \frac{\partial P'}{\partial E_{ij}} \delta E_{ij} + \frac{\partial P'}{\partial \ddot{E}_{ij}} \delta \ddot{E}_{ij} + \frac{\partial P'}{\partial K_{ijk}} \delta \nabla E_{ij} + \frac{\partial P'}{\partial \ddot{K}_{ijk}} \delta \nabla \ddot{E}_{ij} dV dt \end{aligned} \quad (2.A.10)$$

$$\begin{aligned} Integral_{4a} &= \int \frac{\partial P'}{\partial E_{ij}} \delta E_{ij} dV dt = \int \frac{\partial P'}{\partial E_{ij}} \delta U_{i,j} dV dt = \int \left( \frac{\partial P'}{\partial E_{ij}} \delta U_i \right)_{,j} dV dt - \int \nabla_j \left( \frac{\partial P'}{\partial E_{ij}} \right) \delta U_i dV dt \\ &= \int \left( \frac{\partial P'}{\partial E_{ij}} \delta U_i \right) n_j dS dt - \int \frac{\partial}{\partial X_j} \left( \frac{\partial P'}{\partial E_{ij}} \right) \delta U_i dV dt = S_{4a} - \int \frac{\partial}{\partial X_j} \left( \frac{\partial P'}{\partial E_{ij}} \right) \delta U_i dV dt \end{aligned} \quad (2.A.11)$$

## Appendices

$$\begin{aligned}
Integral_{4b} &= \int \frac{\partial P'}{\partial \ddot{E}_{ij}} \delta \ddot{E}_{ij} dVdt = \frac{\partial P'}{\partial \ddot{E}_{ij}} \delta \dot{E}_{ij} \Big|_{\Delta T} - \int \frac{\partial}{\partial t} \left( \frac{\partial P'}{\partial \ddot{E}_{ij}} \right) \delta \dot{E}_{ij} dVdt = \\
&= - \frac{\partial}{\partial t} \left( \frac{\partial P'}{\partial \ddot{E}_{ij}} \right) \delta \dot{E}_{ij} \Big|_{\Delta T} + \int \frac{\partial^2}{\partial t^2} \left( \frac{\partial P'}{\partial \ddot{E}_{ij}} \right) \delta E_{ij} dVdt \\
&= \int \frac{\partial^2}{\partial t^2} \left( \frac{\partial P'}{\partial \ddot{E}_{ij}} \right) \delta U_{i,j} dVdt = \int \frac{\partial^2}{\partial t^2} \left( \frac{\partial P'}{\partial \ddot{E}_{ij}} \right) \delta U_{i,n_j} dSdt - \int \frac{\partial}{\partial X_j} \left( \frac{\partial^2}{\partial t^2} \left( \frac{\partial P'}{\partial \ddot{E}_{ij}} \right) \right) \delta U_i dVdt = \\
&= S_{4b} - \int \frac{\partial}{\partial X_j} \left( \frac{\partial^2}{\partial t^2} \left( \frac{\partial P'}{\partial \ddot{E}} \right) \right) \delta U_i dVdt
\end{aligned} \tag{2.A.12}$$

$$\begin{aligned}
Integral_{4c} &= \int \frac{\partial P'}{\partial K_{ijk}} \delta (\nabla E_{ij}) dVdt = \frac{\partial P'}{\partial K_{ijk}} \delta (E_{ij}) \Big|_{\Delta T} - \int \frac{\partial}{\partial X_k} \left( \frac{\partial P'}{\partial K_{ijk}} \right) \delta (E_{ij}) dVdt \\
&= - \int \left( \frac{\partial}{\partial X_k} \left( \frac{\partial P'}{\partial K_{ijk}} \right) \delta U_{i,n_j} dSdt \right) + \int \left( \frac{\partial^2}{\partial X_k \partial X_j} \left( \frac{\partial P'}{\partial K_{ijk}} \right) \delta U_i dVdt \right) \\
&= S_{4c} + \int \left( \frac{\partial^2}{\partial X_k \partial X_j} \left( \frac{\partial P'}{\partial K_{ijk}} \right) \delta U_i dVdt \right)
\end{aligned} \tag{2.A.13}$$

$$\begin{aligned}
Integral_{4d} &= \int \frac{\partial P'}{\partial \ddot{K}_{ijk}} \delta \nabla \ddot{E}_{ij} dVdt = \frac{\partial P'}{\partial \ddot{K}_{ijk}} \delta \nabla \dot{E}_{ij} \Big|_{\Delta T} - \int \frac{\partial}{\partial t} \left( \frac{\partial P'}{\partial \ddot{K}_{ijk}} \right) \delta \nabla \dot{E}_{ij} dVdt \\
&= - \frac{\partial}{\partial t} \left( \frac{\partial P'}{\partial \ddot{K}_{ijk}} \right) \delta \nabla E_{ij} \Big|_{\Delta T} + \int \frac{\partial^2}{\partial t^2} \left( \frac{\partial P'}{\partial \ddot{K}_{ijk}} \right) \delta U_{i,jk} dVdt \\
&= \int \left( \frac{\partial^2}{\partial t^2} \left( \frac{\partial P'}{\partial \ddot{K}_{ijk}} \right) \delta U_{i,j} \right)_{,k} dVdt - \int \frac{\partial}{\partial X_k} \left( \frac{\partial^2}{\partial t^2} \left( \frac{\partial P'}{\partial \ddot{K}_{ijk}} \right) \right) \delta U_{i,j} dVdt \\
&= S_{4d1} - \int \left( \frac{\partial}{\partial X_k} \left( \frac{\partial^2}{\partial t^2} \left( \frac{\partial P'}{\partial \ddot{K}_{ijk}} \right) \right) \delta U_i \right)_{,j} dVdt + \int \frac{\partial^2}{\partial x_j \partial x_k} \left( \frac{\partial^2}{\partial t^2} \left( \frac{\partial P'}{\partial \ddot{K}_{ijk}} \right) \right) \delta U_i dVdt \\
&= S_{4d1} + S_{4d2} + \int \frac{\partial^2}{\partial X_j \partial X_k} \left( \frac{\partial^2}{\partial t^2} \left( \frac{\partial P'}{\partial \ddot{K}_{ijk}} \right) \right) \delta U_i dVdt
\end{aligned} \tag{2.A.14}$$

$$Integral_5 = \delta \int T' (\dot{E}_{ij}, \nabla \dot{E}_{ij}) dVdt = \int \frac{\partial T'}{\partial \dot{E}_{ij}} \delta \dot{E}_{ij} + \frac{\partial T'}{\partial \dot{K}_{ijk}} \delta \nabla \dot{E}_{ij} dVdt \tag{2.A.15}$$

## Appendices

$$\begin{aligned}
 Integral_{5a} &= \int \left( \frac{\partial T'}{\partial \dot{E}_{ij}} \delta \dot{E}_{ij} = \frac{\partial T'}{\partial \dot{E}_{ij}} \delta E_{ij} \right)_{\Delta T} - \int \frac{d}{dt} \left( \frac{\partial T'}{\partial \dot{E}_{ij}} \right) \delta E_{ij} dV dt = - \int \frac{d}{dt} \left( \frac{\partial T'}{\partial \dot{E}_{ij}} \right) \delta U_{i,j} dV dt \\
 &= - \int \frac{d}{dt} \left( \frac{\partial T'}{\partial \dot{E}_{ij}} \right) \delta U_{i,n_j} dS dt + \int \frac{\partial}{\partial X_j} \frac{\partial}{\partial t} \left( \frac{\partial T'}{\partial \dot{E}_{ij}} \right) \delta U_i dV dt = S_{5a} + \int \frac{\partial}{\partial X_j} \frac{\partial}{\partial t} \left( \frac{\partial T'}{\partial \dot{E}_{ij}} \right) \delta U_i dV dt
 \end{aligned} \tag{2.A.16}$$

$$\begin{aligned}
 Integral_{5b} &= \int \frac{\partial T'}{\partial \dot{K}_{ijk}} \delta \nabla \dot{E}_{ij} dV dt = \int \frac{\partial T'}{\partial \dot{K}_{ijk}} \delta \nabla E_{ij} \Big|_{\Delta T} - \int \frac{\partial}{\partial t} \left( \frac{\partial T'}{\partial \dot{K}_{ijk}} \right) \delta \nabla E_{ij} dV dt \\
 &= - \frac{\partial}{\partial t} \left( \frac{\partial T'}{\partial \dot{K}_{ijk}} \right) \delta E_{ij} \Big|_{\Delta T} + \int \frac{\partial}{\partial X_k} \left( \frac{\partial}{\partial t} \left( \frac{\partial T'}{\partial \dot{K}_{ijk}} \right) \right) \delta U_{i,j} dV dt \\
 &= \int \frac{\partial}{\partial X_k} \left( \frac{\partial}{\partial t} \left( \frac{\partial T'}{\partial \dot{K}_{ijk}} \right) \right) \delta U_{i,n_j} dV dt - \int \frac{\partial}{\partial X_j} \left( \frac{\partial}{\partial X_k} \left( \frac{\partial}{\partial t} \left( \frac{\partial T'}{\partial \dot{K}_{ijk}} \right) \right) \right) \delta U_i dV dt = \\
 S_{5b} &- \int \frac{\partial}{\partial X_j} \left( \frac{\partial}{\partial X_k} \left( \frac{\partial}{\partial t} \left( \frac{\partial T'}{\partial \dot{K}_{ijk}} \right) \right) \right) \delta U_i dV dt
 \end{aligned} \tag{2.A.17}$$

Then, inserting (2.A.4-2.A.17) back into (2.A.3) and deriving with respect to time we get the following macro-equation of motion:

$$\begin{aligned}
 &\int \Sigma_{ij,j} \delta U_i \partial V - \int S_{ijk,jk} \delta U_i dV + \int \frac{\partial}{\partial X_j} \left( \frac{\partial P'}{\partial E_{ij}} \right) \delta U_i dV + \int \frac{\partial}{\partial X_j} \left( \frac{\partial^2}{\partial t^2} \left( \frac{\partial P'}{\partial \dot{E}_{ij}} \right) \right) \delta U_i dV \\
 &+ \int \frac{\partial}{\partial X_j} \frac{\partial}{\partial t} \left( \frac{\partial T'}{\partial \dot{E}_{ij}} \right) \delta U_i dV - \int \frac{\partial^2}{\partial X_j \partial X_k} \left( \frac{\partial^2}{\partial t^2} \left( \frac{\partial P'}{\partial \dot{K}_{ijk}} \right) \right) \delta U_i dV - \int \left( \frac{\partial^2}{\partial X_j \partial X_k} \left( \frac{\partial P'}{\partial K_{ij}} \right) \right) \delta U_i dV \\
 &- \int \frac{\partial}{\partial X_j} \left( \frac{\partial}{\partial X_k} \left( \frac{\partial}{\partial t} \left( \frac{\partial T'}{\partial \dot{K}_{ijk}} \right) \right) \right) \delta U_i dV \\
 &- S_1 - S_{2a} - S_{2b} + S_3 - S_{4a} - S_{4b} - S_{4c} - S_{4d1} - S_{4d2} + S_{5a} + S_{5b} = \int \langle \rho \rangle \delta U_i \ddot{U}_i dV
 \end{aligned} \tag{2.A.18}$$

### 2.A.3 Simplification of $F_i$

In order to simplify the micro-inertia force which is in the last equation of motion (2.A.18), we use the localization tensors of displacement and for deformation to simplify the form of  $F_i$ . Starting with the potential energy  $P'$  :

## Appendices

$$\begin{aligned}
P' &= -\frac{1}{2} \left\langle \rho \ddot{u}_i \left( u_i - E_{ij} x_j - \frac{1}{2} K_{ijk} x_j x_k \right) \right\rangle \\
&= -\frac{1}{2} \left\langle \rho \left( H_{ijk}^E \ddot{E}_{jk} + H_{ijkl}^K \ddot{K}_{jkl} \right) \cdot \left( H_{imn}^E E_{mn} + H_{imnp}^K K_{mnp} - E_{im} x_m - \frac{1}{2} K_{imn} x_m x_n \right) \right\rangle \\
&= -\frac{1}{2} \ddot{E}_{jk} E_{mn} \langle \rho H_{ijk}^E H_{imn}^E \rangle - \frac{1}{2} \ddot{E}_{jk} K_{mnp} \langle \rho H_{ijk}^E H_{imnp}^K \rangle + \frac{1}{2} \ddot{E}_{jk} E_{im} \langle \rho H_{ijk}^E x_m \rangle + \frac{1}{4} \ddot{E}_{jk} K_{imn} \langle \rho H_{ijk}^E x_m x_n \rangle \\
&\quad - \frac{1}{2} \ddot{K}_{jkl} E_{mn} \langle \rho H_{ijkl}^K H_{imn}^E \rangle - \frac{1}{2} \ddot{K}_{jkl} K_{mnp} \langle \rho H_{ijkl}^K H_{imnp}^K \rangle + \frac{1}{2} \ddot{K}_{jkl} E_{im} \langle \rho H_{ijkl}^K x_m \rangle + \frac{1}{4} \ddot{K}_{jkl} K_{imn} \langle \rho H_{ijkl}^K x_m x_n \rangle \\
&\Rightarrow \frac{\partial^2}{\partial t^2} \left( \frac{\partial P'}{\partial \ddot{E}_{ij}} \right) = -\frac{1}{2} \ddot{E}_{mn} \langle \rho H_{kij}^E H_{kmn}^E \rangle - \frac{1}{2} \ddot{K}_{mnp} \langle \rho H_{kij}^E H_{kmnp}^K \rangle + \frac{1}{2} \ddot{E}_{km} \langle \rho H_{kij}^E x_m \rangle + \frac{1}{4} \ddot{K}_{kmn} \langle \rho H_{kij}^E x_m x_n \rangle \\
&\Rightarrow \frac{\partial P'}{\partial E_{ij}} = -\frac{1}{2} \ddot{E}_{mn} \langle \rho H_{kmn}^E H_{kij}^E \rangle + \frac{1}{2} \ddot{E}_{mn} \langle \rho H_{imn}^E x_j \rangle - \frac{1}{2} \ddot{K}_{mnl} \langle \rho H_{kmnl}^K H_{kij}^E \rangle + \frac{1}{2} \ddot{K}_{mkl} \langle \rho H_{imkl}^K x_j \rangle \\
&\Rightarrow \frac{\partial^2}{\partial t^2} \left( \frac{\partial P'}{\partial \ddot{K}_{ijk}} \right) = -\frac{1}{2} \ddot{E}_{mn} \langle \rho H_{lij}^K H_{lmn}^E \rangle - \frac{1}{2} \ddot{K}_{mnp} \langle \rho H_{lmnp}^K H_{lij}^K \rangle + \frac{1}{2} \ddot{E}_{lm} \langle \rho H_{lij}^K x_m \rangle + \frac{1}{4} \ddot{K}_{lmn} \langle \rho H_{lij}^K x_m x_n \rangle \\
&\Rightarrow \frac{\partial P'}{\partial K_{ijk}} = -\frac{1}{2} \ddot{E}_{mn} \langle \rho H_{lmn}^E H_{lij}^K \rangle + \frac{1}{4} \ddot{E}_{mn} \langle \rho H_{imn}^E x_j x_k \rangle - \frac{1}{2} \ddot{K}_{mnp} \langle \rho H_{lmnp}^K H_{lij}^K \rangle + \frac{1}{4} \ddot{K}_{mnp} \langle \rho H_{imnp}^K x_j x_k \rangle
\end{aligned} \tag{2.A.22}$$

Next we derive the micro-kinetic energy:

$$\begin{aligned}
T' &= \left\langle \rho \left( H_{ijk}^E \dot{E}_{jk} + H_{ijkl}^K \dot{K}_{jkl} - \dot{E}_{ij} x_j - \frac{1}{2} \dot{K}_{ijk} x_j x_k \right) \dot{E}_{im} x_m \right\rangle \\
&\quad + \frac{1}{2} \left\langle \rho \left( H_{ijk}^E \dot{E}_{jk} + H_{ijkl}^K \dot{K}_{jkl} - \dot{E}_{jk} x_k - \frac{1}{2} \dot{K}_{ijk} x_j x_k \right) \dot{K}_{imp} x_m x_p \right\rangle \\
&\quad + \frac{1}{2} \left\langle \rho \left( H_{ijk}^E \dot{E}_{jk} + H_{ijkl}^K \dot{K}_{jkl} - \dot{E}_{ij} x_j - \frac{1}{2} \dot{K}_{ijk} x_j x_k \right) \cdot \left( H_{imp}^E \dot{E}_{mp} + H_{impf}^K \dot{K}_{mpf} - \dot{E}_{im} x_m - \frac{1}{2} \dot{K}_{mnp} x_m x_p \right) \right\rangle \\
&= -\frac{1}{2} \dot{E}_{ij} \dot{E}_{im} \langle \rho x_j x_m \rangle - \frac{1}{2} \dot{K}_{ijk} \dot{E}_{im} \langle \rho x_m x_j x_k \rangle - \frac{1}{8} \dot{K}_{ijk} \dot{K}_{imp} \langle \rho x_j x_k x_m x_p \rangle \\
&\quad + \frac{1}{2} \dot{E}_{jk} \dot{E}_{mp} \langle \rho H_{ijk}^E H_{imp}^E \rangle + \dot{K}_{mpf} \dot{E}_{jk} \langle \rho H_{ijk}^E H_{impf}^K \rangle + \frac{1}{2} \dot{K}_{jkl} \dot{K}_{mpf} \langle \rho H_{ijkl}^K H_{impf}^K \rangle \\
&\Rightarrow \frac{\partial}{\partial t} \left( \frac{\partial T'}{\partial \dot{E}_{ij}} \right) = -\dot{E}_{im} \langle \rho x_j x_m \rangle - \frac{1}{2} \dot{K}_{imk} \langle \rho x_m x_j x_k \rangle + \dot{E}_{mp} \langle \rho H_{kij}^E H_{kmp}^E \rangle + \dot{K}_{mpf} \langle \rho H_{kij}^E H_{kmpf}^K \rangle \\
&\Rightarrow \frac{\partial}{\partial t} \left( \frac{\partial T'}{\partial \dot{K}_{ijk}} \right) = -\frac{1}{2} \dot{E}_{im} \langle \rho x_m x_j x_k \rangle - \frac{1}{4} \dot{K}_{imp} \langle \rho x_m x_j x_k x_p \rangle + \dot{E}_{pf} \langle \rho H_{mpf}^E H_{mijk}^K \rangle + \dot{K}_{mpf} \langle \rho H_{ijk}^K H_{impf}^K \rangle
\end{aligned} \tag{2.A.23}$$

After deriving the kinetic and potential energy, we insert these expressions into the last expression of Fi as the following:

$$F_i = \frac{\partial}{\partial X_j} \left( \frac{1}{2} \ddot{E}_{mn} \left\langle \rho \left( H_{imn}^E x_j + H_{mij}^E x_n - 2\delta_i^m x_j x_n \right) \right\rangle + \frac{1}{2} \ddot{K}_{rst} \left\langle \rho \left( H_{irst}^K x_j + \frac{1}{2} H_{rij}^E x_s x_t - \delta_i^r x_s x_j x_t \right) \right\rangle \right) - \frac{\partial^2}{\partial X_j \partial X_k} \left( \ddot{E}_{pq} \left\langle \frac{\rho}{2} \left( H_{pij}^K x_q + \frac{1}{2} H_{ipq}^E x_j x_k - \delta_i^p x_q x_j x_k \right) \right\rangle + \frac{1}{4} \ddot{K}_{rst} \left\langle \rho \left( H_{rij}^K x_s x_t + H_{irst}^K x_j x_k - \delta_i^r x_s x_j x_k x_t \right) \right\rangle \right) \quad (2.A.24)$$

## Appendix 2.B: Higher gradient dynamic homogenization method

Using the definition of internal energy, we expand it in function of the localization tensors:

$$\begin{aligned} 2W^{\text{int}}(E, K) &= (E_{ij} \cdot \Sigma_{ij} + K_{ijk} \cdot S_{ijk}) = \langle \varepsilon_{ij} \sigma_{ij} \rangle + \left\langle \rho \ddot{u}_i \left( u_i - E_{ij} x_j - \frac{1}{2} K_{ijk} x_j x_k \right) \right\rangle \\ &= \left\langle (A_{ijkl}^E \cdot E_{kl} + A_{ijkl}^K \cdot K_{klf}) \cdot C_{ijmn} \cdot (A_{mnrst}^E \cdot E_{rs} + A_{mnrst}^K \cdot K_{rst}) \right\rangle \\ &+ \left\langle \rho \left( H_{ijk}^E \cdot \ddot{E}_{jk} + H_{ijkl}^K \cdot \ddot{K}_{jkl} \right) \cdot \left( H_{igr}^E \cdot E_{qr} + H_{irst}^K \cdot K_{rst} - E_{iq} x_q - \frac{1}{2} K_{igr}^K x_q x_r \right) \right\rangle \\ &= \left\langle A_{ijkl}^E E_{kl} \cdot C_{ijmn} \cdot A_{mnrst}^E E_{rs} + A_{ijkl}^E E_{kl} \cdot C_{ijmn} \cdot A_{mnrst}^K K_{rst} + A_{ijkl}^K K_{klf} \cdot C_{ijmn} \cdot A_{mnrst}^E E_{rs} + A_{ijkl}^K K_{klf} \cdot C_{ijmn} \cdot A_{mnrst}^K K_{rst} \right\rangle \\ &+ \left\langle \rho \left( \begin{aligned} &H_{ijk}^E \ddot{E}_{jk} H_{igr}^E E_{qr} + H_{ijk}^E \ddot{E}_{jk} H_{irst}^K K_{rst} - H_{ijk}^E \ddot{E}_{jk} E_{iq} x_q - \frac{1}{2} H_{ijk}^E \ddot{E}_{jk} K_{igr}^K x_q x_r \\ &+ H_{ijkl}^K \ddot{K}_{jkl} H_{igr}^E E_{qr} + H_{ijkl}^K \ddot{K}_{jkl} H_{irst}^K K_{rst} - H_{ijkl}^K \ddot{K}_{jkl} E_{iq} x_q - \frac{1}{2} H_{ijkl}^K \ddot{K}_{jkl} K_{igr}^K x_q x_r \end{aligned} \right) \right\rangle \end{aligned} \quad (2.B.1)$$

The macroscopic stress is the variation of the internal energy with respect to the macro-deformation:

$$\begin{aligned} \Sigma_{ij}^{\text{dyn}} &= \frac{\partial W^{\text{int}}(E, K, \ddot{E}, \ddot{K})}{\partial E_{ij}} + \frac{\partial^2}{\partial t^2} \left( \frac{\partial W^{\text{int}}(E, K, \ddot{E}, \ddot{K})}{\partial \ddot{E}_{ij}} \right) \\ &= \frac{1}{2} \left\langle \begin{aligned} &A_{klj}^E \cdot C_{klmn} \cdot A_{mnrst}^E \cdot E_{rs} + A_{rskl}^E \cdot C_{rsmn} \cdot A_{mnij}^E \cdot E_{kl} + A_{klj}^E \cdot C_{klmn} \cdot A_{mnrst}^K \cdot K_{rst} + A_{rskl}^K \cdot K_{klf} \cdot C_{rsmn} \cdot A_{mnij}^E \\ &+ \rho H_{qrk}^E \ddot{E}_{rk} H_{pij}^E - \rho H_{iqk}^E \ddot{E}_{qk} x_j + \rho H_{qrkl}^K \ddot{K}_{rkl} H_{qij}^E - \rho H_{iqkl}^K \ddot{K}_{qkl} x_j + \rho H_{kij}^E \ddot{E}_{qr} H_{kqr}^E \\ &+ \rho H_{krst}^K \ddot{K}_{rst} H_{kij}^E - \rho H_{kij}^E \ddot{E}_{kq} x_q - \frac{1}{2} \rho \ddot{K}_{kqr} H_{kij}^E x_q x_r \end{aligned} \right\rangle \\ \Sigma_{ij}^{\text{dyn}} &= E_{dl} \left\langle \frac{1}{2} (A_{krj}^E C_{krmn} A_{mndl}^E + A_{rsdl}^E C_{rsmn} A_{mnij}^E) \right\rangle + K_{rst} \left\langle \frac{1}{2} (A_{klj}^E C_{klmn} A_{mnrst}^K + A_{klrst}^K C_{klmn} A_{mnij}^E) \right\rangle \\ &+ \ddot{E}_{dl} \left\langle \frac{\rho}{2} (H_{qdl}^E H_{qij}^E + H_{kij}^E H_{kdl}^E - H_{idl}^E x_j - H_{dij}^E x_l) \right\rangle \\ &+ \ddot{K}_{rst} \left\langle \frac{\rho}{2} (H_{qrst}^K H_{qij}^E + H_{krst}^K H_{kij}^E - H_{irst}^K x_j - \frac{1}{2} H_{rij}^E x_s x_t) \right\rangle \end{aligned} \quad (2.B.2)$$

The hyper-stress is also the variation of the internal energy with respect to the second gradient deformation:

$$\begin{aligned}
 S_{ijk} &= \frac{\partial W^{\text{int}}(E, K, \ddot{E}, \ddot{K})}{\partial K_{ijk}} + \frac{\partial^2}{\partial t^2} \frac{\partial W^{\text{int}}(E, K, \ddot{E}, \ddot{K})}{\partial \ddot{K}_{ijk}} \\
 &= \frac{1}{2} \left\langle \begin{aligned} &A_{rstl}^E E_{tl} C_{rsmn} A_{mnijk}^K + A_{rsijk}^K C_{rsmn} A_{mndl}^E E_{dl} + A_{rsijk}^K C_{rsmn} A_{mndlt}^K K_{dlt} \\ &+ A_{rstlf}^K C_{rsmn} A_{mnijk}^K K_{tlf} + \rho H_{rst}^E \ddot{E}_{st} H_{rij}^K - \frac{1}{2} \rho H_{igr}^E \ddot{E}_{qr} x_k x_j \\ &+ \rho H_{lqr}^E \ddot{E}_{qr} H_{lij}^K + \rho H_{lij}^K H_{lrst}^K \ddot{K}_{rst} + \rho H_{dstl}^K H_{dijk}^K \ddot{K}_{stl} \\ &-\rho \ddot{E}_{lq} H_{lij}^K x_l - \frac{1}{2} \rho H_{lij}^K K_{lqr} x_q x_r - \frac{1}{2} \rho H_{igr}^K K_{qrl} x_j x_k \end{aligned} \right\rangle \quad (2.B.3) \\
 S_{ijk} &= \left\langle \frac{1}{2} A_{rsdl}^E C_{rsmn} A_{mnijk}^K + \frac{1}{2} A_{rsijk}^K C_{rsmn} A_{mndl}^E \right\rangle \cdot E_{dl} + \left\langle \frac{1}{2} A_{pfijk}^K C_{pfmn} A_{mnrst}^K + \frac{1}{2} A_{dlrst}^K C_{dlmn} A_{mnijk}^K \right\rangle \cdot K_{rst} \\
 &+ \left\langle \frac{\rho}{2} \left( H_{qdl}^E H_{qijk}^K + H_{rdl}^E H_{rij}^K - \frac{1}{2} H_{idl}^E x_k x_j - H_{dijk}^K x_l \right) \right\rangle \cdot \ddot{E}_{dl} + \\
 &\left\langle \frac{\rho}{2} \left( H_{lrst}^K H_{lij}^K + H_{drst}^K H_{dijk}^K - \frac{1}{2} H_{rij}^K x_s x_t - \frac{1}{2} H_{irst}^K x_j x_k \right) \right\rangle \cdot \ddot{K}_{rst}
 \end{aligned}$$

## Appendix 2.C: Elasticity Solution

Using the elasticity theory and Floquet's theorem (Sun et al., 1968) they derive the exact dispersion relation of the longitudinal wave propagating in the direction normal to the layering Eq. (2.C.1) as follows:

$$\cos\left(k(d_f + d_m)\right) = \cos\left(kd_m \frac{c}{c_L^m}\right) \cos\left(kd_f \frac{c}{c_L^f}\right) - \left[\frac{(1+p^2)}{2p}\right] \sin\left(kd_m \frac{c}{c_L^m}\right) \sin\left(kd_f \frac{c}{c_L^f}\right) \quad (2.C.1)$$

$$\text{where } p = \frac{(\lambda_f + 2\mu_f) c_L^m}{(\lambda_m + 2\mu_m) c_L^f}$$

The dispersion of the transverse wave propagating in the direction normal to the layering will be obtained by replacing in Eq. (2.C.1)  $(\lambda_f + 2\mu_f)$  by  $2\mu_f$  and  $(\lambda_m + 2\mu_m)$  by  $2\mu_m$  respectively.

## Appendix 3.A: Identification of micromechanical constants upon normal deformations

We hereby identify the micro-mechanical constants relating micro and macro-scale displacements and strains for the case of longitudinal deformations at the macro-scale of the structure. To that scope, we introduce displacement and strain localization operators, which we fully characterize with the use of boundary and interface conditions. In Fig. 3.2 we summarize the geometric and material parameters of the two material phases contained within the unit-cell of the microscale, further elaborating the definitions of Fig. 4.1a.

## Appendices

We subsequently determine the expressions of the localization operators of Eq. (3) for the case of purely normal macroscopic deformations. In such a deformation mode, the macro displacement field is along the direction  $X$  of periodic structure of Fig. 3.2 (left), so that:

$$U = f(X) \Rightarrow E_{11} \neq 0, K_{111} \neq 0 \quad (3.A.1)$$

The coefficients of the localization tensors for the micro-displacements are denoted  $a_i$  and  $b_i$  for the first and second layer respectively, defined as follows:

$$\begin{aligned} u_1^{(1)}(x) &= \begin{bmatrix} H_{1111}^E & H_{1111}^K \end{bmatrix} \cdot \begin{bmatrix} E_{11} \\ K_{111} \end{bmatrix} = \begin{bmatrix} a_0 + a_1x & a_2 + a_3x + a_4 \frac{x^2}{2} \end{bmatrix} \cdot \begin{bmatrix} E_{11} \\ K_{111} \end{bmatrix} \\ \Rightarrow \left\{ \varepsilon_{11}^{(1)}(x) \right. &= \begin{bmatrix} A_{1111}^E & A_{1111}^K \end{bmatrix} \cdot \begin{bmatrix} E_{11} \\ K_{111} \end{bmatrix} = \begin{bmatrix} a_1 & a_3 + a_4x \end{bmatrix} \cdot \begin{bmatrix} E_{11} \\ K_{111} \end{bmatrix} \\ u_1^{(2)}(x) &= \begin{bmatrix} H_{1111}^E & H_{1111}^K \end{bmatrix} \cdot \begin{bmatrix} E_{11} \\ K_{111} \end{bmatrix} = \begin{bmatrix} b_0 + b_1x & b_2 + b_3x + b_4 \frac{x^2}{2} \end{bmatrix} \cdot \begin{bmatrix} E_{11} \\ K_{111} \end{bmatrix} \\ \Rightarrow \left\{ \varepsilon_{11}^{(2)}(x) \right. &= \begin{bmatrix} A_{1111}^E & A_{1111}^K \end{bmatrix} \cdot \begin{bmatrix} E_{11} \\ K_{111} \end{bmatrix} = \begin{bmatrix} b_1 & b_3 + b_4x \end{bmatrix} \cdot \begin{bmatrix} E_{11} \\ K_{111} \end{bmatrix} \end{aligned} \quad (3.A.2)$$

Eq. (3.A.2) contains a total of 10 unknown parameters  $a_i$  and  $b_i$ , the superscript therein defining in which phase the displacement or the strain is evaluated. The micro-stress developed in each inner material phase is modeled as an isotropic elastic material that is computed as a function of the micro-strains within Eq. (3.A.2), as follows:

$$\begin{cases} \sigma_{11}^{(1)}(x) = (\lambda_1 + 2\mu_1) \cdot \varepsilon_{11}^{(1)}(x) = (\lambda_1 + 2\mu_1) \cdot \begin{bmatrix} a_1 & a_3 + a_4x \end{bmatrix} \cdot \begin{bmatrix} E_{11} \\ K_{111} \end{bmatrix} \\ \sigma_{11}^{(2)}(x) = (\lambda_2 + 2\mu_2) \cdot \varepsilon_{11}^{(2)}(x) = (\lambda_2 + 2\mu_2) \cdot \begin{bmatrix} b_1 & b_3 + b_4x \end{bmatrix} \cdot \begin{bmatrix} E_{11} \\ K_{111} \end{bmatrix} \end{cases} \quad (3.A.3)$$

Where  $\lambda$  in Eq. (3.A.3) defines the first Lamé coefficient. We use the interface continuity condition for the displacement, noting that first and second gradient terms  $E_{ij}$  and  $K_{ijk}$  can be treated as independent variables. The body forces are null within the cell, so we also use the continuity of stresses and stress gradients. As an additional condition, we use the average of the microscopic strains for the first and second gradient to be equal to the corresponding macroscopic strains, so that a sufficient number of equations is derived to determine all constants  $a_i$  and  $b_i$ . These conditions are summarized in Eq. (3.A.4), as follows:

$$\begin{cases} u_1^1(0) = u_2^1(0) \\ u_1^1(-d_1) = -E_{11}d_1 + K_{111}\frac{d_1^2}{2}, u_2^1(d_2) = E_{11}d_2 + K_{111}\frac{d_2^2}{2} \\ \sigma_{11}^1(0) = \sigma_{11}^2(0), \frac{\partial \sigma_{11}^1}{\partial x}(0) = \frac{\partial \sigma_{11}^2}{\partial x}(0) \\ \langle \varepsilon_{11} \rangle_{\Omega} = E_{11}, \langle \nabla \varepsilon_{11} \rangle_{\Omega} = K_{111} \end{cases} \quad (3.A.4)$$

Solving the system of Eqs. (3.A.4) with the use of Eq. (3.A.2) and (3.A.3), one obtains after straightforward computations the following expressions for the microscopic coefficients  $a_i$  and  $b_i$  :

$$\begin{aligned} a_0 &= -\frac{d_1d_2((\lambda_1+2\mu_1)-(\lambda_2+2\mu_2))}{(\lambda_1+2\mu_1)d_2+d_1(\lambda_2+2\mu_2)}, a_1 = \frac{(\lambda_2+2\mu_2)(d_1+d_2)}{(\lambda_1+2\mu_1)d_2+d_1(\lambda_2+2\mu_1)}, \\ a_2 &= -\frac{d_2d_1(-(\lambda_1+2\mu_1)^2d_2d_1+(\lambda_1+2\mu_1)(\lambda_2+2\mu_2)d_1(-d_1+d_2+L)-d_1d_2(\lambda_2+2\mu_2)^2)}{2((\lambda_1+2\mu_1)d_2+d_1(\lambda_2+2\mu_2))^2}, \\ a_3 &= \frac{(\lambda_2+2\mu_2)(d_1(\lambda_2+2\mu_2)(-d_1^2+d_2^2+Ld_1)-d_2(\lambda_1+2\mu_1)(d_1^2+d_2d_1))}{2((\lambda_1+2\mu_1)d_2+d_1(\lambda_2+2\mu_2))^2}, \\ a_4 &= \frac{(\lambda_2+2\mu_2)L}{(\lambda_1+2\mu_1)d_2+d_1(\lambda_2+2\mu_2)} \\ b_0 &= -\frac{d_1d_2((\lambda_1+2\mu_1)-(\lambda_2+2\mu_2))}{(\lambda_1+2\mu_1)d_2+d_1(\lambda_2+2\mu_2)}, b_1 = \frac{(\lambda_1+2\mu_1)(d_1+d_2)}{(\lambda_1+2\mu_1)d_2+d_1(\lambda_2+2\mu_2)}, \\ b_2 &= -\frac{d_2d_1(-(\lambda_1+2\mu_1)^2d_2d_1+(\lambda_1+2\mu_1)(\lambda_2+2\mu_2)d_1(-d_1+d_2+L)-d_1d_2(\lambda_2+2\mu_2)^2)}{2((\lambda_1+2\mu_1)d_2+d_1(\lambda_2+2\mu_2))^2}, \\ b_3 &= \frac{(\lambda_1+2\mu_1)(d_1(\lambda_2+2\mu_2)(Ld_1+d_2^2-d_1^2)-d_2(\lambda_1+2\mu_1)(d_1^2+d_2d_1))}{2((\lambda_1+2\mu_1)d_2+d_1(\lambda_2+2\mu_2))^2}, \\ b_4 &= \frac{(\lambda_1+2\mu_1)L}{(\lambda_1+2\mu_1)d_2+d_1(\lambda_2+2\mu_2)} \end{aligned} \quad (3.A.5)$$

We note that an opposite sign has been used for the boundary conditions of the displacement to the one provided in Chapter 3, which leads to physically accepted results in the problems considered. The coefficients of Eq. (3.A.5) fully define the stress and strain definitions of Eqs. (3.A.2) and (3.A.3) and thus the macroscale stiffness definitions of Eq. (4.3).

### Appendix 4. A: Homogenized elasticity tensors

We write the homogenized equations for the stress and hyperstress tensors in index form in order to use these formulations in the finite element code to compute the effective rigidity tensors.

$$\Sigma_{ij} = C_{ijkl}^{\text{hom}} E_{kl} + B_{ijklm}^{\text{hom}} K_{klm} \quad (4.A.1)$$

Previous equations write explicitly in component form as follows:

$$\begin{pmatrix} \Sigma_{11} \\ \Sigma_{22} \\ \Sigma_{12} \end{pmatrix} = \begin{pmatrix} C_{1111} & C_{1122} & C_{1112} \\ C_{2211} & C_{2222} & C_{2212} \\ C_{1211} & C_{1222} & C_{1212} \end{pmatrix} \begin{pmatrix} E_{11} \\ E_{22} \\ E_{12} \end{pmatrix} + \begin{pmatrix} B_{11111} & B_{11121} & B_{11221} & B_{11222} & B_{11122} & B_{11112} \\ B_{22111} & B_{22121} & B_{22221} & B_{22222} & B_{22122} & B_{22112} \\ B_{12111} & B_{12121} & B_{12221} & B_{12222} & B_{12122} & B_{12112} \end{pmatrix} \begin{pmatrix} K_{111} \\ K_{121} \\ K_{221} \\ K_{222} \\ K_{122} \\ K_{112} \end{pmatrix} \quad (4.A.2)$$

We note that  $K_{ijk}$  is symmetric to the last two indices.

The hyperstress is expressed versus the strain gradient tensor and the coupling tensor with the first gradient term as follows:

$$S_{ijkl} = D_{ijklm}^{\text{hom}} E_{lm} + A_{ijklmn}^{\text{hom}} K_{lmn} \quad (4.A.3)$$

This writes in explicit component form:

$$\begin{pmatrix} S_{111} \\ S_{121} \\ S_{221} \\ S_{222} \\ S_{122} \\ S_{112} \end{pmatrix} = \begin{pmatrix} D_{11111} & D_{11122} & D_{11112} \\ D_{12111} & D_{12122} & D_{12112} \\ D_{22111} & D_{22122} & D_{22112} \\ D_{22211} & D_{22222} & D_{22212} \\ D_{12211} & D_{12222} & D_{12212} \\ D_{11211} & D_{11222} & D_{11212} \end{pmatrix} \begin{pmatrix} E_{11} \\ E_{22} \\ E_{12} \end{pmatrix} + \begin{pmatrix} A_{111111} & A_{111121} & A_{111221} & A_{111222} & A_{111122} & A_{111112} \\ A_{121111} & A_{121121} & A_{121221} & A_{121222} & A_{121122} & A_{121112} \\ A_{221111} & A_{221121} & A_{221221} & A_{221222} & A_{221122} & A_{221112} \\ A_{222111} & A_{222121} & A_{222221} & A_{222222} & A_{222122} & A_{222112} \\ A_{122111} & A_{122121} & A_{122221} & A_{122222} & A_{122122} & A_{122112} \\ A_{112111} & A_{112121} & A_{112221} & A_{112222} & A_{112122} & A_{112112} \end{pmatrix} \begin{pmatrix} K_{111} \\ K_{121} \\ K_{221} \\ K_{222} \\ K_{122} \\ K_{112} \end{pmatrix} \quad (4.A.4)$$

### Appendix 4.B: Corrected higher gradient formulation

As provided in (Li, 2011), we consider that the whole structure  $V$  is decomposed into a finite number of RVE's identical subdomains  $\Omega$ . We use the following Taylor expansion of the microscopic displacement as function of the macroscopic and microscopic spatial variables  $(X, y)$ :

$$u_i(X, y) = \frac{\partial u_i(X)}{\partial X_j} y_j + \frac{1}{2} \frac{\partial^2 u_i(X)}{\partial X_j \partial X_k} y_j y_k + \frac{1}{6} \frac{\partial^3 u_i(X)}{\partial X_j \partial X_k \partial X_l} y_j y_k y_l + o(y^4) \quad (4.B.1)$$

## Appendices

Restricting to the second order we obtain the following displacement and strain at micro-scale as function of macroscopic parameters as follows:

$$\begin{aligned} u_i(X, y) &= E_{ij}y_j + \frac{1}{2}K_{ijk}y_jy_k + o(y^3) \\ \Rightarrow \varepsilon_{ij}(X, y) &= E_{ij} + K_{ijk}y_k + o(y^3) \end{aligned} \quad (4.B.2)$$

Where  $E$  and  $K$  are the first and the second macroscopic strain gradient.

We evaluate using Eq. (B2) the following integral over the entire domain  $V$ :

$$\begin{aligned} \int_V C_{ijkl}^{\text{hom}} \varepsilon_{ij} \varepsilon_{kl} dV &= \int_V C_{ijpl}^{\text{hom}} (E_{ij} + K_{ijk}y_k) (E_{pl} + K_{plm}y_m) dV \\ &= \sum_V \bar{V} \cdot C_{ijpl}^{\text{hom}} E_{ij} E_{pl} + \sum_V \int_{\Omega} y_m C_{ijpl}^{\text{hom}} E_{ij} K_{plm} d\Omega \\ &+ \sum_V \int_{\Omega} y_k C_{ijpl}^{\text{hom}} E_{pl} K_{ijk} d\Omega + \sum_V \int_{\Omega} C_{ijpl}^{\text{hom}} y_k y_m K_{ijk} K_{plm} d\Omega \end{aligned} \quad (4.B.3)$$

Where  $\bar{V}$  is the RVE volume. Since the origin is situated at the center of the RVE ( $\Omega$ ), it holds separating the macroscopic energy terms from Eq. (4.13):

$$\begin{aligned} \Rightarrow \sum_V \bar{V} C_{ijpl}^{\text{hom}} E_{ij} E_{pl} &= \int_V C_{ijkl}^{\text{hom}} \varepsilon_{ij} \varepsilon_{kl} dV - \int_V C_{ijpl}^{\text{hom}} y_k y_m K_{ijk} K_{plm} dV \\ \Rightarrow \sum_V \bar{V} C_{ijpl}^{\text{hom}} E_{ij} E_{pl} &= \int_V C_{ijkl}^{\text{hom}} \varepsilon_{ij} \varepsilon_{kl} dV - \sum_V \bar{V} C_{ijpl}^{\text{hom}} K_{ijk} K_{plm} \left( \int_{\Omega} y_k y_m d\Omega \right) \end{aligned} \quad (4.B.4)$$

We note that  $\bar{V}$  is the RVE surface in the present 2D case.

Integrating the strain energy and using the last expression of the first gradient macroscopic energy across the entire domain (4.B.4) we get the following relation:

$$\begin{aligned} \int_V w dV &= \frac{1}{2} \sum_V \bar{V} (C_{ijpl}^{\text{hom}} E_{ij} E_{pl} + A_{ijklmn}^{\text{hom}} K_{ijk} K_{lmn}) \\ &= \frac{1}{2} \sum_V \bar{V} (A_{ijklmn}^{\text{hom}} K_{ijk} K_{lmn}) + \frac{1}{2} \left( \int_V C_{ijpl}^{\text{hom}} E_{ij} E_{pl} dV - \sum_V \bar{V} C_{ijpl}^{\text{hom}} K_{ijk} K_{plm} \left( \int_{\Omega} y_k y_m d\Omega \right) \right) \\ &= \frac{1}{2} \sum_V \int_{\Omega} A_{ijklmn}^{\text{hom}} K_{ijk} K_{lmn} d\Omega + \frac{1}{2} \left( \int_V C_{ijpl}^{\text{hom}} E_{ij} E_{pl} dV - \sum_V \bar{V} C_{ijpl}^{\text{hom}} K_{ijk} K_{plm} \left( \int_{\Omega} y_k y_m d\Omega \right) \right) \\ &= \frac{1}{2} \int_V A_{ijklmn}^{\text{hom}} K_{ijk} K_{lmn} dV + \frac{1}{2} \left( \int_V C_{ijpl}^{\text{hom}} E_{ij} E_{pl} dV - \int_V C_{ijpl}^{\text{hom}} K_{ijk} K_{plm} I_{km} dV \right) \\ &= \frac{1}{2} \int_V C_{ijpl}^{\text{hom}} E_{ij} E_{pl} dV + \frac{1}{2} \left( \int_V K_{ijk} K_{lmn} (A_{ijklmn}^{\text{hom}} - C_{ijlm}^{\text{hom}} I_{kn}) dV \right) \end{aligned} \quad (4.B.5)$$

## Appendices

Wherein the quadratic inertia tensor is  $I_{km} = \int_{\Omega} y_k \cdot y_m d\Omega$ . We identify from Eq. (4.B5) the

first and second gradient constitutive tensors as follows:

$$\begin{aligned} C_{ijlm}^{\text{hom}*} &= C_{ijlm}^{\text{hom}} \\ A_{ijklmn}^{\text{hom}*} &= A_{ijklmn}^{\text{hom}} - C_{ijlm}^{\text{hom}} I_{kn} \end{aligned} \quad (4.B.6)$$

### Appendix 4. C: Microscopic elastic matrix

We write the elasticity tensor  $C_{ijlm}^0$  of a material evaluated versus the Lamé constants of the matrix as follows:

$$C_{ijlm}^0 = \begin{bmatrix} \lambda + 2\mu & \lambda & 0 \\ \lambda & \lambda + 2\mu & 0 \\ 0 & 0 & 2\mu \end{bmatrix} \quad (4.C.1)$$

$(\lambda, \mu)$  in Eq.(4.C.1) are the Lamé coefficients, evaluated versus the Young modulus and Poisson's ratio as  $(\lambda = E\nu / (1+\nu) / (1-2\nu), \mu = E / (2(1+\nu)))$ .